



Faculty of Sciences  
Department of Biology  
Ecosystem Management Research group

Faculteit Wetenschappen  
Departement Biologie  
Onderzoeksgroep Ecosysteembeheer

# Effects of intertidal ecosystems on estuarine hydrodynamics and flood wave attenuation: a multi-scale study

Dissertation

submitted to obtain the degree of:  
Doctor of Science at the University of Antwerp

to be defended by:

**Jeroen STARK**

Civil Engineer, Delft University of Technology  
born in Schiedam, Netherlands

**Promotor:** Prof. dr. S. Temmerman  
**Co-promotor:** Prof. dr. P. Meire

Antwerp, 2016



# **Effects of intertidal ecosystems on estuarine hydrodynamics and flood wave attenuation: a multi-scale study**

*Effecten van intertidale ecosystemen voor estuariene hydrodynamica en demping van vloedgolven: een meerschelijke studie*

Proefschrift

voorgelegd ter verkrijging van de graad:  
Doctor in de Wetenschappen aan de Universiteit Antwerpen

in het openbaar te verdedigen door:

**Jeroen STARK**

Civil Ingenieur, Technische Universiteit Delft  
geboren te Schiedam, Nederland

Members of the doctoral committee:

Prof. dr. I. Nijs ( <i>chairman</i> )	University of Antwerp
Prof. dr. S. Temmerman ( <i>promotor</i> )	University of Antwerp
Prof. dr. P. Meire ( <i>co-promotor</i> )	University of Antwerp
Prof. dr. ir. T. de Mulder	Ghent University

Other jury members:

Prof. dr. S. Lanzoni	University of Padova
Dr. ir. B. Borsje	University of Twente / Deltares
Prof. dr. ir. Stefan Van Damme	University of Antwerp

© 2016, Jeroen Stark

*All rights reserved. No part of this publication or the information contained herein may be reproduced, stored in a retrieval system, or transmitted in any form or by any means, electronic, mechanical, by photocopying, recording or otherwise, without written prior permission from the author. Reuse of the knowledge and information in this publication is welcomed on the understanding that due credit is given to the source. However, neither the publisher nor the author can be held responsible for any consequences resulting from such use.*

Cover design: Anita Muys, Nieuwe Media Dienst, University of Antwerp

Cover picture: Aerial picture of the Saeftinghe marsh, by Joop van Houdt, <https://beeldbank.rws.nl>, Rijkswaterstaat

---

## Abstract

Estuaries and their intertidal ecosystems, such as marshes and tidal flats, are of great importance to society. They provide for a range of economic activities such as shipping, for ecological functions such as biogeochemical nutrient cycling or biological production and for flood and shoreline protection as intertidal areas have the capacity to attenuate wind waves and storm surges. While historical land reclamations led to a large-scale loss of intertidal habitat, restoration and conservation of intertidal ecosystems is nowadays being implemented as a sustainable strategy to enhance the delivery of these functions again. This thesis addresses the hydrodynamic impact of changes in size and geomorphology of intertidal ecosystems as a result of embankments, de-embankments or natural sedimentation and erosion processes, both locally in marsh channels as well as on estuary scale, with a special focus on the potential of intertidal areas to attenuate storm surges.

For storm surge attenuation across marsh transects, both in-situ water level observations and numerical modelling results in this thesis indicate that intertidal ecosystems have the potential to attenuate peak water levels and reduce storm surges locally (Chapters 2 & 3). A comparison with an analytical approximation of tidal propagation through convergent channels indicates that differences in attenuation rates are induced by variations in cross-sectional averaged friction. In addition, numerical modelling results indicate that peak water level attenuation rates are related to the cross-sectional area of the marsh channels relative to the storage volume on the marsh platform. This implies that storm surge reduction is dependent on marsh geometry as well as on the flood wave height itself. Model simulations also show that storm surge attenuation can be limited by marsh size, due to blockage of the tidal wave against levees or other structures surrounding the marsh.

For regular tidal hydrodynamics, model simulations in this thesis (Chapter 4) show how tidal prism and tidal asymmetry change with the eco-geomorphological development of a tidal marsh, including vegetation establishment, vertical platform growth and changes in marsh channel geometry. In particular, model results show that vegetation establishment leads to marsh-scale flow concentration to the bare channels, causing an increase in tidal prism and a less flood-dominant (or more ebb-dominant) asymmetry of the tide. This decrease in flood-dominance continues as the platform grows vertically and the sediment-demand of the platform decreases. However, as the marsh elevation gets higher in the tidal frame and close to mean high water level, the discharge through the marsh channels decreases again and tidal asymmetry becomes more flood-dominant, indicating an infilling of these channels.

On estuary scale (Chapter 5), model simulations with varying tidal flat elevations indicate that if intertidal areas contribute to the channel cross-section and exert friction for the along-estuary tidal propagation, the elevation of intertidal flats determines their influence on the magnitude and type of tidal asymmetry along estuarine channels. Ebb-dominance is most strongly enhanced for tidal flats around or slightly above mean sea

---

level. Lower tidal flats can even enhance flood-dominance as frictional effects influence low water levels more than high water levels if tidal flats are situated low in the tidal frame. Furthermore, for intertidal storage areas that are situated besides the main estuarine channels and that barely contribute to the tidal propagation along the estuary, model results indicate an along-estuary varying impact on the tidal prism and on tidal asymmetry. In particular, intertidal storage areas enhance ebb-dominance throughout the estuary, except for a stretch directly downstream of the storage area where flood dominance is enhanced due to a velocity surge effect which is stronger during flood than during ebb. The tidal prism generally decreases upstream and increases downstream of intertidal storage areas. However, model simulations indicate that the tidal prism may also decrease far downstream of additional intertidal storage areas due to a decrease in tidal range which gradually reduces the tidal prism in downstream direction.

Overall, this thesis may assist scientists and managers of estuaries and intertidal ecosystems in understanding the impact of intertidal area changes (as a result of de-embankments, estuarine morphological management or the natural eco-geomorphological development of marshes) for estuary scale and marsh scale tidal hydrodynamics. Moreover, as coastal wetland conservation and restoration is starting to be implemented as part of ecosystem-based coastal defense systems, this thesis may also help coastal managers with the design and morphological management of coastal wetlands to optimize their storm surge attenuation functions.

---

## Samenvatting

Estuaria en intertidale ecosystemen zoals zandplaten, slikken en schorren zijn van groot belang voor de maatschappij. Deze gebieden dragen bij aan economische activiteiten zoals de scheepsvaart door estuariene geulen, aan ecologische waarde zoals door de biochemische nutriëntencycli of biologische productie en aan kustbescherming doordat deze gebieden golven en stormvloeden kunnen dempen. Historische inpolderingen hebben het areaal aan intertidale habitat sterk gereduceerd, maar tegenwoordig worden intertidale ecosystemen beschermd en hersteld om de vroegere ecologische en economische functies te herstellen. Deze thesis is een studie naar het effect van veranderingen in de grootte en geometrie van intergetijdengebieden, als gevolg van inpolderingen, ontpolderingen of de natuurlijke morfologische ontwikkeling van deze gebieden, op getijdenhydrodynamica in estuariene geulen en lokaal in de intertidale geulen en kreken in de schorregebieden zelf. Speciale aandacht gaat hierbij uit naar de potentiële kustbeschermingsfunctie van intergetijdengebieden.

De waterstandsmetingen en de resultaten van hydrodynamische modellen in deze thesis (Hoofdstuk 2 & 3) tonen aan dat intergetijdengebieden inderdaad de potentie hebben om hoogwaterstanden in een schorregebied te dempen. Een analytische benadering van getijvoortplanting door convergente geulen laat zien dat variaties in demping tussen verschillende geulsecties en tussen getijden met verschillende hoogwaterniveaus kunnen worden toegeschreven aan variaties in de dwarssectie-gemiddelde wrijving. Uit de resultaten van het hydrodynamisch model volgt ook dat de demping van hoogwaters gerelateerd is aan het watervolume dat door de intertidale geulen stroomt ten opzichte van het watervolume dat over het schorplatform beweegt. Dit betekent dat de lokale demping van vloedgolven afhankelijk is van de geometrie van intergetijdengebieden, maar ook van de hoogte van het stormtij of de vloedgolf zelf. De modelsimulaties laten verder zien dat de grootte van een intergetijdengebied een beperkende factor kan zijn voor de demping van stormvloeden. Als het gebied te klein is, dan wordt de getijgolf geblokkeerd of gereflecteerd tegen dijken of andere hoger gelegen gebieden rondom het intergetijdengebied, wat hogere waterstanden tot gevolg heeft.

Verder laten de modelresultaten in deze thesis zien dat het getijprisma en de getij-asymmetrie in intertidale geulen veranderen tijdens de eco-geomorfologische ontwikkeling van een schorregebied (Hoofdstuk 4). Deze ontwikkeling omvat de vestiging van schorvegetatie, de ophoging van het schorplatform en veranderingen in de geometrie van de intertidale geulen. Vestiging van schorvegetatie leidt tot een concentratie van de getijstroming naar de geulen, zodat het getij-prisma daar toeneemt en de getij-asymmetrie minder vloed-dominant (of meer eb-dominant) wordt. Deze afname in vloed-dominantie zet in eerste instantie door als het schorplatform ophoogt en de vraag naar sediment daar geleidelijk afneemt. Echter, als verdere ophoging van het schorplatform ertoe leidt dat het platform niet meer bij elk getij overstroomt, waardoor het bergingsvolume op het platform en het debiet door de intertidale geulen verminderen, wordt de getij-asymmetrie weer meer vloed-dominant wat duidt op een opvulling van de intertidale geulen.

---

Op estuarium schaal laten modelresultaten in deze thesis (Hoofdstuk 5) zien dat, voor intergetijdengebieden die zich in de stroomvoerende sectie bevinden en wrijving uitoefenen op de voortplanting van het getij, de hoogteligging van intergetijdengebieden bepalend is voor het type en de sterkte van de getij-asymmetrie in de estuariene geulen. Eb-dominantie wordt het meest versterkt voor intergetijdengebieden rond of net boven gemiddeld zeeniveau. Lager gelegen intergetijdengebieden kunnen daarentegen juist vloed-dominantie versterken omdat diepte-afhankelijke wrijvingseffecten in dat geval sterker zijn bij laagwater dan bij hoogwater en er ook bergingscapaciteit is bij lagere waterniveaus. Voor intergetijdengebieden die niet of nauwelijks bijdragen aan de stroomvoerende sectie voor getijvoortplanting van de estuariene geulen laten modelresultaten een ruimtelijk variërende impact op de getij-asymmetrie en het getij-prisma zien. Deze intertidale bergingsgebieden versterken een eb-dominante getij-asymmetrie in het hele estuarium, behalve direct zeewaarts van het gebied. Daar wordt de asymmetrie juist meer vloed-dominant door een lokale piek in de stroomsnelheden die sterker is tijdens vloed dan tijdens eb. In het algemeen neemt het getij-prisma benedenstrooms toe en bovenstrooms af als gevolg van toegevoegde intertidale waterberging. Modelsimulaties in deze thesis laten echter ook zien dat het getij-prisma ver benedenstrooms van intertidale waterberging weer kan afnemen als gevolg van een verminderd getijverschil dat een in zeewaartse richting sterker wordend reducerend effect heeft op het getij-prisma.

De resultaten van deze thesis kunnen wetenschappers en beheerders van estuaria of intertidale ecosystemen helpen bij het begrip van hydrodynamische effecten van veranderingen in intergetijdengebieden. Zo kunnen bijvoorbeeld de gevolgen van in- en ontpolderingen, morfologisch beheer of de natuurlijke eco-geomorfologische ontwikkeling van slikken en schorren beter worden begrepen. Aangezien intertidale ecosystemen tegenwoordig steeds meer als onderdeel van de kustverdediging worden beschouwd, kan deze thesis bovendien bijdragen aan het optimaliseren van het ontwerp en morfologisch beheer van intergetijdengebieden langs kusten en estuaria met het oog op hun kustbeschermingsfunctie.



---

## Acknowledgements

It is now four years ago that my PhD adventure at the University of Antwerp started. During this period, many people have helped me, supported me or have in one or another way contributed to the final result in the form of this thesis.

First, I want to gratefully acknowledge the Port of Antwerp for funding this research and supporting the initial ideas from which this study arose. This PhD wouldn't be possible without this financial support.

Greatest gratitude goes to my promotor Stijn Temmerman for helping me to write this thesis, for always being supportive, for pointing out all the interesting (and publishable) results in what I thought were just ordinary model outcomes or measurements, but above all for being an awesome guide during my PhD adventure. Gratitude also goes to my co-promotor Patrick Meire for introducing me in the magnificent world of the Scheldt Estuary in all its varieties, for the feedback and critical remarks during our progress meetings and for tolerating a civil engineer from the Netherlands in the research group.

I would like to thank the members of my jury and doctoral committee: Tom de Mulder, Stefano Lanzoni, Bas Borsje, Stefan van Damme and Ivan Nijs, who took the time to carefully read this thesis and gave constructive feedback and suggestions during the very last stages of my PhD.

Furthermore, I am grateful to all the people who advised me, helped me or gave feedback during my PhD. I want to specifically acknowledge the members of my "*stuurgroep*": Stefaan Ides, Yves Plancke, Wouter Vandenbruwaene and Els van Duyse, thanks for all the feedback, ideas, suggestions and guidance during our meetings. I want to thank Tomas van Oyen for his help with the second chapter and for brushing up on my math skills; Sven Smolders for his help in learning the TELEMAC modelling system during the early stages of my PhD, for his suggestions and especially for his feedback on the fifth chapter; the nature guides in Saeftinghe: Marc Buise, Walter Poppe and Carla van Dueren den Hollander for helping me during my few fieldwork days and making my visits to this wonderful nature area even more worthwhile; George Schramkowski, Abdel Nnafie and Ronald Brouwer for their suggestions on the fourth chapter; Stefan Becuwe, Geert Borstlap and the other people of CalcUA for their help and support in installing the TELEMAC system on the university's supercomputer and making it possible to do the numerous model exercises that resulted in this thesis; and the people of the TELEMAC consortium who advised me on the model setup and configuration. The bathymetric, topographic, meteorological and part of the hydrodynamic data used in this thesis were made available by Rijkswaterstaat, Flanders Hydraulics Research and the KNMI.

This acknowledgement section would not be complete without a big thank you to all the colleagues at ECOBE for their support, for the sometimes highly intellectual but more often ridiculously funny conversations during lunch and coffee breaks (sorry, Patrick...),

---

for the good-times during the after-work drinks, parties, lunch-sports and all other activities. I especially want to thank my modelling buddies: Christian, Olivier and Veerle. You were a great help to me. There are many others who made these four years much more enjoyable: Lotte, Lindsay, Rebecca, Lennert, Ken, Cedric, Steven, Martijn, Kristine, Leo, Willem-Jan, Jonas, Alexandra, Chen, Eric, Floor, Lucia, Dácil, Dirk, Katrien, Annelies, Jan, Alanna, Dimitri, Stijn, the Tom's, Kerst, Jan-Willem, Goedele, Jean-Philippe, Merche, Johnny, Mérielle and of course our secretaries Magda, Chris and Peter. Thanks a lot!

Last but certainly not least I want to thank my friends and family, who asked me dozens of times what my PhD was about (I can only hope my explanations were at least a bit clear), if I had published anything, when I would finish and more importantly if I was ever coming back to the Netherlands. Above all, I have to thank those who supported me most. Gerlinde, thanks a lot for your encouragements and for understanding and accepting all the times that I worked much too long or came home late, especially in the last couple of months. Mom and Dad, thanks for your unconditional support and encouragements throughout the years.

Jeroen Stark  
Antwerpen, December 2016

---

## Table of contents

<b>Chapter 1:</b>	General introduction	<b>1-20</b>
<b>Chapter 2:</b>	Observations of tidal propagation and storm surge attenuation in a large tidal marsh	<b>21-40</b>
<b>Chapter 3:</b>	Coastal flood protection by a combined nature-based and engineering approach: modelling the effects of marsh geometry and surrounding dikes	<b>41-66</b>
<b>Chapter 4:</b>	Tidal hydrodynamics during different stages of eco-geomorphological development of a tidal marsh: a numerical modelling study	<b>67-96</b>
<b>Chapter 5:</b>	Impact of intertidal area characteristics on estuarine tidal hydrodynamics: a modelling study for the Scheldt estuary	<b>97-124</b>
<b>Appendix 5A:</b>	Tidal constituent analysis	<b>125-130</b>
<b>Appendix 5B:</b>	Effects of the Saeftinghe marsh and its elevation on tidal hydrodynamics in the Scheldt estuary	<b>131-138</b>
<b>Appendix 5C:</b>	Effects of channel enlargement on tidal hydrodynamics in the Scheldt estuary	<b>139-146</b>
<b>Chapter 6:</b>	General discussion and conclusions	<b>147-164</b>
<b>Curriculum Vitae:</b>		<b>165-166</b>



# Chapter 1

## General introduction



*Aerial photograph of the Schelde near Saeftinghe and the Port of Antwerp (<https://beeldbank.rws.nl>, Rijkswaterstaat / Joop van Houdt)*

### 1.1 The importance of estuaries and their intertidal areas

Estuaries can be defined as semi-enclosed water bodies with an open connection to the sea which are influenced by tidal water motion and terrestrial freshwater input (Pritchard, 1967). Intertidal areas along estuaries (i.e., areas with an elevation between low and high water level that are inundated and falling dry along with the tide) consist of tidal flats (or mudflats) and tidal marshes. The latter can be characterized by a high elevated and vegetated marsh platform that is dissected by a branching network of tidal channels that become smaller and shallower in landward direction (Figure 1.1). Estuaries are typically surrounded by high concentrations of industrial, residential, agricultural and recreational activities and are therefore of high economic and societal importance. Moreover, estuaries and in particular their intertidal areas are also of great ecological importance (Barbier et al., 2013; Costanza et al., 1997). They provide numerous ecosystem services to society such as the maintenance of biodiversity as intertidal habitats contain large quantities of varying flora and fauna (Costanza et al., 1997), biogeochemical nutrient cycling linked to the improvement of water quality (e.g. Mitsch et al., 2012), carbon sequestration through the vertical accretion of marshes (e.g. McLeod et al., 2011; Mitsch et al., 2013; Ouyang and Lee, 2014) and they can reduce flood risks in coastal areas (e.g. Bouma et al., 2014; Gedan et al., 2010; Shepard et al., 2011; Temmerman et al., 2013).



**Figure 1.1:** Aerial photograph of the Saeftinghe marsh (Western Scheldt, SW Netherlands), showing the characteristic geomorphology of a tidal marsh with a vegetated marsh platform dissected by a landward branching network of intertidal channels. (Photo by Joop van Houdt, Rijkswaterstaat: <https://beeldbank.rws.nl>)

However, coasts, estuaries and their intertidal areas are under pressure by continuously growing populations and increasing economic activities (Small and Nicholls, 2003). As a result the ecological value of many estuaries deteriorated during the last centuries, mainly due to land reclamation for agricultural and industrial purposes (e.g. Kirwan and Megonigal, 2013; Ma et al., 2014; Moore et al., 2009; Pendleton et al., 2012). Besides,

intensified dredging activities took place in numerous estuaries during the last decades to accommodate larger ships and allow for port expansion, thereby inducing morphological developments (e.g. erosion of intertidal flats and marshes) that might have led to loss of valuable intertidal habitat (e.g. Blott et al., 2006; Meire et al., 2005; Sherwood et al., 1990; Yang et al., 2006). Furthermore, dam construction along major river basins may also have had negative effects to estuarine and coastal ecosystems and intertidal flats in particular, due to a reduction or depletion of the fluvial sediment supply (e.g. Naik and Jay, 2011; Yang et al., 2006). In particular, intertidal areas need sufficient sediment supply to be able to accrete vertically along with sea level rise (e.g. Allen and Rae, 1988; Kirwan and Murray, 2007; Temmerman et al., 2004).

Nowadays, restoration and conservation of estuarine habitats such as tidal flats and marshes is being implemented to enhance the delivery of ecosystem services by estuaries (e.g. de Vriend et al., 2014; Temmerman et al., 2013). This is considered to be a sustainable strategy as biophysical feedback processes are known to accelerate vertical accretion of wetlands along with sea level rise (Kirwan et al., 2016; Temmerman and Kirwan, 2015). In particular, the presence of marsh vegetation reduces flow velocities and enhances sedimentation (Christiansen et al., 2000; De Lima et al., 2015; Mudd et al., 2010), which allows marshes to grow vertically with sea level rise.

## **1.2 The flood protection function of intertidal areas**

Coastal and estuarine wetlands are increasingly valued for their role in mitigation of flood risks during storm surges (Costanza et al., 2008). A storm surge is a rise in the sea surface level caused by low atmospheric pressure (such as during cyclones and hurricanes or typhoons), which in combination with strong landward directed winds leads to a water level setup in coastal and estuarine areas (e.g. Resio and Westerink, 2008). In estuaries, storm surges or storm tides (i.e., storm surges that significantly increase regular high water levels induced by the astronomic tide) propagate as flood waves in a landward direction, through estuarine channels and locally through intertidal areas (such as tidal wetlands), inducing risks of flooding which may lead to loss of human life and destruction of homes, industrial areas or other infrastructure.

Intertidal areas have the potential to locally reduce the height of both wind waves (e.g. Möller et al., 2014, 1999) and storm surges (e.g. Krauss et al., 2009; McGee et al., 2006; Wamsley et al., 2010) during storm conditions through additional flow resistance exerted by the wetland vegetation and by the wetland geomorphology. Moreover, intertidal areas along estuaries can also reduce flood risks on estuary scale as the intertidal storage volume (i.e., the amount of water which can be stored on tidal flats and marshes, situated between low and high water level) can effectively attenuate the peaks of storm surges or storm tides (Meire et al., 2014; Smolders et al., 2015). Hence, the coastal defense potential of intertidal areas can be separated into the potential for the reduction of peak water levels across marshlands or ‘inside marsh attenuation’ and the potential for the reduction of peak water levels along the estuary channels or ‘along

estuary attenuation' (Figure 1.2). Because of their potential coastal defense value, restoration of tidal wetlands and marshes is nowadays starting to be used in addition to conventional coastal defense structures to protect coastal and estuarine areas from flood hazards.

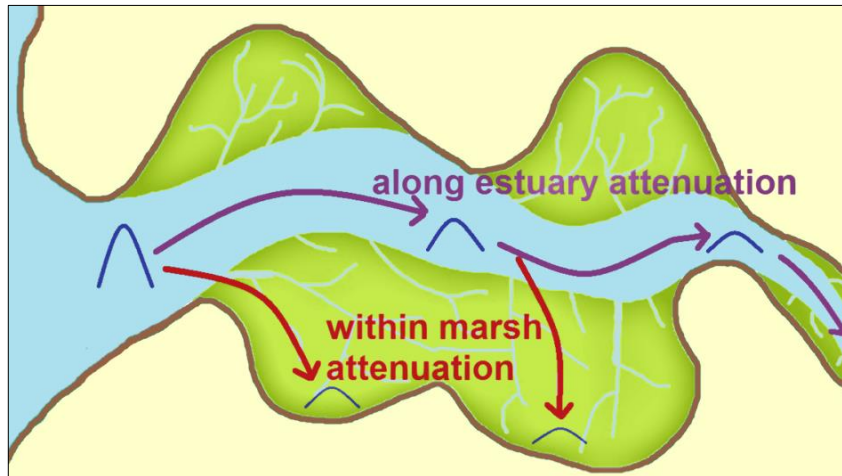


**Figure 1.2:** Schematic overview of the coastal defense potential of intertidal areas along estuaries, consisting of local within marsh attenuation (red) and estuary scale along estuary attenuation (purple).

So far, existing insights on storm surge reduction rates in marshes (i.e., inside marsh attenuation as indicated in Figure 1.2) are limited and based on scarce field studies (McIvor et al., 2012; Chapter 2) and some more numerical modelling studies (e.g. Loder et al., 2009; Resio and Westerink, 2008; Wamsley et al., 2010; Zhang et al., 2012), which were mainly conducted for specific hurricane or storm surge events. Previous studies suggest that the amount of local storm surge reduction by coastal wetlands such as mangroves and tidal marshes is influenced by the geometry of wetlands, including marsh channel width, depth and density (e.g. Loder et al., 2009; Temmerman et al., 2012; Wamsley et al., 2010). For example, numerical modelling studies suggest that marshes with more and wider or deeper channels induce less storm surge reduction rates than marshes which are dissected by fewer or smaller channels (Loder et al., 2009; Temmerman et al., 2012). Other numerical modelling studies have shown that the amount of storm surge reduction over tidal wetlands is also dependent on the vegetation induced flow resistance, which varies with the type of vegetation cover (Hu et al., 2015; Sheng et al., 2012; Zhang et al., 2012). Finally, it has been shown that storm surge reduction varies with the hydrodynamic conditions of the specific flood event, such as storm surge height, storm surge duration and forward speed (e.g. Rego and Li, 2009; Resio and Westerink, 2008; Weisberg and Zheng, 2006). In particular, Resio and Westerink (2008) explained that storm surge attenuation decreases for larger storm surges and longer inundation events as the surge has more time to fill up the entire marsh storage area. Nevertheless, fundamental insights on the combined effect of storm characteristics and specific (geometrical) marsh characteristics on the amount of storm surge reduction rates are still lacking.



### 1.3 Intertidal area changes and tidal hydrodynamics

Variations in the size, geomorphology (i.e., elevation and geometry of the channels, tidal flats and the marsh platform) and topography (i.e., vegetation cover) of intertidal areas may affect tidal hydrodynamics on estuary scale as well as locally in the intertidal marsh channels. On estuary scale, intertidal area changes mainly concern embankments (i.e. building dikes that disconnect intertidal areas from the estuary and hence stop tidal action in the embanked areas), de-embankments such as in managed realignment projects (i.e., building new dikes more landward and breaching or removing existing dikes so that the historically embanked land re-develops into intertidal flats and marshes) or natural sedimentation and erosion processes that alter the elevation and geometry of tidal flats and marshes. On marsh scale, the effect of intertidal area changes on tidal hydrodynamics mainly consists of the natural or human-induced eco-geomorphological development of tidal marshes. This development from a relatively bare and low elevated stage to a higher elevated and vegetated tidal marsh includes changes in vegetation cover, marsh platform elevation (and hence storage area) and marsh channel geometry. The hydrodynamic impact as a result of variations in intertidal area characteristics may include changes in the tidal prism (i.e., the total water volume entering the estuary or marsh during a single tide), (mean) high water levels, (mean) low water levels, tidal range (i.e., the difference between the high and low water levels), the intensity of tidal currents parametrized by (peak) ebb and flood velocities and tidal asymmetry (i.e. the tide becomes asymmetric as its shape deforms and deviates from a symmetrical sinusoidal tidal wave, for instance due to frictional effects in shallow waters; Figure 1.3).

Changes in tidal hydrodynamics may on its turn affect the estuarine or marsh morphology itself (e.g. Dronkers, 1986; Van de Kreeke and Robaczewska, 1993), but also influence ecology (e.g. Meire et al., 2005) and human activities such as shipping (i.e., navigability of estuarine channels). In tidal hydrodynamics, tidal asymmetry is of main importance to coastal and estuarine morphodynamics as asymmetries in tidal current velocities between flood and ebb lead to a residual sediment transport due to the non-linear relation between current velocity and sediment transport (i.e., typically, non-cohesive sediment transport is proportional to the velocity to the power three to five, e.g., Engelund and Hansen, 1967; van Rijn, 1993). If maximum flood velocities exceed maximum ebb velocities, residual non-cohesive sediment fluxes will be in flood direction, implying a net landward import of non-cohesive sediments, and vice versa in case of maximum ebb velocities that exceed maximum flood velocities, which induces a net seaward export of non-cohesive sediments (Lanzoni and Seminara, 2002; Van de Kreeke and Robaczewska, 1993; Wang et al., 1999). Besides its effect on morphodynamics, tidal asymmetry also plays a key role in the chemical and biological functioning of estuaries and marshes. For example, if the asymmetry of the tide causes a net landward transport of sediments (also known as tidal pumping), this may induce risks of sediment infilling of estuaries or estuarine channels and (in case of fine sediments) of high turbidity levels and water quality problems (e.g. Mitchell, 2013;

Winterwerp and Wang, 2013). In marsh channels, the type and magnitude of the tidal asymmetry may determine whether marsh systems are a net sink or source of sediments and other materials such as pollutants, nutrients, seeds or larvae (e.g. Fagherazzi et al., 2008; Friedrichs and Perry, 2001), implying that tidal marsh hydrodynamics is strongly influencing the ecological functioning of the intertidal marsh system.

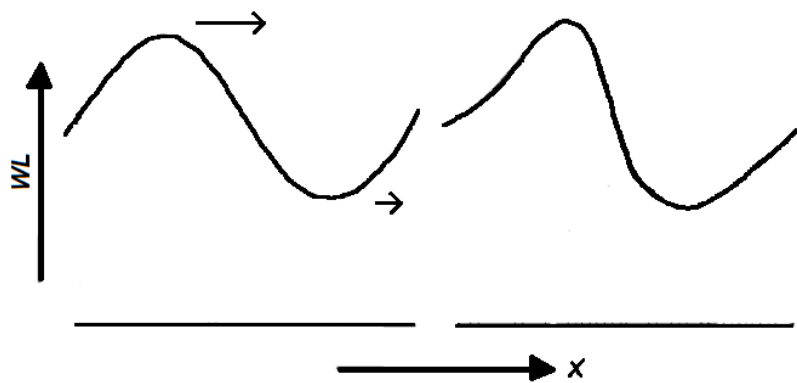


**Figure 1.3:** Sketch of the symmetric tidal wave plotted as vertical water levels against horizontal distance (left), for which the tidal propagation in shallow water is faster during high tide than during low tide, causing the tidal wave to become asymmetric (right).

Besides tidal asymmetry, other hydrodynamic parameters such as the tidal prism and tidal range are also of importance for the morphodynamic behavior and delivery of ecosystem services by estuaries and marshes. The tidal prism can for instance be related to the channel geometry (width, depth, cross-sectional area): several studies have identified relationships between tidal prism and the (equilibrium) cross-sectional area for tidal inlets and estuaries (e.g. D'Alpaos et al., 2009; Jarrett, 1976; O'Brien, 1969, 1931; Stive et al., 2010). In particular, a larger tidal prism due to increased intertidal storage may lead to scouring or erosion of estuarine channels (i.e., as a result of increased flow velocities and bottom shear stress) to increase the cross-sectional area and vice versa. Furthermore, changes in tidal damping or amplification (i.e., decrease or increase in tidal range and high water levels along an estuary or marsh channel) may directly influence flood risks and thereby affect the wellbeing and safety of communities living around estuaries. In this perspective, an interesting question regarding the restoration and management of intertidal areas is whether it can be used to alter tidal hydrodynamics in such a way that positive or desirable effects are obtained with respect to sediment transport patterns, turbidity levels and other estuarine functions such as the navigability of channels, storm surge reduction or the ecological functioning of estuaries and marshes.

### **1.3.1 Tidal asymmetry: a brief description**

As the asymmetry of the tide is of main importance to estuarine and marsh morphodynamics (e.g. Dronkers, 1986; Friedrichs and Perry, 2001; Van de Kreeke and Robaczewska, 1993), a short explanation of the origin and different types of tidal asymmetry is given below. A terminological distinction can be made between the asymmetry of the horizontal tide (i.e., discharges and velocities) and the vertical tide (i.e., water levels), although they are strongly linked (Bolle et al., 2010; Wang et al., 1999, 2002). The asymmetry of the horizontal tide can be expressed by the ratio

between the peak currents or discharges during flood and ebb. If the flood flow is stronger, this asymmetry is called flood-dominant; if the ebb flow is stronger, the horizontal asymmetry is ebb-dominant. The asymmetry of the vertical tide can be expressed as the difference or ratio between the duration of water level rise (flood period) and water level fall (ebb period). If the flood period is shorter, the asymmetry of the vertical tide is flood-dominant; if the ebb-period is shorter, the asymmetry is ebb-dominant. The reasoning behind this is that a shorter duration of the rising tide implies stronger (peak) flood velocities, whereas a shorter duration of the falling tide implies higher (peak) ebb-velocities. In addition, the difference in duration of the slack water periods after high tide and after low tide (i.e., short period around the turn of the tide during which flow velocities are close to zero) are another indicator for horizontal tidal asymmetry, because deposition of fine (suspended) sediment is closely related to the duration during which velocities are low and particles can settle. In particular, longer high water slacks induce a residual transport of fine sediments in flood-direction, while longer low water slack induces a residual transport of fines in ebb-direction (e.g. Dronkers, 1986). However, this type of tidal asymmetry is not assessed in this thesis. Finally, tidal asymmetry can be analyzed by the relative contribution of various tidal constituents to the tidal signal (e.g. Parker, 1984). The amplitude ratios and phase differences between the principal tidal constituents and their superharmonic overtides or compound tides determine the strength and type of the tidal asymmetry (i.e., whether tidal asymmetry is flood- or ebb-dominant). This is further explained in **Appendix 5A**.

Variations in tidal asymmetry along estuarine channels are determined by the estuarine morphology, and by the asymmetry of the incoming tidal wave itself (e.g. Aubrey and Speer, 1985; Dronkers, 1986; Friedrichs and Aubrey, 1988; Friedrichs and Madsen, 1992; Speer and Aubrey, 1985; Wang et al., 2002). Tidal asymmetry originates from non-linear processes in the continuity (Eq. 1.1) and momentum equations (Eq. 1.2) which cause the tidal wave to deform and become asymmetric as the ocean tide propagates in shallow waters such as through estuaries or tidal channels (e.g. Aubrey and Speer, 1985; Friedrichs and Aubrey, 1988; Speer and Aubrey, 1985). Similar nonlinear processes lead to distortion of the tide due to interactions with river discharge (e.g. Parker, 1984). The one-dimensional continuity and momentum equations for channelized flow in tidal channels or estuaries in the presence of tidal flats can be expressed as follows (e.g. Speer and Aubrey, 1985; Wang et al., 2002):

$$b_{tot} \frac{\delta \zeta}{\delta t} + \frac{\delta}{\delta x} \{b_{ch}(h_0 + \zeta)u\} = 0 \quad (1.1)$$

(A)                      (B)

$$\frac{\delta u}{\delta t} + u \frac{\delta u}{\delta x} + g \frac{\delta \zeta}{\delta x} + c_f \frac{u|u|}{h_0 + \zeta} + \frac{\delta}{\delta x} \left( v \frac{\delta u}{\delta x} \right) = 0 \quad (1.2)$$

(C)    (D)    (E)                      (F)                      (G)

in which:  $t$  is time,  $x$  is the distance from the channel entrance,  $u(x,t)$  is the cross-sectional averaged flow velocity,  $\zeta(x,t)$  is the water level relative to mean sea level,  $h_0$  is

the water depth relative to mean sea level,  $b_{tot}$  is the total width of the channel (including tidal flats),  $b_{ch}$  is the width of the channel solely (without tidal flats),  $g$  is the gravitational acceleration,  $c_f$  represents bed friction and  $\nu$  is viscosity. The continuity equation is formed by a storage term (A) and a discharge gradient (B). The momentum equation consists of the local inertia term (C), the advective inertia term (D), the water level gradient (E), a bottom friction term (F) and a horizontal diffusion term (G). If the latter is assumed to be small (i.e., assuming a well-mixed situation) so that the horizontal diffusion can be ignored, the advective inertia term (D) and bottom friction term (F) are left as main sources for non-linear interaction (Wang et al., 1999). The effect of the friction term can be further separated in two parts to distinguish between the effect of depth variation (i.e., the propagation speed of the high tide exceeds the propagation speed of the low tide due to its dependency on water depth) and the effect of non-linear bottom friction, which slows the low tide more than the high tide as the bottom stress will be higher during low tide.

### ***1.3.2 Influence of intertidal areas on estuarine tidal hydrodynamics***

Existing studies on the effect of intertidal areas and their geomorphological properties on estuarine tidal hydrodynamics are in most cases conducted in a highly schematized setting or by analytical approximations (e.g. Fortunato and Oliveira, 2005; Friedrichs and Madsen, 1992; Van Rijn, 2011). In general, it is known that intertidal areas along estuaries and tidal channels affect the tidal prism, the amplification (or damping) of the tide and the tidal asymmetry by enlarging the intertidal storage volume and due to increased friction for tidal propagation. The relative tidal amplitude (i.e., ratio between the tidal amplitude and the channel depth) and the extent of tidal flats (i.e., ratio between the channel width and total estuary width) have been identified as the main determining factors for tidal asymmetry and tidal damping or amplification in estuarine channels (e.g. Friedrichs and Madsen, 1992; Speer and Aubrey, 1985). More specifically, shallow channels with little intertidal storage tend to be flood-dominant as the frictional and inertial distortion in the channels is dominant via the friction term (F) and advective inertia term (D) in the momentum equation (Eq. 1.2) (e.g. Dronkers, 1986; Friedrichs and Aubrey, 1988; Friedrichs and Madsen, 1992; Speer and Aubrey, 1985). Lanzoni and Seminara (2002) even showed one-dimensionally that estuaries without tidal flats are in all cases flood-dominant. Conversely, a large intertidal storage volume in combination with low channel bed friction (i.e., in a deep tidal basin or channel) is known to enhance ebb-dominance through the storage term (A) in the continuity equation (Eq. 1.1) (Friedrichs and Aubrey, 1988; Friedrichs and Madsen, 1992). Intertidal flats may also enhance ebb-dominance by slowing down the propagating high tide more when the tidal flats are inundated, compared to low tide when the tidal flats fall dry (e.g. Fortunato and Oliveira, 2005; Friedrichs and Aubrey, 1988; Friedrichs and Madsen, 1992). In terms of the continuity and momentum equations, the bottom friction term (F) then increases during high tide, while it remains similar during low tide.

However, the effect of some intertidal area characteristics, such as tidal flat elevation or their physiographic setting and location along the estuary, on tidal hydrodynamics and tidal asymmetry in particular is not yet systematically assessed. This implies that there

is still a call for a better understanding of the effect of these specific intertidal area characteristics for estuarine tidal hydrodynamics, especially as restoration of intertidal ecosystems is nowadays being implemented in estuarine management.

### ***1.3.3 Intertidal area changes and marsh scale tidal hydrodynamics***

For marsh scale tidal hydrodynamics, existing studies on the impact of the eco-geomorphological development of tidal marshes on tidal hydrodynamics mainly consist of assessments of channel geometry and platform elevation during different stages of marsh development (e.g. D'Alpaos et al., 2006; Rinaldo et al., 1999; Vandenbruwaene et al., 2015). These studies have shown that the establishment of vegetation patches diverges the flow to the channels where the tidal prism increases, whereas an increase in marsh elevation reduces the storage volume on the marsh platform and thereby leads to a decrease in tidal prism through the marsh channels (D'Alpaos et al., 2006; Vandenbruwaene et al., 2015). Nevertheless, the effect of the different stages of the decadal scale eco-geomorphological development of marshes on tidal asymmetry in (intertidal) marsh channels, being a main force for the morphological development of these intertidal ecosystems, is still poorly studied. In particular, the specific effects of vegetation establishment, platform expansion, vertical platform growth, channel scouring and channel infilling on tidal asymmetry in marsh channels, and hence on the net sediment and material fluxes through these marsh channels, have not yet been systematically assessed.

## **1.4 Thesis objectives**

### ***1.4.1 Potential for storm surge reduction***

As the coastal defense potential of tidal wetlands, including tidal flats and marshes, is increasingly recognized, the first main objective of this thesis is to assess the influence of tidal marsh characteristics on tidal and storm surge propagation across a tidal marsh (i.e., the Saeftinghe marsh). While the effects of specific marsh properties such as marsh size, location and elevation on storm surge propagation along estuary channels have recently been studied (i.e. Smolders et al., 2015), the impact of some specific geomorphological properties of marshes on local storm surge reduction (i.e., inside marsh attenuation as indicated in Figure 1.2) is not yet fundamentally assessed. Moreover, observations of storm surge attenuation in wetlands or tidal marshes are scarce and mainly focusing on one or a few hurricane events.

In **Chapter 2**, the capacity of tidal wetlands to attenuate peak water levels locally is first studied with in-situ water level measurements for regular spring to neap tides and two major storm surge tides. These measurements are conducted in the Saeftinghe marsh, a 3000 ha brackish tidal marsh along the Western Scheldt (see: Section 1.5.2). Besides, a comparison with an analytical approximation of tidal propagation through convergent channels is used to assess the generic character of these observations.

In **Chapter 3**, the water level observations are further used to calibrate a two-dimensional hydrodynamic model (i.e., in TELEMAC-2D; see: Section 1.6) of the Saeftinghe marsh with a special focus on the representation of high water levels in the marsh itself. After validation with the in-situ water level measurements, the hydrodynamic model is used to study the effects of marsh size, marsh geometry and variations in flood wave height on local storm surge attenuation in tidal marshes. Various geomorphological model scenarios are used to assess the effect of varying positions of the dikes surrounding the marsh and of varying elevations of the vegetated marsh platform and of the unvegetated tidal flats and channels on storm surge reduction for a range of storm tides and regular spring- to neap tides. Ultimately, it is intended to relate the amount of storm surge attenuation to marsh geometry and the hydrodynamic boundary conditions.

### ***1.4.2 Marsh scale impact of intertidal area changes on tidal hydrodynamics***

Another objective is to improve general insights on the effect of tidal marsh development on tidal hydrodynamics locally in the marsh channels itself, with a special focus on tidal asymmetry. In particular, the (natural) vertical growth of marshes and the development of the marsh channel network induce changes in tidal storage on the marsh platform and in tidal discharges through the marsh channels (e.g. D'Alpaos et al., 2006; Temmerman et al., 2007). Accordingly, the degree and type of tidal asymmetry in marsh channels, which determines the net import (i.e., in case of flood-dominance) or export (i.e., in case of ebb-dominance) of sediments and other particulate matter (e.g. organic detritus, seeds, larvae, etc.), is also expected to vary between different stages of marsh development (e.g. Fagherazzi et al., 2008; Friedrichs and Perry, 2001). Such variations in tidal asymmetry determine the sink or source function of the marsh during different marsh development stages. This may on its turn influence the ecological functions that are dependent on the sediment or material exchange between marshes and adjacent estuaries or seas, such as carbon or nitrogen burial (Fagherazzi et al., 2013, 2008; Mitsch et al., 2012).

In **Chapter 4**, tidal asymmetry and tidal hydrodynamics in general along the marsh channels are assessed with the TELEMAC-2D hydrodynamic model of the Saeftinghe marsh (i.e., developed in **Chapter 3**). The validation of the model is first extended by a comparison with existing velocity measurements in the marsh channels, after which model scenarios covering different stages of marsh development (i.e., starting from a low-elevated bare tidal flat up to a largely vegetated high tidal marsh) are used to assess tidal hydrodynamics in marsh channels. These geomorphological scenarios include the effect of vegetation establishment and expansion, vertical growth of the marsh platform and variations in marsh channel geometry.

### ***1.4.3 Estuary scale impact of intertidal area changes on tidal hydrodynamics***

The final objective of this study is to assess the impact of intertidal area changes on estuary scale tidal hydrodynamics. Intertidal area changes may consist of embankments, marsh restoration and managed realignment projects (i.e., the creation or restoration of intertidal habitat along estuaries by relocating dikes so that historically embanked land

(re-)develops into intertidal flats and marshes), but also of the natural vertical growth of tidal flats and marshes. Along with such intertidal area changes, tidal hydrodynamics are expected to change along the estuary channels with potential effects on the economic and ecological functions provided by an estuary. For example, changes in high water level have a direct impact on coastal safety, changes in current velocities or low water levels influence the navigability in the channels, while changes in tidal asymmetry influence the residual sediment transport and hence the morphodynamic behavior.

In **Chapter 5**, the impact of specific intertidal area properties (i.e., location along the estuary, relative size and tidal flat elevation) on the characteristics of the tidal wave in the estuary channels is studied with a two-dimensional hydrodynamic model (i.e., set up in TELEMAC-2D; see: Section 1.6) of the Scheldt Estuary that was previously calibrated and validated by Smolders et al. (2015). The Scheldt Estuary model is used for scenario analyses with varying tidal flat elevations and intertidal storage area locations along the Scheldt Estuary (**Chapter 5**). Besides, additional model simulations are performed to assess the impact of variations in elevation of the Saeftinghe marsh specifically (**Appendix 5B**) and to assess the impact of channel deepening or enlargement, being another major human-induced change on estuarine geomorphology, relative to the impact of intertidal area changes (**Appendix 5C**).

## 1.5 Study area

### 1.5.1 The Scheldt Estuary

The Scheldt River originates in France and flows for approximately 355 km through Belgium and the Netherlands until it reaches the North Sea at the estuary mouth near Vlissingen. The total river catchment covers almost 22.000 km<sup>2</sup>. The estuarine part of the Scheldt that is under the influence of tides reaches from the mouth near Vlissingen up to Gent (Figure 1.4), where a weir lock complex prevents further tidal intrusion. The Western Scheldt forms the most downstream part of the Scheldt Estuary in the Netherlands, while the tidally influenced part of the Scheldt Estuary in Belgium is referred to as Sea Scheldt. Parts of the tributary rivers such as the Durme, Rupel, Nete, Dijle and Zenne are also influenced by the tide. The area of interest for this thesis is the tidally influenced part of the Scheldt Estuary (i.e., Sea Scheldt and in particular the Western Scheldt), which has a length of 160 km from Gent to the estuary mouth. The Scheldt estuary is tide-dominated by a meso- to macrotidal regime, with a mean tidal range that varies between 3.8 m at the mouth close to Vlissingen up to 5.2 m in the Sea Scheldt near Hamme, from where the tidal range decreases again. The estuary width is converging from ~5 km near Vlissingen to ~1.5 km at the Dutch-Belgian border and further to ~50 m near Gent. The cross-sectional averaged depth of the estuary converges from about 15 m near Vlissingen to 3m at Gent (Wang et al., 2002). The morphology of the Scheldt Estuary is characterized by a braided pattern of ebb and flood channels with intertidal shoals in the downstream part (i.e. Western Scheldt). Intertidal shoals are typically present at the landward end of flood channels and at the seaward

end of ebb channels and may be intersected by shallow connecting channels (Swinkels et al., 2009). The multichannel system shifts to a single channel system near the Dutch-Belgian border. The channels of the Scheldt estuary form the main shipping lane to the harbors of Antwerp, the third-largest port in Europe (i.e., after Rotterdam and Hamburg), Gent and Vlissingen. Port expansion and the growing need to make the ports accessible for larger ships were main drivers behind the channel deepening program during the last decades. In particular, the navigation depth for the shipping lane to the harbor of Antwerp has been increased in three steps between the 1970s and 2010 to a tide-independent navigable depth of 14.7 m. These works consisted of deepening the shallow sills in the channels, which are mainly present where the braided ebb- and flood channels cross each other. Moreover, continuous maintenance works have to be carried out to ensure the navigation depth in the shipping lanes. Maintenance dredging increased from about 0.5 Mm<sup>3</sup>/year in the 1950s to 7-10 Mm<sup>3</sup>/year in 2010 (before the latest deepening) (Jeuken and Wang, 2010). Sand mining or extraction of sediment from the estuary (on average about 1.7 Mm<sup>3</sup>/year) occurred until 2000 (Jeuken et al., 2004). Nowadays, dredged sediments are relocated in the estuary at strategic locations (i.e., on shoal edges or in channels that are not part of the main shipping lanes) with the aim to reduce dredging costs and maintain the multi-channel system and its diversity of habitats. The boundaries of the estuary are all artificial and determined by man-made dikes. Marshes are only present at specific locations along the estuary and are all bordered by dikes as well.

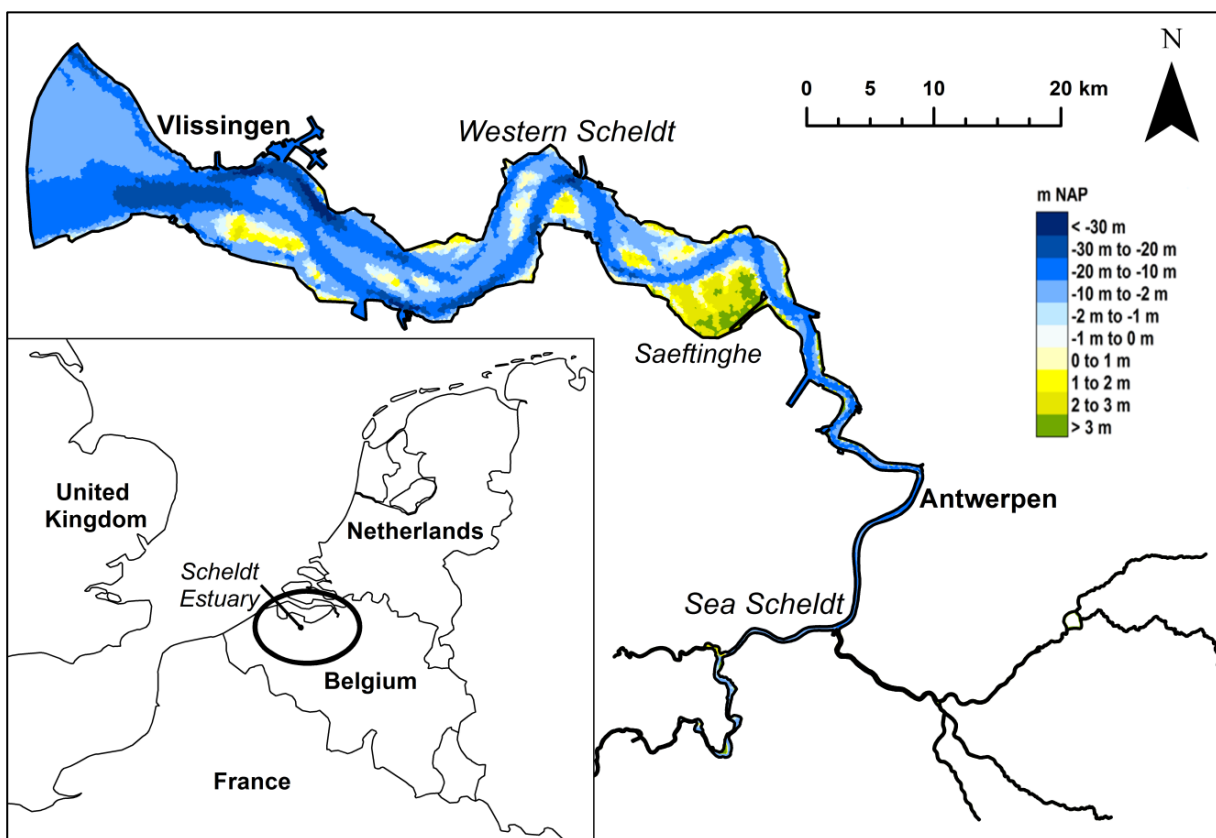


**Figure 1.4:** (a) Location of the Scheldt Estuary in Europe and (b) map of the Scheldt Estuary and its bathymetry.



Historically, large scale wetland reclamation over the last centuries reduced the estuary surface area by approximately 44% between 1650 and 1968. A large part of these intertidal wetlands first built up their elevation through natural sedimentation processes, before they were embanked and converted into agricultural land and human settlements (Van der Spek, 1997). Nowadays, only ~9000 ha of intertidal area remain. Despite the significant decrease in estuarine surface area (ca. 44% between 1650 and 1968), the tidal prism only decreased by less than 10%, leading to a significant increase in the maximum tidal range along the estuary (i.e., from 3.60 m in the 17<sup>th</sup> century to 5.35 m in the 1960s) as well as a faster propagation and increased penetration of the tidal wave into the estuary (Van der Spek, 1997).

Recently, several large scale marsh restoration projects have been put into practice along the Sea Scheldt as part of the so-called Sigma-plan ([www.sigmaplan.be/en](http://www.sigmaplan.be/en)), aiming at the reduction of flood risks and restoration of intertidal habitat along the Belgian part of the Scheldt estuary. Marsh restoration has been implemented along the Sea Scheldt by the creation of flood control areas (FCAs) adjacent to the estuarine channel. Examples are the Lippenbroek FCA (10 ha), Bergenmeersen FCA (40 ha) and the Kruikeke FCA (600 ha). In 2030, a total of 2500 ha of FCAs should be implemented along the Belgian part of the Scheldt estuary (Meire et al., 2014). Other planned de-embankments in the Scheldt Estuary include the Hedwige-Prosperpolder (465 ha) at the Dutch-Belgian border. Some of these new flood control areas (FCAs) are designed with specific inlet and outlet culvert systems to generate a so-called controlled reduced tide (CRT), which means that only limited tidal exchange between the FCA and the estuary channel is allowed to optimize both the coastal defense value as well as the ecological functioning (Cox et al., 2006). In particular, these FCAs with CRT may have a low elevation in the tidal frame and provide large storage volumes during storm surges, while still having normal tidal inundation characteristics to allow marsh development (Beauchard et al., 2013; Cox et al., 2006; Jacobs et al., 2009; Maris et al., 2007; Vandenbruwaene et al., 2012). The FCAs have already proven their coastal defense value by reducing high water levels during a severe storm surge in December 2013 (Meire et al., 2014; Smolders et al., 2015).

### ***1.5.2 The Saeftinghe marsh***

The largest intertidal area along the Scheldt Estuary is 'Het Verdrongen Land van Saeftinghe' or 'Drowned Land of Saeftinghe' (Figure 1.5). This 3000 ha marsh along the Western Scheldt is even the largest brackish tidal marsh in Europe (Dijkema et al., 1984). Nowadays, the marsh is surrounded by levees to the west and south and by the deep estuary channel in the north and the east. The Saeftinghe marsh used to be even larger but stepwise embankments since the former agricultural polder flooded in the 16th century up until around 1900 reduced the intertidal area to its current size (Jongepier et al., 2015). During the last century, the geomorphology of the marsh can be characterized by three main channels dissecting the tidal marsh: Speelmansgat in the west, Ijskelder in the middle and Hondegat in the east (see Figure 1.5). The Hondegat channel and adjacent marshes are of special interest in this study, as water level observations were conducted along this channel (**Chapter 2**). The geomorphology of the

Saeftinghe marsh can further be characterized by the presence of two low man-made dams, one of which is situated close to the dike on the south side of the marsh, while the other stretches along the east side of the marsh (Figure 1.5). Both dams are however intersected by intertidal channels.

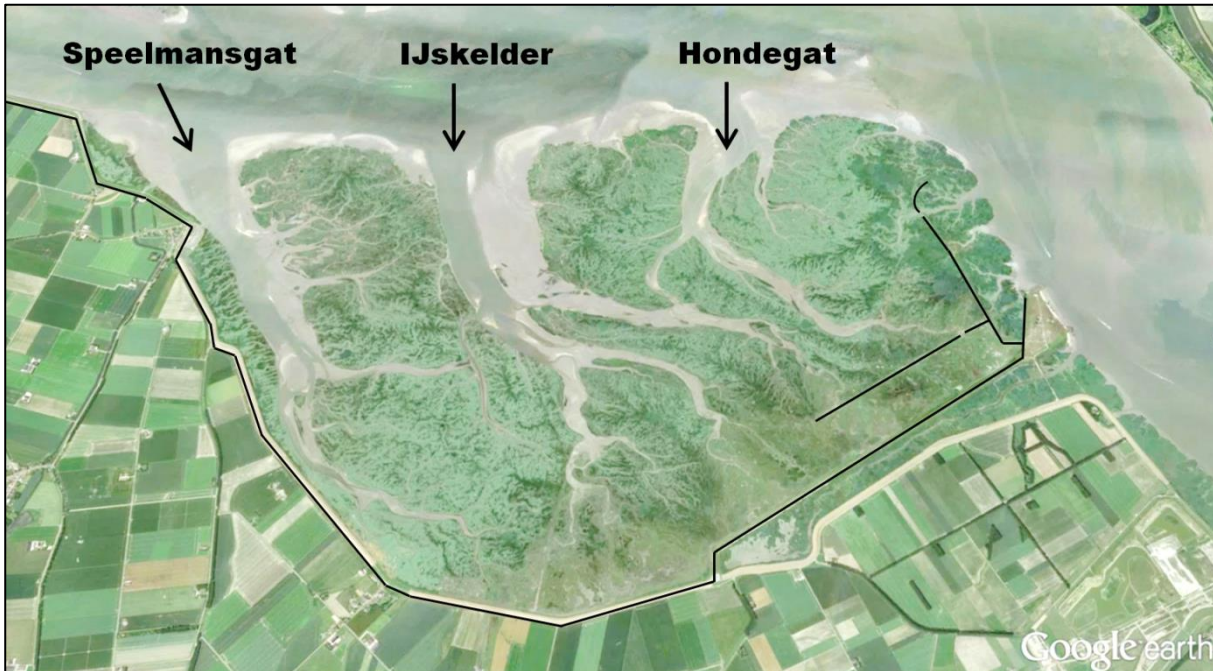


**Figure 1.5:** Aerial picture of the Saeftinghe marsh, obtained from Google Earth, with the surrounding dikes and man-made dams in the marsh indicated in black.

Historically, the vegetated part of the Saeftinghe marsh increased from 48% to 69% of the total area from 1931 to 2010, mainly due to a northward expansion of the marsh platform at the cost of bare tidal flats (Wang and Temmerman, 2013). Consequently, the marsh elevation (i.e., marsh platform, channels and tidal flats) increased by approximately 1.3 m. Nowadays, the marsh vegetation is dominated by *Elymus athericus* on higher elevated and well drained areas such as the natural levees along the tidal channel edges, and *Scirpus maritimus* in lower elevated poorly drained basins further away from channels and creeks, while other species occur in lower densities, including *Puccinellia maritima*, *Aster tripolium* and patches of *Phragmites australis* (Vandenbruwaene et al., 2015). The present-day hydrodynamic conditions at the Saeftinghe marsh consist of a semi-diurnal macrotidal regime which induces a tidal range between 4.0 and 5.6 m for neap and spring tides respectively. High water levels at the study area vary between 2.18 m and 3.15 m above NAP (NAP is the Dutch ordnance level, close to mean sea level) with a mean high water level of 2.76 m NAP, which is slightly below the mean platform elevation of the Saeftinghe marsh of 2.99 m NAP.

### 1.6 Hydrodynamic model

For the hydrodynamic modelling assessments in this thesis, a previously calibrated and validated TELEMAC-2D model of the Scheldt Estuary is adopted as it was available from

earlier studies (i.e. Smolders et al., 2015, 2012). TELEMAC-2D is a widely used process-based hydrodynamic modelling system and is part of the TELEMAC-MASCARET modelling suite. It solves the depth-averaged Saint-Venant equations or shallow water equations (i.e., Eq. 1.1 and 1.2) in two dimensions using the finite-element method and a computation mesh of triangular elements and contains the relevant physical processes with respect to tidal wave propagation in estuaries (Hervouet, 2007). TELEMAC-2D can deal with wetting and drying processes and hence can be used to simulate flow in intertidal systems such as tidal marshes and intertidal channels. In particular, TELEMAC-2D treats wetting and drying in a mass-conservative way by allowing slightly negative depths and smoothing (i.e. adjusting) water level gradients when nodes in the model domain fall dry (i.e., choosing 'Option 1' for the treatment of tidal flats in the model configuration). For more detailed information on the TELEMAC-2D model we refer to the TELEMAC-2D user manual (see: <http://wiki.opentelemac.org/>) and (Hervouet, 2007).

The adopted TELEMAC-2D model of the Scheldt Estuary comprises the tidally influenced part of the Scheldt Estuary from its mouth in the North Sea up until its upstream tributaries (as shown in Figure 1.4). The mesh size ranges from approximately 10-50 m in the most upstream tributaries up to about 150-200 m in the most downstream part of the estuary. Besides, the model is locally refined in some parts of the estuary to include specific bathymetric features in more detail (e.g. large training dams or confluences between the tributaries). Some of the upstream boundaries of the model are forced by discharges, while the downstream boundary is forced by water levels. Disadvantage of this model of the Scheldt Estuary is that it does not include the estuary's entire ebb tidal delta in the North Sea, potentially reducing the model's ability to simulate tidal flow patterns accurately in the most downstream part of the estuary. Nevertheless, model validation shows that the model is able to reproduce observed water level variations (Smolders et al., 2015) and stage-discharge curves (Smolders et al., 2012) in large parts of the estuary. The validation of this model is extended in this thesis by comparing modelled and observed peak water levels (**Chapter 3**) and by a tidal constituent analysis of modelled and observed water levels (**Appendix 5A**), both indicating that the model is able to reproduce (peak) water level variations in the Western Scheldt, including near the Saeftinghe marsh, up until Antwerp in the Sea Scheldt from which the model performance worsens further upstream.

In **Chapter 3** and **Chapter 4**, the Scheldt Estuary model is locally refined at the Saeftinghe marsh to a mesh size of 6-20 m to better represent the complex marsh geomorphology including its branching channel network. An advantage of using a finite element model is herein that the mesh size can easily be reduced at a local scale to implement parts of the marsh channel network with a higher resolution than the surrounding marsh platform. Although efforts are made to include the marsh channel network as good as possible by forcing the mesh on the channels, mesh element sizes of ~6 m or larger imply that some marsh channels are still very roughly schematized (i.e., channel cross-sections that are only represented by less than ~5-6 elements). This holds especially for the inner marsh area where channels are generally narrower. However,

further refinement of the model mesh would significantly increase computation times, which is also undesirable. The model performance on marsh scale is assessed by comparing observed and simulated (peak) water levels (**Chapter 3**) and flow velocities (**Chapter 4**) in the intertidal marsh channels. This model validation indicates that variations in peak water levels across the marsh and between different (storm) tides are captured and that tidally induced water level and velocity variations are fairly well represented in the marsh channels.

The overall performance of the Scheldt Estuary model, including the model performance of the refined Saeftinghe marsh model, can be considered well-suited for the specific applications in this thesis. That is, the model is able to simulate tidally induced water level variations, including the representation of peak water levels, along large parts of the estuary and along intertidal marsh channels. Moreover, discharge variations in the estuarine channels are also captured by the model. This allows for an assessment of large scale variations in (storm) tidal hydrodynamics in estuarine channels (**Chapter 5**) and in marsh channels (**Chapter 3** and **Chapter 4**).

### 1.7 References

- Allen, J.R.L., Rae, J.E., 1988. Vertical salt marsh accretion since the Roman period in the Severn Estuary, Southwest Britain. *Mar. Geol.* 83, 225–235.
- Aubrey, D.G., Speer, P.E., 1985. A Study of Non-linear Tidal Propagation in shallow inlet / estuarine systems Part I : Observations. *Estuar. Coast. Shelf Sci.* 21, 185–205.
- Barbier, E.B., Georgiou, I.Y., Enchelmeyer, B., Reed, D.J., 2013. The value of wetlands in protecting Southeast Louisiana from hurricane storm surges. *PLoS One* 8, e58715. doi:10.1371/journal.pone.0058715
- Beauchard, O., Jacobs, S., Ysebaert, T., Meire, P., 2013. Sediment macroinvertebrate community functioning in impacted and newly-created tidal freshwater habitats. *Estuar. Coast. Shelf Sci.* 120, 21–32. doi:10.1016/j.ecss.2013.01.013
- Blott, S.J., Pye, K., van der Wal, D., Neal, A., 2006. Long-term morphological change and its causes in the Mersey Estuary, NW England. *Geomorphology* 81, 185–206. doi:10.1016/j.geomorph.2006.04.008
- Bolle, A., Bing Wang, Z., Amos, C., De Ronde, J., 2010. The influence of changes in tidal asymmetry on residual sediment transport in the Western Scheldt. *Cont. Shelf Res.* 30, 871–882. doi:10.1016/j.csr.2010.03.001
- Bouma, T.J., van Belzen, J., Balke, T., Zhu, Z., Airoidi, L., Blight, A.J., Davies, A.J., Galvan, C., Hawkins, S.J., Hoggart, S.P.G., Lara, J.L., Losada, I.J., Maza, M., Ondiviela, B., Skov, M.W., Strain, E.M., Thompson, R.C., Yang, S., Zanuttigh, B., Zhang, L., Herman, P.M.J., 2014. Identifying knowledge gaps hampering application of intertidal habitats in coastal protection: Opportunities & steps to take. *Coast. Eng.* 87, 147–157. doi:10.1016/j.coastaleng.2013.11.014
- Christiansen, T., Wiberg, P.L., Milligan, T.G., 2000. Flow and Sediment Transport on a Tidal Salt Marsh Surface. *Estuar. Coast. Shelf Sci.* 50, 315–331. doi:10.1006/ecss.2000.0548
- Costanza, R., Arge, R., Groot, R. De, Farberk, S., Grasso, M., Hannon, B., Limburg, K., Naeem, S., O'Neill, R. V., Paruelo, J., Raskin, R.G., Suttonk, P., van den Belt, M., 1997. The value of the world ' s ecosystem services and natural capital. *Nature* 387, 253–260. doi:10.1038/387253a0
- Costanza, R., Pérez-Maqueo, O., Martinez, M.L., Sutton, P., Anderson, S.J., Mulder, K., 2008. The value of coastal wetlands for hurricane protection. *Ambio* 37, 241–248. doi:10.1579/0044-7447(2008)37[241:TVOCWF]2.0.CO;2
- Cox, T., Maris, T., De Vleeschauwer, P., De Mulder, T., Soetaert, K., Meire, P., 2006. Flood control areas as an opportunity to restore estuarine habitat. *Ecol. Eng.* 28, 55–63. doi:10.1016/j.ecoleng.2006.04.001

- D'Alpaos, A., Lanzoni, S., Marani, M., Rinaldo, A., 2009. On the O'Brien–Jarrett–Marchi law. *Rend. Lincei* 20, 225–236. doi:10.1007/s12210-009-0052-x
- D'Alpaos, A., Lanzoni, S., Mudd, S.M., Fagherazzi, S., 2006. Modeling the influence of hydroperiod and vegetation on the cross-sectional formation of tidal channels. *Estuar. Coast. Shelf Sci.* 69, 311–324. doi:10.1016/j.ecss.2006.05.002
- De Lima, P.H.S., Janzen, J.G., Nepf, H.M., 2015. Flow patterns around two neighboring patches of emergent vegetation and possible implications for deposition and vegetation growth. *Environ. Fluid Mech.* 881–898. doi:10.1007/s10652-015-9395-2
- De Vriend, H., Aarninkhof, S., van Koningsveld, M., 2014. “Building with nature”: the new Dutch approach to coastal and river works. *Proc. ICE - Civ. Eng.* 167, 18–24. doi:10.1680/cien.13.00003
- Dijkema, K.S., Beeftink, W.G., Doody, J.P., Gehu, J.M., Heydemann, B., Rivas Martinez, M., 1984. Salt marshes in Europe, Salt marshes in Europe. European committee for the conservation of nature and natural resources, Strasbourg.
- Dronkers, J., 1986. Tidal asymmetry and estuarine morphology. *Netherlands J. Sea Res.* 20, 117–131. doi:10.1016/0077-7579(86)90036-0
- Engelund, F., Hansen, E., 1967. A monograph on sediment transport in alluvial streams. Copenhagen. doi:10.1017/CBO9781107415324.004
- Fagherazzi, S., Hannion, M., D'Odorico, P., 2008. Geomorphic structure of tidal hydrodynamics in salt marsh creeks. *Water Resour. Res.* 44, 1–12. doi:10.1029/2007WR006289
- Fagherazzi, S., Wiberg, P.L., Temmerman, S., Struyf, E., Zhao, Y., Raymond, P.A., 2013. Fluxes of water, sediments, and biogeochemical compounds in salt marshes. *Ecol. Process.* 2, 3. doi:10.1186/2192-1709-2-3
- Fortunato, A.B., Oliveira, A., 2005. Influence of Intertidal Flats on Tidal Asymmetry. *J. Coast. Res.* 21, 1062–1067. doi:10.2112/03-0089.1
- Friedrichs, C.T., Aubrey, D.G., 1988. Non-linear Tidal Distortion in Shallow Well-Mixed Estuaries: a Synthesis. *Estuar. Coast. Shelf Sci.* 27, 521–545. doi:10.1016/0272-7714(90)90054-U
- Friedrichs, C.T., Madsen, O.S., 1992. Nonlinear diffusion of the tidal signal in frictionally dominated embayments. *J. Geophys. Res.* 97, 5637–5650. doi:10.1029/92JC00354
- Friedrichs, C.T., Perry, J.E., 2001. Tidal salt marsh morphodynamics: A Synthesis. *J. Coast. Res.* 27, 7–37.
- Gedan, K.B., Kirwan, M.L., Wolanski, E., Barbier, E.B., Silliman, B.R., 2010. The present and future role of coastal wetland vegetation in protecting shorelines: Answering recent challenges to the paradigm. *Clim. Change* 106, 7–29. doi:10.1007/s10584-010-0003-7
- Hervouet, J.-M., 2007. Hydrodynamics of Free Surface Flows: Modelling with the finite element method. doi:10.1002/9780470319628
- Hu, K., Chen, Q., Wang, H., 2015. A numerical study of vegetation impact on reducing storm surge by wetlands in a semi-enclosed estuary. *Coast. Eng.* 95, 66–76. doi:10.1016/j.coastaleng.2014.09.008
- Jacobs, S., Beauchard, O., Struyf, E., Cox, T., Maris, T., Meire, P., 2009. Restoration of tidal freshwater vegetation using controlled reduced tide (CRT) along the Schelde Estuary (Belgium). *Estuar. Coast. Shelf Sci.* 85, 368–376. doi:10.1016/j.ecss.2009.09.004
- Jarrett, J.T., 1976. Tidal Prism - Inlet Area Relationships. Vicksburg, MS, U.S.
- Jeuken, C., Wang, Z.B., van der Kaaij, T., Van Helvert, M., Van Ormondt, M., Bruinsma, R., Tanczos, I., 2004. Morfologische ontwikkelingen in het Schelde estuarium bij voortzetting van het huidige beleid en effecten van een verdere verdieping van de vaargeul en uitpoldering langs de Westerschelde. Deelovereenkomst 2 en 3. Morfologie.
- Jeuken, M.C.J.L., Wang, Z.B., 2010. Impact of dredging and dumping on the stability of ebb-flood channel systems. *Coast. Eng.* 57, 553–566. doi:10.1016/j.coastaleng.2009.12.004
- Jongepier, I., Wang, C., Missiaen, T., Soens, T., Temmerman, S., 2015. Intertidal landscape response time to dike breaching and stepwise re-embankment: A combined historical and geomorphological study. *Geomorphology* 236, 64–78. doi:10.1016/j.geomorph.2015.02.012
- Kirwan, M.L., Megonigal, J.P., 2013. Tidal wetland stability in the face of human impacts and sea-level rise. *Nature* 504, 53–60. doi:10.1038/nature12856
- Kirwan, M.L., Murray, a B., 2007. A coupled geomorphic and ecological model of tidal marsh evolution. *Proc. Natl. Acad. Sci. U. S. A.* 104, 6118–6122. doi:10.1073/pnas.0700958104
- Kirwan, M.L., Temmerman, S., Skeeahan, E.E., Guntenspergen, G.R., Fagherazzi, S., 2016. Overestimation of marsh vulnerability to sea level rise. *Nat. Clim. Chang.* 6, 253–260. doi:10.1038/nclimate2909
- Krauss, K.W., Doyle, T.W., Doyle, T.J., Swarzenski, C.M., From, A.S., Day, R.H., Conner, W.H., 2009. Water level observations in mangrove swamps during two hurricanes in Florida. *Wetlands* 29, 142–149. doi:10.1672/07-232.1

- Lanzoni, S., Seminara, G., 2002. Long-term evolution and morphodynamic equilibrium of tidal channels. *J. Geophys. Res.* 107, --. doi:10.1029/2000JC000468
- Loder, N.M., Irish, J.L., Cialone, M.A., Wamsley, T.V., 2009. Sensitivity of hurricane surge to morphological parameters of coastal wetlands. *Estuar. Coast. Shelf Sci.* 84, 625–636. doi:10.1016/j.ecss.2009.07.036
- Ma, Z., Melville, D.S., Liu, J., Chen, Y., Yang, H., Ren, W., Zhang, Z., Piersma, T., Li, B., 2014. Rethinking China's new great wall. *Science (80-. )*. 346, 912–914. doi:10.1126/science.1257258
- Maris, T., Cox, T., Temmerman, S., De Vleeschauwer, P., Van Damme, S., De Mulder, T., Van Den Bergh, E., Meire, P., 2007. Tuning the tide: Creating ecological conditions for tidal marsh development in a flood control area. *Hydrobiologia* 588, 31–43. doi:10.1007/s10750-007-0650-5
- McGee, B.B.D., Goree, B.B., Tollett, R.W., Woodward, B.K., Kress, W.H., 2006. Hurricane Rita Surge Data, Southwestern Louisiana and Southeastern Texas, September to November 2005. U.S. Geological Survey Data Series 220.
- McIvor, A., Spencer, T., Möller, I., Spalding, M., 2012. Storm surge reduction by mangroves. *Natural Coastal Protection Series: Report 2*, Cambridge Coastal Research Unit Working Paper 41.
- McLeod, E., Chmura, G.L., Bouillon, S., Salm, R., Björk, M., Duarte, C.M., Lovelock, C.E., Schlesinger, W.H., Silliman, B.R., 2011. A blueprint for blue carbon: Toward an improved understanding of the role of vegetated coastal habitats in sequestering CO<sub>2</sub>. *Front. Ecol. Environ.* 9, 552–560. doi:10.1890/110004
- Meire, P., Dauwe, W., Maris, T., Peeters, P., Deschamps, M., Rutten, J., Temmerman, S., Ministry, F., Albert, K., 2014. The recent “Saint Nicholas” storm surge in the Scheldt estuary: the Sigma plan proves its efficiency. *ECSA Bull.* 62, 19–23.
- Meire, P., Ysebaert, T., Van Damme, S., Van Den Bergh, E., Maris, T., Struyf, E., 2005. The Scheldt estuary: A description of a changing ecosystem. *Hydrobiologia* 540, 1–11. doi:10.1007/s10750-005-0896-8
- Mitchell, S.B., 2013. Turbidity maxima in four macrotidal estuaries. *Ocean Coast. Manag.* 79, 62–69. doi:10.1016/j.ocecoaman.2012.05.030
- Mitsch, W.J., Bernal, B., Nahlik, A.M., Mander, Ü., Zhang, L., Anderson, C.J., Jørgensen, S.E., Brix, H., 2013. Wetlands, carbon, and climate change. *Landsc. Ecol.* 28, 583–597. doi:10.1007/s10980-012-9758-8
- Mitsch, W.J., Zhang, L., Stefanik, K.C., Nahlik, A.M., Anderson, C.J., Bernal, B., Hernandez, M., Song, K., 2012. Creating Wetlands: Primary Succession, Water Quality Changes, and Self-Design over 15 Years. *Bioscience* 62, 237–250. doi:10.1525/bio.2012.62.3.5
- Möller, I., Kudella, M., Rupprecht, F., Spencer, T., Paul, M., van Wesenbeeck, B.K., Wolters, G., Jensen, K., Bouma, T.J., Miranda-Lange, M., Schimmels, S., 2014. Wave attenuation over coastal salt marshes under storm surge conditions. *Nat. Geosci.* 7, 727–731. doi:10.1038/ngeo2251
- Möller, I., Spencer, T., French, Leggett, D., Dixon, M., 1999. Wave transformation over salt marshes: A field and numerical modelling study from north Norfolk, England. *Estuar. Coast. Mar. Sci.* 49, 411–426. doi:10.1006/ecss.1999.0509
- Moore, R.D., Wolf, J., Souza, A.J., Flint, S.S., 2009. Morphological evolution of the Dee Estuary, Eastern Irish Sea, UK: A tidal asymmetry approach. *Geomorphology* 103, 588–596. doi:10.1016/j.geomorph.2008.08.003
- Mudd, S.M., D'Alpaos, A., Morris, J.T., 2010. How does vegetation affect sedimentation on tidal marshes? Investigating particle capture and hydrodynamic controls on biologically mediated sedimentation. *J. Geophys. Res.* 115, F03029. doi:10.1029/2009JF001566
- Naik, P.K., Jay, D.A., 2011. Distinguishing human and climate influences on the Columbia River: Changes in mean flow and sediment transport. *J. Hydrol.* 404, 259–277. doi:10.1016/j.jhydrol.2011.04.035
- O'Brien, M.P., 1969. Equilibrium flow areas of tidal inlets on sandy coasts, in: *Proceedings of the American Society of Civil Engineers. Journal of the Waterways and Harbors Division.* pp. 43–52-. doi:10.9753/icce.v10.25p
- O'Brien, M.P., 1931. Estuary and tidal prisms related to entrance areas. *Civ. Eng.* 1, 738–739.
- Ouyang, X., Lee, S.Y., 2014. Updated estimates of carbon accumulation rates in coastal marsh sediments. *Biogeosciences Discuss.* 11, 5057–5071. doi:10.5194/bgd-10-19155-2013
- Parker, B.B., 1984. Frictional effects on the tidal dynamics of a shallow estuary, Ph.D. thesis. John Hopkins University, Baltimore, Md., U.S.A.
- Pendleton, L., Donato, D.C., Murray, B.C., Crooks, S., Jenkins, W.A., Sifleet, S., Craft, C., Fourqurean, J.W., Kauffman, J.B., Marb??, N., Megonigal, P., Pidgeon, E., Herr, D., Gordon, D., Baldera, A., 2012. Estimating Global “Blue Carbon” Emissions from Conversion and Degradation of Vegetated Coastal Ecosystems. *PLoS One* 7. doi:10.1371/journal.pone.0043542

- Pritchard, D.W., 1967. What is an estuary: physical viewpoint, in: Lauff, G.H. (Ed.), *Estuaries*. American Association for the Advancement of Science, Washington, DC, pp. 3–5.
- Rego, J.L., Li, C., 2009. On the importance of the forward speed of hurricanes in storm surge forecasting: A numerical study. *Geophys. Res. Lett.* 36. doi:10.1029/2008GL036953
- Resio, D.T., Westerink, J.J., 2008. Modeling the physics of storm surges. *Phys. Today* 61, 33–38. doi:10.1063/1.2982120
- Rinaldo, A., Fagherazzi, S., Lanzoni, S., Marani, M., Dietrich, W.E., 1999. Tidal networks: 3. Landscape-forming discharges and studies in empirical geomorphic relationships. *Water Resour. Res.* 35, 3919–3929.
- Sheng, Y.P., Lapetina, A., Ma, G., 2012. The reduction of storm surge by vegetation canopies: Three-dimensional simulations. *Geophys. Res. Lett.* 39, 1–5. doi:10.1029/2012GL053577
- Shepard, C.C., Crain, C.M., Beck, M.W., 2011. The protective role of coastal marshes: a systematic review and meta-analysis. *PLoS One* 6, e27374. doi:10.1371/journal.pone.0027374
- Sherwood, C.R., Jay, D.A., Harvey, R.B., Hamilton, P., Simenstad, C.A., 1990. Historical changes in the Columbia River Estuary. *Prog. Oceanogr.* 25, 299–352. doi:10.1016/0079-6611(90)90011-P
- Small, C., Nicholls, R.J., 2003. A Global Analysis of Human Settlement in Coastal Zones. *J. Coast. Res.* 19, 584–599.
- Smolders, S., Ides, S., Plancke, Y., Meire, P., Temmerman, S., 2012. Calibrating Discharges in a 2D Hydrodynamic Model of the Scheldt Estuary : Which Parameters Can Be Used and What Is Their Sensitivity ?, in: *Proceedings of 10th International Conference on Hydroinformatics, HIC 2012*, Hamburg, Germany. p. 8.
- Smolders, S., Plancke, Y., Ides, S., Meire, P., Temmerman, S., 2015. Role of intertidal wetlands for tidal and storm tide attenuation along a confined estuary: A model study. *Nat. Hazards Earth Syst. Sci.* 15, 1659–1675. doi:10.5194/nhess-15-1659-2015
- Speer, P.E., Aubrey, D.G., 1985. A study of non-linear tidal propagation in shallow inlet/estuarine systems Part II: Theory. *Estuar. Coast. Shelf Sci.* 21, 207–224. doi:10.1016/0272-7714(85)90097-6
- Stive, M.J.F., Ji, L., Brouwer, R.L., van de Kreeke, J., Ranasinghe, R., 2010. Empirical relationship between inlet cross-sectional area and tidal prism: a re-evaluation, in: *Coastal Engineering Proceedings*. pp. 1–10.
- Swinkels, C.M., Jeuken, C.M.C.J.L., Wang, Z.B., Nicholls, R.J., 2009. Presence of connecting channels in the Western Scheldt Estuary. *J. Coast. Res.* 627–640. doi:10.2112/06-0719.1
- Temmerman, S., Bouma, T.J., Van de Koppel, J., Van der Wal, D., De Vries, M.B., Herman, P.M.J., 2007. Vegetation causes channel erosion in a tidal landscape. *Geology* 35, 631. doi:10.1130/G23502A.1
- Temmerman, S., De Vries, M.B., Bouma, T.J., 2012. Coastal marsh die-off and reduced attenuation of coastal floods: A model analysis. *Glob. Planet. Change* 92–93, 267–274. doi:10.1016/j.gloplacha.2012.06.001
- Temmerman, S., Govers, G., Wartel, S., Meire, P., 2004. Modelling estuarine variations in tidal marsh sedimentation: Response to changing sea level and suspended sediment concentrations. *Mar. Geol.* 212, 1–19. doi:10.1016/j.margeo.2004.10.021
- Temmerman, S., Kirwan, M.L., 2015. Building land with a rising sea. *Science (80-. )*. 349, 588–589. doi:10.1126/science.aac8312
- Temmerman, S., Meire, P., Bouma, T.J., Herman, P.M.J., Ysebaert, T., De Vriend, H.J., 2013. Ecosystem-based coastal defence in the face of global change. *Nature* 504, 79–83. doi:10.1038/nature12859
- Van de Kreeke, J., Robaczewska, K., 1993. Tide-induced residual transport of coarse sediment; Application to the EMS estuary. *Netherlands J. Sea Res.* 31, 209–220. doi:10.1016/0077-7579(93)90022-K
- Van der Spek, A.J.F., 1997. Tidal asymmetry and long-term evolution of Holocene tidal basins in the Netherlands: Simulation of palaeo-tides in the Schelde estuary. *Mar. Geol.* 141, 71–90. doi:10.1016/S0025-3227(97)00064-9
- Van Rijn, L.C., 2011. Analytical and numerical analysis of tides and salinities in estuaries; part I: tidal wave propagation in convergent estuaries. *Ocean Dyn.* 61, 1719–1741. doi:10.1007/s10236-011-0453-0
- Van Rijn, L.C., 1993. *Principles of Sediment Transport in Rivers, Estuaries and Coastal Seas*. Aqua Publications, Amsterdam.
- Vandenbruwaene, W., Meire, P., Temmerman, S., 2012. Formation and evolution of a tidal channel network within a constructed tidal marsh. *Geomorphology* 151–152, 114–125. doi:10.1016/j.geomorph.2012.01.022
- Vandenbruwaene, W., Schwarz, C., Bouma, T.J., Meire, P., Temmerman, S., 2015. Landscape-scale flow patterns over a vegetated tidal marsh and an unvegetated tidal flat: implications for the landform properties of the intertidal floodplain. *Geomorphology* 231, 40–52. doi:10.1016/j.geomorph.2014.11.020

- Wamsley, T. V., Cialone, M. a., Smith, J.M., Atkinson, J.H., Rosati, J.D., 2010. The potential of wetlands in reducing storm surge. *Ocean Eng.* 37, 59–68. doi:10.1016/j.oceaneng.2009.07.018
- Wang, C., Temmerman, S., 2013. Does biogeomorphic feedback lead to abrupt shifts between alternative landscape states?: An empirical study on intertidal flats and marshes. *J. Geophys. Res.* 118, 229–240. doi:10.1029/2012JF002474
- Wang, Z., Jeuken, C., De Vriend, H., 1999. Tidal asymmetry and residual sediment transport in estuaries. A literature study and applications to the Western Scheldt, Z2749.
- Wang, Z.B., Jeuken, M.C.J.L., Gerritsen, H., De Vriend, H.J., Kornman, B.A., 2002. Morphology and asymmetry of the vertical tide in the Westerschelde estuary. *Cont. Shelf Res.* 22, 2599–2609. doi:10.1016/S0278-4343(02)00134-6
- Weisberg, R., Zheng, L., 2006. Hurricane Storm Surge Simulations for Tampa Bay. *Estuaries and Coasts* 29, 899–913. doi:10.1007/BF02798649
- Winterwerp, J.C., Wang, Z.B., 2013. Man-induced regime shifts in small estuaries - I: Theory. *Ocean Dyn.* 63, 1279–1292. doi:10.1007/s10236-013-0662-9
- Yang, S.L., Li, M., Dai, S.B., Liu, Z., Zhang, J., Ding, P.X., 2006. Drastic decrease in sediment supply from the Yangtze River and its challenge to coastal wetland management. *Geophys. Res. Lett.* 33, 4–7. doi:10.1029/2005GL025507
- Zhang, K., Liu, H., Li, Y., Xu, H., Shen, J., Rhome, J., Smith, T.J., 2012. The role of mangroves in attenuating storm surges. *Estuar. Coast. Shelf Sci.* 102-103, 11–23. doi:10.1016/j.ecss.2012.02.021



# Chapter 2

## Observations of tidal propagation and storm surge attenuation in a large tidal marsh

J. Stark, T. van Oyen, P. Meire and S. Temmerman

Based on the paper published in *Limnology and Oceanography* (2015), 60: 1371–1381. doi: 10.1002/lno.10104



*Drawing of the flooding of Saeftinghe during the All Saints' flood in 1570 by Hans Moser*

### **Abstract**

*Tidal wetlands are increasingly valued for their role in coastal defense. Nevertheless, in-situ observations of storm surge attenuation within wetlands are still scarce. We present water level measurements along a 4 km intertidal channel and on the surrounding marsh platform for regular spring to neap tides and two major storm surge tides, showing the effects of flood wave height and marsh geomorphology on the amount of flood wave attenuation. Undermarsh tides with peak water levels below marsh platform elevation are mostly amplified (up to 4 cm/km) within the channels. Overmarsh tides with peak water levels above the marsh platform are generally attenuated along the channels, with maximum attenuation rates of 5 cm/km for tides that inundate the marsh platform by 0.5-1.0 m. For lower or higher flood waves, including storm surges, attenuation rates decrease. Furthermore, the observations show that the maximum attenuation occurs along narrow channel transects where the width of the platform is larger, whereas attenuation rates are lower along wider channels with smaller adjacent marsh platforms. These observations are confirmed by an analytical approximation of tidal wave propagation through convergent channels. The analytical model indicates that differences in attenuation rates are induced by variations in the cross-channel averaged friction between channel sections and between tides with varying peak water levels. Finally, the highest attenuation rates of up to 7 cm over less than 100 m are observed over short distances on the vegetated marsh platform. We conclude that this study provides an empirical basis for the wider implementation of nature-based flood defense strategies.*

## 2.1 Introduction

Low-lying coastal areas are vulnerable to flood hazards caused by storm surges. Global change is expected to increase the risks of flood disasters due to accelerating sea level rise, increasing storm intensity, and growing coastal populations (e.g., Nicholls and Cazenave 2010; Woodruff et al. 2013). As a consequence there is a worldwide growing need for long-term sustainable adaptation to storm surge flood risks, in particular for low-lying deltas and estuaries. Tidal wetlands, including salt marshes and mangroves, are increasingly recognized for their potential value as natural protective barriers (Temmerman et al., 2013; Wamsley et al., 2009). They can reduce the height of wind waves (Möller et al., 2014) and storm surges through additional vegetation roughness and thereby reduce the associated damage during extreme flood events (Barbier et al., 2013; Costanza et al., 2008; Shepard et al., 2011). Tidal wetlands are nowadays starting to be implemented as naturally sustainable coastal defense systems (Temmerman et al., 2013), which calls for a better understanding of flood level reduction by marshes.

In-situ observations of peak water level reduction in coastal wetlands are scarce. Most of the existing field studies considered storm surge attenuation for only one or a few specific hurricane-induced surge events and reported a wide range of attenuation rates, from about 4 to 25 cm of peak water level reduction per kilometer of wetland (Krauss et al., 2009; Lovelace, 1994; McGee et al., 2006; Wamsley et al., 2010). An overview of attenuation rates in coastal marshes and mangroves found in previous field studies is shown in Table 2.1. The large variety in observed storm surge attenuation rates suggests that the attenuation capacity largely depends on the properties of the specific wetland location and specific storm event. Unfortunately, data on the geometrical properties of the marshes and mangroves for which storm surge attenuation rates were reported earlier (Table 2.1) are not always available. Therefore, the effect of wetland geometry on storm surge attenuation can not readily be assessed based on these field observations. Nevertheless, numerical modelling studies have indeed shown that storm surge reduction within coastal marshes varies with site-specific variables, such as offshore bathymetry (Resio and Westerink, 2008), marsh geomorphology, including marsh vegetation cover and local surface roughness (e.g., Loder et al. 2009; Zhang et al. 2012; Temmerman et al. 2012), and with the presence of man-made levees (e.g., Wamsley et al. 2010). These studies have also shown that storm surge reduction may vary with event-specific variables, such as storm surge height, storm track and duration (e.g., Resio and Westerink 2008; Loder et al. 2009; Wamsley et al. 2010). Moreover, modelling studies indicate that larger surge events with higher marsh platform inundation depths are less effectively attenuated than smaller surge events with lower marsh inundation depths and shorter durations (Loder et al., 2009). However, systematic water level observations of events with varying marsh inundation depths, ranging from low tidal inundations to extreme storm surges, are lacking. Even field studies on the attenuation of regular tides in marshes are very scarce. To our knowledge, the only available field study on attenuation of regular tides in a large tidal marsh was conducted by Van der Molen (1997), who focused mainly on spatial differences in mean high water level (HWL) in a

tidal marsh along the U.S. Atlantic coast, showing a reduction of mean high water levels of up to 11 cm/km. Field studies that assess the impact of different marsh inundation depths on tidal and storm surge propagation through marshes are to our knowledge not yet available.

**Table 2.1:** Observed attenuation rates in wetlands from previous field studies.

Location	Description	Attenuation rate (cm/km)	Reference
Louisiana	<i>Hurricane Andrew (1992) surge reduction over 37 km of marsh and open water</i>	4.4 – 4.9	Lovelace (1994), Wamsley et al. (2010)
Great Marshes, Massachusetts	<i>Mean high water level variation across tidal flats and marsh channels with a depth between 0.6 m and 1.8 m relative to mean high water level.</i>	-2.0* – 11.0	Calculated from figures in Van der Molen (1997)
Ten Thousand Islands National Wildlife Refuge, Florida	<i>Hurricane Charley (2004) surge reduction across up to 5.5 km of marshes and mangroves with a maximum inundation depth of 0.1-0.4 m above marsh platform elevation and 0.4-0.8 m in the mangrove area.</i>	9.4 – 15.8	Krauss et al. (2009)
Shark River (Everglades), Florida	<i>Hurricane Wilma (2005) surge reduction over 14 km of riverine mangroves with a maximum inundation depth of 0.5-1.0 m.</i>	4.0 – 6.9	Krauss et al. (2009)
Cameron Prairie, Louisiana	<i>Hurricane Rita (2005) surge reduction in marsh area</i>	10.0	McGee et al. (2006), Wamsley et al. (2010)
Sabine, Louisiana	<i>Hurricane Rita (2005) surge reduction in marsh area</i>	25.0	McGee et al. (2006), Wamsley et al. (2010)
Vermillion, Louisiana	<i>Hurricane Rita (2005) surge reduction in marsh area</i>	4.0	McGee et al. (2006), Wamsley et al. (2010)
Vermillion, Louisiana	<i>Hurricane Rita (2005) surge reduction in marsh area</i>	7.7	McGee et al. (2006), Wamsley et al. (2010)

\*Negative values denote that amplification was observed.

Here, we present a coherent set of field observations on peak water level variations within a large tidal marsh, covering a wide range of marsh inundation depths including neap to spring tides and two storm surges. These observations lead to new insights which are discussed in the discussion section and can be relevant to other locations around the world where marshes or mangroves have the potential to reduce flood risks (e.g. Table 2.1). In addition, in the discussion section, we demonstrate that our findings are consistent with the results of a simplified one-dimensional (1D) analytical model for tidal wave propagation in converging channels which is based on the wave energy flux balance (Van Rijn, 2011). Finally, as large scale in-situ water level observations in tidal marshes are scarce, the data presented in this study provides a valuable dataset to validate numerical modelling studies describing the propagation of tidal waves and storm surges in coastal wetlands.

## 2.2 Methods

Field measurements were conducted in the Saeftinghe marsh, a more than 3000 ha brackish tidal marsh along the Western Scheldt estuary (SW Netherlands; 51.3671°N, 4.1760°E). The local tidal regime is semi-diurnal with high water levels varying between 2.18 m and 3.15 m NAP (NAP is the Dutch ordnance level, close to mean sea level) and a tidal range between 4.02 m and 5.57 m for neap and spring tides respectively. Approximately 70% of Saeftinghe is occupied with marsh vegetation. The marsh vegetation is dominated by *Elymus athericus* and *Scirpus maritimus*, while other species occur in lower densities, including *Puccinellia maritima*, *Aster tripolium* and patches of *Phragmites australis*. The mean canopy height of *E. athericus*, the most abundant species in our study area, is 0.43 m with a standard deviation of 0.1 m (Vandenbruwaene et al., 2015). The remaining 30% of the marsh consists of bare tidal flats and an extensive intertidal channel system (i.e., channels which are dry during low tides).

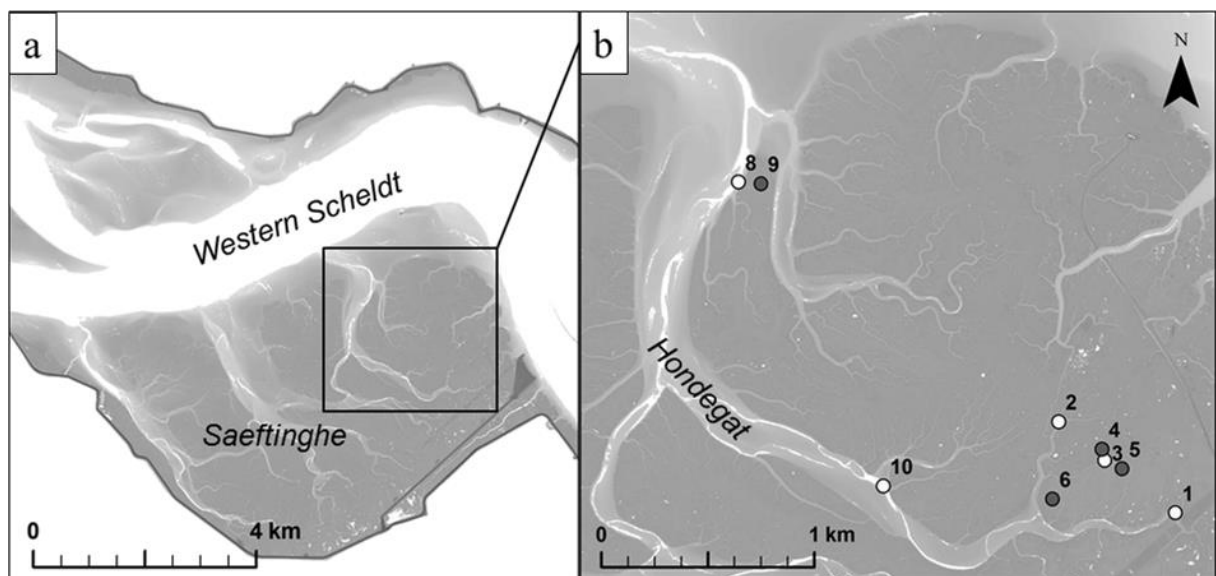


**Figure 2.1:** Study area in the Western Scheldt estuary: (a) Saeftinghe marsh and (b) the Hondegat channel with locations of water level measurements in the marsh channels (light dots) and on the marsh platform (dark dots).

Water level measurements were done in and along the 4 km long Hondegat channel which is over 500 m wide near the main estuarine channel and branches in the landward direction into an extensive network of smaller creeks (Figure 2.1 & Figure 2.2). The marsh platform elevation surrounding this channel varies between 2.89 and 3.45 m NAP, calculated as the 10% and 90% percentiles from a Lidar based digital elevation model. Water levels were measured during two periods of approximately one month (28 August 2013 – 6 October 2013 and 5 December 2013 – 31 December 2013) at several locations in the channel and on the marsh platform. Figure 2.3 shows typical observations at the various locations (see Figure 2.1) of the water level variation for different conditions; i.e., for undermarsh tides (Figure 2.3a), overmarsh tides (Figure 2.3b) and storm tide (Figure 2.3c). The second measurement series includes a severe storm surge that coincided with spring tide and caused two storm tides. The highest storm tide induced peak water levels at several tidal stations in the Western Scheldt

estuary which correspond to a  $1/8 - 1/20 \text{ y}^{-1}$  exceedance probability (water level exceedance probabilities for tidal stations are obtained from Rijkswaterstaat, <http://www.rijkswaterstaat.nl>). In particular, HWLs at the estuary mouth and at tidal stations near the study area were approximately 1.50 m above the astronomical tide during the highest storm tide. While the storm surge was forced by strong northwestern winds on the North Sea, local wind conditions in the study area were less strong at the time HWLs arrived at the entrance of the marsh. In particular, observations from weather stations near the study area indicated hourly averaged wind speeds of 8 to 11 m/s from a west- to northwest direction during the storm tide's high water slack, while maximum wind speeds of 21 to 24 m/s were measured in the Dutch part of the North Sea (wind data obtained from Royal Netherlands Meteorological Institute, <http://www.knmi.nl>). Local wind conditions were milder because the study area is located approximately 60 km inland from the estuary mouth in the North Sea and wind speeds were generally lower there. Secondly, the peak water levels only reached the study area several hours after the peak of the storm.



**Figure 2.2:** Water level loggers installed on the marsh platform (left) and in the marsh channel (right).

The configuration of the measurement locations during the first measurement period consists of one location in the main channel at the marsh edge (location 8), one location in the main channel at the backside of the marsh (location 1), two locations in smaller side-channels at the backside of the marsh (locations 2 and 3) and four locations on the marsh platform (locations 4-6 and 9). During the second campaign measurement devices were only deployed at locations 1, 3, 5 and 8, while location 10 was added halfway the main channel between locations 1 and 8. Locations 1-3 are all situated at approximately similar distances from the marsh edge, measured along the channel

system. However, the channels towards these locations vary in width, depth and cross-sectional area (Table 2.2). Location 1 is situated in the relatively wide main channel, whereas locations 2 and 3 are situated in narrower side-channels with smaller cross-sectional areas. In general, there is a gradual convergence in channel width from  $\sim 500$  m to  $\sim 30$  m between locations 8, 10 and 1, whereas the decrease in channel width towards location 2 and especially location 3 is more abrupt at the entrance of the side-channels. The configuration of measurement locations allows for a comparison of the tidal wave at the marsh edge (location 8) with tides and peak water levels at a variety of sites that are located approximately 4 km from the marsh edge, providing insight into the propagation and attenuation of tides and storm surges in the marsh.

**Table 2.2.** Geometrical properties of channel cross-sections at the measurement locations in the marsh channel system, showing channel width ( $w$ ), mean channel depth below MHWL ( $h_{\text{mean}}$ ), maximum channel depth below MHWL ( $h_{\text{max}}$ ) and cross-sectional area ( $A_c$ ).

Location		Lat. (°)	Lon. (°)	$w$ (m)	$h_{\text{mean}}$ (m)	$h_{\text{max}}$ (m)	$A_c$ (m <sup>2</sup> )
Location 8	<i>marsh edge</i>	51.3695	4.1795	517	2.1	3.9	1105
Location 10	<i>main channel</i>	51.3565	4.1897	167	1.2	2.2	206
Location 1	<i>main channel</i>	51.3559	4.2092	30	0.4	1.1	12
Location 2	<i>side-channel</i>	51.3596	4.2012	8	0.8	1.1	6
Location 3	<i>side-channel</i>	51.3581	4.2044	4	0.5	0.7	2

Water level loggers (Schlumberger, Mini-divers and CERA-divers) were used for the field observations (Figure 2.2). This equipment contains a pressure sensor that measures the water surface level with an accuracy of  $\pm 1$  cm. A BARO-diver, which records the atmospheric pressure, was installed nearby the study area to compensate the water level measurements for the atmospheric pressure (accuracy  $\pm 0.5$  cm). The measurement frequency was set to 2 minutes in order to record the flood propagation accurately. Horizontal coordinates and vertical elevations of the measurement points were determined with RTK-GPS (Trimble 5800), with a maximum vertical measurement error of  $\pm 1$  cm during the first campaign and  $\pm 2$  cm during the second campaign. The combined vertical precision of the water level measurements then becomes  $\pm 1.5$  cm and  $\pm 2.3$  cm for the first and second campaign respectively. In this perspective, it should be stated that when attenuation rates between two measurement points are calculated, the part of the error caused by the BARO-diver affects both measurements and should only be included once. Besides, the part of the vertical error caused by the RTK-GPS measurements remained constant during the measurement period and hence variations in attenuation or amplification between different tides are obtained with a higher accuracy.

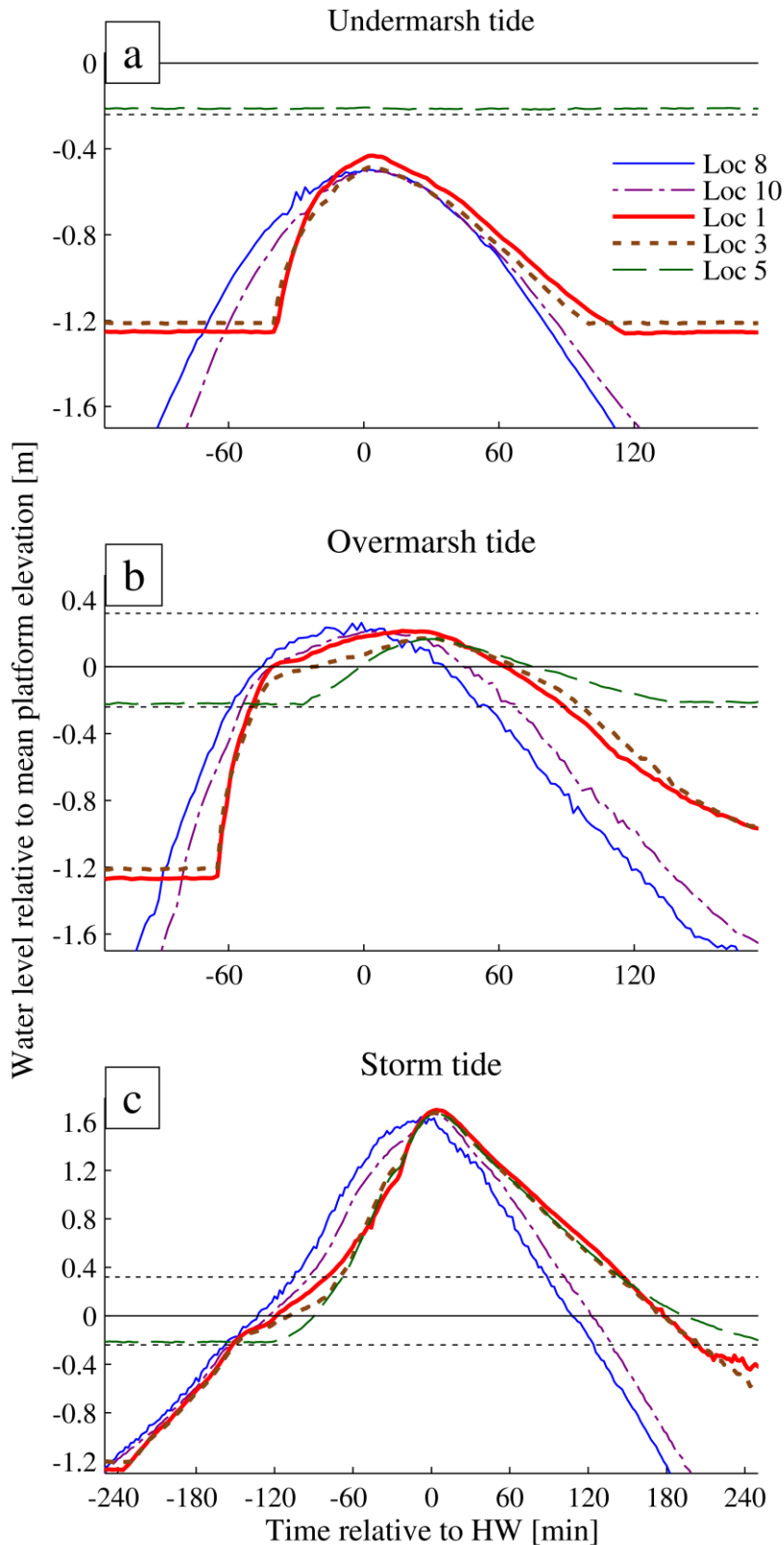


**Figure 2.3:** Tidal water levels at several marsh locations in the channel network (locations 1, 3, 8 and 10) and on the marsh platform (location 5) for: (a) a typical undermarsh tide (10 December 2013), (b) a typical overmarsh tide (5 December 2013) and (c) the highest recorded storm tide (6 December 2013). The overall mean marsh platform elevation is indicated with a solid horizontal line, and 10% and 90% percentiles with dashed horizontal lines.



## 2.3 Results

To evaluate the attenuation rate along the intertidal channels within the marsh, we assess the flood attenuation rate between the marsh edge (location 8) and the inner marsh locations (locations 1-3) in Figure 2.4a, while Figure 2.4b shows the difference in peak water level between location 10 and locations 1-3. Attenuation rates are calculated as the reduction in peak water level between two locations in cm/km. The figures show that the attenuation rate can vary significantly between individual flood events depending on the height of the peak water level. For overmarsh tides (i.e., peak water level above mean platform elevation), the overall attenuation rate from the marsh edge to the inner marsh locations (Figure 2.4a) increases for higher HWL and reaches a maximum of 4 to 5 cm/km for flood events with peak water levels of 0.5-1.0 m above the mean marsh platform elevation. The attenuation rate decreases again for higher tides and there is even a slight amplification measured for the highest recorded storm tide. On the other hand, it is observed that when undermarsh tides occur (i.e., considering HWL below mean platform elevation) the flood attenuation strongly decreases or changes to amplification.

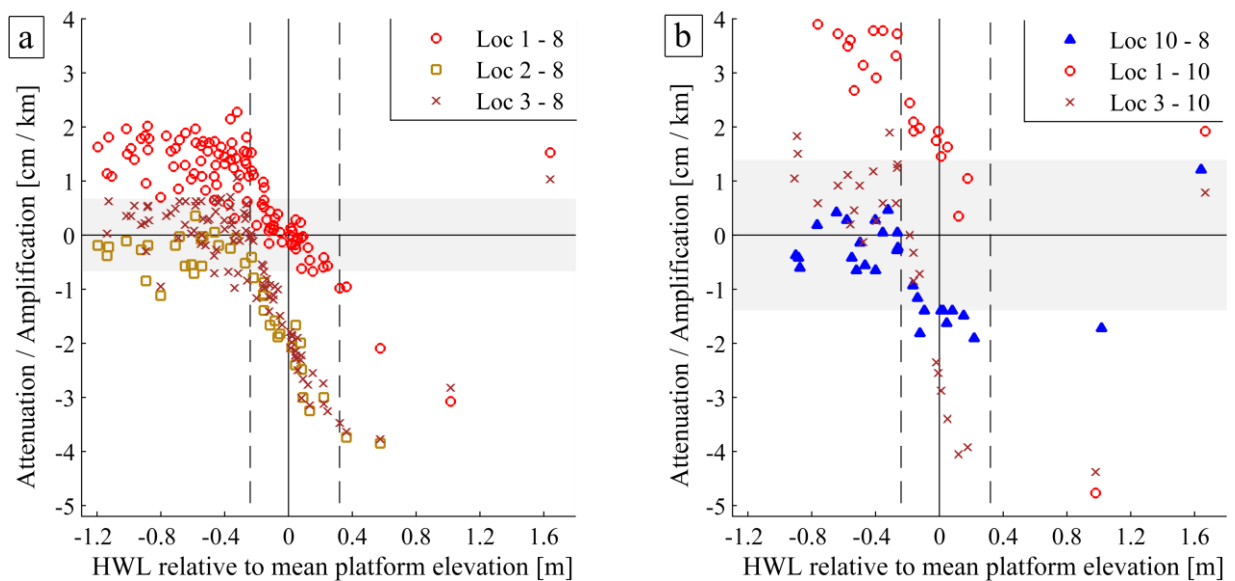


**Figure 2.4.** Amplification and attenuation rates (a) between several inner marsh locations and the marsh edge, and (b) over shorter transects within the marsh channel network (see Figure 2.1 for locations). Amplification and attenuation rates are calculated as the vertical difference in peak water levels in cm per km between locations. The overall mean marsh platform elevation is indicated with a solid vertical line, and 10% and 90% percentiles with dashed vertical lines. The combined vertical error of the calculated attenuation and amplification rates is illustrated in grey.

Second, Figure 2.4 shows that the attenuation rate also varies between different channels in the inner marsh area. In particular, attenuation rates measured along transects through the relatively wide main channel (towards location 1, see Table 2.1) are generally lower than those in the narrower side-channels (towards locations 2-3). For example, considering undermarsh tides, this results in an amplification of the peak water level within the main channel of the marsh (up to 4 cm/km between location 10 and location 1; Figure 2.4b); while in the side-channels, there is still a small decrease of the peak water level (location 2) or the amplification is not so pronounced and within

the vertical precision of the water level measurements (location 3). Moreover, the attenuation rates and the amplification rates measured along the wide outer marsh transect (location 8 to 10) are lower than those measured along the narrower inner marsh transects (location 10 to 1 and 3). Finally, the maximum measured flood wave attenuation over the whole length of the channel system is about 15 cm (or 4 cm/km) from the marsh edge (location 8) towards locations 2 and 3. The maximum attenuation rate within parts of the channel system is approximately 5 cm/km from location 10 towards locations 1 and 3. The maximum attenuation between location 10 and location 2 is not calculated as there are no simultaneous measurements at these locations.

Over non-channeled transects on the vegetated marsh platform, in general, it is found that the peak water level is attenuated, regardless the HWL (see Figure 2.5). Calculated attenuation rates based on the field measurements can rise up to 70 cm/km (Figure 2.5) which is an order of magnitude higher than the maximum rates calculated over transects through the channels (up to 5 cm/km; Figure 2.5b). It must however be stated that the attenuation rates over the marsh platform have been measured over relatively short distances (50-100 m), meaning that the total measured attenuation over these short transects on the platform was only up to 7 cm and especially the lower attenuation rates are within the vertical precision of the water level measurements over such short distances. Finally, it should be stated that these local attenuation rates should not be extrapolated over much longer distances due to their dependence on water depth.

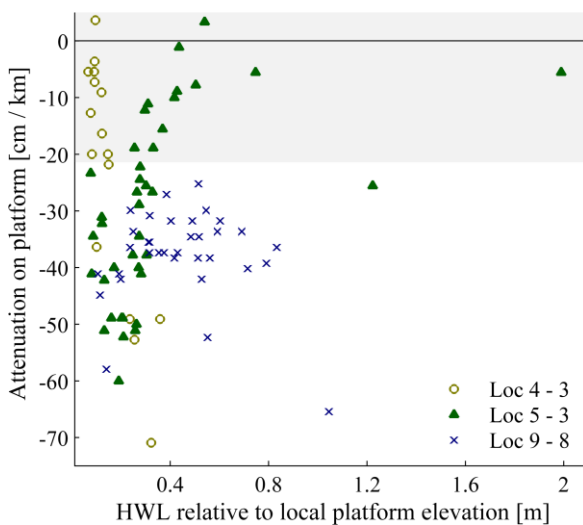


**Figure 2.5.** Attenuation rates between locations on the marsh platform and nearby locations in a marsh channel (see Figure 2.1 for locations), calculated as the vertical difference in peak water levels in cm per km in between locations. The combined vertical error of the calculated attenuation and amplification rates is illustrated in grey.

Figure 2.6 illustrates the changes in the vertical tidal asymmetry as the tide propagates through the marsh. At the marsh edge (location 8, symbols in blue in Figure 2.6a), the ratio  $R$  between flooding period  $T_{flood}$  and ebb period  $T_{ebb}$  is found to vary between 0.7 and 1.2; i.e., both flood-dominant and ebb-dominant asymmetry is observed at the marsh edge. Figure 2.6b describes the ratio between  $R$  at location 1 and  $R$  at location 8 in order to quantify the changes in the vertical asymmetry along the main channel. It is found that  $R$  decreases from the marsh edge (location 8) towards the inner marsh (location 1, symbols in red in Figure 2.6a) for almost all tides. Hence, the tidal asymmetry becomes more flood-dominant (i.e., shorter flood period than ebb period)

from the marsh edge towards the end of the main channel. Moreover, the flood-dominant asymmetry at the inner marsh location gets stronger with increasing peak water levels as long as the marsh platform does not get inundated. As illustrated by Figure 2.6a, at the transition from undermarsh to overmarsh tides, tidal asymmetry at the inner marsh location 1 changes abruptly towards a less flood-dominant ratio. Conversely, there is no measurable effect of platform inundation at the marsh edge location 8. As a result, the difference in tidal asymmetry between the marsh edge and inner marsh location becomes smaller again. This abrupt change in tidal asymmetry at location 1 can also be observed directly from the water level recordings of overmarsh tides as depicted in Figure 2.3, which show that water levels rise slower at inner marsh locations from the moment the platform becomes inundated. As peak water levels increase further above the platform elevation, flood-dominance at the inner marsh location 1 becomes stronger again. Finally, the highest recorded storm tides result in the lowest ratio between flood and ebb periods at location 1 (Figure 2.6). This in contrast to location 8, where the two storm tides were even ebb-dominant due to elongated flood periods of over 6 h, compared to around 3-4 h during normal tides at this location.

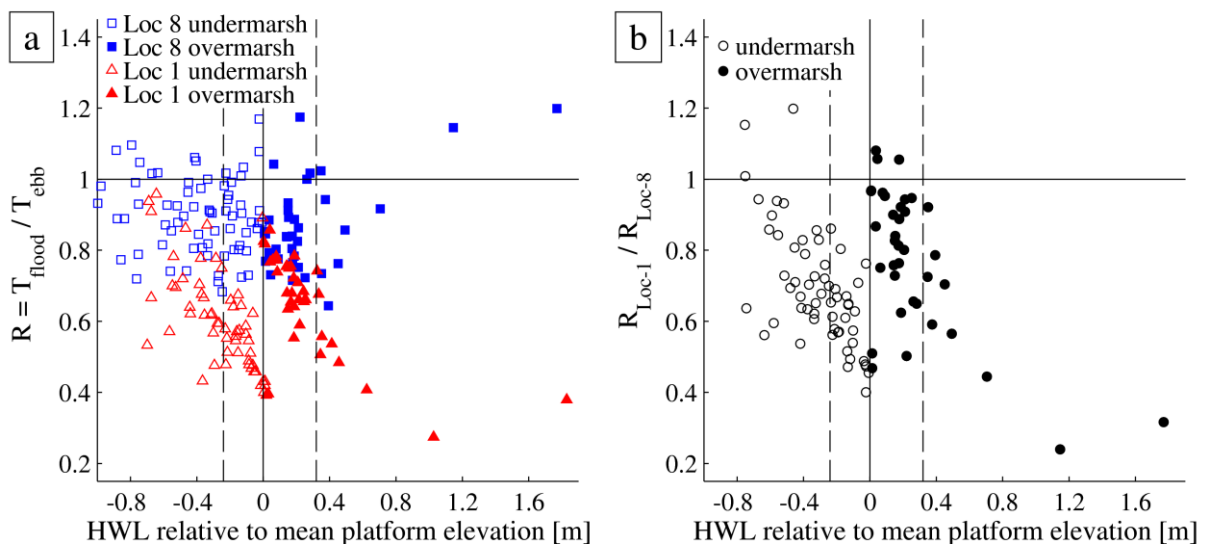


**Figure 2.6.** (a) Tidal asymmetry, expressed as the ratio  $R$  between the duration of the flood and ebb period, at the marsh edge (location 8, blue squares) and the inner marsh (location 1, red triangles) for different undermarsh tides (open symbols) and overmarsh tides (filled symbols), with the global mean platform elevation (solid vertical line) and the 10% and 90% percentiles (dashed vertical lines). (b) Relative change in tidal asymmetry from the outer marsh location towards this inner marsh location. Flood and ebb periods were calculated for the period that water levels were above the water level loggers (i.e., -0.4 m NAP at location 8 and 2.1 m NAP at location 1).

## 2.4 Discussion

While direct measurements of attenuation of tides and storm surges in tidal wetlands (e.g., Van der Molen 1997; Krauss et al. 2009) are scarce and present insights on storm surge attenuation in wetlands are largely based on numerical modelling (e.g., Loder et al.

2009; Wamsley et al. 2010; Temmerman et al. 2012), we performed in-situ measurements of tidal propagation within a large tidal wetland for a wide range of flood events, ranging from neap to spring tides and including two storm surge events. The results of our field study show that the amount of peak water level attenuation along the marsh channels varies with the inundation height above the marsh platform elevation and with the width of channels (relative to the platform width) that dissect the marsh platform (Table 2). The measured attenuation rates for tidal peak water levels in the marsh channel system are in the range of attenuation rates found in previous studies on hurricane-induced surges propagating through mangroves and coastal wetlands (Krauss et al., 2009; Lovelace, 1994; Wamsley et al., 2010) and of attenuation rates calculated from observed spatial differences in mean HWLs in a large tidal marsh by Van der Molen (1997) (Table 2.1).

### ***2.4.1 Comparison with analytical models for tidal flow in tidal channels***

The propagation of overmarsh tides in our observations, which is influenced by both channel geometry and marsh platform characteristics, shows similarities with the characteristics of propagating tides in convergent tidal basins with large intertidal storage area, based on approximate analytical models. In addition, the observed propagation of undermarsh tides, which is mainly influenced by channel geometry, shows similarities with propagating tides in convergent tidal basins with little intertidal storage. For instance, Friedrichs and Aubrey (1994) and Van Rijn (2011) illustrate analytically that tidal wave propagation in convergent channels is dominated by a balance between friction effects (causing attenuation) and convergence (causing amplification). In our observations the amplified undermarsh tides appear to be dominated by convergence, while for the attenuated overmarsh tides friction dominates over convergence. Similarly, Friedrichs and Madsen (1992) found that shallow embayments with large tidal amplitude to water depth ratios and relatively little intertidal storage induce a water level set up and a (flood-dominant) shorter rising asymmetry, whereas relatively deep embayments with ample intertidal storage and low amplitude to depth ratios induce a set down and an (ebb-dominant) shorter falling asymmetry. In our observations, undermarsh tides show an increase in shorter rising asymmetry from the marsh edge towards the end of the main channel and this increase in flood-dominant asymmetry does indeed get smaller at the moment the platform gets inundated (Figure 2.6). The ebb-dominant shorter falling asymmetry as described by Friedrichs and Madsen (1992), however, does not occur at the inner marsh locations.

In order to investigate whether the insights following from the presented observations are generic and not only site-specific, we use the analytical model of Van Rijn (2011) which is based on a basic consideration of the conservation of wave energy flux. It should however be stated that it is not the intention to fit this 1D analytical model to the observed data, as the application of the model to the presented results is not straightforward. In particular, the model is conceived for an idealized setting and is built upon several assumptions which are not completely valid for the present situation. Firstly, the representation of the tidal wave as a single progressive sinusoidal wave is a

rather crude approximation (Van Rijn, 2011). Moreover, the analytical approximation by Van Rijn (2011) was derived for a tidal channel that does not fall dry, which is strongly different from intertidal marsh channels. For example, the model does not account for wetting and drying processes. Furthermore, the complex marsh geometry is simplified to a 1D schematization in which the marsh platform width to channel width ratio is set constant and the branching channel network is schematized as a single channel. Other assumptions are that there is no reflection at the landward end of the channel (i.e., ignoring levees or other structures) and that the impact of platform inundation is solely implemented by increased friction, rather than as additional storage such as in the analytical model for tidal propagation in convergent estuaries by Savenije et al. (2008). This implies that the present analytical approximation can only be used to assess the combined effect of channel convergence and variations in depth-dependent friction on tidal damping or amplification in a setting (parameter configuration) that is similar to that of the study area. Therefore, we use the analytical solution of Van Rijn (2011) solely to investigate the generic character of our findings and to indicate the physical mechanisms that cause the differences in attenuation and amplification rates observed in our measurements. Based on the wave energy flux, Van Rijn (2011) derived that the along-channel variation of the tidal range is governed by the following relation:

$$\frac{dH}{dx} = 0.5\beta H(x) - \frac{f c^2 \cos \varphi}{12\pi g h^3} H(x)^2 \quad (2.1)$$

in which we have made the additional assumption that the channel depth is constant. In (2.1),  $H(x)$  is the tidal range at distance  $x$  from the estuary mouth (or marsh edge in our case),  $\beta$  represents the width convergence coefficient, and  $h$  the constant mean water depth. Frictional effects on the tidal wave propagation are represented by  $f$ , a friction coefficient, which is evaluated as  $f=8g/C^2$  with  $C$  the Chézy coefficient. Finally,  $g$  is the gravitational acceleration,  $c=(gh)^{0.5}$  the local wave speed and  $\varphi$  the phase lead of velocity maximum with respect to water level maximum. As boundary condition, we consider that at the marsh boundary  $H$  is equal to  $H_0$ . Equation 2.1 can then be solved analytically, yielding:

$$H(x) = \left( \left( \frac{C_a + C_b H_0}{H_0 C_a} \right) e^{(-C_a x)} - \frac{C_b}{C_a} \right)^{-1} \quad (2.2)$$

in which  $C_a$  and  $C_b$  are along-channel constants representing:

$$C_a = 0.5\beta \quad (2.3)$$

$$C_b = -\frac{f c^2 \cos \varphi}{12\pi g h^3} \quad (2.4)$$

To take into account the effect of intertidal flats adjacent to the main channel, Van Rijn (2011) further states that  $h$  can be replaced by the effective water depth  $h_{eff} = (b_{ch}/b_{tot})h_{ch} = \alpha h_{ch}$ , with  $b_{ch}$  and  $b_{tot}$  representing the channel width and total width,

respectively. Hence, the scaling factor  $\alpha$  can be used to schematize the influence of the marsh platform surrounding the marsh channel.

In order to apply the analytical solution to an intertidal channel, it is necessary to make some assumptions with respect to the schematization of the marsh (see also Figure 2.7 for a graphical representation). The tidal range is schematized as the difference between the peak water level at the marsh edge ( $HWL$ ) and the channel elevation  $z_{ch}$ , as the marsh channels fall largely dry during low tide. The tide-averaged water depth in the channel  $h$  is assumed to be half of this tidal range and  $h_{eff}$  is only used for overmarsh tides ( $HWL > z_{pl}$ , in which  $z_{pl}$  denotes the platform elevation). The Chézy friction coefficient deployed to evaluate Eq. 2.2 is computed as the width-averaged Chézy coefficient, which means for overmarsh tides that:

$$C = \alpha * C_{ch} + (1 - \alpha) * C_{pl} \tag{2.5}$$

with  $C_{ch}$  and  $C_{pl}$  being the Chézy coefficients representative for the marsh channel and platform, respectively. To implement the effect of vegetation submergence during the highest tides ( $HWL > z_{pl} + k$ ), the friction formula proposed by Baptist et al. (2007) for submerged vegetation is used:

$$C_{pl} = C_{veg} + 2 * \sqrt{g} * \ln\left(\frac{HWL - z_{pl}}{k}\right) \tag{2.6}$$

where  $C_{veg}$  is the Chézy coefficient for friction exerted by the vegetation only and  $k$  the vegetation height. In case of non-submerged vegetation ( $HWL < z_{pl} + k$ ),  $C_{pl}$  equals  $C_{veg}$ . Furthermore, we assume all parameters except for  $H(x)$  to be constant along the channel axis in  $x$ -direction.

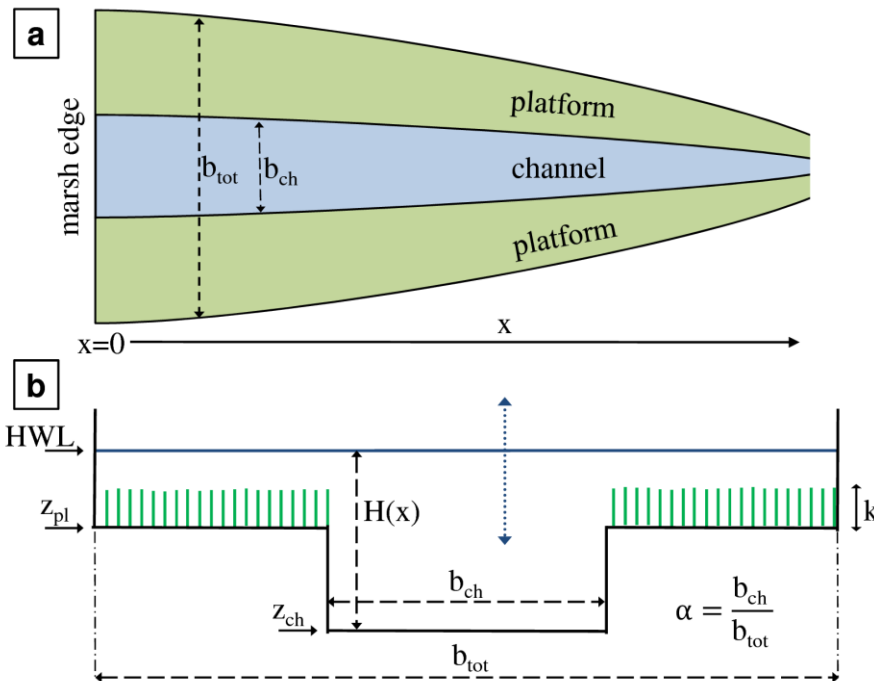


**Figure 2.7:** Schematization of the idealized intertidal channel and adjacent marsh platform, showing (a) a top view of the converging basin and (b) a cross-sectional view of the marsh channel and adjacent platform, in which  $H(x)$  is the tidal range,  $HWL$  the peak water level,  $b_{ch}$  and  $b_{tot}$  are the channel and total width respectively,  $z_{pl}$  is the elevation of the marsh platform,  $z_{ch}$  the elevation of the channel bottom and  $k$  the vegetation height.

The following data have been used to apply the analytical solution to an intertidal channel with adjacent marsh platform. The width convergence length scale  $L_b=1/\beta$  is set equal to 1000 m based on the observed decrease in channel width from the marsh edge location towards the inner marsh locations. The channel elevation  $z_{ch} = +0.5$  m is obtained by averaging the elevation of the channel bottom over the full length of the main channel. The platform elevation is set at  $z_{pl} = +3.0$  m, close to the mean platform elevation in our study area. The vegetation height is set at  $k = 0.4$  m, based on the mean canopy height of the most abundant vegetation type in the study area; i.e., 0.43 m (Vandenbruwaene et al., 2015). To estimate  $\varphi$ , velocity and water level measurements in the main channel close to the marsh edge are used (data obtained from Rijkswaterstaat Zeeland – Meetadviesdienst), leading to  $\varphi = 2$  hr ( $\sim 60^\circ$ ). Finally, we evaluate the spatial variation of the tidal range for different Chézy friction coefficients as it is not straightforward to derive this parameter from the data; i.e.,  $C_{ch}$  equal to 55, 65 and 75  $m^{0.5}s^{-1}$  and  $C_{veg} = 10, 15$  and  $20 m^{0.5}s^{-1}$ . The influence of the marsh platform width on the propagation of overmarsh tides is evaluated by using different values of  $\alpha$  (0.1, 0.35, 0.6 and 0.85). Figure 2.8 shows the resulting amplification and attenuation rates from  $x = 0$  m to  $x = 5000$  m for varying high water levels ( $HWL = 1.5$ - $5.5$  m) at  $x = 0$  m and for the different input values for  $C$  and  $\alpha$ .

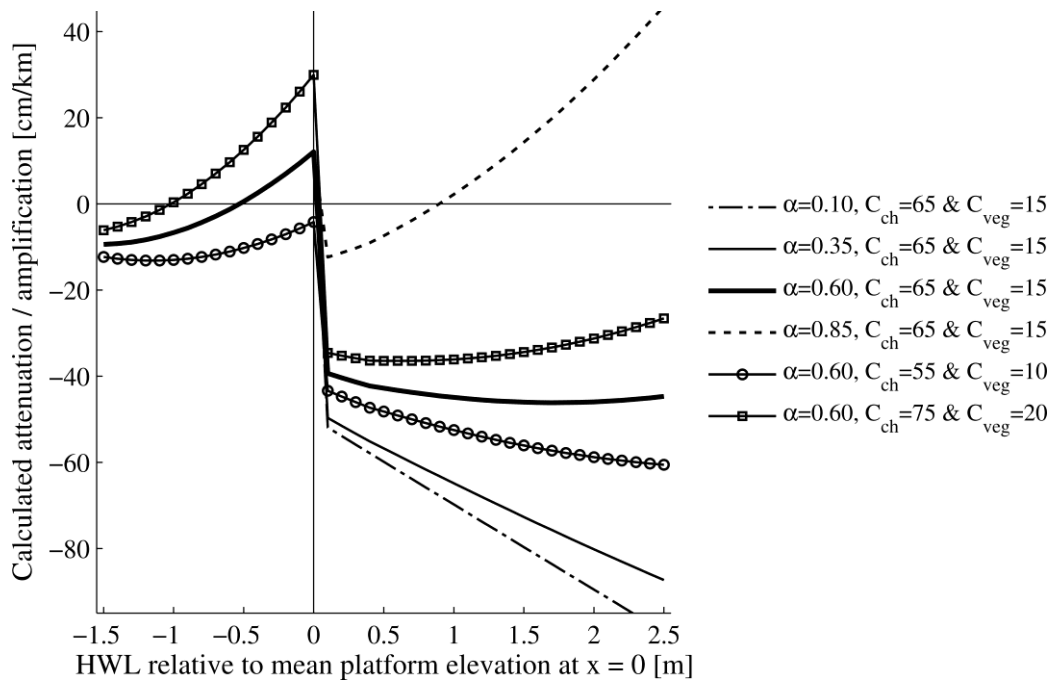


**Figure 2.8** : Results of the analytical model for different Chézy coefficients and different values of  $\alpha$  (i.e., ratio between channel width and total width), showing attenuation and amplification rates for varying undermarsh ( $HWL < z_{pl}$ ) and overmarsh ( $HWL > z_{pl}$ ) high water levels at the marsh edge.

The results of the analytical model show that based on a basic consideration of the wave energy flux balance a similar effect of platform inundation is observed as in our observations. Undermarsh tides are increasingly amplified for higher peak water levels; while friction becomes dominant and attenuation is present when the platform gets inundated and  $h_{eff}$  and  $C$  decrease. The distinct shift to attenuation as the marsh platform gets inundated is consistently obtained from the analytical approximation, regardless of

the configuration of the channel-to-platform width ratio or bottom friction coefficients. Hence, the shift towards attenuation from undermarsh to overmarsh tides in our water level measurements appears to be generic and can (at least partly) be attributed to differences in width-averaged depth and depth-dependent friction. Furthermore, depending on the values of  $C$  and  $\alpha$ , attenuation rates get lower or higher for increasing peak water levels and platform inundation heights. In particular, the results indicate that the width of the platform with respect to the channel width is a key factor to determine whether friction becomes dominant over convergence and tides are attenuated along marsh transects. For higher  $\alpha$  values, the computed attenuation rate decreases or turns into amplification for higher peak water levels, whereas attenuation is persistent for increasing peak water levels if  $\alpha$  is lower. Hence, the geometrical properties of the marsh channel and platform itself may cause attenuation rates to decrease for increasing inundation heights. Conversely, the Chézy friction coefficients themselves appear to play a minor role in the analytical model. In reality, the extent of the marsh platform that is flooded increases for increasing peak water levels, especially for peak water levels around mean platform elevation (i.e.,  $\alpha$  varies with varying  $HWL$ ). This implies that maximum attenuation would occur when the combination of average platform inundation depth, the depth-dependent platform extent and additional friction exerted by the vegetation induces a maximum cross-sectional averaged friction. All in all, the presented results based upon an analytical model for tidal flow in regular tidal basins and estuaries (i.e., channels that are not dry during low tide) support the generic character of our field observations of attenuation and amplification rates in an intertidal channel system.

### **2.4.2 Effect of inundation height**

Our observations indicate that attenuation rates of overmarsh tides first increase for higher platform inundation heights, showing the strongest attenuation for peak water levels that are 0.5-1.0 m above mean platform elevation. Conversely, the highest recorded storm tides were less effectively attenuated or not attenuated at all (Figure 2.4). The latter could be a result of the long duration of the flood period of over 6 h during the highest observed storm tide compared to 3-4 h normally. Because of this longer flood duration, more time was available for the storage area on the marsh platform to fill up to similar water levels as in the adjacent estuary. Numerical modelling studies have also shown that surge attenuation along marsh transects decreases for larger surge events if the surge duration is long compared to the time it takes for the storage area on the marsh platform to get fully inundated (Loder et al., 2009; Resio and Westerink, 2008; Wamsley et al., 2010). In particular, Resio and Westerink (2008) state that additional friction exerted by a marsh may slow storm surge propagation, but if the hydrodynamic (or wind) forcing is long enough the water will eventually fill up the entire marsh storage area. An additional reason for the decrease in attenuation rates concerns the decreasing flow resistance on the vegetated platform for higher water levels which increasingly submerge the marsh vegetation (Baptist et al., 2007; Nepf, 2012). Previous field studies and hydrodynamic modelling studies of regular tides in marshes demonstrated that when the water level is below the vegetation canopy, spatial



flow patterns are controlled by friction by the vegetation canopy, while as soon as the water level overtops the vegetation canopy, more large-scale sheet flow over the vegetation canopy can occur (Temmerman et al., 2005a, 2005b). Our observations of attenuation rates over the full marsh transect (Figure 2.4a) indeed reach a maximum just above the mean canopy height of the most abundant species (i.e., 0.43 m above mean platform elevation; Vandenbruwaene et al., 2014). Nevertheless, limitations in storage area on the marsh platform during long inundation events and the decreasing influence of bottom friction for higher inundation events in general can also reduce attenuation rates for higher inundation events.

#### **2.4.3 Effect of channel geometry**

The observed attenuation rates vary between different locations in the marsh (Figure 2.4), depending on the presence and geometry of nearby channels (Table 2.2). The measured attenuation rates of overmarsh tides are lowest (up to a maximum of 2 cm/km) along the wide and relatively deep outer marsh transect between locations 8 and 10, where the channel width converges from approximately 520 m to 170 m and where the influence of the marsh platform is relatively small. In terms of the analytical model presented above, values for  $\alpha = b_{ch}/b_{tot}$  averaged along the outer marsh transect are estimated to be in the range of 0.4 halfway the main channel to nearly 1.0 at the marsh edge, based on the marsh geometry between the measurement locations. Similarly to the field observations, the results of the analytical model (Figure 2.8) show that attenuation of overmarsh tides is smaller for larger values of  $\alpha$ . Attenuation rates are higher along the inner marsh transects from location 10 towards location 1 and 3 (up to 5 cm/km), where the channel width decreases further to  $\sim 4$ -30 m and the influence of the marsh platform on the propagation of overmarsh tides becomes increasingly important. Averaged values for  $\alpha = b_{ch}/b_{tot}$  along the inner marsh transect are estimated to be in the range of 0.1-0.3. Again, the observation of higher attenuation rates for lower values of  $\alpha$  is supported by the results of the analytical model (Figure 2.8) supporting the generic character of the observations. Furthermore, attenuation rates are generally higher along narrower side-channels towards locations 2 and 3, where the channel width converges to  $\sim 4$ -8 m and cross-sectional areas are small, than along the wider main channel towards location 1, where the channel width converges to  $\sim 30$  m and the cross-sectional area is larger. Only for most strongly damped tide, attenuation rates were similar along the inner marsh channels towards locations 1 and 3 (i.e., 5 cm/km). In addition, the observations also reveal that amplification of undermarsh tides is lower or non-occurring towards locations at the end of narrower side-channels (locations 2 and 3), whereas clear amplification is observed towards the end of the main channel (location 1). These variations in attenuation and amplification rates can be attributed to differences in friction, which is generally higher in narrow and shallow channels compared to wide and deep channels. Over much shorter distances, the highest attenuation rates of up to 70 cm/km are measured on the marsh platform itself (Figure 2.5). This can be expected as the flow field on the marsh platform is frictionally dominated due to the high friction exerted by the vegetation present (e.g., Van Oyen et al. 2012, 2014).

Taken together, our field measurements demonstrate the importance of marsh channel geometry for tidal and storm surge propagation in marshes. The results of the analytical model presented above (see Figure 2.8) confirm the dependency of attenuation rates of overmarsh tides on the ratio between the channel and platform width, showing clear variations in attenuation rates for different  $\alpha$  values. Besides, these findings are in accordance with existing modelling studies, which have shown that marshes with more channels or with wider channels cause relatively lower attenuation rates compared to more continuously vegetated marsh areas (Loder et al., 2009; Temmerman et al., 2012). The observation that attenuation rates are higher in marsh channels with a small cross-sectional area moreover indicates that marshes with a dense network of relatively narrow and shallow channels would induce higher attenuation rates than marshes with a sparser network of larger channels, although they may have a similar channel density. Unfortunately, the currently available dataset does not allow for a quantitative assessment of this hypothesis since the exact quantitative metrics of the along channel averaged channel width, channel cross-section and platform width cannot be readily evaluated for the study area with its complex branching channel network. As these data can only be retrieved by means of a specifically set-up field campaign, this issue falls beyond the scope of the present manuscript.

#### ***2.4.4 Concluding remarks***

In conclusion, this field study emphasizes that flood attenuation rates in a large tidal marsh are not only location-specific, but also event-specific. An important finding of our study is that there appears to be an optimal ratio between tidal and storm surge peak water levels and marsh platform elevation which induces the strongest attenuation along the marsh channels. Hence, protection against storm surges, often attributed to coastal wetlands (e.g., Gedan et al. 2010; Shepard et al. 2011; Temmerman et al. 2013), appears to be optimal only for flood events that cause a specific range of inundation heights (0.5-1 m in this marsh) above the coastal wetland elevation. Reduced attenuation rates for higher inundation events can be caused by (1) limitations in storage area on the marsh platform during long inundation events, (2) the decreasing influence of bottom friction for higher inundation depths and (3) vegetation submergence which also reduces the friction exerted on the flow. According to our findings, high marshes would more effectively attenuate higher flood waves or severe storm surges, whereas low marshes are more effective for the attenuation of lower flood waves or regular tides. Some tidal waves might even experience amplification in higher channelized marshes due to channel convergence, especially if the marsh platform is not yet inundated. Furthermore, distinct differences in attenuation rates are observed between different sized marsh channels, while differences of up to an order of magnitude are found between marsh channels and the vegetated marsh platform, indicating the importance of marsh channel configuration and geometry for storm surge attenuation. For numerical modelling studies it is therefore essential to include the effects of channels on flood wave propagation through marshes to avoid overestimation of storm surge attenuation and correctly simulate spatial differences between surge levels. Finally, our findings contribute to a better understanding of the coastal protection

function of tidal wetlands worldwide and of the mechanisms behind variations in observed storm surge reduction between different locations and different flood wave events (e.g. Table 2.1). Moreover, as coastal wetland conservation and restoration is starting to be implemented as part of ecosystem-based coastal defense systems our findings may help coastal managers and coastal societies with the design and morphological management of coastal wetlands to optimize their coastal defense functions.

## 2.5 References

- Baptist, M.J., Babovic, V., Rodríguez Uthurburu, J., Keijzer, M., Uittenbogaard, R.E., Mynett, A., Verwey, A., 2007. On inducing equations for vegetation resistance. *J. Hydraul. Res.* 45, 435–450.
- Barbier, E.B., Georgiou, I.Y., Enchelmeyer, B., Reed, D.J., 2013. The value of wetlands in protecting Southeast Louisiana from hurricane storm surges. *PLoS One* 8, e58715. doi:10.1371/journal.pone.0058715
- Costanza, R., Pérez-Maqueo, O., Martinez, M.L., Sutton, P., Anderson, S.J., Mulder, K., 2008. The value of coastal wetlands for hurricane protection. *Ambio* 37, 241–248. doi:10.1579/0044-7447(2008)37[241:TVOCWF]2.0.CO;2
- Friedrichs, C.T., Aubrey, D.G., 1994. Tidal propagation in strongly convergent channels. *J. Geophys. Res.* 99, 3321–3336. doi:10.1029/93JC03219
- Friedrichs, C.T., Madsen, O.S., 1992. Nonlinear diffusion of the tidal signal in frictionally dominated embayments. *J. Geophys. Res.* 97, 5637–5650. doi:10.1029/92JC00354
- Krauss, K.W., Doyle, T.W., Doyle, T.J., Swarzenski, C.M., From, A.S., Day, R.H., Conner, W.H., 2009. Water level observations in mangrove swamps during two hurricanes in Florida. *Wetlands* 29, 142–149. doi:10.1672/07-232.1
- Loder, N.M., Irish, J.L., Cialone, M.A., Wamsley, T.V., 2009. Sensitivity of hurricane surge to morphological parameters of coastal wetlands. *Estuar. Coast. Shelf Sci.* 84, 625–636. doi:10.1016/j.ecss.2009.07.036
- Lovelace, J.K., 1994. Storm-tide elevations produced by Hurricane Andrew along the Louisiana coast, August 25–27, 1992. Open File Report 94-371. Baton Rouge, LA, U.S.
- McGee, B.B.D., Goree, B.B., Tollett, R.W., Woodward, B.K., Kress, W.H., 2006. Hurricane Rita Surge Data, Southwestern Louisiana and Southeastern Texas, September to November 2005. U.S. Geological Survey Data Series 220.
- Möller, I., Kudella, M., Rupprecht, F., Spencer, T., Paul, M., van Wesenbeeck, B.K., Wolters, G., Jensen, K., Bouma, T.J., Miranda-Lange, M., Schimmels, S., 2014. Wave attenuation over coastal salt marshes under storm surge conditions. *Nat. Geosci.* 7, 727–731. doi:10.1038/ngeo2251
- Nepf, H.M., 2012. Hydrodynamics of vegetated channels. *J. Hydraul. Res.* 50, 262–279. doi:10.1080/00221686.2012.696559
- Nicholls, R.J., Cazenave, A., 2010. Sea-level rise and its impact on coastal zones. *Science* 328, 1517–1520. doi:10.1126/science.1185782
- Resio, D.T., Westerink, J.J., 2008. Modeling the physics of storm surges. *Phys. Today* 61, 33–38. doi:10.1063/1.2982120
- Savenije, H.H.G., Toffolon, M., Haas, J., Veling, E.J.M., 2008. Analytical description of tidal dynamics in convergent estuaries. *J. Geophys. Res.* 113, C10025. doi:10.1029/2007JC004408
- Shepard, C.C., Crain, C.M., Beck, M.W., 2011. The protective role of coastal marshes: a systematic review and meta-analysis. *PLoS One* 6, e27374. doi:10.1371/journal.pone.0027374
- Temmerman, S., Bouma, T.J., Govers, G., Lauwaet, D., 2005a. Flow paths of water and sediment in a tidal marsh: Relations with marsh developmental stage and tidal inundation height. *Estuaries* 28, 338–352. doi:10.1007/BF02693917
- Temmerman, S., Bouma, T.J., Govers, G., Wang, Z.B., De Vries, M.B., Herman, P.M.J., 2005b. Impact of vegetation on flow routing and sedimentation patterns: Three-dimensional modeling for a tidal marsh. *J. Geophys. Res.* 110, F04019. doi:10.1029/2005JF000301
- Temmerman, S., De Vries, M.B., Bouma, T.J., 2012. Coastal marsh die-off and reduced attenuation of coastal floods: A model analysis. *Glob. Planet. Change* 92–93, 267–274. doi:10.1016/j.gloplacha.2012.06.001

- Temmerman, S., Meire, P., Bouma, T.J., Herman, P.M.J., Ysebaert, T., De Vriend, H.J., 2013. Ecosystem-based coastal defence in the face of global change. *Nature* 504, 79–83. doi:10.1038/nature12859
- Van der Molen, J., 1997. Tidal distortion and spatial differences in surface flooding characteristics in a salt marsh: Implications for sea-level reconstruction. *Estuar. Coast. Shelf Sci.* 45, 221–233. doi:10.1006/ecss.1997.0179
- Van Oyen, T., Carniello, L., D'Alpaos, A., Temmerman, S., Troch, P., Lanzoni, S., 2014. An approximate solution to the flow field on vegetated intertidal platforms: applicability and limitations. *J. Geophys. Res. Earth Surf.* doi:10.1002/2013JF003064
- Van Oyen, T., Lanzoni, S., D'Alpaos, a., Temmerman, S., Troch, P., Carniello, L., 2012. A simplified model for frictionally dominated tidal flows. *Geophys. Res. Lett.* 39, 1–6. doi:10.1029/2012GL051949
- Van Rijn, L.C., 2011. Analytical and numerical analysis of tides and salinities in estuaries; part I: tidal wave propagation in convergent estuaries. *Ocean Dyn.* 61, 1719–1741. doi:10.1007/s10236-011-0453-0
- Vandenbruwaene, W., Schwarz, C., Bouma, T.J., Meire, P., Temmerman, S., 2015. Landscape-scale flow patterns over a vegetated tidal marsh and an unvegetated tidal flat: implications for the landform properties of the intertidal floodplain. *Geomorphology* 231, 40–52. doi:10.1016/j.geomorph.2014.11.020
- Wamsley, T. V., Cialone, M. a., Smith, J.M., Atkinson, J.H., Rosati, J.D., 2010. The potential of wetlands in reducing storm surge. *Ocean Eng.* 37, 59–68. doi:10.1016/j.oceaneng.2009.07.018
- Wamsley, T. V., Cialone, M. a., Smith, J.M., Ebersole, B. a., Grzegorzewski, A.S., 2009. Influence of landscape restoration and degradation on storm surge and waves in Southern Louisiana. *Nat. Hazards* 51, 207–224. doi:10.1007/s11069-009-9378-z
- Woodruff, J.D., Irish, J.L., Camargo, S.J., 2013. Coastal flooding by tropical cyclones and sea-level rise. *Nature* 504, 44–52. doi:10.1038/nature12855
- Zhang, K., Liu, H., Li, Y., Xu, H., Shen, J., Rhome, J., Smith, T.J., 2012. The role of mangroves in attenuating storm surges. *Estuar. Coast. Shelf Sci.* 102–103, 11–23. doi:10.1016/j.ecss.2012.02.021

# Chapter 3

## Coastal flood protection by a combined nature-based and engineering approach: Modelling the effects of marsh geometry and surrounding dikes

J. Stark, Y. Plancke, S. Ides, P. Meire and S. Temmerman

Based on the paper published in *Estuarine, Coastal and Shelf Science* (2016), 175, 34-45, doi: 10.1016/j.ecss.2016.03.027



### **Abstract**

*As ecosystem-based adaptation to global change is gaining ground, strategies to protect coastal and estuarine areas from increasing flood hazards are starting to consist of natural tidal wetland conservation and restoration in addition to conventional coastal defense structures. In this study, the capacity of tidal wetlands to locally attenuate peak water levels during storm tides is analyzed using a two-dimensional hydrodynamic model (TELEMAC-2D) for a 3000 ha intertidal marsh (SW Netherlands). Model results indicate that peak water level reduction largely varies between individual flooding events and between different locations in the marsh. Model scenarios with variable dike positions show that attenuation rates can be minimized by blockage and set up of water levels against dikes or other structures confining the marsh size. This blockage only affects peak water level attenuation across wetlands if the duration of the flood wave is long compared to the marsh size. A minimum marsh width of 6 to 10 km is required to completely avoid blockage effects for the storm tidal cases assessed in this study. If blockage does not affect flood wave propagation, variations in attenuation rates between different locations in the marsh and between tides with varying high water levels can be explained with a single relationship based on the ratio between the water volume on the marsh platform and the total water volume on the platform and in the channels. Attenuation starts to occur when this ratio exceeds 0.2-0.4 and increases from there on up to a maximum of 29 cm/km for a ratio of about 0.85. Furthermore, model scenarios with varying marsh channel depth show that marsh scale attenuation rates increase by up to 4 cm/km if the channel elevation is raised by 0.7 m on average. Conversely, marsh scale attenuation rates decrease by up to 2 cm/km for scenarios in which the channels are lowered by 0.9 m on average. The marsh platform elevation has little effect on the maximum attenuation, but it determines which tides are attenuated. In particular, only overmarsh tides that inundate the platform are attenuated, while undermarsh tides that only flood the marsh channels are not attenuated or even amplified. These findings may assist coastal communities and managers in the optimization of the coastal defense function of tidal wetlands in combination with dikes.*

### 3.1 Introduction

Ecosystem- or nature-based adaptation is an increasingly adopted strategy to cope with natural hazards that may increase with global change (e.g., Barbier, 2014; Hinkel et al., 2014; Jones et al., 2012; Kundzewicz et al., 2014). For coasts and estuaries, which are increasingly exposed to flood hazards from sea level rise and storm surges (e.g., Nicholls and Cazenave, 2010; Woodruff et al., 2013), the potential of tidal wetlands, including mangroves and marshes, for the reduction of flood risks is increasingly recognized around the world (e.g., Gedan et al., 2010; Shepard et al., 2011; Temmerman et al., 2013). In particular, there is growing interest to combine nature-based coastal defense functions of tidal wetlands with engineered coastal defense structures such as dikes (Cheong et al., 2013; Sutton-Grier et al., 2015; Temmerman and Kirwan, 2015). Besides the ecological functions of wetlands, these ecosystems may also contribute to coastal protection as they reduce the height of wind waves (e.g., Möller et al., 2014, 1999) and storm surges (e.g., Krauss et al., 2009; Lovelace, 1994; McGee et al., 2006; Wamsley et al., 2010) through additional flow resistance exerted by the wetland vegetation and wetland geomorphology. Moreover, wetlands may also reduce storm surges by increasing the storage area along estuaries or tidal rivers (e.g., Smolders et al., 2015). The focus of this study is however on the potential of tidal marshes to reduce storm surges locally within and behind the marsh area.

The capacity of tidal marshes and mangroves to attenuate storm surges is typically expressed as the reduction of high water levels (HWLs) per distance that the surge has travelled through a tidal wetland, i.e. the storm surge attenuation rate in cm/km. So far, existing insights on storm surge reduction rates in marshes are limited and based on scarce field studies, which were mainly conducted for one or a few specific hurricane or storm surge events (see McIvor et al. 2012 or Chapter 2 for a more detailed literature review of observed storm surge attenuation rates). Additional insights come from hydrodynamic modelling studies, which are mostly hind-casts of specific hurricane events (e.g., Wamsley et al., 2010; Zhang et al., 2012) or consider marsh geometry in a highly schematized way (e.g., Loder et al., 2009; Temmerman et al., 2012). Peak water level reduction rates ranging from 4 to 25 cm/km are observed in previous field studies. The high variety in observed attenuation rates suggests a strong dependency on the local marsh geomorphology and on the specific hydrodynamic forcing conditions. Besides, the morphological development of marshes may lead to variations of the attenuation capacity over time.

Numerical modelling studies have shown that storm surge attenuation is dependent on event-specific variables such as storm track and duration (Hu et al., 2015; Rego and Li, 2009; Resio and Westerink, 2008; Sheng et al., 2012; Wamsley et al., 2010; Weisberg and Zheng, 2006; Zhang et al., 2012). In particular, Resio and Westerink (2008) explained that attenuation rates decrease for larger storm surges and longer inundation events, because the surge has more time to fill up the entire marsh storage area. Wamsley et al. (2009) drew a similar conclusion to explain amplification of HWLs over marsh sections where levees precluded the surge to move further inland. Lower attenuation rates for

extremely high inundation events were also observed during the in-situ measurements presented in **Chapter 2**, who attributed this to limitations in storage area, vegetation submergence and the decreasing effect of bottom friction on the marsh.

Furthermore, numerical studies on the effect of channel density and channel geometry on storm surge reduction show that marshes with more and wider or deeper channels lead to lower attenuation rates than marshes which are dissected by fewer or smaller channels (e.g., Loder et al., 2009; Temmerman et al., 2012). Similar tendencies were found in field observations (e.g. **Chapter 2**; Krauss et al., 2009; Van der Molen, 1997), where the highest attenuation rates were observed along narrow or shallow channel transects. The effect of the elevation of the marsh platform on surge development over a schematized continuous marsh has been assessed numerically for hurricane induced surges (Loder et al., 2009; Wamsley et al., 2010) and with field observations for the propagation of regular tides and storm tides (**Chapter 2**), which indicate that attenuation only occurs for a specific range of HWLs above the platform elevation. A variety of numerical studies showed that flood wave attenuation is significantly influenced by additional surface roughness due to marsh vegetation cover (e.g., Hu et al., 2015; Loder et al., 2009; Sheng et al., 2012; Temmerman et al., 2012; Zhang et al., 2012). This would suggest that the extent of the vegetated marsh platform relative to the extent of the channels dissecting the platform determines the rate of attenuation. However, no geometrical measure or parameter is found yet in which the effects of variations in marsh geometry are combined with variations in flood wave height, and based on which the storm surge attenuation capacity of tidal wetlands can be predicted. Furthermore, the effect of the position of dikes confining the marsh size on flood level reduction is still poorly studied. To our knowledge, there are no existing studies in which the effect of marsh size is quantified by comparing flood level reduction rates for variable dike positions. As the interest of coastal managers for 'hybrid' coastal defense strategies based on a combination of engineering and nature-based solutions is growing (e.g. Sutton-Grier et al., 2015; Temmerman and Kirwan, 2015), insights on the potential for flood level reduction provided by coastal and estuarine marshes and how they interact with conventional coastal defense structures such as dikes need to be improved.

In this study, we assess the effect of the geometrical properties of an intertidal marsh and the position of the dikes surrounding the marsh on storm surge reduction rates within the marsh itself and consequently at the dikes behind the marsh. A hydrodynamic model is set up for a large tidal marsh including its complex channel network. First the model is calibrated and validated with water level measurements of several spring neap cycles and two storm tides. Scenario analyses are then performed, in which artificial changes are made to the marsh geomorphology and position of dikes surrounding the marsh. In particular, these scenarios focus on the effect of variations in dike position (affecting marsh size), marsh platform elevation and channel depth on the rates of HWL reduction within the marsh. Ultimately, we derive a single parameter based on the model simulations that links the spatial variations (depending on the marsh geometry)



and temporal variations (depending on the height of the flood event) to the HWL reduction rate.

## 3.2 Methods

### 3.2.1 Study area

The studied marsh is the 'Verdronken Land van Saeftinghe' (in the following: 'Saeftinghe'), a 3000 ha brackish intertidal marsh along the Western Scheldt estuary (SW Netherlands) (Figure 3.1). A semi-diurnal macrotidal regime induces HWLs at the study area between 2.18 m and 3.15 m above NAP (the Dutch ordnance level, close to mean sea level) for neap and spring tides respectively. The tidal range varies between 4.02 m and 5.57 m. The Saeftinghe marsh geometry is characterized by three main channels dissecting the marsh platform, called Speelmansgat in the west, IJskelder in the middle and Hondegat in the east (in this study referred to by S-, Y- and H- channels) (Figure 3.2). The three main channels are several hundreds of meters wide at the marsh edge and branch in the landward direction into a complex network of smaller channels. The channels dissecting the marsh are intertidal, implying that they fall dry during low tide. On the marsh platform itself, the most abundant vegetation types are *Elymus athericus* and *Scirpus maritimus*. Other species that occur are *Puccinellia maritima*, *Spartina anglica*, *Aster tripolium* and scattered patches of *Phragmites australis*. Vegetation canopy height depends on the local species composition and may be estimated as around 0.42 m on average (Vandenbruwaene et al., 2015). An artificial dam that is only flooded during high storm tides is present within the eastern part of the marsh (Figure 3.2b).

Wang and Temmerman (2013) presented a historical analysis of the geomorphological and vegetation development of the Saeftinghe marsh from the 1930s until 2004, which is extended to 2010 in this thesis (see: **Chapter 4**). During this period, the vegetated part of the marsh increased from 48% to 69% of the total area. The mean elevation of Saeftinghe increased from 1.13 m to 2.41 m above NAP, while mean high water levels increased from 2.36 m to 2.76 m. Accordingly, the mean elevation of the bare flats and intertidal channels increased from NAP +0.56 m in 1931 to NAP +1.06 m in 2010, while the mean elevation of the vegetated platform increased even more from NAP +1.92 m to 2.99 m in 2010. This latter value is used for the analyses in this study.

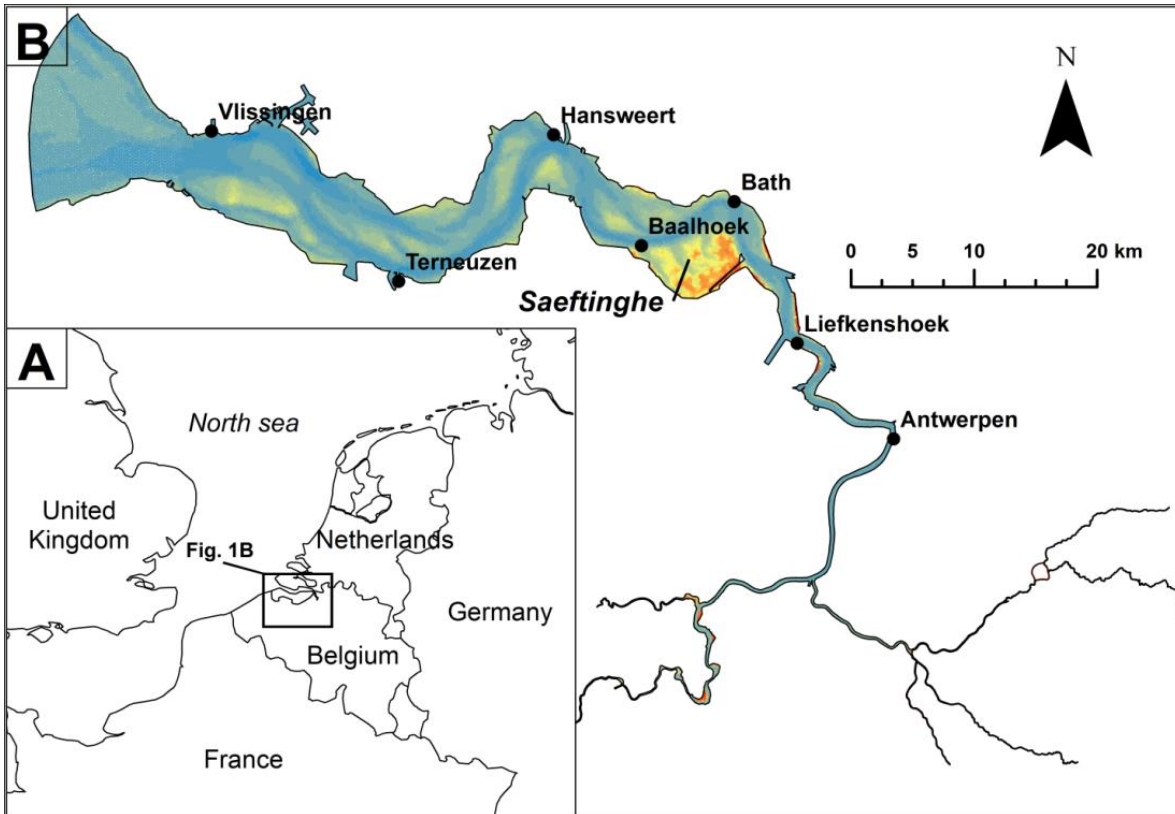


**Figure 3.1:** (a) Location of the Scheldt Estuary in Europe and (b) the Scheldt Estuary with its intertidal areas, including the tidal stations that are used in the model validation.

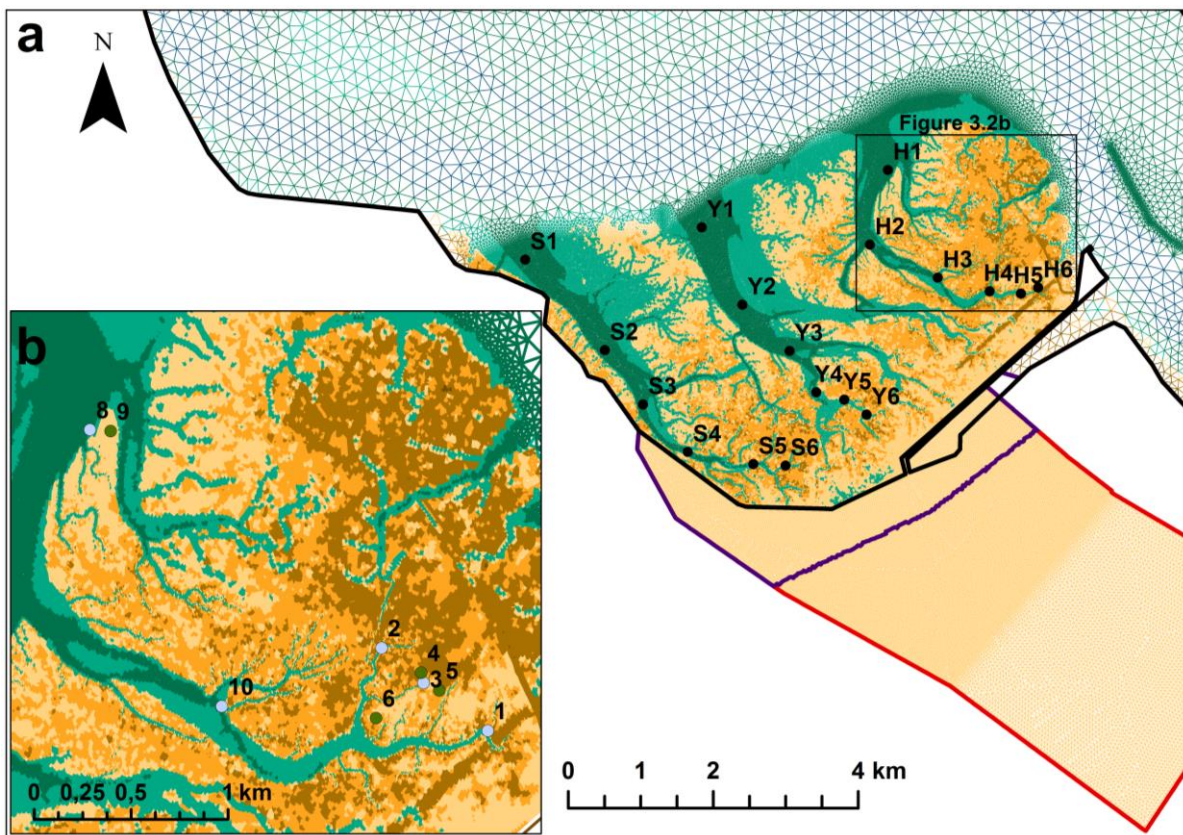


**Figure 3.2:** Model mesh at the Saeftinghe marsh with (a) the locations along the S-, Y- and H-transects, the present dikes and model boundary (bold black line) and the model boundary for the scenarios with 1 km (purple line) and 5 km (red line) marsh platform extensions and (b) the locations of the water level observations in the channels (blue dots) and on the platform (green dots).

### 3.2.2 Hydrodynamic model

The numerical model used in this study is set up with TELEMAC-2D (version 6.3), a widely used hydrodynamic modelling system that is part of the TELEMAC-MASCARET modelling suite and contains the relevant physical processes with respect to tidal wave propagation in estuaries (Hervouet, 2007). TELEMAC-2D solves the Saint-Venant equations or shallow water equations for continuity (Eq. 3.1) and momentum (Eq. 3.2 and 3.3), of which the one-dimensional form was already introduced in **Chapter 1** (i.e., Eq. 1.1 and 1.2), simultaneously in two dimensions:

$$\frac{\delta U}{\delta x} + \frac{\delta V}{\delta y} = S_h \quad (3.1)$$

$$\frac{\delta U}{\delta t} + U \frac{\delta U}{\delta x} + V \frac{\delta U}{\delta y} = -g \frac{\delta h}{\delta x} + \nu \Delta U + S_x \quad (3.2)$$

$$\frac{\delta V}{\delta t} + U \frac{\delta V}{\delta x} + V \frac{\delta V}{\delta y} = -g \frac{\delta h}{\delta y} + \nu \Delta V + S_y \quad (3.3)$$

in which  $U$  and  $V$  ( $\text{m}\cdot\text{s}^{-1}$ ) represent the flow velocity components in Cartesian coordinates,  $S_h$  ( $\text{s}^{-1}$ ) is a source or sink term for fluid,  $g$  ( $\text{m}\cdot\text{s}^{-2}$ ) is the gravity acceleration,  $h$  (m) is the water depth,  $\nu$  ( $\text{m}^2\cdot\text{s}^{-1}$ ) is a momentum diffusivity coefficient which represents the molecular and the turbulent viscosity and gives a weight to the diffusion terms in Eq. 3.2 and Eq. 3.3. Finally,  $S_x$  and  $S_y$  ( $\text{m}\cdot\text{s}^{-2}$ ) are sources or sinks of momentum in the dynamic equations (such as wind force, Coriolis force and bottom friction). Furthermore, TELEMAC-2D can deal with wetting and drying processes and hence can be used to simulate flow in intertidal systems such as tidal marshes and intertidal channels. In particular, wetting and drying processes are treated numerically in a mass-conservative way by allowing slightly negative depths and smoothing (i.e. adjusting) water level gradients when nodes in the model domain fall dry. For more detailed information on the TELEMAC-2D model and how wetting and drying processes are treated numerically we refer to (Hervouet, 2007) and the TELEMAC-2D user manual (see: <http://wiki.opentelemac.org/>).

#### Model description

The model mesh used in this study is adopted from Smolders et al. (2015) who calibrated and validated a tidal model (including storm tides) for the Scheldt estuary from its mouth in the North Sea up to its most upstream tidal boundaries (Figure 3.1). The mesh size ranges from approximately 10-50 m in the most upstream tributaries up to about 150-200 m in the most downstream part of the estuary. For this study, the model is locally refined to a mesh size of 6-20 m at the Saeftinghe study area to include the complex marsh geomorphology as good as possible and to represent the locations of the water level measurements more accurately (see Figure 3.2b for these locations). The refinement increases the number of nodes to a total of 130175. The extensive network of channels and creeks that dissect the marsh platform is included in the mesh by forcing the mesh to follow the marsh channel network to the extent possible. This

channel network has been extracted from a Lidar-based Digital Elevation Model (DEM) with a resolution of 2x2 m using GIS-software. Although efforts are made to include the complex marsh channel network as good as possible, element sizes of ~6 m or larger imply that part of the marsh channel system, especially in the inner marsh area where channels become narrower, is still roughly schematized (i.e., less than ~5-6 elements to represent the channel width) and results should therefore be taken with care. However, further refinement of the model mesh would significantly increase computation times, which is in our case also undesirable.

Bathymetric and topographic data from 2009 to 2011 are used to implement the bathymetry of the estuary, its tributaries and the Saeftinghe geomorphology in the model. The effect of vegetation on tidal propagation through the marsh is included by assigning higher bottom friction coefficients to vegetated areas than to non-vegetated areas. Vegetation maps (Huijs, 1995; Reitsma, 2006) are used to distinguish vegetated from non-vegetated areas. All types of vegetation are wrapped into a single Manning bottom friction coefficient because the spatial distribution of the vegetation types is too scattered to distinguish large areas with different vegetation characteristics on the scale we are modelling. Moreover, the dominant vegetation species have rather similar characteristics (i.e., flexible wetland grass types). The value for the overall bottom friction coefficient representing the combined effect of all types of marsh vegetation is derived by calibration. Drawback of implementing vegetation by constant Manning friction coefficients is that the depth-dependent effect of the vegetation (i.e., submerged versus emerged) on the flow is not incorporated (Baptist et al., 2007). However, previous modelling studies on storm surge propagation in wetlands have shown that reasonable results can be obtained while using constant or depth-independent Manning coefficients (e.g. Wamsley et al., 2009; Zhang et al., 2012).

The North Sea boundary of the model is forced with tidal water levels obtained from nearby tidal stations in the North Sea and along the coast. The upstream boundaries of the tributaries are closed, as the influence of the small discharges from these tributaries can be considered negligible compared to the tidal forcing at the study area. In particular, during the simulated periods the total upstream discharge ranged between 35-75 m<sup>3</sup>s<sup>-1</sup> (for 30/8/2013 until 27/9/2013) and up to a maximum of ~95 m<sup>3</sup>s<sup>-1</sup> during the severe storm surge event in December 2013 (based on weekly averaged discharges in Vanlierde et al., 2014). Wind effects are not taken into account in the model, implying that the wind set up that develops locally in the estuary or over the marsh area is not simulated. However, storm surges in the Western Scheldt are mainly generated by wind and atmospheric pressure effects on the North Sea, which is outside the model domain. Surge generation in the estuary itself is relatively small due to shorter fetch lengths and relatively low water depths. In the model, storm surges are included as boundary conditions at the North Sea model boundary.

### Model calibration

The hydrodynamic model of the Scheldt Estuary, without considering the Saeftinghe study area, was calibrated on tidal water levels by implementing zones with different

Manning's bottom friction coefficients  $n$ , varying from  $0.010 \text{ s}\cdot\text{m}^{-1/3}$  to  $0.026 \text{ s}\cdot\text{m}^{-1/3}$  (Smolders et al., 2015). For this study, the performance of the model was optimized further for tidal stations near the Saeftinghe marsh by slightly tuning bottom friction coefficients. Nevertheless, here we focus specifically on the model performance with respect to the representation of tidal wave propagation and storm surge attenuation within the Saeftinghe marsh. In-situ water level observations in **Chapter 2** are used for the calibration of the model in the marsh study area itself. These water level measurements were conducted in and around the 4 km Hondegat channel in the Saeftinghe marsh at the locations shown in Figure 3.2b and include several spring-to-neap cycles and two storm tides, the highest of which induced HWLs at tidal stations near the study area with an exceedance probability of  $1/5$ - $1/10 \text{ y}^{-1}$ . Calibration of the model part representing the Saeftinghe marsh is done by tuning Manning's bottom friction coefficients  $n_f$  and  $n_v$  for unvegetated and vegetated parts of the marsh respectively. In addition, the spatially and temporally constant velocity diffusivity coefficient  $\nu$  is tuned to optimize the representation of tidal propagation through the marsh channels. However, the user-implemented diffusivity  $\nu$  only influences the model results if its value is significant compared to the artificial diffusivity caused by the numerical model itself. As  $\nu$  is related to (local) mesh size and will be optimized for the Saeftinghe marsh where the mesh is refined, its value might not be optimal for the entire model domain in which large parts of the mesh are coarser. Therefore, care is taken during the calibration to make sure changes in  $\nu$  and in the Manning coefficients for the Saeftinghe marsh do not affect the model performance of the estuary scale model, which was validated previously. Values used in the calibration are  $n_f = 0.01, 0.015, 0.02$  and  $0.03 \text{ s}\cdot\text{m}^{-1/3}$  for the bottom friction on the unvegetated tidal flats and channels,  $n_v = 0.04, 0.08$  and  $0.12 \text{ s}\cdot\text{m}^{-1/3}$  for the bottom friction coefficient on the vegetated marsh platform and  $\nu = 0.01, 0.1, 0.5, 1.0, 2.0$  and  $10 \text{ m}^2\cdot\text{s}^{-1}$  for the velocity diffusivity coefficient. Ultimately, best results are obtained with  $\nu = 0.5 \text{ m}^2\cdot\text{s}^{-1}$ ,  $n_f = 0.01 \text{ s}\cdot\text{m}^{-1/3}$  and  $n_v = 0.08 \text{ s}\cdot\text{m}^{-1/3}$ . Figure 3.3 shows a map of the spatial variations in calibrated Manning friction coefficients around the Saeftinghe marsh).

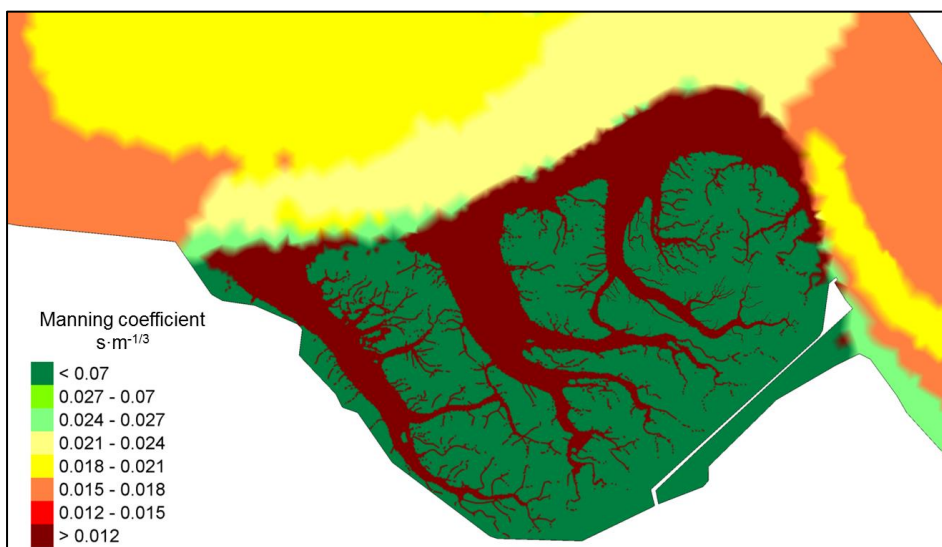


**Figure 3.3:** Manning coefficients for the Saeftinghe marsh and adjacent channels as implemented in the TELEMAC-2D model.

Model validation

The model performance on estuary scale is assessed by comparing simulated and observed water levels at several tidal stations from the estuary mouth near Vlissingen up to Antwerp (see Figure 3.1 for locations of the tidal stations) for a full spring-neap cycle (i.e., 30/8/2013-27/9/2013). Similarly, the model performance in the Saeftinghe marsh is assessed by comparing simulated water levels with the in-situ field observations in **Chapter 2** (i.e., 30/8/2013-27/9/2013 & 1/12/2013-15/12/2013). We calculate the mean error (Eq. 3.4), mean absolute error (Eq. 3.5) and root mean squared error (Eq. 3.6) for the total water level series. For high water levels specifically, we calculate the mean error (Eq. 3.7) and phase difference at high water (Eq. 3.8):

$$ME = \frac{1}{t} \sum_{i=1}^t (WL(i)_{sim} - WL(i)_{obs}) \quad (3.4)$$

$$MAE = \frac{1}{t} \sum_{i=1}^t |WL(i)_{sim} - WL(i)_{obs}| \quad (3.5)$$

$$RMSE = \sqrt{\frac{\sum_{i=1}^t (WL(i)_{sim} - WL(i)_{obs})^2}{t}} \quad (3.6)$$

$$ME_{HWL} = \frac{1}{n} \sum_{j=1}^n (HWL(j)_{sim} - HWL(j)_{obs}) \quad (3.7)$$

$$\Delta\varphi_{HWL} = \frac{1}{n} \sum_{j=1}^n (T_{HW}(j)_{sim} - T_{HW}(j)_{obs}) \quad (3.8)$$

in which  $WL_{sim}$  and  $WL_{obs}$  (m) are the simulated and observed water level series,  $i$  represents the individual time steps and  $t$  is the total number of time steps. Furthermore,  $HWL_{sim}$  and  $HWL_{obs}$  (m) are the simulated and observed high water levels,  $T_{HW-sim}$  and  $T_{HW-obs}$  (min) are the simulated and observed time steps of high water,  $j$  represents the individual high waters and  $n$  is the total number of high waters.

In addition, we compare simulated attenuation and amplification rates with observed rates for a variety of HWLs.

Finally, the sensitivity of the simulated tidal propagation through the marsh channels to variations in  $n_f$  and  $v$  is assessed in Section 3.3.1 based on their impact on the MAE of the total water level series and on  $\Delta\varphi_{HWL}$  and  $ME_{HWL}$  for the high water levels. Additionally, the sensitivity of the simulated attenuation rates to  $n_v$  is briefly assessed in section 3.3.2.

**3.2.3 Model scenarios**

Model scenarios are set up in which the marsh geometry is altered to assess the influence of marsh scale geomorphology on the attenuation of peak water levels (Table 3.1). Although marsh platform elevation and marsh channel elevation are not independent, they are independently lowered or raised in the model scenarios in order

to gain fundamental insights in their individual impacts on storm surge attenuation. Artificial elevation changes within the tidal frame are applied to the elevation of the marsh platform ( $\pm 0.4$  m) and channels ( $\pm 0.9$  m). To prevent the local platform elevation from becoming lower than adjacent channels, the elevation of the vegetated platform was restricted to a minimum of NAP +2.4 m, while the local elevation of the bare channels was restricted to a maximum of NAP +2.4 m to ensure that the channel elevation does not rise above the surrounding platform. This leads to scenarios in which the channel elevation is lowered by 0.9 m on average (Run 3) or raised by 0.7 m on average (Run 4) and in which the platform elevation is either raised or lowered by 0.4 m on average (Run 5 & Run 6). Furthermore, simulations are performed in which the marsh size is increased by repositioning the dike on the south side of Saeftinghe to a more landward position and hence extending the marsh width by approximately 1 km (Run 1) and 5 km (Run 2).

**Table 3.1.** Overview of model scenarios.

Simulation	Description of scenario
<b>Run 0</b>	Reference scenario with 2011 bathymetry of Saeftinghe
<b>Run 1</b>	Marsh platform extended / Dike behind marsh moved landward by 1 km
<b>Run 2</b>	Marsh platform extended / Dike behind marsh moved landward by 5 km
<b>Run 3</b>	Channel elevation lowered by 0.9 m
<b>Run 4</b>	Channel elevation increased by 0.7 m
<b>Run 5</b>	Platform elevation lowered by 0.4 m
<b>Run 6</b>	Platform elevation increased by 0.4 m

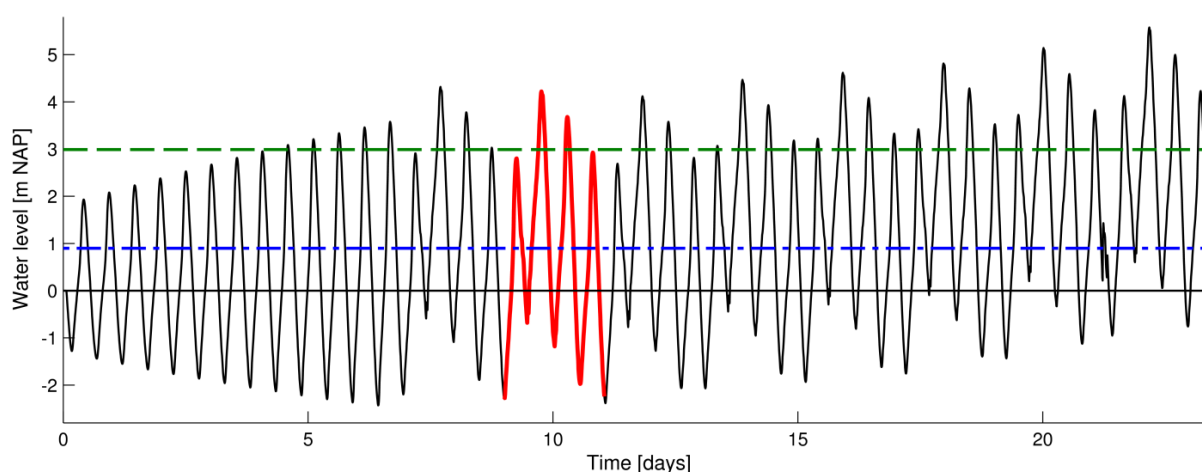


**Figure 3.4:** Modelled water level series near the study area. The measured storm tide is indicated by the red bold part. The mean platform elevation is indicated with the green dashed line and the mean elevation of the bare channels is indicated with the blue dot-dashed line.

The extended part of the marsh is schematized as a continuous vegetated marsh or grassland ( $n_v = 0.08 \text{ s} \cdot \text{m}^{-1/3}$ ) at an elevation of NAP +3.0 m (i.e., approximately the mean platform elevation of the study area) and without any channels dissecting the platform. These simulations are used to assess the effect of marsh size (i.e. storage area on the

platform) and whether it is a limiting factor for storm surge attenuation in case of larger surge events. All model simulations consist of a series of regular tides and storm tides, set up by manually altering the amplitude of a regular tide and of the measured storm tide in December 2013 (see Figure 3.4). Attenuation and amplification rates are calculated over the S-, Y- and H channels (see Figure 3.2) for all geomorphological scenarios.

### ***3.2.4 Analysis of relations between attenuation rates and marsh geometry***

The three main channels of the marsh are divided in shorter transects to analyze the relation between the spatially varying marsh geometry and attenuation rates more specifically. In particular, we attempt to relate HWL reduction rates over shorter channel sections to local geometrical properties of the marsh. Local attenuation rates are calculated for the simulation in which the platform area is extended by 5 km (Run 2 in Table 3.1) to exclude the effects of water level setup against the dikes and hence isolate the effects of marsh geomorphology on tidal attenuation or amplification. The analysis is only done for the S- and Y-transects as storm surge propagation along the H-transect for the highest HWLs is affected by water entering the marsh over the low man-made dam in the eastern part of the marsh (see Figure 3.2). This makes the analysis of storm surge propagation along the H-transect more complex. To avoid miscellaneous results, the S5-S6 section is also excluded, because the direction of the flood wave propagation (i.e. direction of the water level gradient) for high overmarsh tides differs from the orientation of this channel section. Only overmarsh tides with HWLs of at least 0.4 m above mean platform elevation are included in the analysis. For these higher tides, large scale sheet flow over the marsh surface occurs in the model simulations, reducing the influence of flow routing through the channels on water level variations (Temmerman et al., 2005a, 2005b). Attenuation rates are calculated as the HWL difference along each section (i.e., S1-S2-...-S5 and Y1-Y2-...-Y5 sections) divided by the difference in distance from the front edge of the marsh between the beginning and end of each section (calculated as the bird's fly distance between the marsh edge and the along-channel locations). Various geometrical parameters, which relate the marsh geometry to the amount of friction exerted on the propagating storm tides, are computed for each section in an attempt to relate them to simulated attenuation rates. Geometrical parameters include mean channel width, mean cross-sectional area of the channel, mean channel depth, maximum channel depth, width and depth convergence length scales of the channel, mean platform elevation and an estimate for the ratio ( $\alpha_A$ ) between the vegetated surface area ( $A_{pl}$ ) and the total surface area ( $A_{ch}+A_{pl}$ ) along each channel section. These vegetated ( $A_{pl}$ ) and non-vegetated ( $A_{ch}$ ) surface areas are derived from vegetation maps for a 500 m wide band on both sides along the thalweg (corresponding to the minimum distance needed to include the marsh platform along the widest of the investigated channel sections) with GIS software (ArcGIS, version 10.1). This parameter is considered as a proxy for the ratio between marsh platform width and the total width of the channel and the platform, which is adopted from Van Rijn (2011) and used in **Chapter 2** to explain differences in attenuation rates between marsh channels with varying geometry. Ultimately, attenuation rates are for each tide



compared to the ratio between the water volume above the platform and the total water volume (i.e. above the channels and above the platform) present in each section ( $\alpha_v = V_{pl}/(V_{ch}+V_{pl})$ ).

### 3.3 Results

#### 3.3.1 Model Validation

To validate the model performance on the estuary scale, observed and modelled series of water levels are compared in Table 3.2, which also contains the mean error and average phase difference between the observed and modelled HWLs. Average phase differences near the study area (i.e. Bath and Baalhoek tidal stations, see Figure 3.1) are smaller than 5 minutes. Values for  $ME_{HWL}$  range from -0.04 to +0.01 m near the Saeftinghe marsh, where the tidal range is  $\sim 4.0$ -5.5 m. The model performance in the Saeftinghe marsh itself is validated by a comparison between modelled and observed tidal water level series at several measurement locations in the channel system and on the marsh platform (Table 3.3, see Figure 3.2 for measurement locations). Mean errors for the full series of simulated water levels vary between -0.02 m and -0.11 m, indicating that the water levels are slightly underestimated throughout the marsh system. HWLs at the marsh edge location (loc. 8) are simulated with a  $ME_{HWL}$  of -0.03 m and phase difference of -2 minutes, which is a similar accuracy as at the nearby tidal stations in the estuary (Table 3.2). Halfway along the main channel (loc. 10), HWLs are represented with a  $ME_{HWL}$  and  $\Delta\phi_{-HWL}$  of +0.02 m and -1.8 min respectively. At the inner marsh locations (loc. 1, 2 and 3), situated at the end of the main channel and narrower side-channels, values for  $ME_{HWL}$  range from 0.00 m to +0.05 m and average phase differences are 3.8 and 16 minutes respectively. It should be stated that the model validation for the locations on the platform is only based on a limited number of tides (i.e., two tides at loc. 5 and six tides at loc. 6).

**Table 3.2:** Comparison between observed and simulated series of tidal water levels along the estuary (see Fig. 1 for locations of the tidal stations), showing the distance from the estuary mouth ( $x$ ), mean error (ME), mean absolute error (MAE) and root mean squared error (RMSE), and comparison between observed and simulated HWLs, showing the  $ME_{HWL}$  and  $\Delta\phi_{-HWL}$ .

Tidal station	$x$ <i>km</i>	ME <i>m</i>	MAE <i>m</i>	RMSE <i>m</i>	$ME_{HWL}$ <i>m</i>	$\Delta\phi_{-HWL}$ <i>min</i>
<b>Vlissingen</b>	2	0.02	0.05	0.06	0.07	0.2
<b>Terneuzen</b>	24	-0.03	0.09	0.10	0.03	-2.1
<b>Hansweert</b>	42	-0.06	0.09	0.12	0.01	-8.5
<b>Baalhoek</b>	52	-0.06	0.07	0.09	-0.04	-2.7
<b>Bath</b>	61	-0.05	0.08	0.10	0.01	0.8
<b>Liefkenshoek</b>	74	-0.06	0.10	0.13	-0.01	3.8
<b>Antwerpen</b>	91	-0.09	0.13	0.16	-0.04	8.4

**Table 3.3:** Comparison between observed and simulated series of tidal water levels in the marsh (see Figure 2 for measurement locations), including mean error (ME), mean absolute error (MAE) and root mean squared error (RMSE), and for the HWLs specifically the mean error ( $ME_{HWL}$ ) and mean phase difference ( $\Delta\phi_{HWL}$ ).

Measurement location		ME	MAE	RMSE	$ME_{HWL}$	$\Delta\phi_{HWL}$
		<i>m</i>	<i>m</i>	<i>m</i>	<i>m</i>	<i>min</i>
<b>Loc. 8</b>	<i>marsh edge</i>	-0.11	0.11	0.12	-0.03	-2.0
<b>Loc. 10</b>	<i>main channel</i>	-0.08	0.12	0.14	0.02	-1.8
<b>Loc. 1</b>	<i>main channel</i>	-0.10	0.14	0.24	0.00	-3.5
<b>Loc. 2</b>	<i>side channel</i>	-0.07	0.16	0.21	0.05	-3.8
<b>Loc. 3</b>	<i>side channel</i>	-0.10	0.13	0.19	0.01	16
<b>Loc. 5</b>	<i>platform</i>	-0.02	0.06	0.07	-0.01	-20
<b>Loc. 6</b>	<i>platform</i>	-0.05	0.06	0.08	-0.02	0.0

Besides, water level variations during the two storm tides are fairly well represented. For the highest storm tide, during which no attenuation was present in the observations, the model results do not show any attenuation either. For the second highest storm tide, the model slightly underestimates the measured HWL reduction between locations 10 and 1 (i.e. -6.6 cm instead of -7.4 cm reduction). HWLs during the storm tides are generally underestimated throughout the domain of the model. At the study area, HWLs are underestimated by approximately 16 cm for this second highest storm tide, probably due to the absence of wind in the model schematization. During the high water slack of the highest storm tide, hourly averaged wind speeds of 8 to 11 m/s from a west- to northwest direction were present at the study area (data obtained from Royal Netherlands Meteorological Institute, <http://www.knmi.nl>). According to the basic formula for wind setup by Keulegan (1951), these wind speeds induce water level setup of several centimeters across the estuary channel and of around 5 cm (in WNW direction) locally in the marsh itself.

Furthermore, an artificial series of regular tides and storm tides (Figure 3.4) is simulated to compare amplification and attenuation rates ( $dHWL/dx$ ) for a wider range of HWLs than those of the measurements only (Figure 3.5). The water level observations show a tendency of slight amplification for tides with peak water levels below the marsh platform elevation. Once the platform gets inundated, attenuation starts to occur and attenuation rates increase up to a maximum of about 5 cm/km for inundation heights around 0.5-1.0 m, after which attenuation rates decrease again. Along the inner marsh sections (i.e., loc. 10 to loc. 1 and 3), this observed relation between attenuation rates and marsh flooding depth is captured by the model (Figure 3.5). In the outer marsh section (loc. 8 to loc. 10), the model predicts a slight amplification up to 1 cm/km for most tides while attenuation of up to 2 cm/km was observed. For undermarsh tides specifically, the model underestimates the observed amplification along the inner marsh

sections by 1 to 4 cm/km between loc. 1 and 3. Nevertheless, the model reproduces the dependency of the amount of attenuation or amplification on the HWL relative to the platform elevation, especially for overmarsh tides (Figure 3.5).

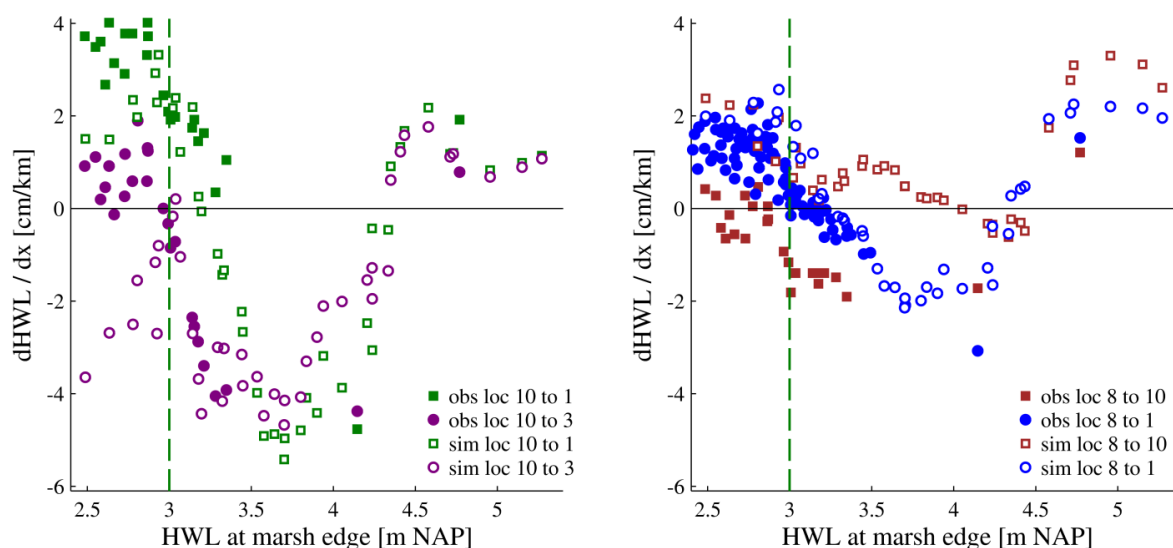


**Figure 3.5:** Observed (full markers) and modelled (open markers) attenuation and amplification rates from locations 10 to 3 (purple), 10 to 1 (green) (left graph) and 8 to 10 (brown) and 8 to 1 (blue) (right graph). The mean platform elevation is indicated by a dashed vertical green line.

### Sensitivity analysis

The impact of the velocity diffusivity coefficient ( $\nu$ ) and the Manning friction coefficient for unvegetated tidal flats and channels ( $n_f$ ) on the simulated tidal propagation through the intertidal channels of the Saefinghe marsh is briefly assessed by comparing the results of various calibration runs. In particular, Table 3.4 shows the impact of variations in  $\nu$  and Table 3.5 depicts the impact of variations in  $n_f$ , both relative to a reference simulation. This sensitivity analysis indicates that lower velocity diffusivity coefficients lead to a slightly faster propagation of HWLs through the marsh channels, while the HWLs themselves get somewhat higher towards the landward end of the marsh channel. Conversely, higher values of  $\nu$  lead to lower HWLs and slow down their propagation. The impact of variations in  $\nu$  on the MAE is limited if  $\nu$  is reduced. However, if its value is increased to 1.0 or 2.0  $\text{m}^2\cdot\text{s}^{-1}$ , the MAE increases and hence the overall representation of the tidal wave worsens a bit. Similarly, the effect of increased bottom friction coefficients in the intertidal channels is that the propagation of HWLs is increasingly slowed down for higher values of  $n_f$ . The impact on the HWLs themselves ranges from a negligible increase to a small decrease (i.e., for  $n_f = 0.03 \text{ s}\cdot\text{m}^{-1/3}$ ). Furthermore, higher values for  $n_f$  generally lead to a larger MAE, implying that the model performance gets less good if the friction coefficient in the channels is increased.

**Table 3.4:** Relative changes in mean absolute error ( $\Delta\text{MAE}$ ), average high water level ( $\Delta\text{HWL}$ ) and in the moment of high water ( $\Delta\text{T}_{\text{HW}}$ ) at the marsh edge (loc. 8) and the landward end of the main channel (loc. 1) for simulations with variable velocity diffusivity coefficients ( $\nu$ ) relative to the reference scenario with  $\nu = 0.5 \text{ m}^2\cdot\text{s}^{-1}$ ,  $n_f = 0.01 \text{ s}\cdot\text{m}^{-1/3}$  and  $n_v = 0.08 \text{ s}\cdot\text{m}^{-1/3}$ .

$\nu$ ( $\text{m}^2\cdot\text{s}^{-1}$ )	$\Delta\text{MAE}$ ( $\text{m}$ )		$\Delta\text{HWL}$ ( $\text{m}$ )		$\Delta\text{T}_{\text{HWL}}$ ( $\text{min}$ )	
	Loc. 8	Loc. 1	Loc. 8	Loc. 1	Loc. 8	Loc. 1
<b>0.01</b>	-0.003	-0.004	+0.013	+0.030	-0.3	-4.3
<b>0.1</b>	0.0	-0.008	+0.002	+0.013	0.0	-2.8
<b>0.5</b>	-	-	-	-	-	-
<b>1.0</b>	0.0	+0.026	-0.002	-0.017	+0.3	+4.0
<b>2.0</b>	+0.004	+0.076	-0.006	-0.058	0.0	+13.0

**Table 3.5:** Relative changes in mean absolute error ( $\Delta\text{MAE}$ ), average high water level ( $\Delta\text{HWL}$ ) and in the moment of high water ( $\Delta\text{T}_{\text{HW}}$ ) at the marsh edge (loc. 8) and the landward end of the main channel (loc. 1) for simulations with variable Manning friction coefficients for the unvegetated tidal channels ( $n_f$ ) relative to the reference scenario with  $\nu = 0.1 \text{ m}^2\cdot\text{s}^{-1}$ ,  $n_f = 0.01 \text{ s}\cdot\text{m}^{-1/3}$  and  $n_v = 0.08 \text{ s}\cdot\text{m}^{-1/3}$ .

$n_f$ ( $\text{s}\cdot\text{m}^{-1/3}$ )	$\Delta\text{MAE}$ ( $\text{m}$ )		$\Delta\text{HWL}$ ( $\text{m}$ )		$\Delta\text{T}_{\text{HWL}}$ ( $\text{min}$ )	
	Loc. 8	Loc. 1	Loc. 8	Loc. 1	Loc. 8	Loc. 1
<b>0.01</b>	-	-	-	-	-	-
<b>0.015</b>	+0.001	+0.019	0.0	+0.005	+0.6	+0.3
<b>0.02</b>	+0.003	+0.039	-0.002	+0.004	+0.9	+5.0
<b>0.03</b>	+0.014	+0.094	-0.009	-0.016	+0.6	+14.2

### 3.3.2 Model scenarios with varying marsh geometry and dike position

Along-channel water level variations ( $d\text{HWL}/dx$ ) are calculated for all geomorphological scenarios described in Table 3.1. When the variation of HWLs along the S-, Y- and H-channel sections is considered for the reference scenario (Run 0), distinct spatial differences in HWLs arise (Figure 3.6). Modelled HWLs of the 4 m storm tide increase from the marsh edge into the outer 1.5-3.0 kilometers of the S- and Y-transects and remain fairly constant along the outer part of the H-transect. Over the inner sections of the marsh channels (i.e., S3-S6, Y3-Y6, H3-H6), HWLs decrease again, resulting in a net attenuation along the full Y- and H-transects and negligible net changes along the full S-transect. Along the innermost part of the Y- and H-transects, HWLs do not decrease any further. This can be attributed to set up and reflection against the dike on the south side of the marsh. Furthermore, scenario analyses with varying platform and channel elevation show that attenuation rates along intertidal channels vary largely with marsh geomorphology. In these analyses attenuation rates are only given for the inner marsh sections (i.e. S3-S6 and Y3-Y6) as the focus is on attenuation of HWLs along marsh channels, rather than on the slight amplification along the outer sections where the influence of the marsh platform is small. Finally, spatial variations in attenuation or amplification of HWLs are assessed by comparing them with local geometrical characteristics of the marsh (Section 3.3.3).

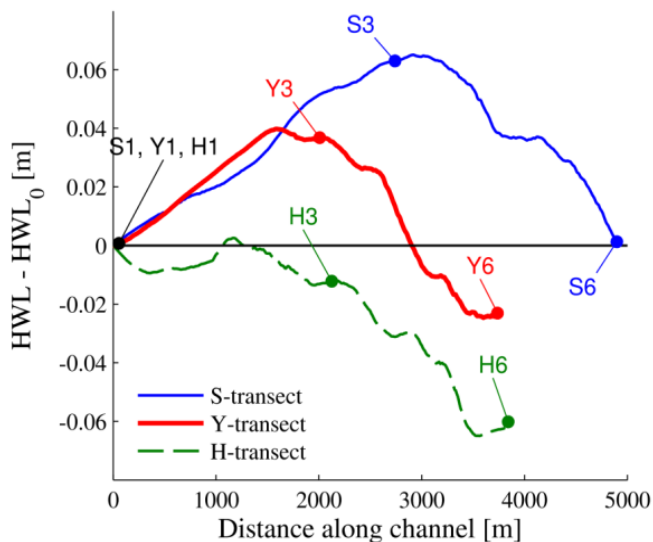


**Figure 3.6:** Variation in HWLs for a NAP +4.0 m storm tide along the S-, Y- and H-transects based on the reference scenario (Run 0). The distance along the channel is given from S1, Y1 and H1 respectively. HWLs are computed relative to the high water level at these marsh edge locations ( $HWL_0$ ).

#### Impact of dike position and marsh size

From a comparison between the reference simulation (Run 0 in Figure 3.7) and simulations in which the dike south of the marsh is repositioned and the marsh platform is extended by 1 km (Run 1 in Figure 3.7) and by 5 km (Run 2 in Figure 3.7), it becomes clear that attenuation rates are highly influenced by the dike position and hence the marsh size. If the dike is positioned too close to the seaward marsh edge, making the marsh extent shorter than a certain critical width (here smaller than 6 to 10 km of marshland), the highest tides and storm tides are not much attenuated or even slightly amplified (Figure 3.7e and 3.7f). The result of the simulation with the 1 km extended platform indicates that even a small strip of additional marsh platform area can significantly improve the storm surge attenuation capacity of a marsh. While HWLs of around 1.5 m above platform elevation are not attenuated at all in the reference simulation, a platform extension of 1 km leads to maximum attenuation rates of 7 cm/km along the S3-S6 section and of over 10 cm/km along the Y3-Y6 section. Similar to the reference scenario, attenuation rates in the simulation with 1 km platform extension decrease again and turn into amplification for even higher storm tides (i.e., > 2 m above platform elevation). The results of the simulation with the 5 km extended platform do not show this strong decrease in attenuation rates for the highest HWLs. Instead, attenuation rates remain similar or appear to decrease slightly for the highest storm tides.

#### Impact of channel depth

The model results show that deeper marsh channels result in lower attenuation rates compared to the reference scenario, while shallower marsh channels lead to an increase in attenuation rates. In particular, maximum attenuation rates along the Y3-Y6 transect change from 6 cm/km for the reference simulation (Run 0 in Figure 3.7b) to 4 cm/km for a simulation in which the channel elevation is lowered by 0.9 m (Run 3 in Figure 3.7b) or increase to 10 cm/km for the simulation in which the channel elevation is raised by 0.7 m on average (Run 4 in Figure 3.7b). Maximum attenuation rates along the S3-S6 transect are around 2.5 cm/km, 4 cm/km and 7 cm/km for the simulations with a lowered channel elevation (Run 3), the reference simulation (Run 0) and the simulation

with increased channel elevation (Run 4) respectively (Figure 3.7a). The general trend of increased attenuation rates for overmarsh tides up until a certain maximum and decreasing attenuation or even amplification for the highest storm tides is persistent for all scenarios with varying channel elevations.

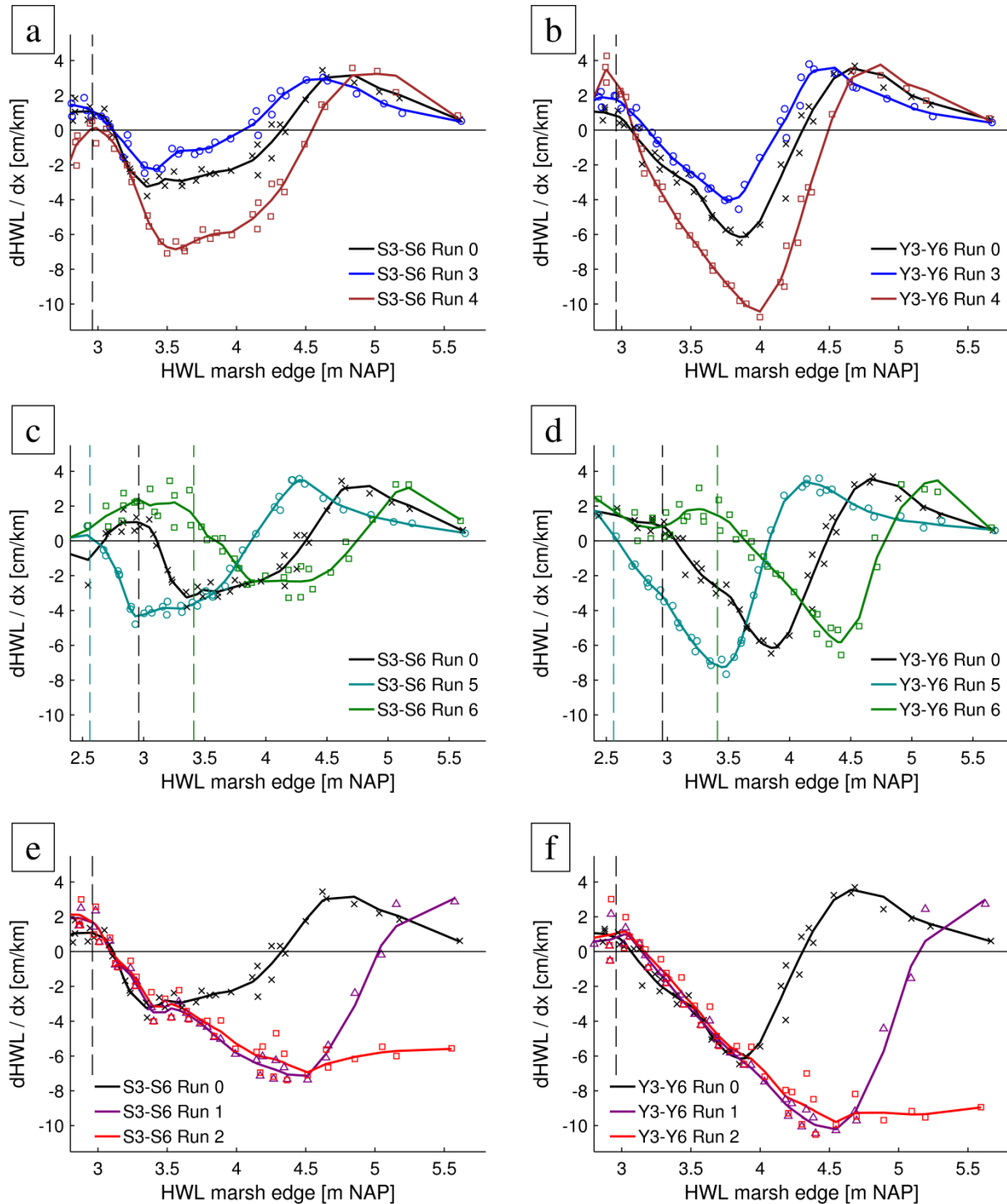


**Figure 3.7:** Modelled attenuation and amplification rates of tides with different high water levels for scenarios in which the channel elevation is varied (top), scenarios in which the platform elevation is varied (mid) and scenarios in which the dike is moved landward and the marsh platform is extended by 1 km or 5 km (bottom) over the S3-S6 (left) and Y3-Y6 transect (right) (see Fig. 3.2 for transect locations). The model scenarios are explained in Table 3.1. Each marker represents an individual tide and the lines represent the moving average. The mean platform elevations for the different scenarios are indicated with dashed vertical lines.

Impact of platform elevation

Model results show that the elevation of the marsh platform determines the range of HWLs for which attenuation takes place (Figure 3.7c and 3.7d). In all scenarios with varying platform elevations, attenuation only occurs for overmarsh tides that inundate the marsh platform up to about 1.2 m. On the other hand, undermarsh tides with HWLs below the marsh platform elevation are not attenuated in the model results. Modelled attenuation rates are highest for overmarsh tides that are approximately 0.5 to 1.0 m above the mean marsh platform elevation. For higher tides, attenuation rates are decreasing or changing into amplification, which is shown to be the result of blockage by the dike behind the marsh area (Figure 3.7e and 3.7f). Maximum attenuation rates are all within the range of 6.5 to 7.5 cm/km along the Y3-Y6 transect for simulations in which platform elevations have been either lowered (Run 5 in Figure 3.7d) or raised (Run 6 in Figure 3.7d) by 0.4m. Along the S3-S6 transect, maximum attenuation rates are lower; ranging from 3.5 to 5 cm/km.

Relations between attenuation rates and marsh geometry

For storm tides with HWLs of at least 0.4 m above mean platform elevation, a correlation can be found between the simulated attenuation rates ( $dHWL/dx$ ) and the ratio ( $\alpha_v$ ) between the water volume on the vegetated platform and the total water volume on the marsh platform and in the channels ( $r^2 = 0.92$  and  $p < 0.001$ , see Figure 3.8):

$$dHWL/dx = -36.2 * \alpha_v + 8.0 \quad (3.9)$$

The relationship is based on Run 2, in which the marsh platform is extended to avoid the influence of blockage against the dikes on the modelled water level variations. Attenuation starts to occur when  $\alpha_v$  exceeds 0.2-0.4 and increases gradually from there on. As  $\alpha_v$  is dependent on marsh geometry and the height of the flood wave, this correlation explains both spatial variations (between marsh sections) and temporal variations (between tides with different HWLs) in attenuation rates. The highest computed attenuation rates are up to 29 cm/km over the Y5-Y6 channel section. Attenuation does not occur for any of the simulated storm tides along the outer marsh sections S1-S2-S3 and Y1-Y2-Y3. Sensitivity analyses show that the coefficients in Eq. 3.9 alter if the bottom friction on the marsh platform is changed. In particular, if  $n_v$  for the vegetated platform is lowered to  $0.04 \text{ s}\cdot\text{m}^{-1/3}$ , Eq. 3.9 changes to  $dHWL/dx = -27.2*\alpha_v + 6.2$  ( $r^2 = 0.86$  and  $p < 0.001$ ) and the maximum modelled attenuation decreases to 23 cm/km. Conversely, if  $n_v$  increases to  $0.12 \text{ s}\cdot\text{m}^{-1/3}$ , Eq. 3.9 changes to  $dHWL/dx = -41.1*\alpha_v + 9.2$  ( $r^2 = 0.92$  and  $p < 0.001$ ), while the maximum attenuation increases to 32 cm/km.

Other cross-sectional geometrical properties such as width and depth convergence length scales, channel width, the water depth in the channel or on the platform, total cross-sectional area or the ratio between water depth on the platform and in the channels could not be related to the modelled attenuation rates and are therefore not shown. Only the tide-independent ratio between the platform surface area and the total surface area of the channel and adjacent platform ( $\alpha_A$ ) can be used to explain differences in maximum attenuation rates between different channel sections (Figure 3.9).

Attenuation only occurs along relatively small channels where  $\alpha_A$  is larger than 0.5. From there, maximum attenuation rates are increasing with increasing values for  $\alpha_A$ . Conversely, amplification is persistent for all tides along channel sections with  $\alpha_A$  below 0.5, except for the slight attenuation for some tides along the Y2-Y3 section. However,  $\alpha_A$  does not account for variations in attenuation rates between different tides with varying HWLs.

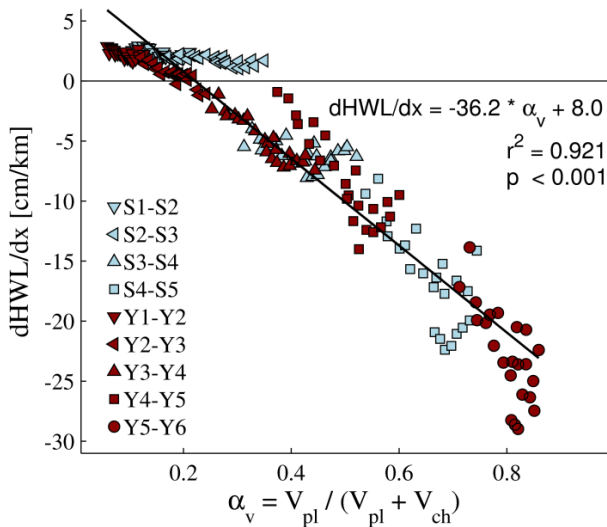


**Figure 3.8:** HWL reduction rates along channel sections in the S- (light blue) and Y- (dark red) transect for Run 2 plotted against the ratio between water volume above the platform and the total water volume ( $\alpha_v$ ). These water volumes are computed above the vegetated and non-vegetated surface areas in a strip of 500 m around each channel section.

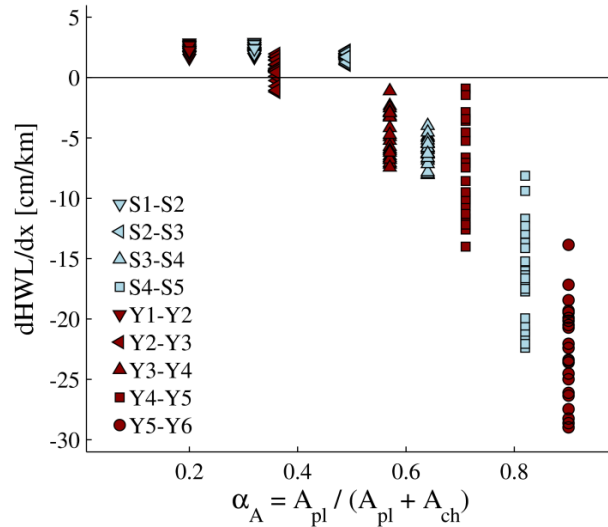


**Figure 3.9:** HWL reduction rates along the S- (light blue) and Y- (dark red) transects for Run 2 plotted against the ratio between platform surface area and total surface area ( $\alpha_A$ ), calculated based on the vegetated and non-vegetated surface area in a strip of 500 m around each channel section.

### 3.4 Discussion

#### 3.4.1 Model performance

The hydrodynamic model that is used to compute HWL attenuation rates across marshes represents observed water level variations (**Chapter 2**) along intertidal marsh channels over a distance of several kilometers fairly well (Table 3.3). The model results capture the observed dependency of attenuation rates on the HWL relative to the platform elevation (Figure 3.5). In particular, modelled attenuation rates increase (or amplification rates decrease) as HWLs increase above the platform elevation up until a maximum for HWLs of around 0.7-0.8 m above platform elevation, from which attenuation rates decrease (or amplification rates increase) again. The model also captures observed attenuation and amplification rates for overmarsh tides along the inner marsh sections (i.e., loc. 10 to 1 and 3) where attenuation is strongest and on which the main conclusions of this study are based. Nevertheless, some discrepancy between the model results and the observations exists. Firstly, the model underestimates observed attenuation in the outer part of the channel where slight



amplification is predicted for most overmarsh tides. This suggests that bottom friction applied in the model along this section is too low to simulate the observed dampening of the tidal wave (Friedrichs and Aubrey, 1994; Van Rijn, 2011). Bottom friction along the outer part of the marsh channel could indeed be higher in reality due to the presence of coarser (sandy) sediments (Jongepier et al., 2015) and large bed forms (Huijs, 1995), which may be the result of higher flow velocities in the deeper and wider outer channel parts as compared to the shallower and smaller inner channel parts. Results from the model calibration show that attenuation along this section increases if a higher Manning coefficient is applied. Hence, spatially varying Manning coefficients (i.e., higher in the outer than in the inner channel parts) could improve the overall model performance. However, it would reduce the generic character of our model scenarios and conclusions on the effect of marsh channel and platform geometry, as differences in attenuation rates between the scenarios could then be attributed to spatial differences in channel bed friction, instead of solely differences in marsh channel geometry and platform extent. A second discrepancy is the underestimation of observed amplification by 1 to 4 cm/km for undermarsh tides along the narrowest inner marsh section (i.e., loc. 10 to 3) by the model. This could be due to limitations in the resolution of the bathymetry data and of the mesh itself, which causes some deeper parts of the channels to be missing or smoothed out in the model bathymetry, especially affecting lower tides (i.e., due to the inverse relationship between water depth and bottom friction). Despite the above-discussed discrepancies between observed and modelled attenuation for the outer marsh sections and for undermarsh tides, we emphasize that the conclusions of our study are based on the model results for overmarsh tides along the inner marsh sections, where observations are indeed well reproduced by the model.

#### ***3.4.2 Effect of marsh size and dike position***

One important finding of this study is that limitations in storage area or marsh extent have a considerable impact on storm surge attenuation and may drastically reduce attenuation rates (Figure 3.7e and 3.7f). Storage area limitations can be caused by the blockage or reflection against a dike or similar structure confining the marsh surface area (Wamsley et al., 2010, 2009) and prevent a marsh from reaching its full attenuation capacity. This mechanism was hypothesized by Resio and Westerink (2008), who argued that attenuation rates decrease if the duration of the hydrodynamic forcing is long compared to the time needed to fill the available storage area. In that case, the propagating flood wave is blocked or reflected before HWLs reach the end of a basin or marsh platform, leading to higher HWLs at the landward end of the marsh and hence lower attenuation rates. Moreover, attenuation rates can even be minimized or amplification of HWLs can occur, as is the case for the highest storm tides in the reference simulation and the simulation in which the dike is moved landward by 1 km (Figure 3.7). The simulation in which the platform is extended much further by 5 km does not show a drastic decrease in attenuation rates for higher overmarsh storm tides. In that simulation, the propagating peak of the tidal wave has not yet reached the dike behind the marsh before the ebb tide starts and water levels decrease again. Therefore, storage area limitations do not affect HWL reduction in the studied marsh section in this

simulation. Sensitivity of storm surge reduction to limitations in storage area relative to the duration of the hydrodynamic forcing implies that the duration of a storm surge or flood wave affects storm surge reduction rates across a given wetland (Hu et al., 2015; Liu et al., 2013; Resio and Westerink, 2008). In this context it should be mentioned that only tidal waves with a more or less constant period are considered in this study. In micro-tidal cases however, faster moving storms cause flood waves with a shorter duration and are found to result in higher storm surge reduction rates than slower moving storms with longer flood wave durations (Hu et al., 2015; Liu et al., 2013; Sheng et al., 2012; Zhang et al., 2012).

Following the reasoning of Resio and Westerink (2008), we hypothesize that a minimum wetland size exists for which the attenuation capacity of the area is fully used and is not anymore affected by blockage effects against dikes of other structures behind the marsh. This minimum wetland size would depend on the duration of the flood wave and on site-specific variables that affect the landward propagation of the flood wave, such as the presence and size of channels and friction exerted by the vegetation. Based on the present model results for storm tides only, the minimum extent of the studied marsh should be between 6 and 10 km to completely avoid blockage effects for the highest modelled storm tides and to optimize the attenuation capacity of the marsh. It must be stated however that the extended part of the marsh is rather schematically implemented and does not contain any channels. In reality, a larger marsh area would yield larger channels in the existing part of the marsh due to the relation between channel size and tidal prism or drainage volume (D'Alpaos et al., 2010; Vandenbruwaene et al., 2015), while a channel network would develop in the extended marshland as well. However, our model assessments consist solely of hydrodynamic modelling and do not include morphodynamic feedbacks or sediment transport. The present schematization of the marsh extension could rather be seen as supra-tidal marshland. Because of these limitations in the model schematization and the dependency on event-specific variables, a general definition of this minimum wetland size cannot readily be evaluated with the present model results.

### **3.4.3 Influence of marsh geometry**

The model results show that the depth of marsh channels affects the amount of HWL reduction (Figure 3.7a and 3.7b). Deeper channels exert less friction and lead to a reduction of marsh scale attenuation rates, while shallow marsh channels exert more friction and increase marsh scale attenuation rates. Nevertheless, the model results did not reveal a distinct relationship between the water depth in the channel and the attenuation rate that holds for tides with varying HWLs. These results are consistent with findings of existing numerical studies (Loder et al., 2009; Temmerman et al., 2012) and can be explained by the inverse relationship between channel depth and bottom friction exerted on the flow. If local surge generation would be of importance, marsh channel depth could have a contrasting effect on  $dHWL/dx$  as surge generation decreases with increasing depth (Rego and Li, 2009; Resio and Westerink, 2008). In our study, surge generation occurs outside the model domain and surge height is incorporated as boundary condition for the model.

In contrast to channel depth, the marsh platform elevation barely affects the maximum attenuation rate along marsh sections. Platform elevation is however an indicator for the range of tides that are attenuated and which tides are most heavily damped (Figure 3.7c and 3.7d). Undermarsh tides with HWLs below marsh platform elevation and, which only flood the marsh channel network, are not attenuated or are even slightly amplified. Overmarsh tides that also inundate the vegetated marsh platform are increasingly attenuated for higher HWLs, as long as limitations in storage area are not considered. These findings are in accordance with the observations in **Chapter 2** on which the model is based. Furthermore, the model results indicate that marshes with a lower platform elevation induce the highest attenuation rates for relatively low inundation events compared to marshes with a higher platform elevation (i.e., as long as the limitation in storage area due to confinement by the dikes does not affect the HWL reduction) (see Figure 3.7c and 3.7d, HWLs between 2.5 m and 3.5 m). As limitations in storage area reduce attenuation rates on the lower marsh for increasing HWLs, the higher marsh becomes more effective. If the platform elevation is higher, blockage effects only start to affect attenuation rates for higher HWLs. This can be attributed to slower flood wave propagation on higher marsh platforms due to smaller water depths. A greater effectiveness of high marshes in a confined system was also found by Wamsley et al. (2009). Moreover, Loder et al. (2009) found that for high platform elevations smaller surge events are generally attenuated, while larger surge events are amplified. Our results are consistent with these findings and show as well that decreased attenuation rates or amplification for larger surge events can be due to set up against dikes confining the marsh, especially if such larger surge events have a longer duration.

#### ***3.4.4 Relationship between marsh geometry, peak water levels and attenuation rates***

As attenuation rates vary temporally between flood events and spatially between marsh sections, parameters solely based on marsh geometry, such as the ratio  $\alpha_A$  between platform surface area and total surface area, can only explain spatial variations in attenuation rates for single flood events. However, they do not explain variations in attenuation rates between tides with different HWLs (Figure 3.9), implying that a tide-varying parameter is needed. The present model results provide for a relation between along channel variations in HWLs and the tide-varying ratio  $\alpha_v$  between water volume on the vegetated platform and the total water volume (Eq. 3.9). This relationship combines geometrical and hydrodynamic variations (both present in  $\alpha_v$ ) to explain differences in attenuation rates (Figure 3.8). The relationship applies only to a situation without confinement by dikes or other structures, as it is based on the model simulation with the extended marsh platform (i.e., Run 2 in Table 3.1). Moreover, we assume that large-scale sheet flow occurs over the marsh platform, implying that flow routing through the channel network does not affect attenuation rates. Previous studies showed that this is the case for tides with HWLs above the canopy height of the vegetation (Temmerman et al., 2005a, 2005b; Vandenbruwaene et al., 2015), which is around 0.4 m for the most abundant species in our study area. Although the vegetation stem height is not explicitly implemented in the model, Eq. 3.9 is also based on storm tides with HWLs

that are at least 0.4 m above the mean platform elevation for which sheet flow over the marsh platform actually occurs in the model simulations. The coefficients in Eq. 3.9 likely vary with site-specific parameters such as vegetation-type and bottom roughness. In this study, a constant Manning's coefficient of  $n = 0.08 \text{ s}\cdot\text{m}^{-1/3}$  is used to implement the additional friction and drag force exerted by the marsh vegetation. More dense vegetation such as mangrove forests would exert higher friction and drag forces on the flow, leading to higher attenuation rates (e.g., Krauss et al., 2009) and hence a different relationship between  $\alpha_v$  and  $dH_{HWL}/dx$ . A sensitivity analysis with model simulations in which the Manning coefficient of the vegetated marsh platform is altered indicates that Eq. 3.9 indeed varies for different friction coefficients. The flood wave period will also affect attenuation rates (e.g., Sheng et al., 2012; Zhang et al., 2012) and hence the relationship described above. Hypothetically, similar relationships could be found for different wetland types (i.e., different friction coefficients) and for flood waves with a different duration, ranging from tidal inundation events as described in this study to long flood waves caused by large cyclones or hurricanes. Further research is necessary to test this hypothesis and possibly find relationships between attenuation rates, HWLs and marsh geometry for various wetland types and storm surge durations. Nonetheless, the present model results are potentially applicable to attenuation of storm tides in other marshes with similar characteristics (i.e., macrotidal marshes which are dominated by flexible wetland grasses). In reality, marsh channel and platform elevations may vary between marsh sites (due to differences in tidal range or sediment availability) or may change over time (due to long-term morphological development or changing hydrodynamic conditions). Our model scenarios with varying marsh size and different marsh channel and platform elevations contribute to fundamental insights on how flood attenuation rates vary with such space- and time-dependent marsh geomorphological properties. Therefore, the presented results are of interest to coastal managers that want to implement wetlands or marshes as part of their coastal defense structures or coastal managers and scientists who want to examine the coastal defense capacity of existing marshes.

### 3.5 References

- Baptist, M.J., Babovic, V., Rodríguez Uthurburu, J., Keijzer, M., Uittenbogaard, R.E., Mynett, A., Verwey, A., 2007. On inducing equations for vegetation resistance. *J. Hydraul. Res.* 45, 435–450.
- Barbier, E.B., 2014. A global strategy for protecting vulnerable coastal populations. *Science* (80-. ). 345, 1250–1251. doi:10.1126/science.1254629
- Cheong, S.-M., Silliman, B., Wong, P.P., van Wesenbeeck, B., Kim, C.-K., Guannel, G., 2013. Coastal adaptation with ecological engineering. *Nat. Clim. Chang.* 3, 787–791. doi:10.1038/nclimate1854
- D'Alpaos, A., Lanzoni, S., Marani, M., Rinaldo, A., 2010. On the tidal prism-channel area relations. *J. Geophys. Res. Earth Surf.* 115, 1–13. doi:10.1029/2008JF001243
- Friedrichs, C.T., Aubrey, D.G., 1994. Tidal propagation in strongly convergent channels. *J. Geophys. Res.* 99, 3321–3336. doi:10.1029/93JC03219
- Gedan, K.B., Kirwan, M.L., Wolanski, E., Barbier, E.B., Silliman, B.R., 2010. The present and future role of coastal wetland vegetation in protecting shorelines: Answering recent challenges to the paradigm. *Clim. Change* 106, 7–29. doi:10.1007/s10584-010-0003-7

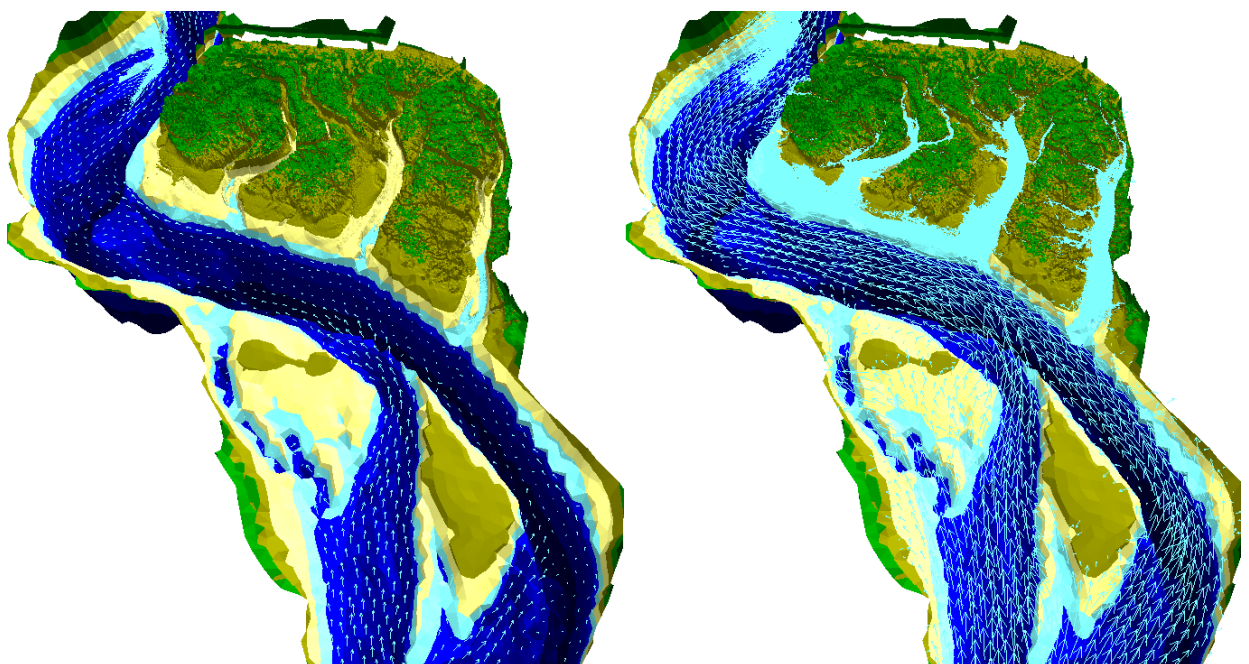
- Hervouet, J.-M., 2007. Hydrodynamics of Free Surface Flows: Modelling with the finite element method. doi:10.1002/9780470319628
- Hinkel, J., Lincke, D., Vafeidis, A.T., Perrette, M., Nicholls, R.J., Tol, R.S.J., Marzeion, B., Fettweis, X., Ionescu, C., Levermann, A., 2014. Coastal flood damage and adaptation costs under 21st century sea-level rise. *Proc. Natl. Acad. Sci. U. S. A.* 111, 3292–7. doi:10.1073/pnas.1222469111
- Hu, K., Chen, Q., Wang, H., 2015. A numerical study of vegetation impact on reducing storm surge by wetlands in a semi-enclosed estuary. *Coast. Eng.* 95, 66–76. doi:10.1016/j.coastaleng.2014.09.008
- Huijs, S., 1995. Geomorfologische ontwikkeling van het intergetijdgebied in de Westerschelde 1935-1989. Middelburg, The Netherlands.
- Jones, H.P., Hole, D.G., Zavaleta, E.S., 2012. Harnessing nature to help people adapt to climate change. *Nat. Clim. Chang.* 2, 504–509. doi:10.1038/nclimate1463
- Jongepier, I., Wang, C., Missiaen, T., Soens, T., Temmerman, S., 2015. Intertidal landscape response time to dike breaching and stepwise re-embankment: A combined historical and geomorphological study. *Geomorphology* 236, 64–78. doi:10.1016/j.geomorph.2015.02.012
- Krauss, K.W., Doyle, T.W., Doyle, T.J., Swarzenski, C.M., From, A.S., Day, R.H., Conner, W.H., 2009. Water level observations in mangrove swamps during two hurricanes in Florida. *Wetlands* 29, 142–149. doi:10.1672/07-232.1
- Kundzewicz, Z.W., Kanae, S., Seneviratne, S.I., Handmer, J., Nicholls, N., Peduzzi, P., Mechler, R., Bouwer, L.M., Arnell, N., Mach, K., Muir-Wood, R., Brakenridge, G.R., Kron, W., Benito, G., Honda, Y., Takahashi, K., Sherstyukov, B., 2014. Flood risk and climate change: global and regional perspectives. *Hydrol. Sci. J.* 59, 1–28. doi:10.1080/02626667.2013.857411
- Liu, H., Zhang, K., Li, Y., Xie, L., 2013. Numerical study of the sensitivity of mangroves in reducing storm surge and flooding to hurricane characteristics in southern Florida. *Cont. Shelf Res.* 64, 51–65. doi:10.1016/j.csr.2013.05.015
- Loder, N.M., Irish, J.L., Cialone, M.A., Wamsley, T.V., 2009. Sensitivity of hurricane surge to morphological parameters of coastal wetlands. *Estuar. Coast. Shelf Sci.* 84, 625–636. doi:10.1016/j.ecss.2009.07.036
- Lovelace, J.K., 1994. Storm-tide elevations produced by Hurricane Andrew along the Louisiana coast, August 25-27, 1992. Open File Report 94-371. Baton Rouge, LA, U.S.
- McGee, B.B.D., Goree, B.B., Tollett, R.W., Woodward, B.K., Kress, W.H., 2006. Hurricane Rita Surge Data, Southwestern Louisiana and Southeastern Texas, September to November 2005. U.S. Geological Survey Data Series 220.
- McIvor, A., Spencer, T., Möller, I., Spalding, M., 2012. Storm surge reduction by mangroves. *Natural Coastal Protection Series: Report 2*, Cambridge Coastal Research Unit Working Paper 41.
- Möller, I., Kudella, M., Rupprecht, F., Spencer, T., Paul, M., van Wesenbeeck, B.K., Wolters, G., Jensen, K., Bouma, T.J., Miranda-Lange, M., Schimmels, S., 2014. Wave attenuation over coastal salt marshes under storm surge conditions. *Nat. Geosci.* 7, 727–731. doi:10.1038/ngeo2251
- Möller, I., Spencer, T., French, Leggett, D., Dixon, M., 1999. Wave transformation over salt marshes: A field and numerical modelling study from north Norfolk, England. *Estuar. Coast. Mar. Sci.* 49, 411–426. doi:10.1006/ecss.1999.0509
- Nicholls, R.J., Cazenave, A., 2010. Sea-level rise and its impact on coastal zones. *Science* 328, 1517–1520. doi:10.1126/science.1185782
- Rego, J.L., Li, C., 2009. On the importance of the forward speed of hurricanes in storm surge forecasting: A numerical study. *Geophys. Res. Lett.* 36. doi:10.1029/2008GL036953
- Reitsma, J.M., 2006. Vegetatiekartering van de Westerschelde 2004-2005 op basis van false colour-luchtfoto's 1:5000 / 1:10.000. Delft, The Netherlands.
- Resio, D.T., Westerink, J.J., 2008. Modelling the physics of storm surges. *Phys. Today* 61, 33–38. doi:10.1063/1.2982120
- Sheng, Y.P., Lapetina, A., Ma, G., 2012. The reduction of storm surge by vegetation canopies: Three-dimensional simulations. *Geophys. Res. Lett.* 39, 1–5. doi:10.1029/2012GL053577
- Shepard, C.C., Crain, C.M., Beck, M.W., 2011. The protective role of coastal marshes: a systematic review and meta-analysis. *PLoS One* 6, e27374. doi:10.1371/journal.pone.0027374
- Smolders, S., Plancke, Y., Ides, S., Meire, P., Temmerman, S., 2015. Role of intertidal wetlands for tidal and storm tide attenuation along a confined estuary: A model study. *Nat. Hazards Earth Syst. Sci.* 15, 1659–1675. doi:10.5194/nhess-15-1659-2015
- Sutton-Grier, A.E., Wowk, K., Bamford, H., 2015. Future of our coasts: The potential for natural and hybrid infrastructure to enhance the resilience of our coastal communities, economies and ecosystems. *Environ. Sci. Policy* 51, 137–148. doi:10.1016/j.envsci.2015.04.006

- Temmerman, S., Bouma, T.J., Govers, G., Lauwaet, D., 2005a. Flow paths of water and sediment in a tidal marsh: Relations with marsh developmental stage and tidal inundation height. *Estuaries* 28, 338–352. doi:10.1007/BF02693917
- Temmerman, S., Bouma, T.J., Govers, G., Wang, Z.B., De Vries, M.B., Herman, P.M.J., 2005b. Impact of vegetation on flow routing and sedimentation patterns: Three-dimensional modelling for a tidal marsh. *J. Geophys. Res.* 110, F04019. doi:10.1029/2005JF000301
- Temmerman, S., De Vries, M.B., Bouma, T.J., 2012. Coastal marsh die-off and reduced attenuation of coastal floods: A model analysis. *Glob. Planet. Change* 92-93, 267–274. doi:10.1016/j.gloplacha.2012.06.001
- Temmerman, S., Kirwan, M.L., 2015. Building land with a rising sea. *Science* (80-. ). 349, 588–589. doi:10.1126/science.aac8312
- Temmerman, S., Meire, P., Bouma, T.J., Herman, P.M.J., Ysebaert, T., De Vriend, H.J., 2013. Ecosystem-based coastal defence in the face of global change. *Nature* 504, 79–83. doi:10.1038/nature12859
- Van der Molen, J., 1997. Tidal distortion and spatial differences in surface flooding characteristics in a salt marsh: Implications for sea-level reconstruction. *Estuar. Coast. Shelf Sci.* 45, 221–233. doi:10.1006/ecss.1997.0179
- Van Rijn, L.C., 2011. Analytical and numerical analysis of tides and salinities in estuaries; part I: tidal wave propagation in convergent estuaries. *Ocean Dyn.* 61, 1719–1741. doi:10.1007/s10236-011-0453-0
- Vandenbruwaene, W., Schwarz, C., Bouma, T.J., Meire, P., Temmerman, S., 2015. Landscape-scale flow patterns over a vegetated tidal marsh and an unvegetated tidal flat: implications for the landform properties of the intertidal floodplain. *Geomorphology* 231, 40–52. doi:10.1016/j.geomorph.2014.11.020
- Vanlierde, E., Ferket, B., Michielsens, S., Vereycken, K., Van Hoestenbergh, T., Levy, Y., Plancke, Y., Deschamps, M., Verwaest, T., Mostaert, F., 2014. MONEOS - jaarboek monitoring WL 2013: Factual data rapportage van monitoring hydrodynamiek en fysische parameters zoals gemeten door WL in het Zeescheldebekken in 2013. Versie 4.0. WL Rapporten, 12\_070. Antwerpen.
- Wamsley, T. V., Cialone, M. a., Smith, J.M., Atkinson, J.H., Rosati, J.D., 2010. The potential of wetlands in reducing storm surge. *Ocean Eng.* 37, 59–68. doi:10.1016/j.oceaneng.2009.07.018
- Wamsley, T. V., Cialone, M. a., Smith, J.M., Ebersole, B. a., Grzegorzewski, A.S., 2009. Influence of landscape restoration and degradation on storm surge and waves in Southern Louisiana. *Nat. Hazards* 51, 207–224. doi:10.1007/s11069-009-9378-z
- Wang, C., Temmerman, S., 2013. Does biogeomorphic feedback lead to abrupt shifts between alternative landscape states?: An empirical study on intertidal flats and marshes. *J. Geophys. Res.* 118, 229–240. doi:10.1029/2012JF002474
- Weisberg, R., Zheng, L., 2006. Hurricane Storm Surge Simulations for Tampa Bay. *Estuaries and Coasts* 29, 899–913. doi:10.1007/BF02798649
- Woodruff, J.D., Irish, J.L., Camargo, S.J., 2013. Coastal flooding by tropical cyclones and sea-level rise. *Nature* 504, 44–52. doi:10.1038/nature12855
- Zhang, K., Liu, H., Li, Y., Xu, H., Shen, J., Rhome, J., Smith, T.J., 2012. The role of mangroves in attenuating storm surges. *Estuar. Coast. Shelf Sci.* 102-103, 11–23. doi:10.1016/j.ecss.2012.02.021

# Chapter 4

## Changing tidal hydrodynamics during different stages of eco-geomorphological development of a tidal marsh: a numerical modelling study

J. Stark, P. Meire and S. Temmerman



### **Abstract**

*The eco-geomorphological development of tidal marshes, from initially low-elevated bare tidal flats up to a high-elevated marsh and its typical network of channels and creeks, induces long-term changes in tidal hydrodynamics in a marsh, which will have feedback effects on the marsh development. Here we study tidal hydrodynamics and tidal asymmetry in particular along marsh channels during different stages of eco-geomorphological development, including vegetation establishment, vertical platform growth and changes in channel geometry. A validated two-dimensional hydrodynamic model of the 3000 ha Saeftinghe marsh (The Netherlands) is used to simulate several eco-geomorphological scenarios covering different stages of marsh development that have been observed here over the past 80 years. Tidal asymmetry is quantified along a 4 km marsh channel by (1) the difference in peak flood and peak ebb velocities, (2) the ratio between duration of the rising tide and the falling tide and (3) a proxy for residual sediment transport based on the dimensionless bed shear stress. Although spatial variations in tidal asymmetry are large and the different indicators for tidal asymmetry do not always respond similarly to eco-geomorphological changes, some general trends can be obtained from the model results. Flood-dominance prevails during the initial bare stage of the low-lying tidal flat. Vegetation establishment and rapid platform expansion lead to marsh-scale flow concentration to the bare channels, causing an increase in tidal prism along with a less flood-dominant asymmetry of the tide. The decrease in flood-dominance continues as the platform grows vertically and the sediment-demand of the platform decreases. However, as the marsh elevation gets higher in the tidal frame and close to mean high water level, the tidal discharge in the channels decreases again and tidal asymmetry becomes more flood-dominant, indicating an infilling of the marsh channels. If the channel size becomes too small, the model results suggest that hydro-morphodynamic feedbacks based on tidal prism to channel cross-sectional area relationships keep the marsh channels from filling in completely by enhancing ebb-dominance as long as the tidal volume and flow velocities remain sufficiently high. Overall, this study increases insight of the hydro-morphodynamic interactions between tidal flow and marsh geomorphology during various stages of eco-geomorphological development of marshes and marsh channels in particular.*



## 4.1 Introduction

Tidal marshes occur along estuaries and coasts in temperate zones, on sheltered shores where tidal currents and wave forces are relatively weak (Allen, 2000). They form a unique habitat and are highly valuable (Barbier et al., 2013) as their ecological functioning provides benefits to society such as improvement of water quality (e.g., Mitsch et al., 2012), carbon sequestration (e.g., McLeod, 2011; Mitsch et al., 2013; Ouyang and Lee, 2014) and flood and shoreline erosion protection (e.g., **Chapter 3**; Gedan et al., 2010; Spalding et al., 2014; Temmerman and Kirwan, 2015; Temmerman et al., 2013). The sustainability of tidal marshes and their valuable functions is however under pressure by among others sea level rise and anthropogenic impacts (Kirwan and Megonigal, 2013; Kirwan et al., 2016). A key aspect for the functioning and sustainability of tidal marshes are the fluxes of water and the physical, chemical and biological materials it contains (i.e., sediments, nutrients, pollutants, seeds, larvae, plankton, etc.) through tidal channels that connect marshes with the adjacent estuary or sea. The degree of tidal asymmetry in the channels, which describes the difference in magnitude and duration of flood and ebb fluxes, is thereby determining whether marsh systems are a net sink (import) or source (export) of these materials (e.g. Fagherazzi et al., 2013; French and Stoddart, 1992; Friedrichs and Perry, 2001). Moreover, a flood or ebb dominant asymmetry respectively generates net sediment import or export and ultimately determines the marshes' ability to build up sediments and hence to sustain themselves in balance with sea level rise or not (e.g. Ganju et al., 2015, 2013; Reed, 2002).

In general it is known that the tidal wave is distorted as it propagates through shallow channels due to processes including bottom friction, channel convergence and advective inertia (e.g. Aubrey and Speer, 1985; Friedrichs and Aubrey, 1988; Parker, 1984; Speer and Aubrey, 1985; Wang et al., 1999). Changes in the shape of the tidal wave can be quantified and analyzed by variations in tidal asymmetry, which links the shape of the tidal wave to residual sediment transport directions (Dronkers, 1986; Van de Kreeke and Robaczewska, 1993; Wang et al., 1999). A distinction can be made between the asymmetry of the vertical tide (i.e., water levels) and of the horizontal tide (i.e., discharges and velocities). The asymmetry of the vertical tide is often quantified by the difference in duration of the flood and ebb periods. The asymmetry of the horizontal tide can be expressed by the difference between peak currents or discharges during flood and ebb. The horizontal tide is considered flood dominant in case the peak flood velocities are higher than the peak ebb velocities, and vice versa. Similarly, the vertical tide is considered flood dominant if the duration of the flood period is shorter than the duration of the ebb (i.e. a shorter flood than ebb period implies a stronger flood than ebb flow if the flood and ebb discharges are equal), and vice versa (e.g. Wang et al., 2002). In addition, the difference in duration of the slack water periods (i.e. with negligible flow velocities) after high and low tide is another indicator for tidal asymmetry, as it relates to the settlement of fine sediments after flood and ebb respectively (Dronkers, 1986). However, as marsh channels are often intertidal and hence fall partly or entirely dry

around low tide inducing elongated periods of low water slack without any physical meaning for sediment transport, this characterization of tidal asymmetry is deemed not applicable in an intertidal channel.

For tidal marshes specifically, numerous field studies have quantified the tidal asymmetry and associated net import or export of materials through marsh channels, showing that in certain situations the tidal asymmetry is flood-dominant and associated with net import of materials (e.g. sediments), while other studies showed ebb-dominance and net export (e.g. Boon, 1975; French and Stoddart, 1992; Ganju et al., 2015, 2013; Green and Hancock, 2012; Pethick, 1980). However, the factors determining the direction and magnitude of tidal asymmetry in marsh channels are still poorly understood. We hypothesize that one such factor may be the stage of eco-geomorphological development of the combined channel-marsh system. The development of a channel network on an originally bare intertidal sand or mudflat is most likely initiated by small perturbations in the topography. Small topographic depressions lead to a concentration of tidal flow and thereby locally to higher shear stresses and eventually to creek formation (D'Alpaos et al., 2005; Stefanon et al., 2010). Further development towards a marsh system with a channel network and a vegetated platform is strongly influenced by the establishment of pioneer vegetation patches on the originally bare intertidal flat. Vegetation patches reduce flow velocities locally and enhance sedimentation inside the patches (Christiansen et al., 2000; De Lima et al., 2015; Mudd et al., 2010), while the flow is accelerated and shear stresses are higher leading to erosion adjacent to the patches (Bouma et al., 2013; D'Alpaos et al., 2006; Temmerman et al., 2007; Vandenbruwaene et al., 2013; Zong and Nepf, 2010). This positive feedback mechanism causes vegetation patches to expand due to increased sedimentation wherever vegetation is present and marsh channels to grow due to increased erosion in between vegetation patches, eventually leading to merging of vegetation patches and the formation of the typical marsh landscape consisting of elevated vegetated platforms dissected by a non-vegetated channel network (Allen, 2000; D'Alpaos et al., 2007; Kirwan and Murray, 2007; Stefanon et al., 2010; Temmerman et al., 2012; Vandenbruwaene et al., 2013). Ultimately, sedimentation on the vegetated areas raises the elevation of the marsh platform up until around mean high water level (MHWL) for which the marsh can be considered as a high or mature marsh (Allen, 2000; Temmerman et al., 2003). Marsh platforms that have not yet accreted to elevations around MHWL and that are situated lower in the intertidal frame are considered low or young marshes. The rise in elevation of the marsh platform towards elevations around MHWL occurs relatively fast (i.e. over the course of a few decades) (e.g., D'Alpaos et al., 2006; Gunnell et al., 2013; Sheehan and Ellison, 2014; Wang and Temmerman, 2013), depending on external factors including sediment supply and rate of sea level rise (e.g., French, 2006; Kirwan et al., 2010; Temmerman et al., 2004). It may be expected that the establishment of marsh vegetation and the elevation increase of the vegetated platform induces contradicting effects on the flow pattern through the marsh channels. Both the friction caused by vegetation establishment as well as the expansion and elevation increase of the marsh platform is expected to

enhance flow concentration towards the channels and to increase the tidal discharge in the channels on the one hand; but less water can be stored on higher platforms on the other hand, leading to a lower tidal prism and lower tidal discharge through the channels are expected (D'Alpaos et al., 2006; Temmerman et al., 2007). Along with these effects of marsh developmental stage on tidal discharges in the channels, we may expect that the degree of tidal asymmetry, and hence its effect on net material fluxes, will change during different stages of marsh development, but this has not been systematically documented.

This paper assesses tidal hydrodynamics in marsh channels during different stages of marsh development, starting from a low-lying, almost bare tidal flat situation up to a high-elevated, vegetated marsh with a platform elevation around mean high water level. The selection of these marsh developmental stages is based on observations over a long time scale (ca. 80 years) in a large marsh (ca. 3000 ha) in the Netherlands (Wang and Temmerman, 2013). A validated two-dimensional hydrodynamic model for this channel-marsh system (**Chapter 3**) is used to assess vertical and horizontal tidal asymmetry for a number of observed successive stages of marsh development. Finally, we discuss the implications of our model results in terms of expected effects on net material fluxes, in particular sediment fluxes, and how this evolves during different stages of marsh development.

## 4.2 Methods

### 4.2.1 Study area

We study tidal hydrodynamics in the intertidal channels of the 'Verdrongen Land van Saeftinghe' (in the following: 'Saeftinghe'), which is a ca. 3000 ha brackish intertidal flat and marsh system along the Western Scheldt estuary (51.3671°N, 4.1760°E). The present-day marsh is surrounded by levees in the south and the west and bordered by the subtidal estuary channel in the north and east. The Saeftinghe marsh used to be larger but stepwise embankments since the 17<sup>th</sup> century (the last of which around 1900) confined the marsh to its current size (Jongepier et al., 2015). Three large intertidal channels characterize the marsh geomorphology throughout its development since 1900: Speelmansgat in the west, Ijskelder in the middle and Hondegat in the east (Figure 4.1a-c). The latter Hondegat channel and adjacent marshes are subject for this study, as detailed field measurements of tidal water level movements are available for this channel-marsh system from previous studies (i.e., **Chapter 2**; Vandenbruwaene et al., 2015) and a validated two-dimensional hydrodynamic model (**Chapter 3**) is available for this area (see model description below). The marsh platform is covered by various types of vegetation, of which *Elymus athericus* and *Scirpus maritimus* are the most abundant (Vandenbruwaene et al., 2015). Nowadays, a semi-diurnal macrotidal regime induces a tidal range between 4.0 and 5.6 m for neap and spring tides respectively in the estuary channel bordering the study area. High water levels at the

study area vary between 2.18 m and 3.15 m above NAP (NAP is the Dutch ordnance level, close to mean sea level), with a mean high water level (MHWL) in the estuary channel adjacent to the marsh system of 2.76 m.

Wang and Temmerman (2013) presented a historical analysis of the geomorphological development and vegetation establishment in the Saeftinghe marsh from the 1930s until 2004 based on historical digital elevation models (DEMs) and vegetation maps. The topographic surveys and aerial photographs they used were originally provided by Rijkswaterstaat (Huijs, 1995; Tolman and Pranger, 2012). Here, we extend their analysis until 2010-2013. The vegetation cover and elevation change of Saeftinghe is visualized in Figure 4.1a-c and summarized in Table 4.1 for the 1930s (1931 DEM and 1935 vegetation map), 1960s (1963 DEM and 1959 vegetation map) and 2010s (2013 DEM and 2010 vegetation map). The elevation changes are specifically visualized in Figure 4.2. Marsh expansion occurred mostly towards the northern part of Saeftinghe, but also locally at the marsh-channel edges. The most southern and eastern parts of Saeftinghe, close to the levees had already developed to a relatively high vegetated marsh state in the 1930s, while the remaining part of the marsh developed from a low and mostly unvegetated tidal flat to a high and vegetated marsh and channel system during the studied period.

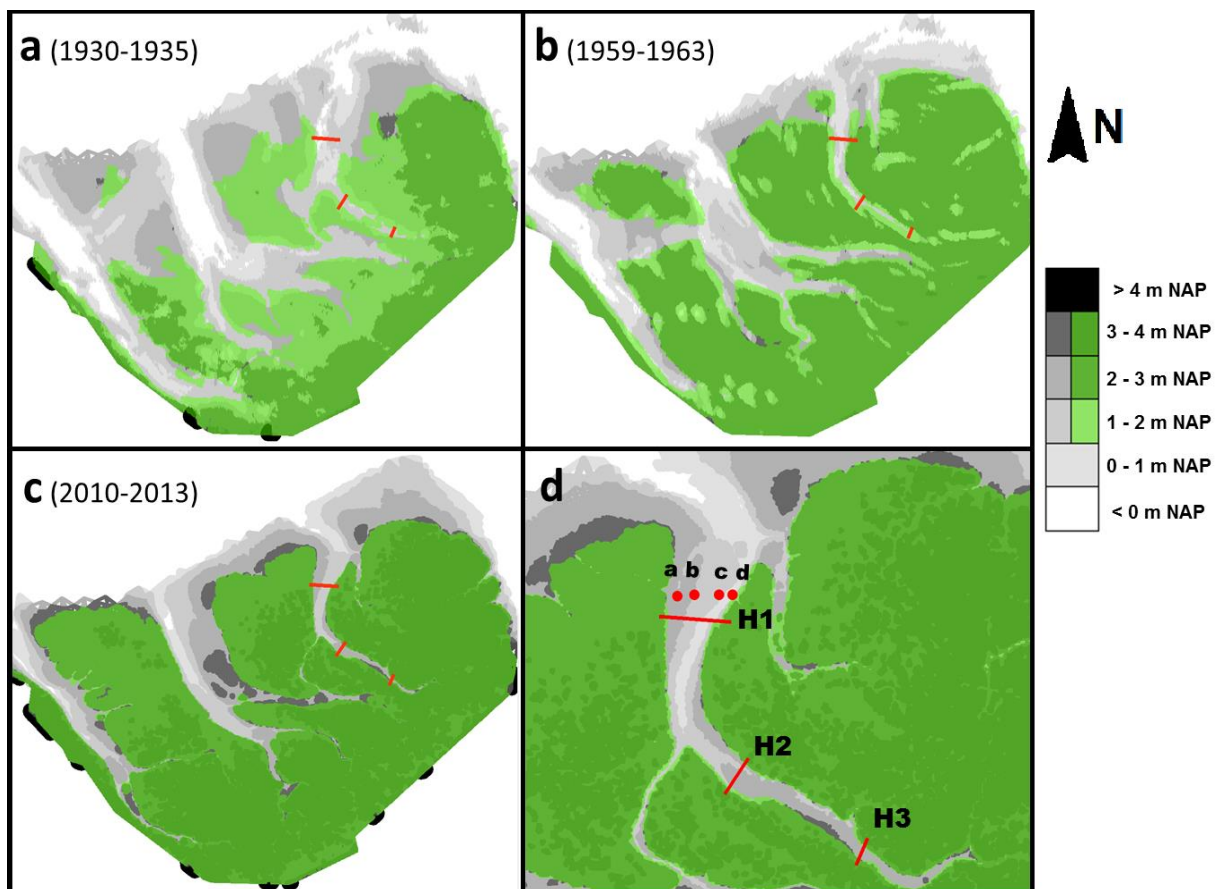


**Figure 4.1:** Map of the Saeftinghe marsh, shown with the bathymetry and vegetation cover of a) 1930-1935 (top left), b) 1959-1963 (top right) and c) 2010-2013 (bottom left) and d) the studied marsh channel with the locations of the velocity measurements and the sections where tidal hydrodynamics are assessed indicated in red (bottom right).

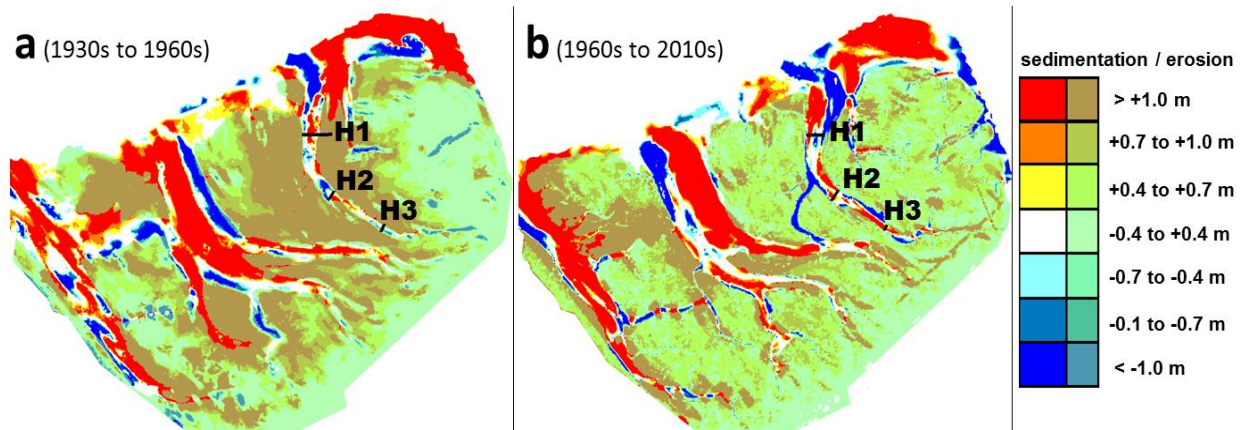


**Figure 4.2:** Historical elevation changes between (a) the 1930s and 1960s and (b) the 1960s and 2010s in the Saeftinghe marsh, including the elevation cover (transparent green) and with the locations of the sections where tidal hydrodynamics are assessed indicated in black.

**Table 4.1:** Development of the elevation and vegetation cover of the Saeftinghe marsh and of the mean high water level (MHWL) in the adjacent estuary channel.

Period	1931-1935	1959-1963	2010-2013
Mean elevation	1.13 m NAP	2.18 m NAP	2.41 m NAP
Mean elevation bare flats	0.56 m NAP	0.99 m NAP	1.05 m NAP
Mean elevation vegetated platform	1.92 m NAP	2.69 m NAP	2.99 m NAP
Vegetation cover	48%	67%	69%
MHWL	2.36 m NAP	2.53 m NAP	2.76 m NAP

#### 4.2.2 Hydrodynamic model

The numerical model used in this study is set up with TELEMAC-2D (version 6.3), a two-dimensional hydrodynamic model which is part of the TELEMAC-MASCARET modelling suite. This modelling system solves the Saint-Venant equations or shallow water equations, of which the one-dimensional form was discussed in **Chapter 1** (i.e., Eq. 1.1 and 1.2) and the two-dimensional form was shown in **Chapter 3** (i.e., Eq. 3.1-3.3). TELEMAC-2D contains the relevant physical processes with respect to tidal wave propagation in estuaries (Hervouet, 2007), including wetting and drying processes. These play an important role in an intertidal marsh and are dealt with by TELEMAC-2D while ensuring mass-conservation. In particular, wetting and drying is treated numerically in a mass-conservative way by allowing slightly negative depths and smoothing (i.e. adjusting) water level gradients when nodes in the model domain fall dry. For more detailed information on the TELEMAC-2D model and how wetting and drying processes are treated numerically we refer to (Hervouet, 2007) and the TELEMAC-2D user manual (see: <http://wiki.opentelemac.org/>).

#### Model description

The hydrodynamic model that is set up for the current study comprises the entire Scheldt Estuary, from the North Sea up to the upstream tributaries where tidal action is stopped by weirs or sluices near Gent (Figure 4.3). The model is locally refined at the studied marsh area to a mesh resolution of ~6-20 m. The historical elevation data of the

marsh (see above, Figure 4.1a-c), which is used to implement the bathymetry of the study area in the model, consists roughly of 1 data point per 0.4 ha and is interpolated to a 20 x 20 m DEM by Wang and Temmerman (2013). The 2013 DEM, which has an original resolution of 2 x 2 m, is also converted to a 20 x 20 m resolution, to implement the bathymetries with an equal level of representation of the marsh geomorphology and its channel network.

The Scheldt Estuary model was previously calibrated for tidal water levels and discharges within the estuarine channel by Smolders et al. (2015) and at a finer scale for tidal water level movement within the Saeftinghe marsh area in **Chapter 3**. Calibration for tidal water levels along the intertidal marsh channels was done by tuning the velocity diffusivity coefficient ( $\nu$ ), which represents the molecular and the turbulent viscosity, and Manning's bottom friction coefficients for the non-vegetated intertidal flats and channels ( $n_f$ ) and vegetated marsh platform ( $n_v$ ) respectively. Vegetation effects on tidal flow over the platform are thus implemented by increased bottom friction, which means that the depth-dependent effect of the vegetation (i.e., submerged versus emerged) on the flow is not incorporated (Baptist et al., 2007). The model calibration showed that best results are obtained with  $\nu = 0.5 \text{ m}^2 \cdot \text{s}^{-1}$ ,  $n_f = 0.01 \text{ s} \cdot \text{m}^{-1/3}$  and  $n_v = 0.08 \text{ s} \cdot \text{m}^{-1/3}$  (**Chapter 3**).

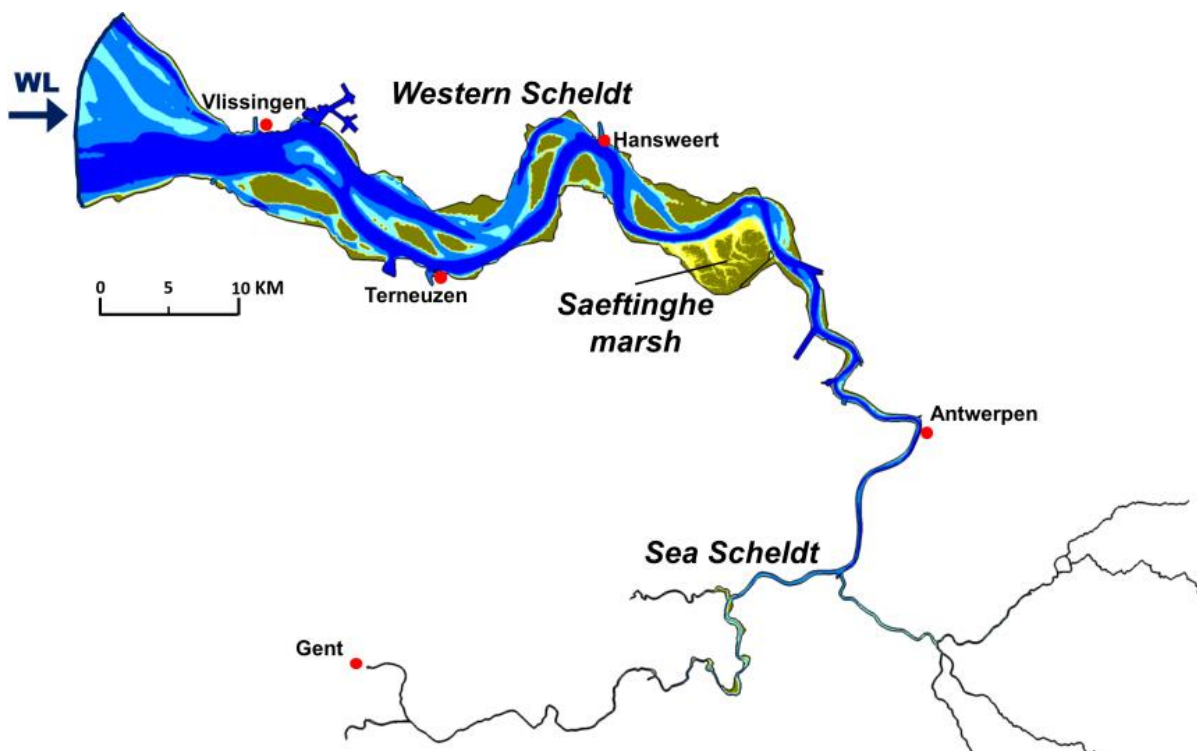


**Figure 4.3:** Scheldt Estuary model domain, showing the North Sea water level boundary (WL) and intertidal areas along the estuary (in brown and yellow), including the Saeftinghe marsh.

In the present model assessment, the North Sea boundary is forced with 28 days (i.e., 1/7/2012-28/7/2012) of observed tidal water levels at tide gauges in the coastal zone, for the model validation as well as the scenario analysis. Upstream discharges are not implemented as the influence of the upstream freshwater discharge on tidal hydrodynamics in the studied marsh can be considered negligible. In particular, the total

discharge of the upstream tributaries ranged between 50 and 174 m<sup>3</sup>/s during the simulation period (Vanlierde et al., 2013), which is less than one percent of the amplitude of the tide-induced discharges through the estuarine channel adjacent to the Saeftinghe marsh.

#### Model validation

The hydrodynamic model performance on estuary scale was assessed previously for simulated and observed water levels (**Chapter 3**; Smolders et al., 2015) and stage-discharge curves (Smolders et al., 2012). On the marsh scale, the model was validated based on simulated and observed water level data in the marsh channels and on the vegetated marsh platform (**Chapter 3**). This model validation indicates that observed water levels in the marsh channels are represented with mean errors between -0.02 m and -0.11 m, indicating that the water levels are slightly underestimated in the marsh system. Peak water levels are represented with mean errors between -0.03 m and +0.05 m (or ~1% of the local tidal range), which is a similar accuracy as in the adjacent estuarine channels. Besides, the sensitivity of the model performance to variations in  $\nu$  and  $n_f$  was also assessed in **Chapter 3**.

Here we extend the model validation by comparing modelled flow velocities with velocity measurements in the Hondegat channel (provided by Rijkswaterstaat Zeeland – Meetadviesdienst). The velocity measurements were conducted near the marsh edge at locations a, b, c and d (from west to east; see locations in Figure 4.1d). It must be stated that the model bathymetry is based on a DEM from 2013, while the water level measurements were conducted in 2012, possibly leading to a (slightly) different cross-sectional geometry and velocity profile along the measurement transect. Mean errors (ME, see: Eq. 3.4) root mean squared errors (RMSE, see: Eq. 3.6) and normalized root mean squared errors (NRMSE; i.e., RMSE normalized by the range of the total dataset) are calculated for the full series of flow velocities (Table 4.2). Validation is also done for peak velocities specifically (Table 4.2; Figure 4.4).

**Table 4.2:** Validation of the hydrodynamic model with observed flow velocities at the locations shown in Figure 4.1d, depicting the mean error, root mean squared error and normalized root mean squared error of the full series of flow velocities and for the flood and ebb peak flow velocities.

Measurement location	Total series			Flood peak			Ebb peak		
	ME <i>m/s</i>	RMSE <i>m/s</i>	NRMSE -	ME <i>m/s</i>	RMSE <i>m/s</i>	NRMSE -	ME <i>m/s</i>	RMSE <i>m/s</i>	NRMSE -
<b>a</b>	-0.08	0.07	0.17	+0.01	0.06	0.25	-0.05	0.08	0.18
<b>b</b>	-0.04	0.08	0.15	+0.16	0.17	0.36	+0.06	0.10	0.17
<b>c</b>	0.00	0.08	0.15	+0.18	0.19	0.32	+0.10	0.13	0.21
<b>d</b>	+0.05	0.08	0.16	+0.11	0.16	0.30	+0.05	0.06	0.24

The model represents the full series of observed flow velocities quite well, with ME ranging between -0.08 m/s and 0.05 m/s. These mean errors are highest relative to the observed velocities at location a and location d where the velocities are lower (i.e., approximately -30%). The relative mean errors at locations b and c, where the velocities

are higher, are only -18% and -1% respectively. Values for RMSE are all around  $\sim 0.08$  m/s, which is 15-17% of the range of the observations depending on the location (Table 4.2). Peak flood currents and to a lesser extent peak ebb currents are generally overestimated (Figure 4.4), except for the peak ebb velocities at location a where the peak ebb velocities are underestimated (Table 4.2). The RMSE values for peak flood velocities are between 0.06-0.19 m/s (i.e., 25-36% of the range in observed peak velocities) and the RMSE for peak ebb velocities varies between 0.06-0.13 m/s (i.e., 17-24% of the range in peak ebb velocities), depending on the measurement location. At location d, situated in the channel thalweg where flow velocities are highest, peak flows are overestimated by 0.11 m/s on average during flood and 0.05 m/s on average during ebb. As peak flood velocities are generally overestimated more than peak ebb velocities, this will also influence tidal asymmetry. In particular, the difference between peak flood and peak ebb velocities is on average overestimated by 0.19 m/s, 0.21 m/s, 0.11 m/s and 0.09 m/s for locations a, b, c and d respectively. Therefore, the results on tidal asymmetry in this study should be taken with care.

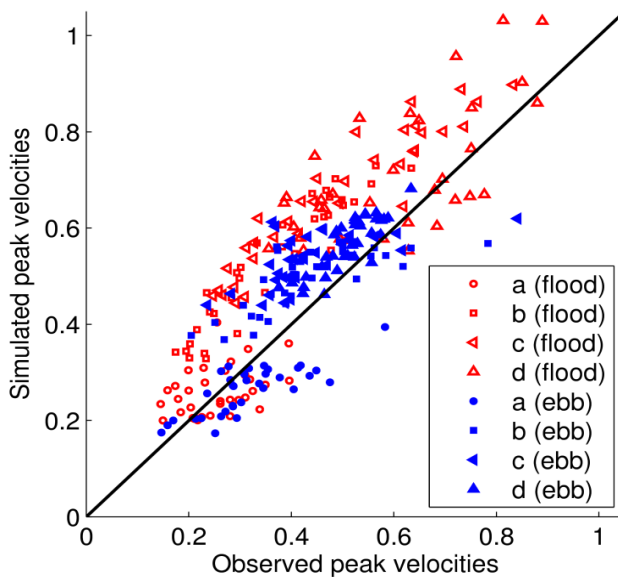


**Figure 4.4:** Simulated against observed peak flow velocities during flood (red markers) and ebb (blue markers) at velocity measurement locations a, b, c and d.

### 4.2.3 Model scenarios

Eight model scenarios are set up to analyze the effect of successive development stages of marsh topography (based on historical DEMs) and vegetation cover (based on vegetation maps) on tidal asymmetry in an intertidal marsh channel (Table 4.3). Scenario sc1 can be seen as the mudflat stage as the effects of vegetation are left out and the elevation of the marsh platform was rather low in the 1930s, especially in the outer marsh parts near location H1. Scenarios sc2, sc5 and sc6 contain the historical development from a relatively low marsh in the 1930s (sc2) to the 1960s (sc5) and finally a high marsh in the 2010s scenario (sc6). Scenarios sc3 and sc4 consider a stepwise development of vegetation expansion and platform elevation increase between the 1930s scenario and 1960s scenario. With these scenarios, we attempt to separate the effect of vegetation establishment (sc1 to sc2 and sc3) and vertical platform growth (sc3 to sc4) on tidal asymmetry in marsh channels. In addition, scenarios sc7 and sc8 investigate the effect of a fictitious situation in which continuous sedimentation in the



marsh channels would occur, as the channel elevation is raised by 0.5 m and 1.0 m respectively. As in **Chapter 3**, this elevation increase is limited to a maximum elevation of 2.5 m above NAP, to avoid that the channels are higher than the surrounding marsh platform in these scenarios, leading to a final elevation increase of the channels of 0.4 m in sc7 and 0.7 m in sc8.

**Table 4.3:** Overview of the model scenarios.

Scenario	Geomorphology	Vegetation cover	Marsh development steps / stage
sc1	1931	None	<i>'low and bare tidal flat'</i>
sc2	1931	1935	<i>vegetation establishment</i>
sc3	1931	1959	<i>vegetation establishment</i>
sc4	1931 channels / 1963 platform	1959	<i>vertical platform growth</i>
sc5	1963	1959	<i>channel infilling</i>
sc6	2013	2010	<i>vertical platform growth &amp; channel infilling</i>
sc7	2013 (channels + 0.4 m)	2010	<i>continued channel infilling</i>
sc8	2013 (channels + 0.7 m)	2010	<i>continued channel infilling</i>

Only the topography and vegetation cover of the marsh itself vary between the different scenarios, while the bathymetry in the rest of the model is kept constant to exclude effects of external changes (i.e., morphological development in the rest of the Scheldt estuary). The hydrodynamic boundary conditions, consisting of a full spring neap cycle of water level series at the North Sea boundary (i.e., 1/7/2012-28/7/2012), are kept constant as well. This implies however that the MSL, tidal range and MHWL at the studied marsh are higher in some model scenarios than in the real historical situation in the 1930s and 1960s. Therefore, the present model scenarios do not represent the historical situation as such, but allows for an analysis of changing tidal hydrodynamics as a result of the geomorphological development of a tidal marsh without having to account for long term variations in external factors such as changes in tidal range, MHWL or sea level rise. The impact of changing MHWLs on the model results is assessed by two additional model runs in which scenarios sc2 (1930s) and sc5 (1960s) are simulated with adjusted boundary conditions. In these model runs, the tidal amplitude at the boundary is reduced such that the simulated MHWL near the study area is similar to the MHWL of the 1930s for sc2 and of the 1960s for sc5 (see: Section 4.4.4).

#### **4.2.4 Quantification of channel geometry and analysis of tidal asymmetry**

We analyze the simulated variation in tidal asymmetry throughout different stages of marsh development more specifically at three cross-sections along the Hondegat channel (see Figure 4.1d). Section H1 is situated near the most seaward marsh edge in the present-day situation. Sections H2 and H3 are situated in the channel at a more landward distance of 1 km and 2 km from H1. The geomorphological development of the marsh channel is assessed locally by calculating the mean and minimum channel elevation (i.e., corresponding to the mean and maximum water depth in the channel), channel width and channel cross-sectional area. In reality, intertidal flats with a higher

elevation than 0.7 to 0.5 m below MHWL are likely to become part of the marsh platform as a shift between bare and vegetated states is present around this elevation in the studied marsh (Wang and Temmerman, 2013). Therefore, bare areas above +2.0 m (or approximately MHWL -0.7m) NAP are not considered part of the channel network anymore in our study. The vegetation cover in the proximity of the channel sections is computed for a 500 m wide buffer zone around the channel sections. Finally, the geomorphological development of the marsh platform surrounding the Hondegat channel is qualitatively assessed based on the elevation changes in Figure 4.2.

Tidal asymmetry is quantified here in two ways: (1) as the average ratio between the duration of rising and falling tide,  $R_T$ , and (2) as the average difference between flood and ebb peak velocities ( $\Delta V_{max}$ ):

$$R_T = \frac{1}{n} \sum_{j=1}^n \left( \frac{T_{rise}(j)}{T_{fall}(j)} \right) \quad (4.1)$$

$$\Delta V_{max} = \frac{1}{n} \sum_{j=1}^n (V_{max}flood(j) - V_{max}ebb(j)) \quad (4.2)$$

in which  $T_{rise}$  and  $T_{fall}$  are the durations (in min) of water level rise and water level fall for each tide,  $V_{max}flood$  and  $V_{max}ebb$  represent the maximum cross-sectional averaged flood and ebb velocities per tide (in m/s),  $j$  represents an individual tide and  $n$  is the amount of tides in the simulation. For the calculation of  $R_T$ , the long period of gravity-induced ebb drainage with relatively slow flow velocities, low water depths and hence little physical meaning for particle transport is excluded from the calculation by limiting  $T_{fall}$  to the period during which the water level fall is higher than 0.4 cm/min. This limit corresponds reasonably well with a shift, visible in the model results by a breakpoint in the rate of water level change, from faster tidally induced outflow to slower gravity-induced outflow due to friction-induced lagging effects on the ebb. For the assessment of horizontal tidal asymmetry, we use the difference instead of the ratio between peak flood and peak ebb velocities as the low cross-sectional averaged ebb velocities in some of the model simulations would lead to extremely high ratios between peak flood and peak ebb velocities. As the sediment in the main channels of the Saefthinghe is mainly sandy (Jongepier et al., 2015), the difference between maximum flood and ebb velocities can be considered as an indicator for the residual sediment transport load and direction (Van de Kreeke and Robaczewska, 1993; Wang et al., 1999).

An additional indicator for tidal asymmetry that is considered here is the dimensionless bed shear stress (also referred to as Shields mobility parameter) during flood flow and during ebb flow. The bed shear stress or the bed shear stress relative to the critical bed shear stress for the initiation of particle motion is often used in sediment transport formulas (e.g. Chollet and Cunge, 1979; Engelund and Hansen, 1967) and may be used as a proxy for the residual sediment transport and hence as an indicator for tidal asymmetry. In particular, it provides indicative insight in the variations in horizontal tidal asymmetry between the three sections and between the different model scenarios,

while considering the full velocity time series (i.e., the entire tidal wave) instead of solely the peak velocities. Besides, using a real sediment transport formula would not have any additional quantitative meaning as estimated sediment transports cannot be validated against any measurements. According to Van Rijn (1993), total sediment transport correlates with the excess dimensionless bed shear stress to the power  $\sim 1.5$ , which is again calculated at sections H1, H2 and H3:

$$Q_s \sim \frac{1}{t} \sum_{i=1}^t (\theta(i) - \theta_{cr})^{1.5} \quad \text{for } \theta(i) > \theta_{cr} \quad (4.3)$$

in which  $Q_s$  represents a proxy for the cumulated sediment transport over the entire simulation of  $t$  time steps,  $\theta(i)$  is the time-varying non-dimensional bed shear stress and  $\theta_{cr}$  is the critical non-dimensional shear stress for the initiation of particle motion. Here, we distinguish between flood and ebb flow by assigning positive values to the results during flood and negative values during ebb. By doing so, we obtain a residual value for  $(\theta - \theta_{cr})^{1.5}$  over a full spring-neap cycle which can be in flood or in ebb direction (i.e., flood- or ebb-dominant). The dimensionless bed shear stress  $\theta$  is calculated as follows:

$$\theta(i) = \frac{1}{d_{50} \cdot (s - 1)} \cdot \left( \frac{V(i)}{C(i)} \right)^2 \quad (4.4)$$

in which  $V(i)$  represents the flow velocity per time step (m/s), extracted from the model results at every 5 m along cross-sections H1, H2 and H3. Furthermore,  $s$  is the relative density of the sediment (-) and  $d_{50}$  is the median grain size (m). The Chézy friction coefficient  $C(i)$  ( $\text{m}^{1/2}/\text{s}$ ) depends on the time-varying water depth based on:

$$C(i) = 5.75 \cdot \sqrt{g} \cdot \log \left( \frac{12h(i)}{6d_{50}} \right) \quad (4.5)$$

with  $h(i)$  being the time-varying water depth (m), which is also extracted from the hydrodynamic model results, and  $g$  the gravitational acceleration ( $\text{m}/\text{s}^2$ ). The critical dimensionless shear stress  $\theta_{cr}$  is a function of the dimensionless particle parameter  $D_*$  (Van Rijn, 2007a) and can be estimated by:

$$\theta_{cr} = 0.115 \cdot (D_*)^{-0.5} \quad \text{for } D_* < 4 \quad (4.6a)$$

$$\theta_{cr} = 0.14 \cdot (D_*)^{-0.64} \quad \text{if } 4 \leq D_* < 10 \quad (4.6b)$$

$$\text{with: } D_* = d_{50} \cdot \left( \frac{(s-1) \cdot g}{\nu_k^2} \right)^{1/3} \quad (4.6c)$$

in which  $\nu_k$  is a kinematic viscosity coefficient ( $\text{m}^2/\text{s}$ ). For the calculations, the parameters are set as follows:  $s = 2.65$ ,  $d_{50} = 150 \mu\text{m}$  (the large main channels of Saeftinghe typically consist of fine sand with median grain sizes of 125 to 250  $\mu\text{m}$ ; Jongepier et al., 2015; Ysebaert and Herman, 2002),  $g = 9.81 \text{ m}/\text{s}^2$ ,  $\nu_k = 10^{-6} \text{ m}^2/\text{s}$  (Van Rijn, 2007b), while  $C(i)$  mostly ranges between 55 and 75  $\text{m}^{1/2}/\text{s}$  depending on the

water depth. These settings result in a critical dimensionless shear stress for the initiation of particle motion (or Shields mobility criterion) of  $\theta_{cr} = 0.0595$ . The latter implies that the velocity threshold for particle motion varies from 0.21 m/s to 0.29 m/s along with the depth-dependent Chézy coefficient. Ultimately, the results are cumulated per cross-section to compute one indicator for tidal asymmetry per cross-section (i.e., H1, H2 and H3) for each simulation. Furthermore, a brief sensitivity analysis indicates that varying the median grain size within  $63 < d_{50} < 500 \mu\text{m}$  (i.e., very fine sand and fine sand) only influences the magnitude of the results, while the qualitative trends between the model scenarios and the differences between the locations remain similar. However, it should be stated this approach is based on the assumption that the sediment is non-cohesive, while in reality grain sizes vary along the studied marsh channel and cohesive sediments are present as well. Especially smaller marsh channels often consist of much finer and more cohesive silty sediments (e.g. Hampel et al., 2003), for which the mobility criterion (i.e.,  $\theta_{cr}$ ) and the relation between excess bed shear stress and sediment transport are different (e.g. Van Rijn, 2007a, 1993). Therefore, we want to emphasize that this proxy for residual sediment transport should solely be interpreted as an indicator for horizontal tidal asymmetry in this scenario analysis and has little predictive value for the actual sediment transport due to the simplifications and assumptions that are made.

Finally, we also compute the mean spring tidal prism ( $P$ ) and compare it with a typical power law relationship between channel cross-sectional area ( $\Omega$ ) and tidal prism. Such general relationships have been found for tidal inlet channels (e.g. D'Alpaos et al., 2009; Jarrett, 1976; O'Brien, 1969, 1931; Stive et al., 2010), but also for salt marsh channels (e.g. Rinaldo et al., 1999; Steel and Pye, 1997; Vandenbruwaene et al., 2015) where the watershed was in some cases used as a proxy for tidal prism. Here, a  $\Omega$ -to- $P$  relationship is obtained by making a power law fit through the simulated tidal prisms and the cross-sectional areas at multiple cross-sections along the Hondegat channel for the present-day scenario (i.e., sc6 for which the marsh geomorphology is considered mature).

## **4.3 Results**

### ***4.3.1 Geomorphological development***

The eco-geomorphological development of the marsh is quantified by the changes in vegetation cover and channel geometry at sections H1, H2 and H3 (see Figures 4.1d) along the studied marsh channel (Figure 4.5). In addition, Figure 4.2 shows the vertical elevation changes along the studied marsh channel and the surrounding platform between the 1930s (sc2), 1960s (sc5) and 2010s (sc6). Vegetation cover increased the strongest in the outer part of the marsh near location H1, while the vegetation cover was already high in the 1930s at the more inland locations H2 and H3 where a smaller increase occurred (Figure 4.5a). From the 1960s onwards (i.e., sc5 to sc8), the vegetation cover remained nearly constant around all three sections. The platform elevation along the marsh channel increases strongly between the 1930s scenario to the

1960s scenario (i.e., sc3 to sc4) and slightly less pronounced between the 1960s and 2010s scenarios (i.e., sc4/5 to sc6) (Figure 4.2). The cross-sectional area of the channels generally decreases between the consecutive model scenarios at all three locations (i.e., sc3 to sc8), except for the channel size increase at H1 between the 1960s (sc5) and 2010s (sc6). This local increase in channel size at section H1 between sc5 and sc6 is likely due to the development of a connecting channel between the Hondegat channel and the Ijskelder channel (i.e., the middle main channel of the Saeftinghe marsh), which established in the 2010s scenario (Figure 4.1 & 4.2) and enlarges the watershed, storage volume and hence tidal prism of the Hondegat channel at section H1, while sections H2 and H3 sections are not affected as these are located ‘upstream’ of this side-branch of the main Hondegat channel. At section H3, the entire channel cross-section is higher than +2.0 m NAP for sc8 so that the cross-sectional area and channel width are reduced to zero. The decrease in cross-sectional area can be attributed to an increasing elevation of the marsh channel bed for scenarios sc4 to sc5 and sc6 to sc8 at H1, sc5 to sc8 at H2 and sc5 to sc8 at H3. For scenarios sc7 to sc8 at section H1 and sc6 to sc8 at sections H2 and H3, the elevation increase of the marsh channel bed is also accompanied by a reduction in channel width. Deepening of the channel is present as well between scenarios sc3 to sc4 and sc5 to sc6 at H1 and sc3 to sc5 at H3, implying that the decrease in cross-sectional area between sc3 and sc4 at section H1 and between sc3 and sc5 at section H3 is solely the result of channel narrowing.

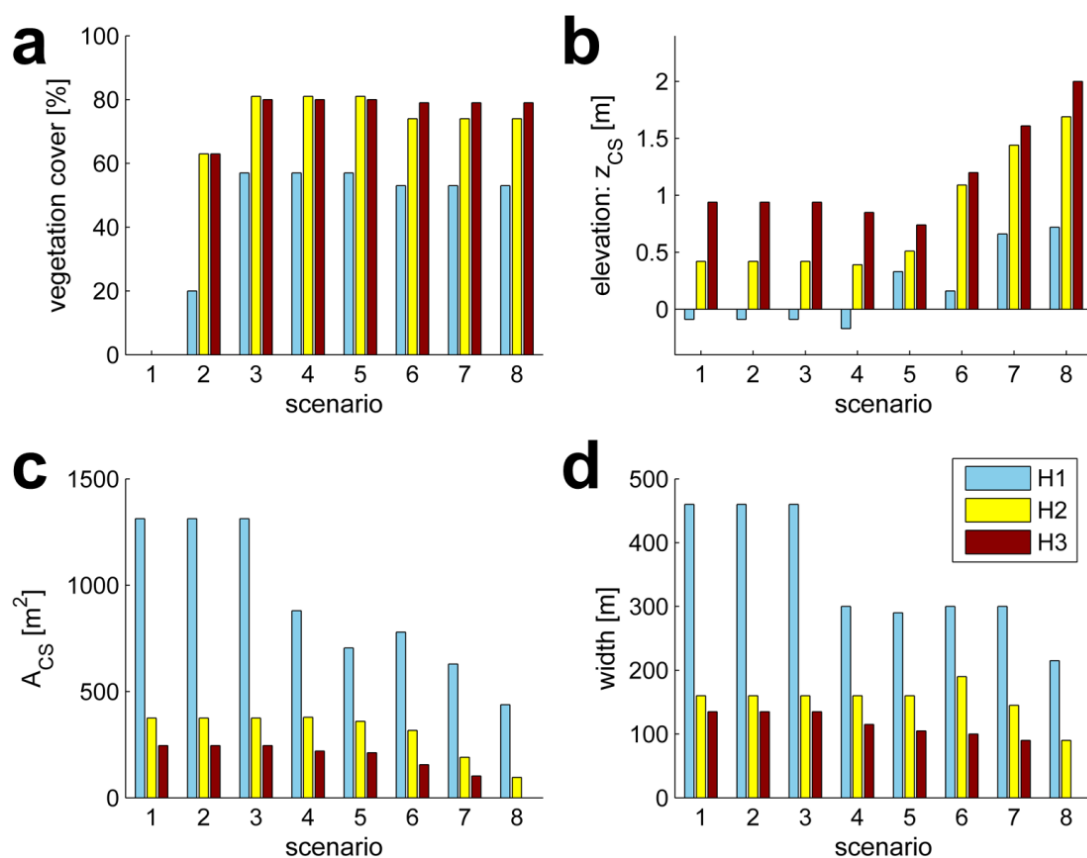


**Figure 4.5:** Geomorphological development of the Hondegat channel for the modelled scenarios at cross sections H1, H2 and H3 (see Figure 4.2 for locations) showing (a) the vegetation cover for a 500 m wide buffer zone around the channel cross-section, (b) the mean elevation of the cross-section, (c) the cross-sectional area below MHWL and (d) the channel width.

In the following, the results of the model scenarios are grouped based on specific eco-geomorphological developments of the marsh: vegetation establishment (sc1, sc2 and sc3); vertical platform growth (sc3, sc4 and sc6); channel size increase (sc5 to sc6 at section H1); and channel size decrease (sc4 to sc5 and sc7 to sc8 at H1 and sc4 to sc8 at H2 and H3).

### 4.3.2 Tidal Prism

The tidal prism in the studied marsh channel generally decreases between the consecutive scenarios (Figure 4.6a) as a result of overall marsh elevation increase (Table 4.1 and Figure 4.2) and consequently decreasing storage volume. In Figure 4.6b, the simulated tidal prism is plotted against the cross-sectional areas of each channel section for all scenarios and compared with a cross-sectional area to prism relationship for the marsh channel based on the simulation results of the present-day scenario (sc6). This power-law relationship yields:

$$\Omega = 0.0124 \cdot P^{0.79} \quad (4.7)$$

in which  $\Omega$  is the cross-sectional area in  $m^2$  of the marsh channel below MHWL (i.e., below 2.76 m NAP) and  $P$  is the mean tidal prism in  $m^3$  over the 28-days simulation.

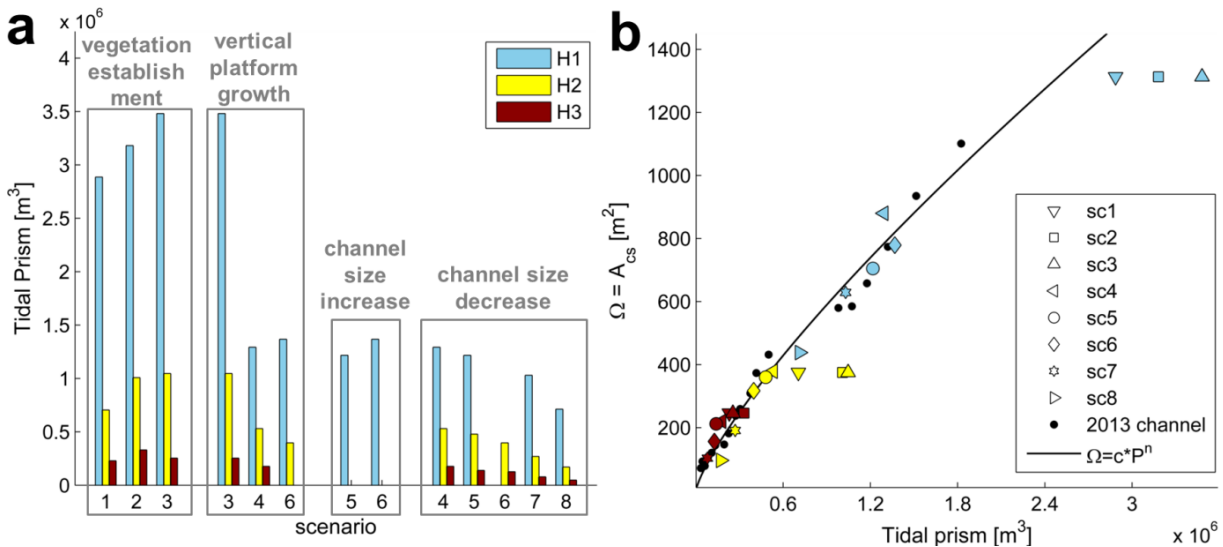


**Figure 4.6:** (a) Simulated mean flood tidal prism through cross-sections H1, H2 and H3 and (b) tidal prism plotted against the cross-sectional areas of section H1 (blue), H2 (yellow) and H3 (dark red) for model scenarios sc1-sc8. The plotted power law relationship (Eq. 4.7) is based on the simulated tidal prism through multiple cross-sections of the marsh channel in the 2013 bathymetry (black dots).

Adding the effect of vegetation generally induces a tidal prism increase in the marsh channels, which causes  $P$  to become relatively large for the cross-section based on the above  $\Omega$ -to- $P$  relationship. An exception is the remarkable decrease in tidal prism through section H3 from sc2 to sc3. Vertical platform growth towards the 1960s level (i.e., sc3 to sc4) leads to a significant decrease in tidal prism and makes  $P$  closer to equilibrium or even too small for the cross-sectional area of the channels, based on the estimated  $\Omega$ -to- $P$  relationship. At section H2, the tidal prism decreases further for the 2010s scenario (sc6). Conversely, at section H1 the increase in channel size towards the

2010s scenario (i.e., sc5 to sc6) causes the tidal prism to increase despite the vertical platform growth between those scenarios. In both cases, the tidal prism and cross-sectional area are close to equilibrium based on the estimated  $\Omega$ -to-P relationship. Infilling of the marsh channels or channel size decrease is accompanied by a reduction in tidal prism in accordance with the above relationship.

#### 4.3.3 Asymmetry of the vertical tide

The asymmetry of the vertical tide, quantified by the ratio  $R_T$  between the duration of the rising tide  $T_{rise}$  and the duration of the falling tide  $T_{fall}$  (Figure 4.7), is consistently shorter-rising along the marsh channel for all eco-geomorphological scenarios. Including the effect of vegetation has varying effects on  $R_T$  along the marsh channel:  $R_T$  increases slightly between sc1 and sc2 at locations H1 and H2, whereas  $R_T$  decreases between sc2 and sc3 at locations H1 and H2 and in general at location H3. Model results indicate that the decrease in  $R_T$  in the vegetated scenarios is induced by longer durations of the falling tide, as the duration of the rising tide remained fairly constant. Adding the effect of vegetation thus induces a lagging effect on the falling tide. Vertical platform growth (i.e., sc3 to sc4) generally leads to an increase in  $R_T$  and hence a development towards a less flood-dominant asymmetry of the vertical tide. The channel size increase from sc5 to sc6 at section H1 induces a slight increase in  $R_T$ . The reduction in channel cross-sectional area that is present between various scenarios has varying effects on  $R_T$ . At the outer section H1,  $R_T$  increases at first between sc4 and sc5, but  $R_T$  decreases in the scenarios in which the channel elevation is artificially increased (i.e., sc7 and sc8). Conversely,  $R_T$  decreases at the inner marsh sections H2 and H3 between scenarios sc4 and sc6, whereas  $R_T$  increases in the following scenarios sc7 and sc8 where the shortening of the falling tide is more profound than the shortening of the rising tide.

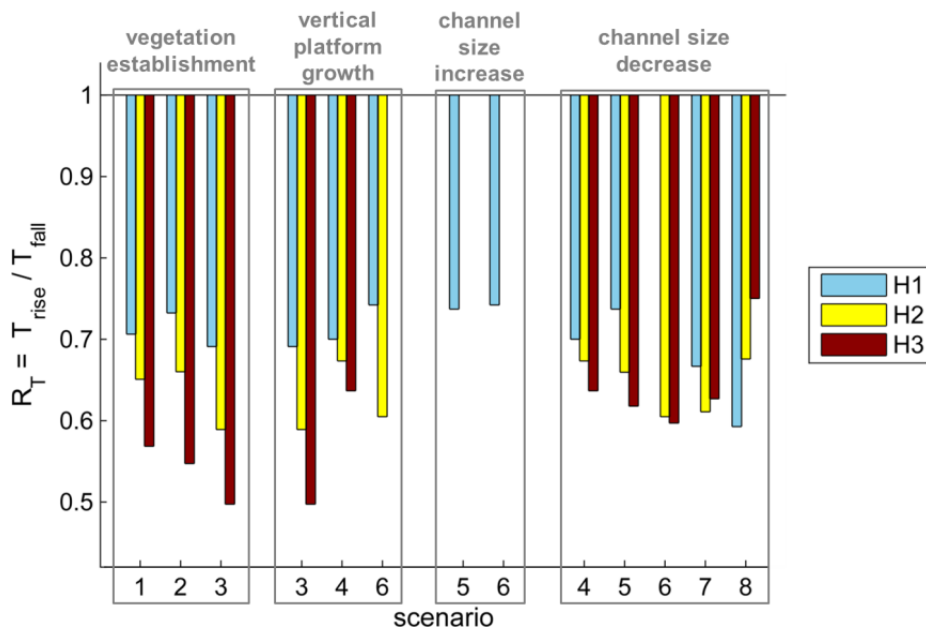


**Figure 4.7:** Modelled ratio between flood and ebb periods at locations H1, H2 and H3 for the different model scenarios sc1-8.

With respect to the implications of the vertical tidal asymmetry quantified by  $R_T$  for the horizontal tidal asymmetry, it must be stated that the total flood volumes and total ebb

volumes are not equal for all examined sections and scenarios. In particular, sc1 gives total flood volumes that are 1.26 times higher than the total ebb volume at loc. H1 and the flood tidal prism is 0.86 to 0.94 times smaller than the ebb tidal prism for sc2-5 at location H3. For the other scenarios, the cumulated ebb- and flood discharges are nearly equal at all three sections.

#### 4.3.4 Asymmetry of the horizontal tide

The horizontal tidal asymmetry is depicted by (1) the difference  $\Delta V_{max}$  between the maximum flood and maximum ebb velocities averaged over a spring-neap cycle at sections H1, H2 and H3 (Figure 4.8); (2) the difference  $\Delta V_{max}$  between the peak flood and maximum ebb velocities along the marsh channel and its surrounding platform for a typical spring tide with high water level of 3.15 m NAP (Figure 4.9); and (3) a proxy for the residual sediment transport based on the dimensionless bed shear stress (see: Eq. 4.3) at sections H1, H2 and H3 (Figure 4.10). Horizontal tidal asymmetry varies both spatially as well as between the model scenarios. Besides, as Figure 4.9 is based on a single tide and Figure 4.8 on a spring-neap average, results do not necessarily correspond between the two types of tidal asymmetry quantification.

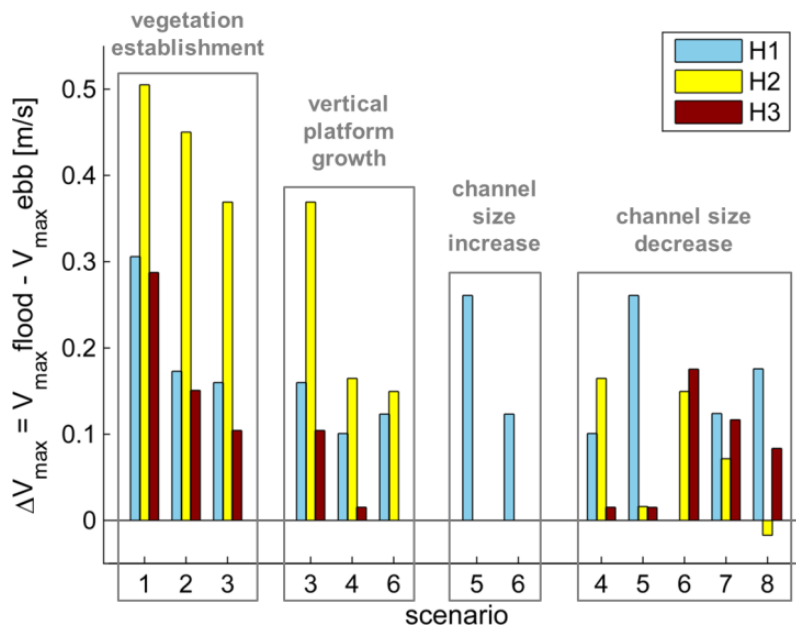


**Figure 4.8:** Difference between cross-sectional averaged peak flood and ebb peak velocities ( $\Delta V_{max}$ ) through cross-sections H1, H2 and H3 for the different model scenarios sc1-8.

Inclusion of the effects of vegetation (i.e., comparing sc1 with sc2 and sc3) leads to a decrease in flood-dominant asymmetry (i.e.,  $\Delta V_{max} > 0$ ) across the majority of the study area, especially where vegetation is present (Figure 4.9), but also in the marsh channels (Figure 4.8). If the platform elevation is increased (i.e., from sc3 to sc4), the strongly flood-dominant character of the intertidal channel diminishes (Figure 4.8 & 4.9) due to a stronger decrease in peak flood velocities than in peak ebb velocities; although a slight increase in  $\Delta V_{max}$  is modelled at section H1 between scenarios sc4 and sc6. A reduction in channel size has again varying effects on  $\Delta V_{max}$  and hence the tidal asymmetry along the marsh channel. If the spatial patterns of  $\Delta V_{max}$  are considered (Figure 4.9), artificial



infilling of the marsh channels (i.e., comparing scenarios sc6 with sc7 and sc8) appears to enhance ebb-dominance in the outer part of the marsh channel between sections H1 and H2, whereas flood-dominance is enhanced in the inner part (i.e., upstream of section H3) where the channel elevation is increased up to the maximum level of 2.0 m NAP (i.e., close to platform elevation). For sections H1, H2 and H3 specifically (Figure 4.8),  $\Delta V_{max}$  decreases at the inner sections H2 and H3 if the channel elevation is artificially increased (i.e., sc6 to sc7 and sc8), whereas  $\Delta V_{max}$  increases at the outer section H1 between these scenarios. Finally, an increase in channel size and tidal prism at section H1 between sc5 and sc6 is accompanied by a reduction in  $\Delta V_{max}$ , implying a decrease in flood-dominant asymmetry of the horizontal tide (Figure 4.8). It should however be stated that distinct spatial differences in  $\Delta V_{max}$  are present along the channel, especially in the proximity of section H2 for sc5, with some channel parts showing a strong flood-dominance, whereas nearby channel parts are strongly ebb-dominant (Figure 4.9). Such distinct local variations are probably caused by the local channel morphology. For example, narrow and shallow parts along the channel can lead to a local acceleration of the tidal flow, inducing stronger ebb flow downstream of this 'bottleneck' and stronger flood flow upstream of the 'bottleneck'. Therefore, values for  $\Delta V_{max}$  may differ locally from the large scale spatial pattern.

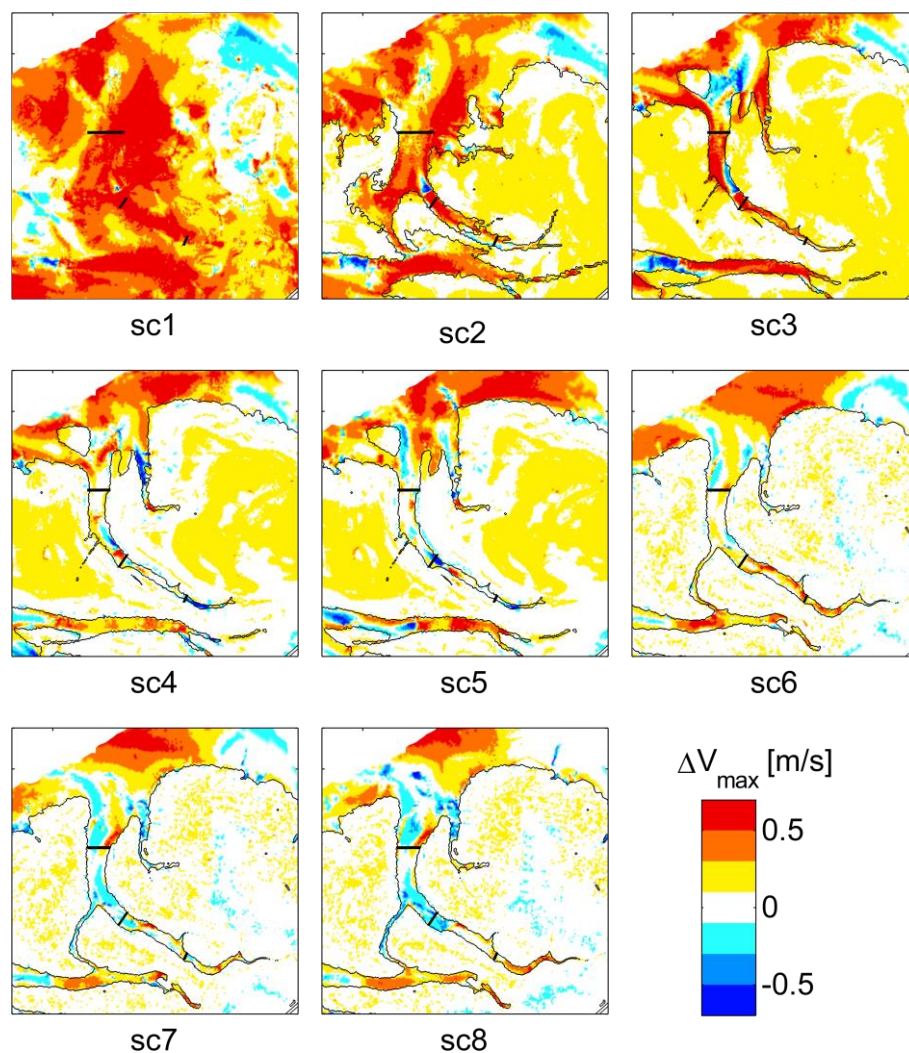


**Figure 4.9:** Difference between peak flood velocities and peak ebb velocities ( $\Delta V_{max}$ ) along the Hondegat channel and its surrounding platform for a single spring tide with a high water level of +3.15 m NAP for model scenarios sc1-8. The contour lines represent the border between the vegetated and non-vegetated parts of the marsh for each scenario.

The last indicator for horizontal tidal asymmetry is a proxy for the residual sediment transport based on the excess dimensionless bed shear stress  $\theta$  to the power 1.5 (Eq. 4.3). Adding the effect of vegetation has varying effects, but this indicator is in all cases less flood-dominant for the scenario with the 1960s vegetation cover (i.e., sc3) than in the unvegetated scenario (i.e., sc1). Vertical platform growth results in a strong decrease in flood-dominance at all sections (i.e., mainly comparing sc3 with sc4) based on  $(\theta - \theta_{cr})^{1.5}$ . However, flood-dominance increases again at section H1 towards the 2010s scenario (i.e., between sc4 and sc6) for which also the cross-sectional area of the channel decreases. A decrease in channel size has contrasting effects in different scenarios. In general, flood-dominance increases between the historical 1960s and 2010s scenarios (i.e., sc4, sc5 and sc6) based on this proxy for residual sediment transport, except for the remarkable shift towards strong ebb-dominance at section H2 for sc5 which is probably caused by a local peak in ebb-directed asymmetry around this section (Figure 4.9). The flood-dominant asymmetry weakens if the channel elevation is increased relative to the present-day situation (i.e., from sc6 to sc7 and sc8). This even leads to an ebb-dominant asymmetry at section H3 for scenario sc8.

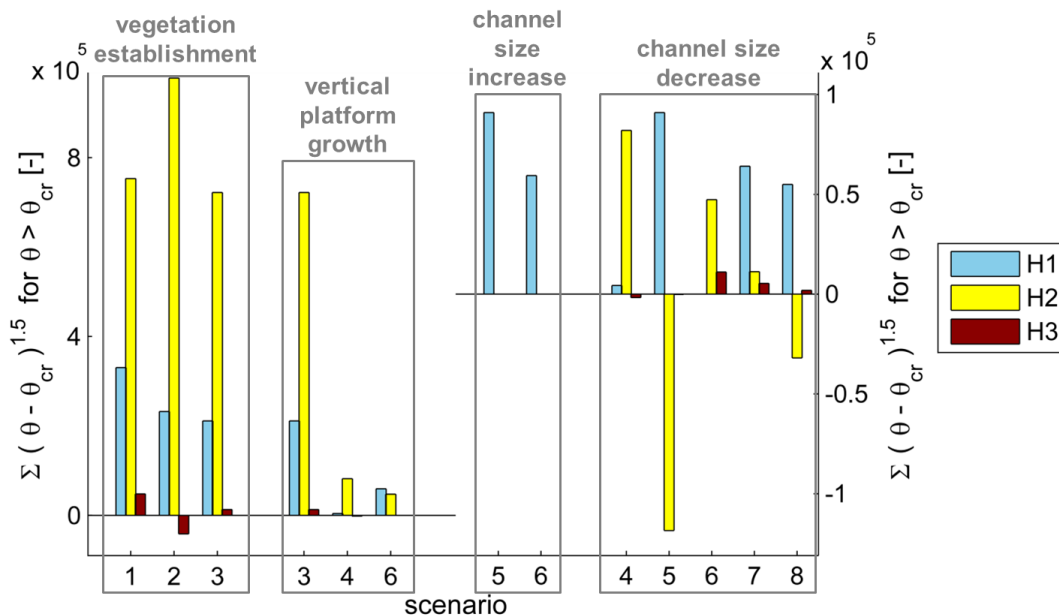


**Figure 4.10:** Proxy for the residual sediment transport based on the excess dimensionless bed shear stress (see: Eq. 4.3-4.6), calculated at sections H1, H2 and H3 for scenarios 1-8. Positive values denote a flood-dominant asymmetry and negative values an ebb-dominant asymmetry. Note the different scaling of the vertical axes on the left and right side of the figure.

## 4.4 Discussion

The aim of this study was to analyze the long-term changes in tidal asymmetry between subsequent stages of the eco-geomorphological development of a tidal marsh, starting from a relatively bare and low elevated stage to a higher elevated and vegetated tidal marsh. The present model results confirm our hypothesis of changing tidal asymmetry

along with the eco-geomorphological development of tidal marshes, implying that marsh development stage indeed influences the net transport of sediments or other materials in marsh channels. In addition, the development in tidal prism is mostly according to previous observations by Vandenbruwaene et al. (2013) and results of an idealized model by D'Alpaos et al. (2006). That is, vegetation establishment causes flow concentration towards the marsh channels, while marsh elevation increase and reduced storage volume on the marsh platform lead to a decrease in tidal prism through the marsh channels. In the following paragraphs, these changes in tidal asymmetry and tidal prism during specific steps in eco-geomorphological marsh development (i.e., vegetation establishment, vertical platform growth and changes in channel geometry) are discussed in more detail.

It should be stated that based on the model results different indicators for tidal asymmetry (i.e.,  $\Delta V_{max}$ ,  $R_T$  and the proxy for sediment transport) do not always show similar trends during the different stages of marsh development. Moreover, local spatial differences in horizontal tidal asymmetry along the marsh channel appear to be large (Figure 4.9) compared to the long term trends or differences between the model scenarios (Figure 4.8). Furthermore, flood-dominance of the horizontal tide is generally overestimated by the Saeftinghe marsh model according to the model validation. Although this complicates the quantitative interpretation of the model results, the qualitative impact of specific eco-geomorphological changes (i.e., comparing between model scenarios) on tidal asymmetry can still be obtained.

#### **4.4.1 Effect of vegetation establishment**

Inclusion of the effect of vegetation in the model simulations (i.e., comparing sc1 with sc2 and sc3) induces a less flood-dominant tidal asymmetry (Figures 4.8, 4.9 & 4.10).. While a deepening of the channels due to vegetation establishment as found in previous studies (e.g. D'Alpaos et al., 2006; Temmerman et al., 2007) would suggest an ebb-dominant asymmetry associated with a net sediment export through the channel network (e.g. Dronkers, 1986; French and Stoddart, 1992; Van de Kreeke and Robaczewska, 1993), the less flood-dominant asymmetry in the present results would imply that the net import of sediment and other materials through the marsh channels only reduces as a result of vegetation establishment. However, the flood-dominant tidal asymmetry is overestimated in our model assessment (see: Section 4.2.2). Besides, a net sediment import is more likely to contribute to the vertical growth of the vegetated parts of the marsh rather than to the infilling of the channel network itself as a consequence of enhanced settling and limited erosion on the vegetated parts of the marsh (e.g. Christiansen et al., 2000; de Lima et al., 2015; Mudd et al., 2010). Accordingly, higher sediment concentrations are generally moving into a marsh during the flood phase than out of the marsh during ebb (e.g. Krone, 1987). Following the above, net sediment import through marsh channels could even be accompanied by channel erosion if sedimentation on the platform exceeds erosion in the channels. However, only the horizontal tidal asymmetry becomes less flood-dominant if vegetation is implemented (Figure 4.8 & 4.10), while the flood-dominance of the vertical

tide increases (Figure 4.7). This means that the lag effect vegetation has on tidal flow damps the peak flood velocities more than the peak ebb velocities, but it also elongates the ebb outflow. Besides, further examination of the model results indicates that the increase in total ebb volumes exceeds the increase in total flood volumes as a result of vegetation-induced flow routing, which may explain the development towards a shorter-rising tide. This suggests that part of the outflow during ebb entered the marsh through a different channel, or that part of the inflow during the flood stage occurred as so-called sheet flow over the marsh platform (Temmerman et al., 2005a, 2005b).

Furthermore, vegetation establishment increases the tidal prism in the channels (Figure 4.6). Hence, the additional friction exerted by the vegetation on the intertidal platform results in marsh scale flow concentration towards the channels, while absence of vegetation leads to more divergent sheet flow. An exception is the decrease in tidal prism in the innermost part of the marsh channel (i.e., comparing sc2 with sc3 at section H3), which can be attributed to the lagging effect which the vegetation has on the propagation of the tidal wave into the marsh (e.g. **Chapter 2**). Previous studies showed similar effects of vegetation on flow routing on a smaller scale, with highly schematized or idealized models as well as in laboratory experiments (e.g. D'Alpaos et al., 2006; Temmerman et al., 2007; Vandenbruwaene et al., 2015; Zong and Nepf, 2010). Based on the  $\Omega$ -to-P relationship for the Hondegat channel (Eq. 4.7), adding the effect of vegetation brings the tidal prism further from equilibrium with the cross-sectional area at sections H1 and H2 (Figure 4.6b), which would imply a similar development towards channel scouring and hence towards ebb-dominance (or less flood-dominance).

### **4.4.2 Effect of vertical platform growth**

Model results show that vertical platform growth (primarily analyzed as the difference between sc3 and sc4) mainly leads to a significant decrease in tidal prism through the channel, especially at marsh edge section H1 (Figure 4.6a). Vertical platform growth may induce contrasting effects for tidal asymmetry: it leads to a decrease in sediment demand on the marsh platform as the remaining accommodation space decreases (potentially reducing flood-dominance), but a lower storage volume and tidal prism also imply that the channel cross-section becomes relatively large according to  $\Omega$ -to-P relationships (enhancing flood-dominance). Besides, the impact of vertical platform growth on tidal asymmetry shows similarities with the differences in tidal asymmetry between overmarsh tides (i.e., tides that do inundate the marsh platform) with varying HWLs, for which flood-dominance increases with the inundation height on the marsh platform and hence decreases with the platform elevation (see **Chapter 2**). In particular, higher marsh platforms (or tides with lower inundation depths on the marsh platform) exert more friction on the propagating high waters, leading to a less flood-dominant or even ebb-dominant asymmetry and vice versa. On the other hand, if the platform elevation becomes so high in the tidal frame that only a few high tides actually inundate the marsh platform, this may enhance flood-dominance as the additional bottom friction and storage volume provided by the marsh platform are then largely lost.

In the present study, vertical platform growth is at first accompanied by a development towards a less flood-dominant and more ebb-dominant asymmetry (Figure 4.7-4.10). This suggests that the marsh elevation (including the marsh platform and channels) gets closer to equilibrium with the tidal boundary conditions and in particular with the MHWL (Allen and Rae, 1988; Fagherazzi et al., 2012; Temmerman et al., 2004, 2003). However, the model validation indicates that flood dominance is generally overestimated by the model. The cross-sectional area of the marsh channel sections is fairly close to equilibrium with the tidal prism after the platform elevation increase according to the estimated  $\Omega$ -to-P relationship (i.e., for sc4; Figure 4.6b), implying that the channel size is not exceptionally large for the tidal prism in this scenario and that enhanced flood-dominance is not to be expected. Later on, as the platform elevation increases further and gets so high in the tidal frame that a majority of the tides is confined within the channels (i.e. sc6), the horizontal tide becomes more flood-dominant again.

#### ***4.4.3 Effect of changing channel geometry***

Changes in marsh channel depth, width and hence cross-sectional area generally relate to variations in tidal prism through empirical relationships between tidal prism and cross-sectional areas of tidal inlets (e.g. Jarrett, 1976; O'Brien, 1969, 1931; Stive et al., 2010) but also of marsh channels (e.g. Rinaldo et al., 1999; Steel and Pye, 1997; Vandenbruwaene et al., 2015), including the  $\Omega$ -to-P relationship which is established for the Hondegat channel specifically in this study (Figure 4.6b). In this perspective, the effect of channel infilling on tidal asymmetry may be twofold. On one hand, channel infilling reduces the cross-sectional area of the channels, which would imply that the cross-sectional area of the channel becomes relatively small based on  $\Omega$ -to-P relationships, likely leading to enhanced ebb-dominance associated with channel scouring. On the other hand, marsh scale channel infilling also reduces the tidal prism itself as the water storage in the channel network decreases. The effect of changes in channel size thus depends on the position of the tidal prism and cross-sectional area relative to the  $\Omega$ -to-P equilibrium curve and hence how important the water storage in the marsh channel network is for the total tidal prism. In addition, shallower channels may induce an increase in flood-dominant asymmetry due to stronger advective inertia and non-linear friction effects, which result in a faster propagation of the high tide than of the low tide in shallow waters and thereby enhance a flood-dominant shorter-rising asymmetry (e.g. Friedrichs and Aubrey, 1988; Speer and Aubrey, 1985).

In our model results, both decreasing and increasing flood-dominance occur as a result of reduced marsh channel size (Figure 4.7, 4.8 & 4.10). For the historical scenarios in which the reduction in channel size is solely caused by channel elevation increase and in which the channel width remains constant (i.e., sc4 to sc5 at section H1, sc5 to sc6 at section H2 and H3), there is indeed an increase in flood-dominance of the horizontal tide (Figure 4.8 & 4.10). The channel size decrease in these is also accompanied by an increase in platform elevation to levels around or above MHWL, causing some tides to become undermarsh and thereby reducing the net effect of the marsh platform on tidal

asymmetry. Conversely, a further decrease in channel size compared to the present-day situation reduces channel depth as well as channel width (i.e., between sc7 and sc8 at section H1 and between sc6, sc7 and sc8 at sections H2 and H3; Figure 4.5d), and induces a development towards a more ebb-dominant asymmetry (Figure 4.8, 4.9 & 4.10). This implies that hydro-morphodynamic feedbacks may enlarge the channel size to its equilibrium cross-section based on the above mentioned  $\Omega$ -to-P relationships if the cross-sectional area is reduced. However, along the innermost part of the channel (i.e., upstream of section H3), flood-dominance increases again in sc8 in which the elevation of the inner part of the channel is almost increased up to platform elevation (Figure 4.9), suggesting that the hydro-morphodynamic feedback mechanism that keeps the channel open does not persist if the channel elevation increases too much (i.e. in this case for channel elevations > 2.0 m NAP) or the tidal prism becomes too small. Based on this, we hypothesize that there are two morphological states to which intertidal marsh channels may develop if they are brought out of equilibrium by a reduction in channel size or tidal prism; (1) a state in which velocities remain high enough to erode the channel bed and enlarge the channel depth according to typical  $\Omega$ -to-P relationships and (2) a state in which velocities are too low to erode the channel bed leading to a complete infilling and siltation of the marsh channel. This reasoning is similar to the response of tidal inlets to changes in cross-sectional area or tidal prism and flow velocities, typically examined by closure curves such as the Escoffier (1940) curve (e.g. De Swart and Zimmerman, 2009).

#### **4.4.4 Effect of changing MHWL**

Although the present model results are based on scenarios that comprise the historical development of the marsh geomorphology and vegetation cover, they do not represent the historical tidal hydrodynamics as such. In particular, the marsh has a lower position in the tidal frame in our model scenarios than in the actual 1930s and 1960s situation as the scenarios are simulated with present-day tidal boundary conditions, implying a higher MHWL than the historical MHWLs in the 1930s and 1960s (i.e., 2.36 m in 1930, 2.53 m in 1960 and 2.76 m in 2010). Additional model runs in which the scenarios sc2 (1930s) and sc5 (1960s) are simulated with a reduced tidal amplitudes (i.e., reducing the MHWL to its historical height) result in similar trends between the model scenarios and eco-geomorphological development stages. Nevertheless, applying historical tidal boundary conditions reduces the tidal prism in the marsh channels by up to 25% compared to the scenarios with present-day boundary conditions. As the marsh elevation relative to MHWL is an important factor for sedimentation rates on the marsh platform (e.g. Allen and Rae, 1988; Temmerman et al., 2004, 2003), the marsh's relatively high position in the tidal frame for the 1930s scenarios (i.e., sc1-3) and 1960s scenarios (i.e., sc4-5) partly explains the high tidal prism and strong flood dominance in our model results, especially for the 1930s scenarios (Figure 4.8 & 4.9). Remarkably, the main indicators for tidal asymmetry  $\Delta V_{max}$  (< 0.03 m/s) and  $R_T$  (< 0.03%) only differ slightly between the simulations with and without reduced tidal amplitudes. However, the proxy for residual load based on the dimensionless bed shear stress changes significantly. For the 1930s scenario (sc2), the estimated residual sediment import decreases by about 15% at sections H1 and H2, while ebb-dominance is minimized at

section H3 if the tidal amplitude is reduced to that of the 1930s. For the 1960s scenario (sc5), flood-dominance at section H1 increases by  $\sim 12\%$ , while the ebb-dominance at section H2 is minimized if the tidal amplitude is reduced to that of the 1960s. It must be stated that the simulations with reduced tidal amplitudes do not represent the exact historical situation either, as sea level rise is not incorporated and the distortion of the tidal wave along the estuary has also changed during the last decades as a result of geomorphological changes in the rest of the estuary (e.g. Wang et al., 2002).

#### ***4.4.5 Concluding remarks***

Our results show that tidal asymmetry in marsh channels varies with the eco-geomorphological development of marshes. This implies that the eco-geomorphological development stage of marshes determines the net import or export through the channels and whether marsh systems act as a sink or source of sediments or other materials. This does not only affect the geomorphological development of marshes, it may also influence their ecological functioning. In particular, many of the ecological functions provided by marshes depend on the exchange of sediments and other particulate matter (e.g. organic detritus, seeds, larvae, etc.) between marshes and adjacent estuaries or seas (e.g. Fagherazzi et al., 2013, 2012). For example, carbon and nitrogen burial in marshes are related to sediment deposition in marshes (McLeod et al., 2011; Mitsch et al., 2012) and hence to the net sediment import through marsh channels, which is according to our results highest on low marshes during the early stages of marsh development and strongly decreases with the vertical growth of the marsh platform. Other ecological functions such as denitrification (e.g. Mitsch et al., 2012) or biogenic silica recycling (e.g. Struyf et al., 2005) depend amongst others on the water exchange between marshes and adjacent seas or estuaries and are therefore closely related to the tidal prism (Fagherazzi et al., 2013), which generally decreases during the eco-geomorphological development from low tidal flats to high elevated marshes and may even diminish if marsh channels silt up completely. However, other functions provided by marshes, such as coastal protection, may be optimized for higher marsh elevations (e.g. **Chapter 2; Chapter 3**; Smolders et al., 2015). The time-varying impact of marsh development on tidal hydrodynamics is also reflected in the ecosystem services provided by these areas and should be accounted for in impact assessments of for example marsh restoration projects (Boerema et al., 2016).

Overall, the present study may assist scientists and managers of tidal marshes in understanding the interactions between tidal hydrodynamics and the geomorphological development of marshes and marsh channels in particular. It could also open a route for research on the stability of marsh channels as a result of changes in tidal hydrodynamics or sediment supply and whether channel siltation may occur or not. On the other hand, areas where sea level rise or sediment depletion cause drowning and die-off of tidal wetlands (e.g. Kirwan and Megonigal, 2013; Kirwan et al., 2016) could also benefit from this study, especially as the effect of higher tidal amplitudes and mean high water levels was indirectly assessed in the historical scenarios. Finally, the present results may as well be of interest to scientists or estuarine managers studying marsh ecology as long-

term variations in tidal marsh hydrodynamics also influence the ecological functioning of marshes through the transport of other materials such as nutrients or pollutants.

## 4.5 References

- Allen, J.R.L., 2000. Morphodynamics of Holocene salt marshes: A review sketch from the Atlantic and Southern North Sea coasts of Europe. *Quat. Sci. Rev.* 19, 1155–1231. doi:10.1016/S0277-3791(99)00034-7
- Allen, J.R.L., Rae, J.E., 1988. Vertical salt marsh accretion since the Roman period in the Severn Estuary, Southwest Britain. *Mar. Geol.* 83, 225–235.
- Aubrey, D.G., Speer, P.E., 1985. A Study of Non-linear Tidal Propagation in shallow inlet / estuarine systems Part I : Observations. *Estuar. Coast. Shelf Sci.* 21, 185–205.
- Baptist, M.J., Babovic, V., Rodríguez Uthurburu, J., Keijzer, M., Uittenbogaard, R.E., Mynett, A., Verwey, A., 2007. On inducing equations for vegetation resistance. *J. Hydraul. Res.* 45, 435–450.
- Barbier, E.B., Georgiou, I.Y., Enchelmeyer, B., Reed, D.J., 2013. The value of wetlands in protecting Southeast Louisiana from hurricane storm surges. *PLoS One* 8, e58715. doi:10.1371/journal.pone.0058715
- Boerema, A., Geerts, L., Oosterlee, L., Temmerman, S., Meire, P., 2016. Ecosystem service delivery in restoration projects: The effect of ecological succession on the benefits of tidal marsh restoration. *Ecol. Soc.* 21. doi:10.5751/ES-08372-210210
- Boon, J.D.I., 1975. Tidal discharge asymmetry in a salt marsh drainage system. *Limnol. Oceanogr.* 20, 71–80. doi:10.4319/lo.1975.20.1.0071
- Bouma, T.J., Temmerman, S., van Duren, L.A., Martini, E., Vandenbruwaene, W., Callaghan, D.P., Balke, T., Biermans, G., Klaassen, P.C., van Steeg, P., Dekker, F., van de Koppel, J., de Vries, M.B., Herman, P.M.J., 2013. Organism traits determine the strength of scale-dependent bio-geomorphic feedbacks: A flume study on three intertidal plant species. *Geomorphology* 180–181, 57–65. doi:10.1016/j.geomorph.2012.09.005
- Chollet, J.P., Cunge, J.A., 1979. New interpretation of some head loss-flow velocity relationships for deformable movable beds. *J. Hydraul. Res.* 17, 1–13. doi:10.1080/00221687909499596
- Christiansen, T., Wiberg, P.L., Milligan, T.G., 2000. Flow and Sediment Transport on a Tidal Salt Marsh Surface. *Estuar. Coast. Shelf Sci.* 50, 315–331. doi:10.1006/ecss.2000.0548
- D’Alpaos, A., Lanzoni, S., Marani, M., Fagherazzi, S., Rinaldo, A., 2005. Tidal network ontogeny: Channel initiation and early development. *J. Geophys. Res. Earth Surf.* 110, 1–14. doi:10.1029/2004JF000182
- D’Alpaos, A., Lanzoni, S., Marani, M., Rinaldo, A., 2009. On the O’Brien–Jarrett–Marchi law. *Rend. Lincei* 20, 225–236. doi:10.1007/s12210-009-0052-x
- D’Alpaos, A., Lanzoni, S., Marani, M., Rinaldo, A., 2007. Landscape evolution in tidal embayments: Modeling the interplay of erosion, sedimentation, and vegetation dynamics. *J. Geophys. Res. Earth Surf.* 112, 1–17. doi:10.1029/2006JF000537
- D’Alpaos, A., Lanzoni, S., Mudd, S.M., Fagherazzi, S., 2006. Modeling the influence of hydroperiod and vegetation on the cross-sectional formation of tidal channels. *Estuar. Coast. Shelf Sci.* 69, 311–324. doi:10.1016/j.ecss.2006.05.002
- De Lima, P.H.S., Janzen, J.G., Nepf, H.M., 2015. Flow patterns around two neighboring patches of emergent vegetation and possible implications for deposition and vegetation growth. *Environ. Fluid Mech.* 881–898. doi:10.1007/s10652-015-9395-2
- De Swart, H.E., Zimmerman, J.T.F., 2009. Morphodynamics of Tidal Inlet Systems. *Annu. Rev. Fluid Mech.* 41, 203–229. doi:10.1146/annurev.fluid.010908.165159
- Dronkers, J., 1986. Tidal asymmetry and estuarine morphology. *Netherlands J. Sea Res.* 20, 117–131. doi:10.1016/0077-7579(86)90036-0
- Engelund, F., Hansen, E., 1967. A monograph on sediment transport in alluvial streams. Copenhagen. doi:10.1017/CBO9781107415324.004
- Escoffier, F.F., 1940. The stability of tidal inlets. *Shore and Beach* 8, 114–115.
- Fagherazzi, S., Kirwan, M.L., Mudd, S.M., Guntenspergen, G.R., Temmerman, S., Rybczyk, J.M., Reyes, E., Craft, C., Clough, J., 2012. Numerical models of salt marsh evolution: Ecological, geomorphic, and climatic factors 1–28. doi:10.1029/2011RG000359
- Fagherazzi, S., Wiberg, P.L., Temmerman, S., Struyf, E., Zhao, Y., Raymond, P.A., 2013. Fluxes of water, sediments, and biogeochemical compounds in salt marshes. *Ecol. Process.* 2, 3. doi:10.1186/2192-1709-2-3



- French, J.R., Stoddart, D.R., 1992. Hydrodynamics of Salt Marsh Creek Systems: Implications for Marsh Morphological Development and Material Exchange. *Earth Surf. Process. Landforms* 17, 235–252.
- French, P.W., 2006. Managed realignment - The developing story of a comparatively new approach to soft engineering. *Estuar. Coast. Shelf Sci.* 67, 409–423. doi:10.1016/j.ecss.2005.11.035
- Friedrichs, C.T., Aubrey, D.G., 1988. Non-linear Tidal Distortion in Shallow Well-Mixed Estuaries: a Synthesis. *Estuar. Coast. Shelf Sci.* 27, 521–545. doi:10.1016/0272-7714(90)90054-U
- Friedrichs, C.T., Perry, J.E., 2001. Tidal salt marsh morphodynamics: A Synthesis. *J. Coast. Res.* 27, 7–37.
- Ganju, N.K., Kirwan, M.L., Dickhudt, P.J., Guntenspergen, G.R., Cahoon, D.R., Kroeger, K.D., 2015. Sediment transport-based metrics of wetland stability. *Geophys. Res. Lett.* 42, 7992–8000. doi:10.1002/2015GL065980
- Ganju, N.K., Nidzieko, N.J., Kirwan, M.L., 2013. Inferring tidal wetland stability from channel sediment fluxes: Observations and a conceptual model. *J. Geophys. Res. Earth Surf.* 118, 2045–2058. doi:10.1002/jgrf.20143
- Gedan, K.B., Kirwan, M.L., Wolanski, E., Barbier, E.B., Silliman, B.R., 2010. The present and future role of coastal wetland vegetation in protecting shorelines: Answering recent challenges to the paradigm. *Clim. Change* 106, 7–29. doi:10.1007/s10584-010-0003-7
- Green, M.O., Hancock, N.J., 2012. Sediment transport through a tidal creek. *Estuar. Coast. Shelf Sci.* 109, 116–132. doi:10.1016/j.ecss.2012.05.030
- Hampel, H., Catrijsse, A., Vincx, M., 2003. Morphometric variation among sardine (*Sardina pilchardus*) populations from the northeastern Atlantic and the western Mediterranean. *ICES J. Mar. Sci. J. du ...* 60, 278–289. doi:10.1016/S1054
- Hervouet, J.-M., 2007. Hydrodynamics of Free Surface Flows: Modelling with the finite element method. doi:10.1002/9780470319628
- Huijs, S., 1995. Geomorfologische ontwikkeling van het intergetijdegebied in de Westerschelde 1935–1989. Middelburg, The Netherlands.
- Jarrett, J.T., 1976. Tidal Prism - Inlet Area Relationships. Vicksburg, MS, U.S.
- Jongepier, I., Wang, C., Missiaen, T., Soens, T., Temmerman, S., 2015. Intertidal landscape response time to dike breaching and stepwise re-embankment: A combined historical and geomorphological study. *Geomorphology* 236, 64–78. doi:10.1016/j.geomorph.2015.02.012
- Kirwan, M.L., Guntenspergen, G.R., D’Alpaos, A., Morris, J.T., Mudd, S.M., Temmerman, S., 2010. Limits on the adaptability of coastal marshes to rising sea level. *Geophys. Res. Lett.* 37, n/a–n/a. doi:10.1029/2010GL045489
- Kirwan, M.L., Megonigal, J.P., 2013. Tidal wetland stability in the face of human impacts and sea-level rise. *Nature* 504, 53–60. doi:10.1038/nature12856
- Kirwan, M.L., Murray, a B., 2007. A coupled geomorphic and ecological model of tidal marsh evolution. *Proc. Natl. Acad. Sci. U. S. A.* 104, 6118–6122. doi:10.1073/pnas.0700958104
- Kirwan, M.L., Temmerman, S., Skeeahan, E.E., Guntenspergen, G.R., Fagherazzi, S., 2016. Overestimation of marsh vulnerability to sea level rise. *Nat. Clim. Chang.* 6, 253–260. doi:10.1038/nclimate2909
- Krone, R.B., 1987. A method for simulating historic marsh elevations, in: Krause, N.C. (Ed.), *Coastal Sediments '87*. American Society of Civil Engineers, New York, NY, pp. 316–323.
- McLeod, E., Chmura, G.L., Bouillon, S., Salm, R., Björk, M., Duarte, C.M., Lovelock, C.E., Schlesinger, W.H., Silliman, B.R., 2011. A blueprint for blue carbon: Toward an improved understanding of the role of vegetated coastal habitats in sequestering CO<sub>2</sub>. *Front. Ecol. Environ.* 9, 552–560. doi:10.1890/110004
- Mitsch, W.J., Bernal, B., Nahlik, A.M., Mander, Ü., Zhang, L., Anderson, C.J., Jørgensen, S.E., Brix, H., 2013. Wetlands, carbon, and climate change. *Landsc. Ecol.* 28, 583–597. doi:10.1007/s10980-012-9758-8
- Mitsch, W.J., Zhang, L., Stefanik, K.C., Nahlik, A.M., Anderson, C.J., Bernal, B., Hernandez, M., Song, K., 2012. Creating Wetlands: Primary Succession, Water Quality Changes, and Self-Design over 15 Years. *Bioscience* 62, 237–250. doi:10.1525/bio.2012.62.3.5
- Mudd, S.M., D’Alpaos, A., Morris, J.T., 2010. How does vegetation affect sedimentation on tidal marshes? Investigating particle capture and hydrodynamic controls on biologically mediated sedimentation. *J. Geophys. Res.* 115, F03029. doi:10.1029/2009JF001566
- O’Brien, M.P., 1969. Equilibrium flow areas of tidal inlets on sandy coasts, in: *Proceedings of the American Society of Civil Engineers. Journal of the Waterways and Harbors Division.* pp. 43–52–. doi:10.9753/icce.v10.25p
- O’Brien, M.P., 1931. Estuary and tidal prisms related to entrance areas. *Civ. Eng.* 1, 738–739.

- Ouyang, X., Lee, S.Y., 2014. Updated estimates of carbon accumulation rates in coastal marsh sediments. *Biogeosciences Discuss.* 11, 5057–5071. doi:10.5194/bgd-10-19155-2013
- Parker, B.B., 1984. Frictional effects on the tidal dynamics of a shallow estuary, Ph.D. thesis. John Hopkins University, Baltimore, Md., U.S.A.
- Pethick, J.S., 1980. Velocity surges and asymmetry in tidal channels. *Estuar. Coast. Mar. Sci.* 11, 331–345. doi:10.1016/S0302-3524(80)80087-9
- Reed, D.J., 2002. Sea-level rise and coastal marsh sustainability: Geological and ecological factors in the Mississippi delta plain. *Geomorphology* 48, 233–243. doi:10.1016/S0169-555X(02)00183-6
- Rinaldo, A., Fagherazzi, S., Lanzoni, S., Marani, M., Dietrich, W.E., 1999. Tidal networks: 3. Landscape-forming discharges and studies in empirical geomorphic relationships. *Water Resour. Res.* 35, 3919–3929.
- Sheehan, M.R., Ellison, J.C., 2014. Intertidal morphology change following *Spartina anglica* introduction, Tamar Estuary, Tasmania. *Estuar. Coast. Shelf Sci.* 149, 24–37. doi:10.1016/j.ecss.2014.07.006
- Smolders, S., Ides, S., Plancke, Y., Meire, P., Temmerman, S., 2012. Calibrating Discharges in a 2D Hydrodynamic Model of the Scheldt Estuary : Which Parameters Can Be Used and What Is Their Sensitivity ?, in: *Proceedings of 10th International Conference on Hydroinformatics, HIC 2012*, Hamburg, Germany. p. 8.
- Smolders, S., Plancke, Y., Ides, S., Meire, P., Temmerman, S., 2015. Role of intertidal wetlands for tidal and storm tide attenuation along a confined estuary: A model study. *Nat. Hazards Earth Syst. Sci.* 15, 1659–1675. doi:10.5194/nhess-15-1659-2015
- Spalding, M.D., McIvor, A.L., Beck, M.W., Koch, E.W., Möller, I., Reed, D.J., Rubinoff, P., Spencer, T., Tolhurst, T.J., Wamsley, T. V., van Wesenbeeck, B.K., Wolanski, E., Woodroffe, C.D., 2014. Coastal Ecosystems: A Critical Element of Risk Reduction. *Conserv. Lett.* 7, 293–301. doi:10.1111/conl.12074
- Speer, P.E., Aubrey, D.G., 1985. A study of non-linear tidal propagation in shallow inlet/estuarine systems Part II: Theory. *Estuar. Coast. Shelf Sci.* 21, 207–224. doi:10.1016/0272-7714(85)90097-6
- Steel, T.J., Pye, K., 1997. The development of saltmarsh tidal creek networks: evidence from the UK., in: *Proceedings of the Canadian Coastal Conference*, 22-25 May 1997. pp. 267–280.
- Stefanon, L., Carniello, L., D’Alpaos, A., Lanzoni, S., 2010. Experimental analysis of tidal network growth and development. *Cont. Shelf Res.* 30, 950–962. doi:10.1016/j.csr.2009.08.018
- Stive, M.J.F., Ji, L., Brouwer, R.L., van de Kreeke, J., Ranasinghe, R., 2010. Empirical relationship between inlet cross-sectional area and tidal prism: a re-evaluation, in: *Coastal Engineering Proceedings*. pp. 1–10.
- Struyf, E., Van Damme, S., Gribsholt, B., Meire, P., 2005. Freshwater marshes as dissolved silica recyclers in an estuarine environment (Schelde estuary, Belgium). *Hydrobiologia* 540, 69–77. doi:10.1007/s10750-004-7104-0
- Temmerman, S., Bouma, T.J., Govers, G., Lauwaet, D., 2005a. Flow paths of water and sediment in a tidal marsh: Relations with marsh developmental stage and tidal inundation height. *Estuaries* 28, 338–352. doi:10.1007/BF02693917
- Temmerman, S., Bouma, T.J., Govers, G., Wang, Z.B., De Vries, M.B., Herman, P.M.J., 2005b. Impact of vegetation on flow routing and sedimentation patterns: Three-dimensional modeling for a tidal marsh. *J. Geophys. Res.* 110, F04019. doi:10.1029/2005JF000301
- Temmerman, S., Bouma, T.J., Van de Koppel, J., Van der Wal, D., De Vries, M.B., Herman, P.M.J., 2007. Vegetation causes channel erosion in a tidal landscape. *Geology* 35, 631. doi:10.1130/G23502A.1
- Temmerman, S., Govers, G., Meire, P., Wartel, S., 2003. Modelling long-term tidal marsh growth under changing tidal conditions and suspended sediment concentrations, Scheldt estuary, Belgium. *Mar. Geol.* 193, 151–169. doi:10.1016/S0025-3227(02)00642-4
- Temmerman, S., Govers, G., Wartel, S., Meire, P., 2004. Modelling estuarine variations in tidal marsh sedimentation: Response to changing sea level and suspended sediment concentrations. *Mar. Geol.* 212, 1–19. doi:10.1016/j.margeo.2004.10.021
- Temmerman, S., Kirwan, M.L., 2015. Building land with a rising sea. *Science (80-. )*. 349, 588–589. doi:10.1126/science.aac8312
- Temmerman, S., Meire, P., Bouma, T.J., Herman, P.M.J., Ysebaert, T., De Vriend, H.J., 2013. Ecosystem-based coastal defence in the face of global change. *Nature* 504, 79–83. doi:10.1038/nature12859
- Temmerman, S., Moonen, P., Schoelynck, J., Govers, G., Bouma, T.J., 2012. Impact of vegetation die-off on spatial flow patterns over a tidal marsh. *Geophys. Res. Lett.* 39. doi:10.1029/2011GL050502
- Tolman, M.E., Pranger, D.P., 2012. *Toelichting bij de Vegetatiekartering Westerschelde 2010*.
- Van de Kreeke, J., Robaczewska, K., 1993. Tide-induced residual transport of coarse sediment; Application to the EMS estuary. *Netherlands J. Sea Res.* 31, 209–220. doi:10.1016/0077-7579(93)90022-K

- Van Rijn, L.C., 2007a. Unified View of Sediment Transport by Currents and Waves. I: Initiation of Motion, Bed Roughness, and Bed-Load. *J. Hydraul. Eng.* 133, 649–667. doi:van Rijn, L.C., 2007. Unified View of Sediment Transport by Currents and Waves. I: Initiation of Motion, Bed Roughness, and Bed-Load. *J. Hydraul. Eng.* 133, 649–667.
- Van Rijn, L.C., 2007b. Unified View of Sediment Transport by Currents and Waves. II: Suspended Transport. *J. Hydraul. Eng.* 133, 668–389. doi:10.1061/ASCE0733-94292007133:6668?CE
- Van Rijn, L.C., 1993. *Principles of Sediment Transport in Rivers, Estuaries and Coastal Seas.* Aqua Publications, Amsterdam.
- Vandenbruwaene, W., Bouma, T.J., Meire, P., Temmerman, S., 2013. Bio-geomorphic effects on tidal channel evolution: Impact of vegetation establishment and tidal prism change. *Earth Surf. Process. Landforms* 38, 122–132. doi:10.1002/esp.3265
- Vandenbruwaene, W., Schwarz, C., Bouma, T.J., Meire, P., Temmerman, S., 2015. Landscape-scale flow patterns over a vegetated tidal marsh and an unvegetated tidal flat: implications for the landform properties of the intertidal floodplain. *Geomorphology* 231, 40–52. doi:10.1016/j.geomorph.2014.11.020
- Vanlinder, E., Vereecken, H., Plancke, Y., Taverniers, E., Mostaert, F., 2013. MONEOS - jaarboek monitoring WL 2012: Factual data rapportage van monitoring hydrodynamiek en fysische parameters zoals gemeten door WL in het Zeescheldebekken in 2012. Versie 2.0. WL Rapporten, 12\_070. Antwerpen.
- Wang, C., Temmerman, S., 2013. Does biogeomorphic feedback lead to abrupt shifts between alternative landscape states?: An empirical study on intertidal flats and marshes. *J. Geophys. Res.* 118, 229–240. doi:10.1029/2012JF002474
- Wang, Z., Jeuken, C., De Vriend, H., 1999. Tidal asymmetry and residual sediment transport in estuaries. A literature study and applications to the Western Scheldt, Z2749.
- Wang, Z.B., Jeuken, M.C.J.L., Gerritsen, H., De Vriend, H.J., Kornman, B.A., 2002. Morphology and asymmetry of the vertical tide in the Westerschelde estuary. *Cont. Shelf Res.* 22, 2599–2609. doi:10.1016/S0278-4343(02)00134-6
- Ysebaert, T., Herman, P.M.J., 2002. Spatial and temporal variation in benthic macrofauna and relationships with environmental variables in an estuarine, intertidal soft-sediment environment. *Mar. Ecol. Prog. Ser.* 244, 105–124. doi:10.3354/meps244105
- Zong, L., Nepf, H., 2010. Flow and deposition in and around a finite patch of vegetation. *Geomorphology* 116, 363–372. doi:10.1016/j.geomorph.2009.11.020



# Chapter 5

## Impact of intertidal area characteristics on estuarine tidal hydrodynamics: a modelling study for the Scheldt estuary

J. Stark, S. Smolders, P. Meire and S. Temmerman



*Creation of an intertidal area by de-embankment of the Perkpolder*

### **Abstract**

*Marsh restoration projects are nowadays being implemented as ecosystem-based strategies to reduce flood risks and to restore intertidal habitat along estuaries. Changes in estuarine tidal hydrodynamics are expected along with these intertidal area changes. A validated hydrodynamic model of the Scheldt estuary is used to gain fundamental insights in the role of intertidal area characteristics on tidal hydrodynamics and tidal asymmetry in particular through several geomorphological scenarios in which intertidal area elevation and location along the estuary is varied. Model results indicate that the location of intertidal areas and their storage volume relative to the local tidal prism determine the intensity and reach along the estuary over which tidal hydrodynamics are affected. Our model results also suggest that intertidal storage areas that are located within the main estuarine channel system, and hence are part of the flow-carrying part of the estuary, may affect tidal hydrodynamics differently than intertidal areas that are side-basins of the main estuarine channel, and hence only contribute little to the flow-carrying cross-section of the estuary. If tidal flats contribute to the channel cross-section and exert frictional effects on the tidal propagation, the elevation of intertidal flats influences the magnitude and direction of tidal asymmetry along estuarine channels. Ebb-dominance is most strongly enhanced if tidal flats are around mean sea level or slightly above. Conversely, flood-dominance is enhanced if the tidal flats are situated low in the tidal frame. For intertidal storage areas at specific locations besides the main channel, flood-dominance in the estuary channel peaks in the vicinity of those areas and generally reduces upstream and downstream compared to a reference scenario. Finally, the model results indicate an along-estuary varying impact on the tidal prism as a result of adding intertidal storage at a specific location. In addition to known effects of tidal prism decrease upstream and tidal prism increase downstream of additional storage areas, our model results indicate a reduction in tidal prism far downstream of intertidal storage areas as a result of a decreasing tidal range. This study may assist estuarine managers in assessing the impact of marsh restoration and managed shoreline realignment projects, as well as with the morphological management of estuaries through dredging and disposal of sediment on intertidal areas.*

## 5.1 Introduction

Estuaries and their intertidal areas are of great importance to society, providing for a range of economic activities (e.g. ports and shipping), but also for many ecological functions such as biogeochemical nutrient cycling, biological production and the maintenance of biodiversity (e.g. Barbier et al., 2013; Costanza et al., 1997). Furthermore, coastal wetlands are also valued for their flood and shoreline protection function, as they attenuate wind waves and storm surges (e.g. **Chapter 2; Chapter 3; Möller et al., 2014, 2001; Shepard et al., 2011; Temmerman et al., 2013**). However, coastal and estuarine habitats are under pressure by continuously growing populations and increasing economic activities (Small and Nicholls, 2003). As a result, the ecological value of many estuaries deteriorated during the last decades to centuries, mainly due to land reclamation for agricultural and industrial purposes (e.g. Kirwan and Megonigal, 2013; Moore et al., 2009; Pendleton et al., 2012; Barbier et al. 2011). Moreover, intensive dredging activities took place in numerous estuaries around the world to accommodate larger ships and allow for port expansion, thereby inducing morphological developments that might have led to loss of valuable intertidal habitat (e.g. Blott et al., 2006; Meire et al., 2005; Sherwood et al., 1990; Yang et al., 2006). Nowadays, conservation and restoration of (former) intertidal marshes and tidal flats along estuaries is gaining ground as a sustainable strategy to re-establish the coastal defense value as well as the ecological functions provided by these areas (e.g. Cox et al., 2006; French, 2006; Temmerman and Kirwan, 2015). The influence of the above-described intertidal area changes, resulting from embankments, de-embankments, natural or human induced erosion or accretion of tidal flats, on tidal hydrodynamics at the larger scale of adjacent estuaries is the main subject of this study.

### 5.1.1 Tidal asymmetry

Along with intertidal area changes, we may expect hydrodynamic changes in tidal range, tidal prism and tidal asymmetry, which on its turn induce effects on estuarine morphology, ecology and human activities such as shipping (i.e., navigability of estuarine channels). Tidal asymmetry is herein of particular importance to coastal and estuarine morphodynamics as asymmetries in tidal current velocities between flood and ebb lead to a residual sediment transport due to the non-linear relation between current velocity and sediment transport (i.e., typically, non-cohesive sediment transport is proportional to the velocity to the power three to five). In particular, if maximum flood velocities exceed maximum ebb velocities, residual non-cohesive sediment fluxes will be in flood direction, implying a net import of non-cohesive sediments, and vice versa (Lanzoni and Seminara, 2002; Van de Kreeke and Robaczewska, 1993; Wang et al., 1999). Although the asymmetry of the vertical tide (i.e., water levels) is strongly linked to asymmetry of the horizontal tide (i.e., discharges and velocities) and they are generally of the same type (i.e., either flood-dominant or ebb-dominant), a terminological distinction can be made between them (Wang et al., 1999, 2002). The asymmetry of the vertical tide is often described by the difference or ratio between the duration of rising tide (flood) and falling tide (ebb). If the flood period is shorter, the

asymmetry of the vertical tide is flood-dominant; if the ebb-period is shorter, the asymmetry is ebb-dominant. The reasoning behind this is that a shorter duration of flood would imply stronger (peak) flood velocities and hence higher transport rates in the flood direction and vice versa (i.e., shorter ebb duration with higher ebb-velocities and higher sediment transport during ebb), which is often the case (e.g. Dronkers, 1998) but not necessarily true in the presence of tidal flats (e.g. Brown and Davies, 2010). Similarly, the asymmetry of the horizontal tide can be described by the ratio between the peak currents or discharges during flood and ebb. If the flood currents are stronger, this asymmetry is flood-dominant; if the ebb-currents are stronger, the horizontal asymmetry is ebb-dominant. Furthermore, the difference in duration of the slack water periods after high and low tide is another indicator for horizontal tidal asymmetry. Deposition of fine (suspended) sediment is closely related to the settling time of particles. Longer high water slacks induce a residual transport of fine sediments in flood-direction and hence flood-dominance, while longer low water slacks induce a residual transport of fines in ebb-direction and ebb-dominance (e.g. Dronkers, 1986). However, this type of tidal asymmetry is not assessed in this study. Finally, tidal asymmetry can also be characterized by the relative contribution of different tidal constituents to the tidal signal, as the amplitude ratios and phase differences between the principal constituents and their overtides or compound tides are indicators for the strength and nature of the tidal asymmetry (e.g. Friedrichs and Aubrey, 1988; Parker, 1984; Wang et al., 1999, 2002).

Variations in tidal asymmetry along an estuary are for a large part determined by estuarine morphology, including the cross-sectional geometry of estuarine channels and adjacent intertidal flats and marshes, as well as by the asymmetry of the incoming tidal wave itself (e.g. Aubrey and Speer, 1985; Dronkers, 1986; Friedrichs and Aubrey, 1988; Friedrichs and Madsen, 1992; Speer and Aubrey, 1985; Wang et al., 2002). More specifically, asymmetries in the tidal wave originate from the mechanisms described by the non-linear terms in the continuity (Eq. 5.1) and momentum equations (Eq. 5.2) which cause the tidal wave to deform and become asymmetric as the ocean tide propagates in shallow waters such as estuaries (e.g. Aubrey and Speer, 1985; Friedrichs and Aubrey, 1988; Parker, 1984). In the presence of tidal flats, these shallow water equations can be described as follows (e.g. Wang et al., 2002):

$$b_{tot} \frac{\delta \zeta}{\delta t} + \frac{\delta}{\delta x} \{b_{ch}(h_0 + \zeta)u\} = 0 \quad (5.1)$$

(A)                      (B)

$$\frac{\delta u}{\delta t} + u \frac{\delta u}{\delta x} + g \frac{\delta \zeta}{\delta x} + c_f \frac{u|u|}{h_0 + \zeta} + \frac{\delta}{\delta x} \left( v \frac{\delta u}{\delta x} \right) = 0 \quad (5.2)$$

(C)    (D)    (E)                      (F)                      (G)

in which:  $t$  is time,  $x$  is the distance from the channel entrance,  $u(x,t)$  is the cross-sectional averaged flow velocity,  $\zeta(x,t)$  is the water level relative to mean sea level,  $h_0$  is



the water depth relative to mean sea level,  $b_{tot}$  is the total width of the channel (including tidal flats),  $b_{ch}$  is the width of the channel solely (without tidal flats),  $g$  is the gravitational acceleration,  $c_f$  represents bed friction and  $\nu$  is viscosity. The continuity equation is formed by a storage term (A) and a discharge gradient (B). The momentum equation consists of the local inertia term (C), the advective inertia term (D), the water level gradient (E), a bottom friction term (F) and a horizontal diffusion term (G). If the latter is assumed to be small (i.e., assuming a well-mixed situation) so that the horizontal diffusion can be ignored, the advective inertia term (D) and bottom friction term are left as main sources for non-linear interaction (Wang et al., 1999). The effect of the friction term (F) can be further separated in two parts to distinguish between the effect of variations in water depth (i.e., the propagation speed of the high tide exceeds the propagation speed of the low tide due to its dependency on water depth) and the effect of non-linear bottom friction itself, which slows the low tide more than the high tide as the bottom stress will be higher during low tide.

### **5.1.2 Intertidal areas and tidal asymmetry**

The relative tidal amplitude (i.e., ratio between the tidal amplitude and the channel depth) and the relative extent of tidal flats have been identified as the most important factors for tidal asymmetry in estuarine channels (e.g. Friedrichs and Madsen, 1992; Speer and Aubrey, 1985). In general, shallow channels with little intertidal storage tend to be flood-dominant, whereas estuaries or tidal basins with deep channels and a large intertidal storage volume tend to be ebb-dominant (e.g. Dronkers, 1986; Friedrichs and Aubrey, 1988; Friedrichs and Madsen, 1992; Speer and Aubrey, 1985). More specifically, a flood-dominant-asymmetry arises if frictional and inertial distortion in the channels is dominant via the friction term (F) and advective inertia term (D) in the momentum equation (Eq. 5.2) (e.g. Dronkers, 1986; Friedrichs and Aubrey, 1988; Friedrichs and Madsen, 1992; Speer and Aubrey, 1985). Lanzoni and Seminara (2002) even showed one-dimensionally that estuaries without tidal flats are invariably flood-dominant. If tidal flats are present, ebb-dominance is enhanced through the storage term (A) in the continuity equation (Eq. 5.1) (Friedrichs and Aubrey, 1988; Friedrichs and Madsen, 1992). Moreover, the bottom friction term (F) also increases during high tide when tidal flats are inundated, while it remains similar during low tide when they fall dry. However, tidal flats that are situated low in the tidal frame may exert friction and provide storage volume for the propagating low tide as well, especially if their position in the estuary is such that they contribute to the flow-carrying cross-section of the estuarine channel system (i.e., allowing the along estuary propagation of the tidal wave over the intertidal flats). The presence of tidal flats then exerts friction and reduces the cross-sectional averaged channel depth during most part of the tidal cycle. Fortunato and Oliveira (2005), who assessed the impact of tidal flats on the propagation speed of the high and low tide based on water depth variations only (i.e., only considering advective inertia), showed that low tidal flats may even enhance flood-dominance as they slow the propagation of the low tide more.

In addition, one could distinguish between two types of restored intertidal areas or flood control areas (Townend and Pethick, 2002): (1) restored intertidal areas that only

have limited connection with the adjacent estuarine channels and that only provide for intertidal storage without any compensatory increase in cross-sectional area of the estuarine channels; and (2) intertidal areas that are part of the flow-carrying cross-section of the estuarine channel and flat system and hence enlarge the cross-sectional area and exert friction on the tidal flow. It can be expected that these two types of intertidal storage areas have a different impact on tidal hydrodynamics and tidal asymmetry along the estuarine channels. Therefore, we hypothesize that the position of intertidal storage areas with respect to the flow-carrying cross-section of the estuarine channel system may also be a determining factor for the impact of intertidal storage on estuarine tidal hydrodynamics.

So far, existing studies mostly assess the effect of intertidal area characteristics on tidal hydrodynamics in a highly schematized setting or by analytical approximations (e.g. Fortunato and Oliveira, 2005; Friedrichs and Madsen, 1992; Van Rijn, 2011). However, the effect of tidal flat elevation and the physiographic setting and location along the estuary on tidal asymmetry is not yet systematically assessed. This implies that there is still a call for a better understanding of the effect of these specific intertidal area characteristics for estuarine tidal hydrodynamics.

### **5.1.3 Objectives**

Here, we address the influence of intertidal areas on along-estuary tidal hydrodynamics and tidal asymmetry in particular, based on a range of model scenarios simulated with a two-dimensional model of the Scheldt estuary. This study may provide more generic insights on the effect of intertidal area characteristics on tidal hydrodynamics along the estuary by systematically varying the intertidal flat elevation (i.e., assessing depth-varying friction and storage effects) and the intertidal flat location along the estuary (and hence varying the intertidal storage volume relative to the tidal prism) in different model scenarios. Moreover, we attempt to distinguish between different effects of intertidal areas based on their physiographic setting, i.e. (1) intertidal areas that do not contribute to the flow-carrying cross-section, which affect the tidal propagation along the estuary mainly by increasing the intertidal storage volume; and (2) intertidal areas that are situated within the main estuarine channel and flat system, which additionally enhance bottom friction for the propagating tidal wave.

## **5.2 Study area**

The area of interest for this study is the tidally influenced part of the Scheldt estuary, which has a length of 160 km from Gent to the estuary mouth (Figure 5.1). The most downstream part of the Scheldt estuary in The Netherlands is referred to as Western Scheldt, while the tidally influenced part of the Scheldt River in Belgium is referred to as Sea Scheldt. The Scheldt estuary is tide-dominated by a meso- to macrotidal regime, with a mean tidal range that varies between 3.8 m at the mouth near Vlissingen up to 5.2 m in the Sea Scheldt near KM-100, from where the tidal range decreases again towards

Gent (Pieters, 2002). The estuary width is converging from  $\sim 5$  km near Vlissingen to  $\sim 1.5$  km at the Dutch-Belgian border and further to  $\sim 50$  m near Gent. Likewise, the cross-sectional averaged depth of the estuary converges from about 15 m near Vlissingen to 3 m at Gent (Wang et al., 2002). The morphology of the Western Scheldt is characterized by a braided pattern of ebb and flood channels with intertidal shoals or bars which may be intersected by shallow shortcut channels that connect the flood and ebb channels (Swinkels et al., 2009) (Figure 5.1). The multichannel system shifts to a single channel system in the landward direction near the Dutch-Belgian border.

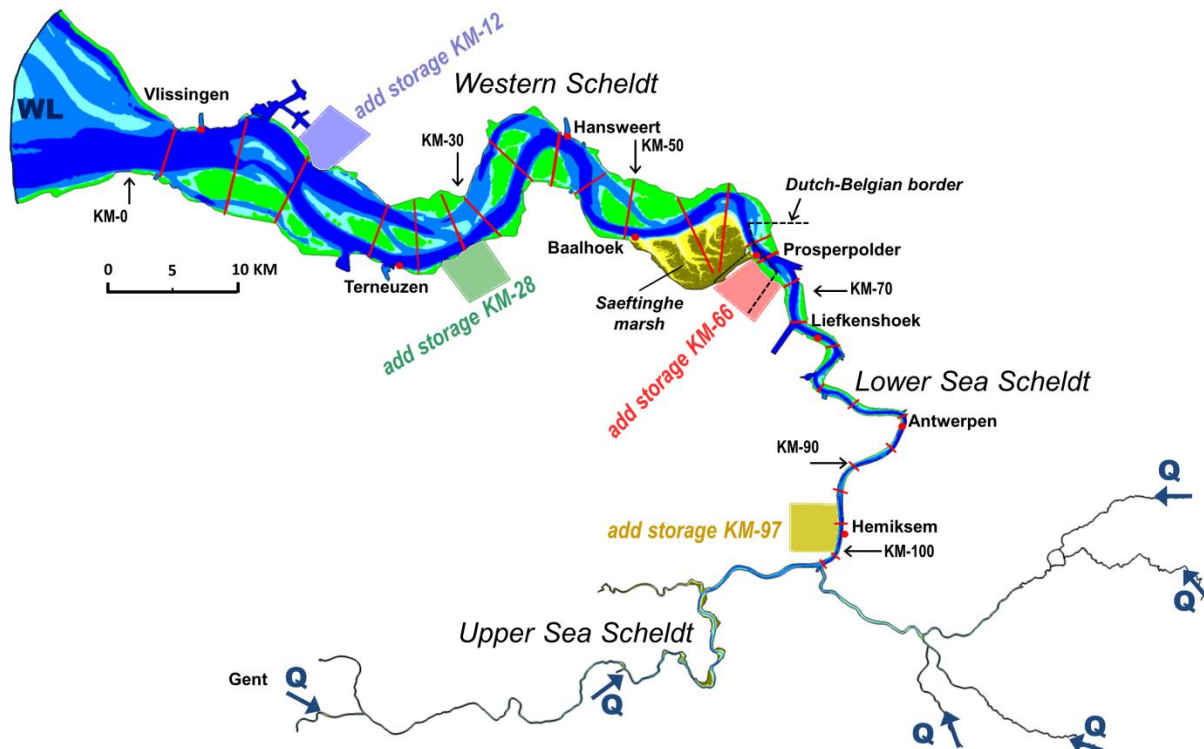


**Figure 5.1:** Map of the Scheldt estuary model, including the locations of the North Sea water level boundary and the six upstream discharge boundaries. The tidal stations for the model validation are indicated with red dots and the cross-sections for the scenario analysis with red lines. Tidal flats for which the elevation is varied in the scenario analysis are indicated in green, while the artificial additional storage areas at KM-12, KM-28, KM-66 and KM-97 are shown as well.

Historically, numerous embankments of former intertidal areas (i.e. tidal flats and marshes) reduced the estuarine surface area by approximately 44% between 1650 and 1968. Due to sediment accretion the elevation of marshes rose above mean high water level (MHWL) before being embanked (Van der Spek, 1997). Nowadays, only  $\sim 9000$  ha of intertidal area remain, out of which the Saeftinghe marsh, the biggest intertidal area along the Western Scheldt, accounts for 3500 ha. Despite the significant decrease in estuarine surface area (ca. 44% between 1650 and 1968), the tidal prism only decreased by less than 10%, leading to a significant increase in the maximum tidal range along the estuary (i.e., from 3.60 m in 1650 to 5.35 m in 1968) as well as a faster propagation and increased penetration of the tidal wave into the estuary, especially along the Sea Scheldt (Van der Spek, 1997).

Recently, several marsh restoration projects have been put into practice or will be realized within the next coming years along both the Western Scheldt and the Sea

Scheldt. On the one hand, this is realized by building new dikes more landward and breaching or removing existing dikes so that the historically embanked land re-develops into intertidal flats and marshes (similar to so-called managed coastal realignment in the UK, e.g., French, 2006; Rupp-Armstrong and Nicholls, 2007). Such de-embankments were recently implemented along the Western Scheldt (Perkpolder, 75 ha) and will be further realized within a few years (Hedwige-Prosperpolder, 465 ha; Zwin, 120 ha). On the other hand, marsh restoration along the Sea Scheldt is part of the so-called Sigma-plan and includes the creation of flood control areas (FCAs) adjacent to the estuarine channel aiming at the reduction of flood risks and restoration of intertidal habitat along the Belgian part of the Scheldt estuary. Some of these FCAs are designed with specific inlet and outlet culvert systems to generate a so-called controlled reduced tide, which means that only limited tidal exchange between the FCA and the estuary channel is allowed to optimize both the flood defense value as well as the ecological functioning. In particular, the FCAs may have a low elevation in the tidal frame and provide large storage volumes during storm surges, while still having normal tidal inundation characteristics to allow marsh development (Cox et al., 2006; De Mulder et al., 2013; Maris et al., 2007). By 2030, a total of over 2500 ha of FCAs will be realized along the Belgian part of the Scheldt estuary.

## 5.3 Numerical methods

### 5.3.1 Model description

A two-dimensional depth-averaged hydrodynamic model of the Scheldt Estuary was used in this study. This model was set up in TELEMAC-2D (version v7p0) and presented in previous studies (**Chapter 3**; **Chapter 4**; Smolders et al., 2015, 2012). TELEMAC-2D is a widely used hydrodynamic model that is part of the TELEMAC-MASCARET modelling suite (Hervouet, 2007) and solves the shallow water equations for continuity (Eq. 5.1) and momentum (Eq. 5.2) in two dimensions (Eq. 5.3-5.5):

$$\frac{\delta U}{\delta x} + \frac{\delta V}{\delta y} = S_h \quad (5.3)$$

$$\frac{\delta U}{\delta t} + U \frac{\delta U}{\delta x} + V \frac{\delta U}{\delta y} + g \frac{\delta h}{\delta x} - \nu \Delta U = S_x \quad (5.4)$$

$$\frac{\delta V}{\delta t} + U \frac{\delta V}{\delta x} + V \frac{\delta V}{\delta y} + g \frac{\delta h}{\delta y} - \nu \Delta V = S_y \quad (5.5)$$

in which  $U$  and  $V$  ( $\text{m}\cdot\text{s}^{-1}$ ) represent the flow velocity components in Cartesian coordinates,  $S_h$  ( $\text{s}^{-1}$ ) is a source or sink term for fluid,  $g$  ( $\text{m}\cdot\text{s}^{-2}$ ) is the gravity acceleration,  $h$  (m) is the water depth,  $\nu$  ( $\text{m}^2\cdot\text{s}^{-1}$ ) is a momentum diffusivity coefficient which represents the molecular and the turbulent viscosity and gives a weight to the diffusion terms in Eq. 5.4 and Eq. 5.5. Finally,  $S_x$  and  $S_y$  ( $\text{m}\cdot\text{s}^{-2}$ ) are sources or sinks of momentum in the dynamic equations (such as wind force, Coriolis force and bottom friction). For the bottom friction term (i.e., part of  $S_x$  and  $S_y$ ), the Manning's friction coefficient is used in

this study, from which a dimensionless friction coefficient is calculated in TELEMAC-2D based on Eq. 5.6.

$$c_f = \frac{2gn^2}{h^{1/3}} \quad (5.6)$$

in which  $c_f$  is a dimensionless friction coefficient and  $n$  ( $\text{s}\cdot\text{m}^{-1/3}$ ) the Manning's friction coefficient. The sink terms in Eq. 5.4 and 5.5 as a result of bottom friction in two dimensions then become (Hervouet, 2007):

$$S_x = -\frac{1}{2h} c_f U \sqrt{(U^2 + V^2)} \quad (5.7)$$

$$S_y = -\frac{1}{2h} c_f V \sqrt{(U^2 + V^2)} \quad (5.8)$$

For more detailed information on the implementation of bottom friction in TELEMAC-2D or on the TELEMAC-2D modelling system in general we refer to (Hervouet, 2007) and the TELEMAC-2D user manual (see: <http://wiki.opentelemac.org/>).

The Scheldt estuary model covers the estuary from its mouth in the North Sea up to the most landward boundaries of tidal influence, including all tidal tributaries (Figure 5.1). The model has a triangular mesh, consisting of 52076 nodes and 94849 elements. Mesh sizes range from  $\sim 5$  m in the upstream tributaries,  $\sim 50$  m at the Saeftinghe marsh, to  $\sim 150$  m along the Western Scheldt and  $\sim 300$  m near the estuary mouth. The North Sea boundary of the model is forced by a series of tidal water levels based on observed water levels at tidal stations in the mouth area, while the boundaries at some of the upstream tributaries are forced by fluvial discharges (see Figure 5.1 for the locations of the upstream discharge boundaries). Wind effects are not taken into account. Bathymetric data from 2009 to 2011 are used to implement the bathymetry of the Western Scheldt, Sea Scheldt, its tributaries and the geomorphology of the Saeftinghe marsh in the model. Spatially varying Manning roughness coefficients ranging from  $0.01 \text{ s}\cdot\text{m}^{-1/3}$  up to  $0.026 \text{ s}\cdot\text{m}^{-1/3}$  are obtained from calibration (**Chapter 3**; Smolders et al., 2015). Besides, the viscosity coefficient is set to  $\nu = 10^{-4} \text{ m}^2/\text{s}$  for the entire model domain, similar to the model validation by Smolders et al. (2015).

### 5.3.2 Model validation

The Scheldt estuary model was validated previously by comparing observed and modelled water level time series with a special focus on high water levels and storm tides (**Chapter 3**; Smolders et al., 2015) and by comparing modelled and observed stage-discharge curves at several stations along the estuary (Smolders et al., 2012). The model validation shows that the model represents observed water level variations with a mean error ranging from  $+0.02$  m near the estuary mouth to  $-0.09$  m at KM-87 near Antwerpen and  $-0.07$  m at KM-100 (see Figure 5.1 for locations). Root mean square errors range from  $0.06$  m at the estuary mouth to  $0.16$  m at KM-87 to KM-100. High water levels are represented with mean errors between  $-0.04$  m and  $0.07$  m, while

average phase differences between the modelled and observed high water levels are smaller than the time interval of 10 minutes of the water level measurements at all stations. For this study the model validation is extended with harmonic analyses on observed and modelled water level time series along the Scheldt estuary. Harmonic analyses are conducted with the T-TIDE toolbox in Matlab (Pawlowicz et al., 2002). Amplitudes and phases are computed for the M2 main tidal constituent and the M4 overtide based on the observed and modelled water level series at several tidal stations along the estuary. The validation based on harmonic analyses is shown in **Appendix 5A**.

### **5.3.3 Model scenarios**

Several artificial model scenarios (i.e., they do not represent real marsh restoration projects) are used in this study to gain generic insights in the impact of intertidal flat characteristics on tidal hydrodynamics along estuarine channels (Table 5.1). We herein attempted to separate between effects of two different types of physiographic settings of intertidal areas, i.e. (1) intertidal basins located adjacent to the main estuarine channel, which affect tidal propagation along the estuary mainly by increasing the intertidal storage volume; and (2) intertidal bars located within the main estuarine channel and flat system, which additionally enhance bottom friction for the propagating tidal wave. We attempt to simulate the separate effects by (1) alternatively adding intertidal storage basins at different locations adjacent to the estuary and (2) varying the elevation of the tidal flats that are present within the main estuarine channel system (i.e., the bottom friction term is water-depth dependent, see Eq. 5.6).

First, a reference scenario based on the 2011 bathymetry of the Western Scheldt is simulated. Four scenarios are set up in which additional intertidal storage areas are attached at different locations along the estuary (Figure 5.1). These additional storage areas all have a surface area of ~1500 ha and an elevation of NAP +0 m (i.e., NAP is the Dutch ordnance level, close to mean sea level) and all have an open connection with the main estuarine channel. Their storage volume slightly varies due to along estuary variations in MHWL and small differences in the additional surface area (i.e., 47-58 Mm<sup>3</sup>, calculated below the local highest high water or HHW). Relative to the local tidal prism, the additional storage volume approximates 3%, 5%, 19% and 59% of the local tidal prism for the added intertidal areas at KM-12, KM-28, KM-66 and KM-97 respectively. Furthermore, five scenarios are set up in which the elevation of the intertidal flats (i.e., defined as areas with a bottom elevation above -2.0 m NAP) is varied up until ~KM-80 between NAP -2.0 m and NAP +2.0 m with a one meter interval, along with a scenario in which the tidal flat elevation is increased above the highest high water level and hence excluding the intertidal areas from the model. The elevation and morphology of the Saeftinghe marsh (Figure 5.1) is kept constant in these model scenarios. Because of its position in a bend along the estuary channel, we expect that large parts of the Saeftinghe marsh only provide for intertidal storage and barely exert friction on the along-estuary propagating tidal wave (i.e., only the northeastern part of Saeftinghe contributes to the propagation of the tidal wave through the estuary channel in the model simulations). As these model scenarios specifically aim at investigating the combined effect of storage

and friction for the propagating tide, and large parts of Saeftinghe only have a storage function (see **Appendix 5B**), we decided to keep the geomorphology of Saeftinghe constant. Moreover, the effect of intertidal areas that are not within the flow-carrying cross-section is already assessed in other model scenarios. Besides, due to its size (i.e., ~3000 ha, ~43 Mm<sup>3</sup> of intertidal storage in the reference scenario in which the mean elevation of Saeftinghe is +2.4 m NAP), the impact of changes in the elevation and hence storage volume of the Saeftinghe marsh would exceed the more subtle effects of other tidal flats that are situated along the estuarine channel and flat system. The specific impact of elevation changes of the Saeftinghe marsh on tidal hydrodynamics along the estuary is assessed in **Appendix 5B**. In all model scenarios, the Manning's bottom friction coefficient  $n$  for the intertidal areas is set to  $n_{flat} = 0.02 \text{ s}\cdot\text{m}^{-1/3}$  (representative for bare sand) for all intertidal flats and increased to  $n_{veg} = 0.08 \text{ s}\cdot\text{m}^{-1/3}$  (representative for vegetated marshes, e.g. Temmerman et al., 2012; Wamsley et al., 2010) to include the effect of additional vegetation-induced friction on the platform of Saeftinghe.

In the scenario analysis, the North Sea boundary is forced by 28 days of water level observations (i.e. 31/8/2013-28/9/2013), while the upstream river discharge is forced by constant monthly averaged discharges of 3.0 to 12.0 m<sup>3</sup>s<sup>-1</sup> at the upstream boundary of the Sea Scheldt near Gent and at six other tributaries (average discharges are calculated based on available discharge data from <http://www.waterinfo.be>).

**Table 5.1:** Overview of model scenarios for the analysis of the effect of intertidal flat location and elevation on along-estuary tidal hydrodynamics, including the total intertidal storage volume below highest high water (excluding the Saeftinghe marsh which accounts for ~40 Mm<sup>3</sup> of the total intertidal storage in the reference scenario) for scenarios in which the tidal flat elevation is varies and the additional intertidal storage volume for scenarios in which storage areas are added along the estuary.

Scenario description	Abbreviation	(additional) intertidal storage volume
<i>Reference scenario based on the 2011 bathymetry (without recently restored intertidal areas along the Sea Scheldt)</i>	REF	248 Mm <sup>3</sup>
<i>Scenario with a ~1600 ha intertidal area at KM-12 along the estuary</i>	add storage KM-12	+50 Mm <sup>3</sup>
<i>Scenario with a ~1500 ha intertidal area at KM-28 along the estuary</i>	add storage KM-28	+47 Mm <sup>3</sup>
<i>Scenario with a ~1400 ha intertidal area at KM-66 along the estuary</i>	add storage KM-66	+50 Mm <sup>3</sup>
<i>Scenario with a ~1500 ha intertidal area at KM-97 along the estuary</i>	add storage KM-97	+58 Mm <sup>3</sup>
<i>Scenario with tidal flats at an elevation of -2.0 m NAP</i>	$z_{flats} = \text{NAP} - 2$	448 Mm <sup>3</sup>
<i>Scenario with tidal flats at an elevation of -1.0 m NAP</i>	$z_{flats} = \text{NAP} - 1$	368 Mm <sup>3</sup>
<i>Scenario with tidal flats at an elevation of +0 m NAP</i>	$z_{flats} = \text{NAP} + 0$	292 Mm <sup>3</sup>
<i>Scenario with tidal flats at an elevation of +1.0 m NAP</i>	$z_{flats} = \text{NAP} + 1$	213 Mm <sup>3</sup>
<i>Scenario with tidal flats at an elevation of +2.0 m NAP</i>	$z_{flats} = \text{NAP} + 2$	137 Mm <sup>3</sup>
<i>Scenario without tidal flats</i>	no flats	0 Mm <sup>3</sup>

### 5.3.4 Quantifying tidal hydrodynamics

Tidal characteristics are quantified at cross-sections along the estuary with a regular spacing of 5-8 km and a more frequent spacing of 3-5 km in the vicinity of the additional storage areas, as shown in Figure 5.1.

The vertical tide is described by the mean tidal range ( $TR$ ), mean high water level ( $MHWL$ ), mean low water level ( $MLWL$ ) and the phase of the high water ( $T_{HW}$ ) and low water ( $T_{LW}$ ) compared to a reference scenario. The horizontal tide is described by the cross-sectional averaged peak velocities during flood ( $V_{CS-flood}$ ) and during ebb ( $V_{CS-ebb}$ ). Furthermore, the flood tidal prism ( $P$ ) is calculated through all these cross-sections. It should be stated that the flood tidal prism differs slightly from the ebb tidal prism due to the presence of an upstream river discharge. However, the effect of the river discharge is considered to be small, especially at the Western Scheldt where the river discharge accounts for less than one percent of the tidal discharge amplitude (Vanlierde et al., 2014). All parameters are averaged over the model simulation period of two spring-neap cycles.

Tidal asymmetry is quantified here in two ways: (1) as the average ratio between the duration of rising and falling tide,  $R_T$ , and (2) as the average ratio between peak cross-sectional averaged velocities during flood and during ebb,  $R_V$ :

$$R_T = \frac{1}{n} \sum_{j=1}^n \left( \frac{T_{rising}(j)}{T_{falling}(j)} \right) \quad (5.9)$$

$$R_V = \frac{1}{n} \sum_{j=1}^n \left( \frac{\max(V_{CS-flood}(j))}{\max(V_{CS-ebb}(j))} \right) \quad (5.10)$$

in which  $T_{rising}$  and  $T_{falling}$  are the durations (in min) of water level rise and water level fall for each tide,  $\max(V_{CS-flood})$  and  $\max(V_{CS-ebb})$  represent the maximum cross-sectional averaged flood and ebb velocities per tide (in m/s),  $j$  represents an individual tide and  $n$  is the amount of tides in the simulation.

In addition, classical harmonic analyses are performed on the model results, using the T-TIDE toolbox in MATLAB (Pawlowicz et al., 2002), in order to further demonstrate the effect of our model scenarios on indicators for tidal asymmetry based on harmonic constituents. Methods and results are shown in **Appendix 5A**.

## 5.4 Results

### 5.4.1 Scenarios with additional intertidal storage

Adding intertidal storage basins adjacent to the estuarine channels reduces the tidal range along the estuary (Figure 5.2a), implying a damping of the tidal wave. The highest tidal range reduction is directly downstream of the additional storage areas, from where the tidal range reduction decreases further downstream. Upstream of the added storage



areas, the reduction in tidal range remains more or less constant compared to the reference scenario. In general, tidal range reduction is larger if the added intertidal storage is located further upstream and hence when the intertidal storage volume is relatively larger compared to the local tidal prism that passes through the estuary. The reduction in tidal range is mainly due to lower MHWLs (Figure 5.2b), while a slight increase in MLWLs is also present (Figure 5.2c). Furthermore, the propagation of the high water (Figure 5.2d) is delayed upstream of additional intertidal storage basins (i.e., 15 to 45 minutes phase lag directly upstream of the added storage areas). Conversely, the high water propagation is accelerated downstream of the additional storage areas (i.e., phase lead of 2 to 8 minutes directly downstream of the added storage areas). The phase of the low water is delayed throughout the estuary if intertidal storage is added (Figure 5.2e), with the longest phase lags if the additional storage area is located further upstream and hence affects a larger portion of the local tidal prism (i.e., up to 12 min for the scenario with additional storage at KM-97).

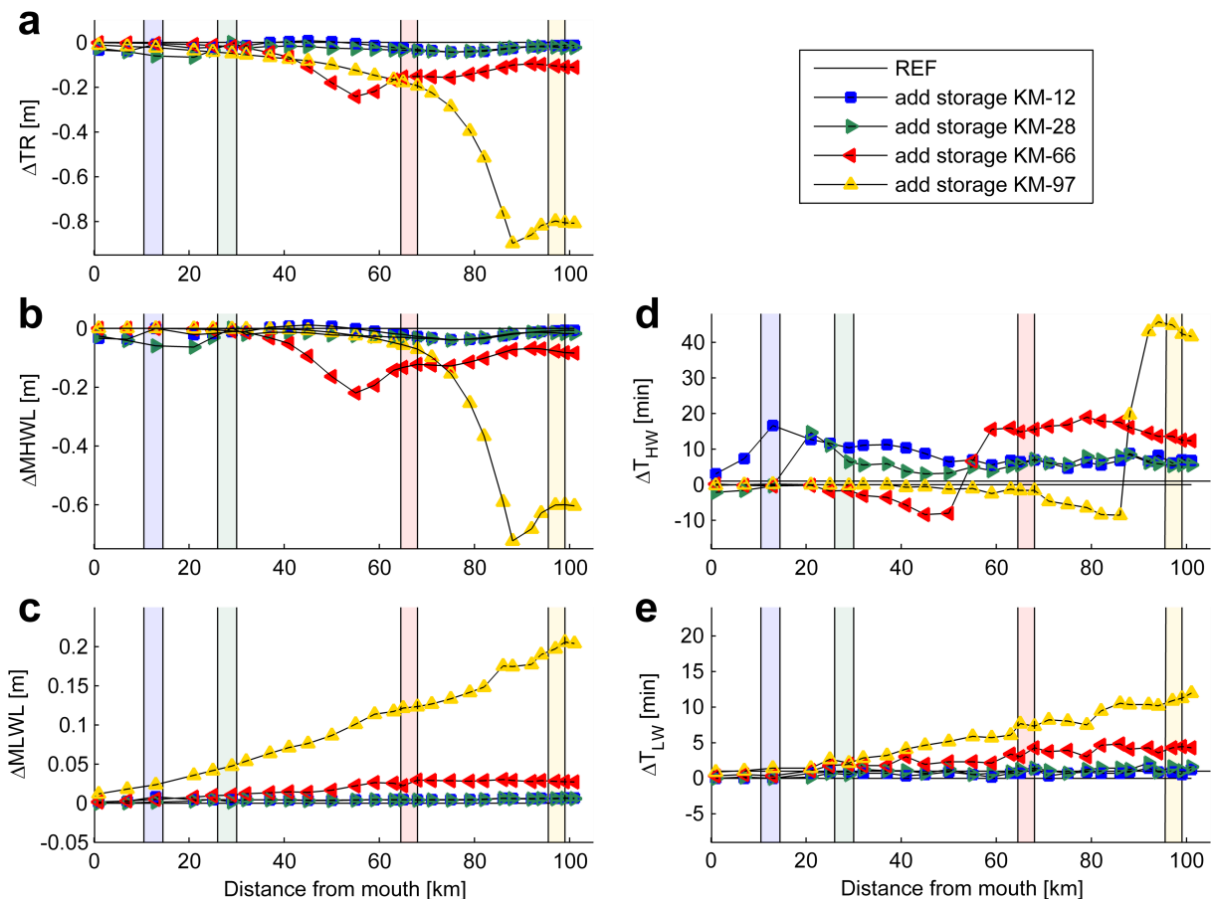


**Figure 5.2:** Modelled change in (a) tidal range, (b) mean high water level (MHWL), (c) mean low water level (MLWL) and the phase differences of (d) high water ( $T_{HW}$ ) and (e) low water ( $T_{LW}$ ) for the scenarios with additional intertidal storage at KM-12 (blue), KM-28 (green), KM-66 (red) and KM-97 (yellow), relative to the reference scenario (zero line).

The effect of additional intertidal storage areas on the tidal prism varies along the estuary (Figure 5.3). Upstream of the additional storage areas, there is a reduction in tidal prism, which is relatively stronger if the area is located further upstream. The tidal prism strongly increases directly downstream of the additional storage area (i.e., by  $\sim 30 \text{ Mm}^3$  in all scenarios). The relative effect is again stronger if the storage area is

located further upstream along the estuary channels (i.e., up to a 30% increase for the scenario with added storage area at KM-97) and therefore affects a larger part of the original tidal prism. However, the tidal prism increase weakens downstream and even turns into a decrease for the scenarios in which intertididal storage is added at KM-66 and KM-97. In contrast, for the scenarios in which intertididal storage is added in the downstream part of the estuary (i.e., KM-12 or KM-28), the tidal prism increase remains fairly constant up until the estuary mouth.  $V_{cs-flood}$  and  $V_{cs-ebb}$  (Figure 5.4) show a similar pattern as the tidal prism, with a reduction in both flood and ebb velocities upstream of the added storage areas and an increase in peak velocities downstream of the additional intertididal storage. Generally, peak flood velocities are more affected than the peak ebb velocities.

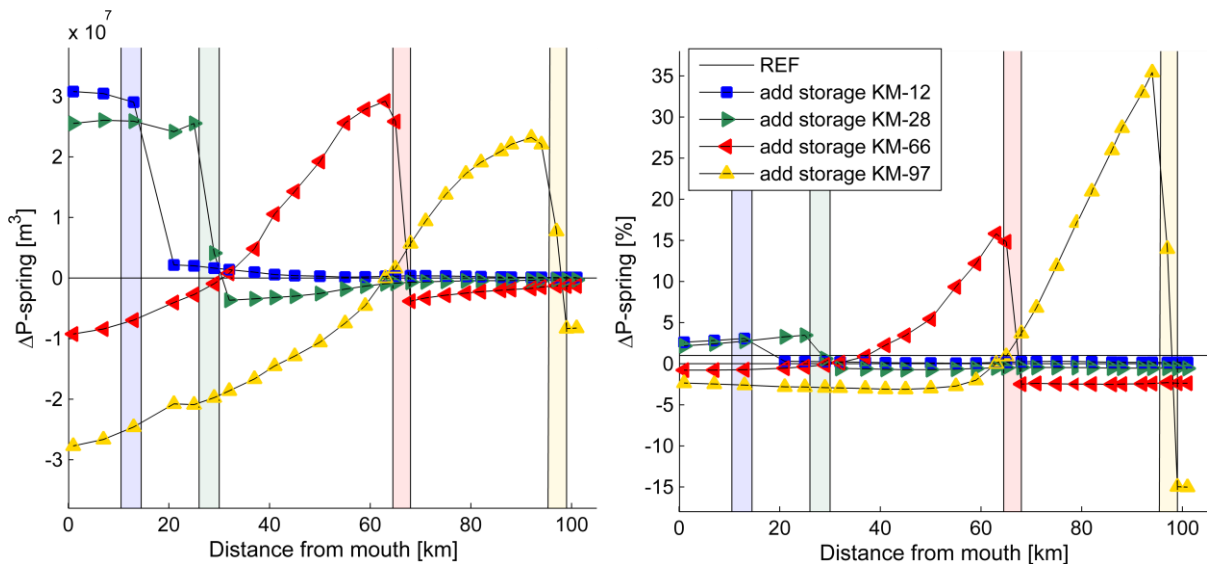


**Figure 5.3:** Modelled absolute (left) and percentage (right) change in tidal prism for the scenarios with additional intertididal storage at KM-12 (blue), KM-28 (green), KM-66 (red) and KM-97 (yellow) compared to the reference scenario (zero line).

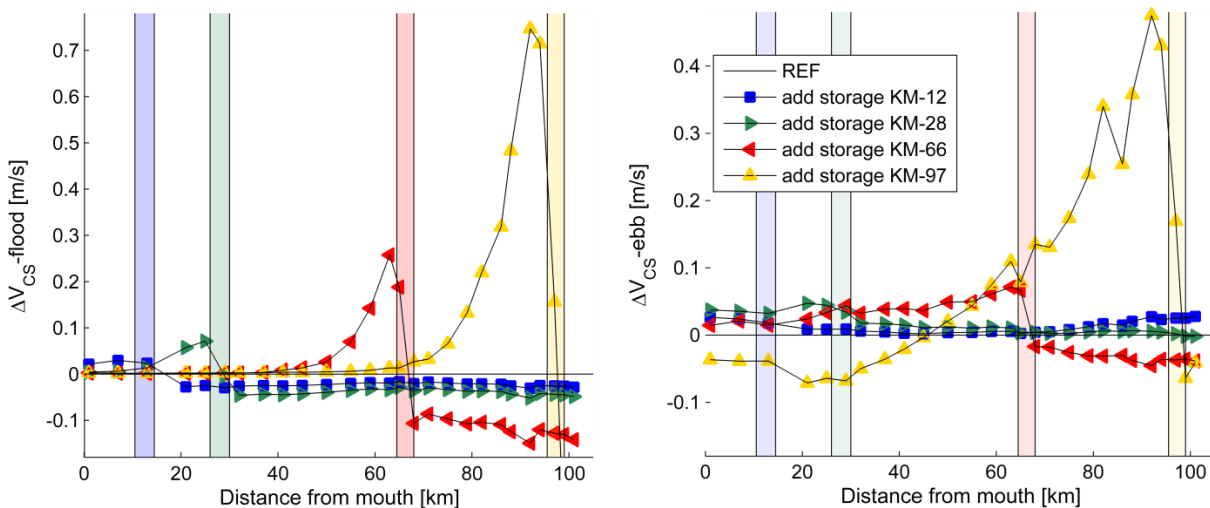


**Figure 5.4:** Modelled difference in cross-sectional averaged peak flood velocities (left) and cross-sectional averaged peak ebb velocities (right) between scenarios with additional intertididal storage at KM-12 (blue), KM-28 (green), KM-66 (red) and KM-97 (yellow) compared to the reference scenario (zero line).

Tidal asymmetry along the estuarine channels is also affected by additional intertididal storage. Based on  $R_T$  (i.e., the ratio between the duration of the rising and the falling tide;

Figure 5.5), flood-dominance of the vertical tide is enhanced downstream of the added storage areas (i.e., lower  $R_T$ -values) and is reduced upstream of those areas (i.e., higher  $R_T$ -values). A shift between the strongest decrease in  $R_T$  to the strongest increase in  $R_T$  is present just downstream of the additional storage areas in all artificial scenarios. Similar patterns are present in  $R_V$  (i.e., the ratio between cross-sectional averaged peak velocities during flood and ebb), which shifts abruptly from enhanced flood-dominance (i.e., higher  $R_V$ -values) directly downstream of additional intertidal storage areas to a reduction in flood-dominance or even a shift to ebb-dominance (i.e., lower  $R_V$ -values) upstream of these areas (Figure 5.5). Further downstream, the impact of additional storage areas located in the upstream part (i.e., at KM-66 and KM-97) on  $R_T$  diminishes, while  $R_V$  shifts back to slightly enhanced ebb-dominance. An exception is the model scenario with additional intertidal storage at KM-97 which shows a remarkable increase in  $R_V$  near the estuary mouth. If the relative contribution and phase differences of the M4 and M2 tidal constituents obtained from harmonic analysis in **Appendix 5A** are considered as indicators for tidal asymmetry, the effects of additional storage areas are largely similar but more subtle. In particular flood-dominance is slightly enhanced directly downstream of additional storage areas and flood-dominance is generally reduced upstream. However, the local increase in flood-dominance of the horizontal tide directly downstream of the added storage areas is not present based on harmonic analysis of the velocity time series.

In addition, the model results indicate some general characteristics of the along-estuary variation in tidal asymmetry. For instance, flood dominance of the vertical tide generally increases along the estuary, although it decreases slightly between KM-20 and KM50, with for the reference scenario  $R_T = 0.95$  near the mouth and  $R_T = 0.77$  at KM-100. Along-estuary variations in  $R_V$  are less gradual but consistently flood-dominant for the reference scenario, ranging between  $R_V = 1.05$  and  $R_V = 1.30$ .

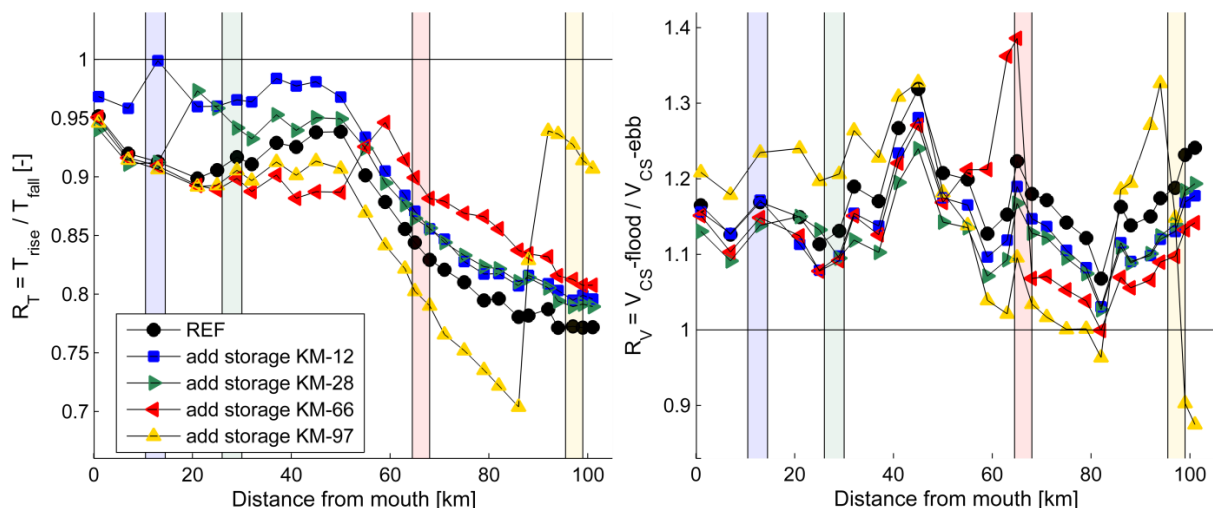


**Figure 5.5:** Modelled vertical tidal asymmetry based on the ratio between the duration of the rising tide and of the falling tide (left) and horizontal asymmetry based on the ratio between cross-sectional averaged peak velocities during flood and during ebb (right) for scenarios with additional intertidal storage at KM-12 (blue), KM-28 (green), KM-66 (red) and KM-97 (yellow) and for the reference scenario (black dots and line).

**5.4.2 Scenarios with varying tidal flat elevation**

The presence of intertidal flats within the main estuarine channel has a significant impact on the damping or amplification of the tidal wave along the estuary, depicted by the tidal range in Figure 5.6a. In particular, inclusion of tidal flats reduces the tidal range by up to 0.20 m, depending on the elevation of the intertidal areas. In the downstream part of the estuary (i.e., up until KM-50), lower tidal flats result in the strongest tidal range reduction, whereas intertidal flats that are higher in the tidal frame result in less reduction of the tidal range (Figure 5.6b). Conversely, tidal range reduction is stronger for higher intertidal flats in the upstream part of the estuary (i.e., from KM-50 onwards). In the most upstream part of the analyzed transect where there are barely any tidal flats present (i.e., from KM-75 onwards), there is even an increase in tidal range for scenarios with  $z_{\text{flat}} < 0$  m NAP, as well as for the reference scenario. Variations in tidal range between the different model scenarios are mostly the result of differences in high water levels, rather than in low water levels (Figure 5.6c-f) as variations in MHWL show similar trends as the tidal range (Figure 5.6c & 5.6d), whereas variations in MLWL are all within  $\pm 0.03$  m, except for the scenario with low intertidal flats (i.e.,  $z_{\text{flat}} = -2.0$  m NAP) for which a maximum MLWL increase of 0.08 m is modelled (Figure 5.6e & 5.6f). For this simulation, the impact on MLWL even exceeds impact on MHWL along large parts of the estuary. Furthermore, the propagation of the high water as well as the low water are slowed down due to the presence of tidal flats (Figure 5.6g-j). The low water phase lag is longest for lower tidal flats throughout the estuary (i.e., up to 24 minutes for  $z_{\text{flat}} = \text{NAP} - 2.0$  m; Figure 5.6j). The high water phase lag is longer for tidal flats around or slightly above MSL in the upstream part of the estuary (i.e., from KM-50 onwards for  $z_{\text{flat}} = \text{NAP} + 0.0$  m and  $z_{\text{flat}} = \text{NAP} + 1.0$  m) and for lower tidal flats in the downstream part (i.e., up until KM-50; Figure 5.6h).

The modelled tidal prism is also strongly affected by the inclusion of tidal flats within the estuarine channel (Figure 5.7). Scenarios with lower tidal flats and hence more intertidal storage result in the strongest tidal prism increase of up to 33%, whereas higher tidal flats with less storage volume result in a maximum tidal prism increase of only 3% compared to the scenario without tidal flats within the estuary. The relative increase in tidal prism is strongest between KM-30 and KM-50. Further upstream, the differences in tidal prism between the model scenarios become smaller and are even minimized from KM-90 onwards, where the analyzed transect ends and upstream of which there are no bathymetrical differences between the scenarios. Similar trends can be observed from the cross-sectional averaged peak velocities (Figure 5.8), especially during flood, which are highest in scenarios with low tidal flats and lowest for scenarios with high tidal flats. For peak ebb velocities, the scenario with a tidal flat elevation of  $z_{\text{flat}} = 0$  m NAP results in the highest velocity increase up until  $\sim$ KM-75. Velocity differences between the model scenarios become smaller upstream and even diminish in the most upstream part (i.e., from KM-75 onwards).

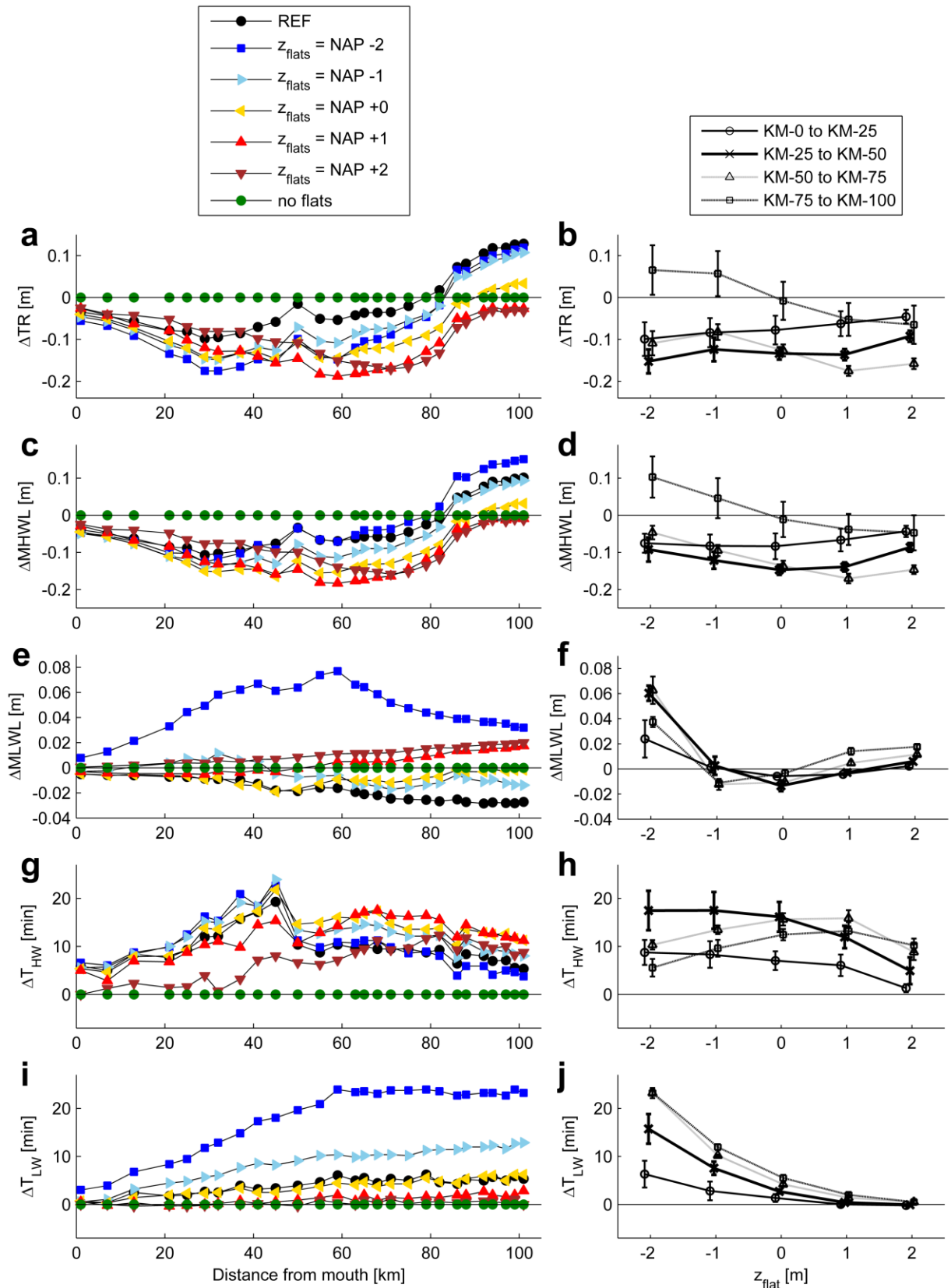


**Figure 5.6:** Modelled difference in tidal range (a & b), mean high water level (c & d), mean low water level (e & f) and the phase differences of high water  $T_{HW}$  (g & h) and low water  $T_{LW}$  (i & j) for the reference scenario and scenarios with varying elevations of tidal flats within the main estuarine channel compared to the scenario without tidal flats (left); and also plotted against the tidal flat elevation, averaged over four parts of the estuary, with error bars representing the standard deviation per section (right).

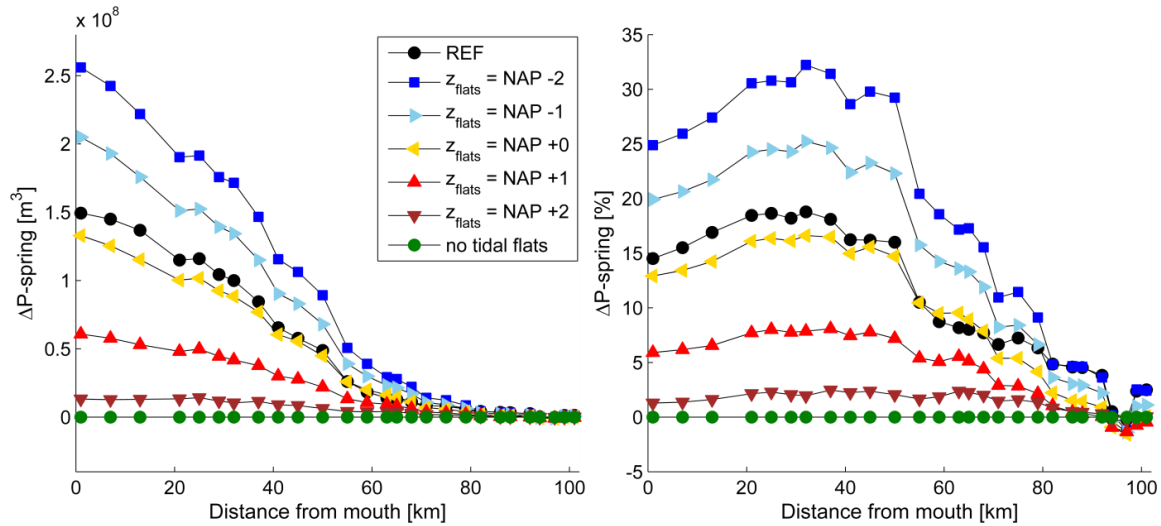


**Figure 5.7:** Modelled absolute (left) and relative (right) difference in tidal prism for the reference scenario and for scenarios with varying elevations of tidal flats within the main estuarine channel, compared to the scenario without tidal flats.

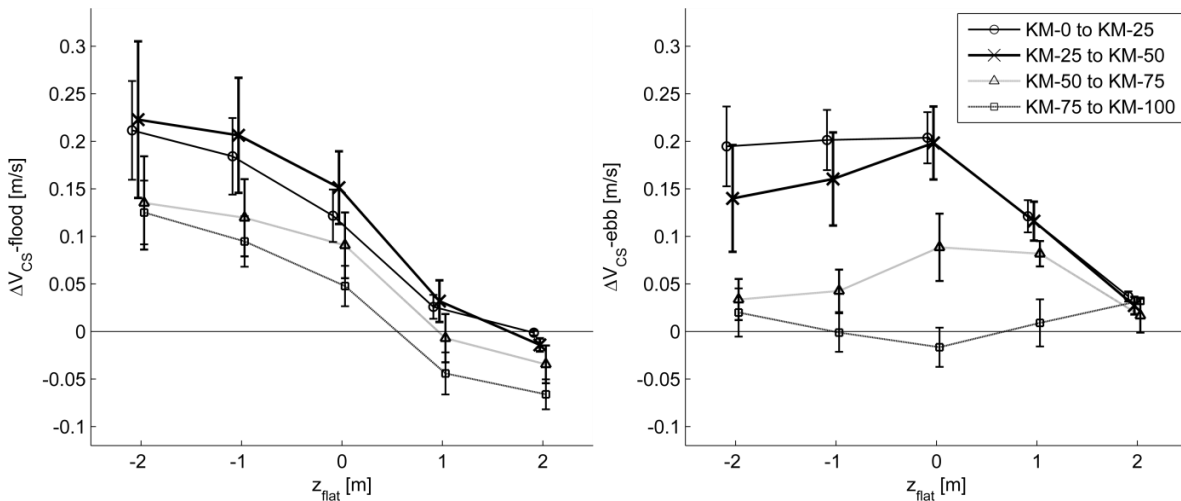


**Figure 5.8:** Modelled difference in cross-sectional averaged peak velocities during flood (left) and ebb (right) between scenarios with specific tidal flat elevations and the scenario without tidal flats, averaged over four parts of the estuary, with error bars representing the standard deviation per section.

Horizontal and vertical tidal asymmetry along the estuary vary between model scenarios with different tidal flat elevations (Figures 5.9 and 5.10), but tidal asymmetry is in all cases flood-dominant based on  $R_T$  (i.e., the ratio between the duration of the rising and the falling tide) and  $R_V$  (i.e., the ratio between cross-sectional averaged peak velocities during flood and ebb). The strength of the flood-dominant asymmetry is weakest for  $z_{flat} = 0.0$  m NAP and  $z_{flat} = +1.0$  m NAP along large parts of the estuary. Conversely, in the most upstream part (from KM-75 onwards) the least flood-dominant horizontal asymmetry (i.e., lowest  $R_V$ -values) is modelled for  $z_{flat} = +2.0$  m NAP (Figure 5.10). Furthermore, the most flood-dominant asymmetry is modelled for scenarios with low tidal flats (i.e., in the upstream part of the estuary) or for the scenario without tidal flats (i.e., in the downstream part of the estuary). The trends in  $R_V$  and  $R_T$  for scenarios with varying tidal flat elevations are all consistent with the results of a harmonic component analysis on the water level time series and cross-sectional averaged velocity time series (see **Appendix 5A**). However, based on the phase difference between the M4 and M2 tidal constituents, an ebb-dominant asymmetry of the vertical tide and the

horizontal tide is present along parts of the estuary for the model scenarios with  $z_{\text{flat}} = 0.0$  m NAP and  $z_{\text{flat}} = +1.0$  m NAP, whereas  $R_V$  and  $R_T$  only become less flood-dominant. Besides, in the most downstream part of the estuary, ebb-dominance prevails for all scenarios except the scenario with  $z_{\text{flat}} = -2.0$  m NAP, based on the harmonic component analysis.

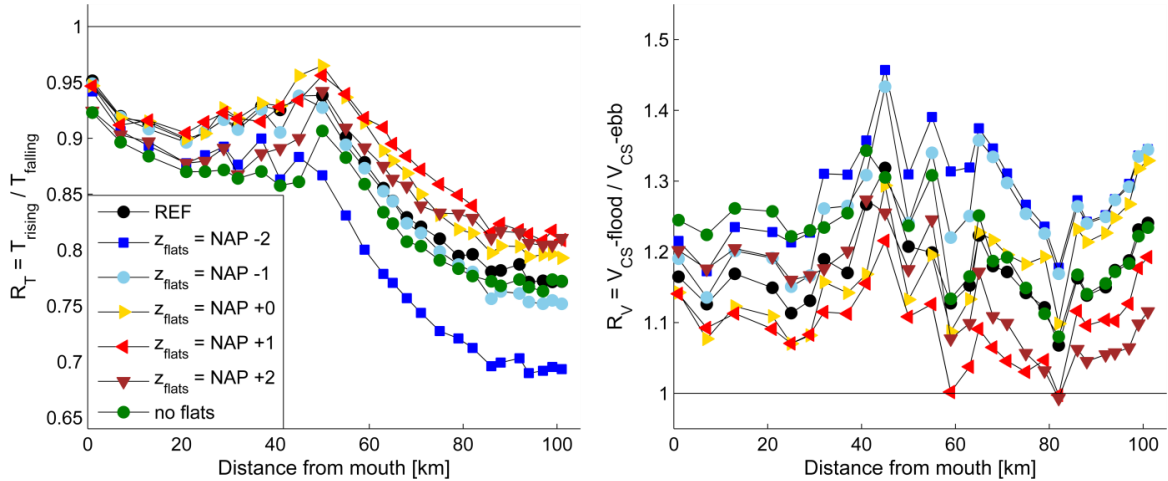


**Figure 5.9:** Modelled vertical tidal asymmetry based on the ratio between the duration of the rising tide and of the falling tide (left) and horizontal asymmetry based on the ratio between cross-sectional averaged peak velocities during flood and during ebb (right) for scenarios with varying elevations of tidal flats within the main estuarine channel.

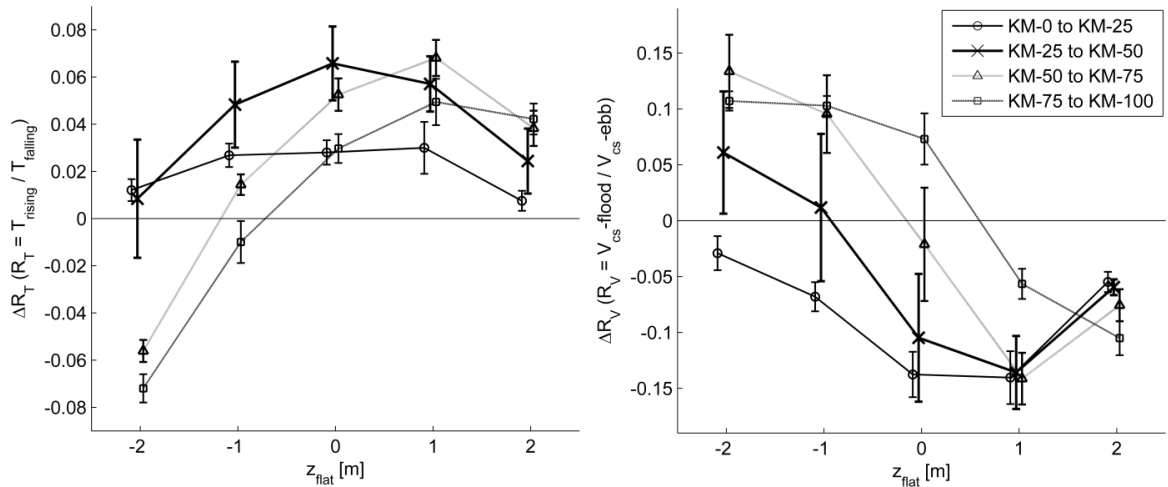


**Figure 5.10:** Modelled difference in vertical tidal asymmetry based on the ratio between the duration of the rising tide and of the falling tide (left) and in horizontal tidal asymmetry based on the ratio between cross-sectional averaged peak velocities during flood and during ebb (right) between scenarios with specific tidal flat elevations and the scenario without tidal flats, averaged over four parts of the estuary and plotted against the tidal flat elevation, with error bars representing the standard deviation per section.

## 5.5 Discussion

The impact of specific intertidal area characteristics on tidal hydrodynamics was assessed with a hydrodynamic model of the Scheldt Estuary. We show that intertidal areas can have varying effects on tidal hydrodynamics depending on their elevation and location along the main estuary channels. While previous studies often only considered

the storage function of tidal flats (e.g. Friedrichs and Aubrey, 1994, 1988; Friedrichs and Madsen, 1992), we show that friction exerted by the tidal flats is also a determining factor for tidal asymmetry and that low tidal flats may even enhance flood-dominance. In particular, our results indicate that the elevation of tidal flats and hence the amount of friction exerted and storage provided at different water levels determines the influence of tidal flats on the type of tidal asymmetry in estuarine channels (i.e., whether tidal flats enhance ebb-dominance or flood-dominance). It is also shown that tidal flats that are part of the flow-carrying cross-section of the estuary (i.e., located within the estuarine channel system) and exert friction on the propagating tidal wave may, depending on their elevation, have a different influence on tidal hydrodynamics than intertidal areas that contribute little to the flow-carrying cross-section of the estuary and mainly provide for intertidal storage (i.e., such as intertidal side-basins adjacent to the estuarine channel system). Furthermore, the locations of intertidal storage areas as well as their size relative to the local tidal prism determine the strength and along-estuary stretch of the impact on tidal prism, tidal range and tidal asymmetry.

### **5.5.1 Effects on tidal asymmetry**

The impact of intertidal area characteristics on tidal asymmetry is assessed by (1) the ratio between the duration of the rising and falling tide, (2) the ratio between peak flood and peak ebb velocities and (3) by a tidal constituent analysis (**Appendix 5A**). For the different parameters for tidal asymmetry, the impact of changes in intertidal area characteristics on tidal asymmetry is qualitatively similar, although the strength and type of tidal asymmetry may differ between these indicators (i.e., one parameter tends to become more flood- or ebb-dominant than the other).

If the intertidal flats contribute to the flow-carrying cross-section (i.e. located within the estuarine channel system), the storage and frictional effects on the shallow intertidal flats both affect the tidal propagation along the estuary. Friction and storage effects on the tidal flats generally slow the propagation of the high water more than the propagation of the low water, enhancing ebb-dominance (Friedrichs and Aubrey, 1988). However, our model results show that this mechanism only enhances ebb-dominance for a specific range of tidal flat elevations (Figures 5.9, 5.10 and **Appendix 5A**). In particular, tidal flats with an elevation between  $\sim$ MSL and  $\sim$ MHWL enhance ebb-dominance or decrease flood-dominance the most in our simulations, with the strongest reduction in flood-dominant asymmetry for tidal flat elevations slightly above MSL (i.e.,  $z_{\text{flat}} = \text{NAP} + 0.0 \text{ m}$  to  $\text{NAP} + 1.0 \text{ m}$ ) (Figure 5.10). The latter was also found by Fortunato and Oliveira (2005), who assessed the propagation speed of the high and low tide analytically and showed that a tidal flat elevation slightly above mean sea level induces the strongest ebb-dominance. Furthermore, our model results indicate that tidal flats that are situated low in the tidal frame do not always enhance ebb-dominance. Instead, they may even enhance a flood-dominant asymmetry as they do not only slow the propagating high tide, but also affect the propagating low tide. While the storage volume increases for low tidal flats, the friction effect on the propagating high tide will decrease as the water depth on the tidal flats becomes larger and the friction exerted on low water levels increases. Very low tidal flats may even become subtidal during neap tides



(i.e., with relatively high low water levels) and hence reduce the effective depth of the flow-carrying cross-section (i.e., cross-sectional averaged depth according to Van Rijn, 2011). In that case, the situation can also be interpreted as that of an estuarine channel with a relatively large amplitude-to-depth ratio, which is generally characterized by flood-dominance due to the frictional interaction between the tide and the shallow channel bottom (e.g. Friedrichs and Aubrey, 1988; Friedrichs and Madsen, 1992; Speer and Aubrey, 1985). On the other hand, for intertidal flats that are situated very high in the tidal frame, the intertidal storage volume minimizes and hence the propagation of the tidal wave and high water in particular is less affected by the intertidal storage. According to our model results, the decrease in flood-dominance is weaker in this situation (i.e.,  $z_{\text{flat}} = \text{NAP} + 2.0 \text{ m}$ ) compared to the situation without tidal flats. In the extreme case without tidal flats, flood-dominance prevails throughout the estuary, which is consistent with the findings of Lanzoni and Seminara (2002).

The above mechanisms enhance flood-dominance for low intertidal flats if they are part of the flow-carrying cross-section of the estuary. However, in case the location of the intertidal storage within the estuary is such that it does barely contribute to the flow-carrying cross-section of the estuary (i.e. intertidal side-basins), frictional effects of the intertidal flats on the propagation of the tidal wave through the estuary are expected to be small. Generally, a large intertidal storage volume in the absence of friction is known to enhance ebb-dominance through the storage term in the continuity equation as the intertidal storage is always larger at high water than at low water (Friedrichs and Aubrey, 1988; Friedrichs and Madsen, 1992). This is indeed observed in the simulation results, in which ebb-dominance is enhanced upstream of the additional storage areas (Figure 5.5 and **Appendix 5A**) as the propagation of the tidal wave is slowed down due to the presence of the additional intertidal storage. Besides, a slower propagation of the high waters upstream of additional intertidal storage was also modelled by Maximova et al. (2010) in a previous modelling study on the effect of fictitious de-embankments of historical branches and marshes along the Scheldt Estuary. In contrast, flood-dominance is enhanced along a stretch of several kilometers downstream of the additional intertidal storage areas (i.e., up to 20 km for the horizontal tide and up to 40 km for the vertical tide, depending on the relative size of the storage area). This appears to be the result of a faster propagating high tide (Figure 5.2d) and to a stronger increase in peak flood velocities than in peak ebb velocities (Figure 5.4) related to a velocity surge at the moment the intertidal flats become inundated. Further downstream, the effect on vertical tidal asymmetry diminishes or remains slightly more flood-dominant, whereas the horizontal tidal asymmetry shifts back to slightly enhanced ebb-dominance as a result of the additional storage areas. Hence, the horizontal and vertical tidal asymmetries are not always similar in the presence of tidal flats.

### ***5.5.2 Effects on tidal range and tidal prism***

In addition to tidal asymmetry, intertidal areas also affect the tidal range and tidal prism along estuarine channels. For the scenarios in which intertidal storage is added at specific locations along the estuary, tidal prism and tidal range decrease upstream as the tidal wave is damped by the intertidal storage area (i.e., the tidal range decreases and

the propagation of especially the high tide is slowed down). The impact of added storage areas is stronger if the surface area and hence storage volume of the side-basins are larger relative to the local tidal prism (i.e., for more upstream located side-basins). It has been shown analytically that the impact of storage basins on the upstream tidal amplitude relates to the 'basin admittance' (Li et al., 2016; Roos and Schuttelaars, 2015). The basin admittance is a proportionality coefficient between the water volume entering the basin and the local tidal amplitude, and is a function of the basin's surface area, the local channel geometry and of the geometry of the connection between the side-basin and the estuarine channel. Relatively large basins with narrow connections to the estuary channel have high basin admittances and exert a strong influence on upstream tidal amplitude, while small basins with wide connections have low basin admittances and have a less pronounced impact on tidal amplitude. Similar to the analytical results of Li et al. (2016) on additional storage basins along the Ems estuary, additional intertidal storage basins always reduce the upstream tidal amplitude in our model results.

The tidal prism strongly increases directly downstream of an intertidal storage area, which can be related to the additional storage volume of the area itself. Further downstream of the storage area, the increase in tidal prism gradually becomes smaller and may even switch to a remarkable decrease in tidal prism in the most downstream part of the estuary. This can be explained by the decrease in tidal range due to the additional intertidal storage volume (Jeuken et al., 2004; Maximova et al., 2010). In particular, as the tidal prism strongly increases downstream of additional intertidal areas as a direct result of the added storage volume (Figure 5.3) and there is no compensatory increase in the cross-sectional area of the channels, flow velocities in the tidal channels increase as well (Figure 5.4), leading to higher bottom friction and hence a reduced tidal range (Figure 5.2a). This second-order effect on the tidal prism increases downstream as a larger area is influenced (Figure 5.3). While the most downstream additional storage areas still induce a tidal prism increase near the estuary mouth, the scenarios in which the additional storage areas are located far upstream induce a strong tidal prism decrease at the estuary mouth, implying that far downstream this second-order effect of tidal range reduction can be stronger than the first-order effect of storage volume increase. This conclusion differs as compared to previous modelling studies on the de-embankment of historical side-branches and marshes along the Scheldt Estuary (i.e., Coen et al., 2008; Jeuken et al., 2004) in which it was concluded that the second-order effect of tidal range reduction on the tidal prism is always weaker than the tidal prism increase due to the additional storage volume itself. In conclusion, the variation in the impact of (additional) intertidal storage areas on the tidal prism along the estuary appears to depend on the along-estuary location: a reduction in tidal prism arises at the seaward edge of the estuary if the intertidal storage is located far enough upstream, otherwise the tidal prism increases in the most downstream part of the estuary.

Furthermore, the presence of tidal flats along the estuarine channels reduces the tidal range in large parts of the estuary independent of tidal flat elevation, indicating that damping due to friction and (additional) intertidal storage dominates over inertia and convergence (Friedrichs and Aubrey, 1994; Friedrichs and Madsen, 1992). Model results

indicate that in the downstream part of the analyzed transect (i.e., up until KM-50), the tidal range decreases most for low tidal flats which add the largest intertidal storage volume, which suggests that the effect of increasing storage volume is stronger than the effect of decreasing friction (due to a larger water depth). Conversely, in the upstream part of the analyzed transect (i.e., from KM-50 onwards), tidal range and MHWL decrease most for higher tidal flats, which provide for less storage but exert more friction for the propagating high tide. In the most upstream part of the analyzed transect where there are barely any tidal flats present (i.e., upstream of KM-75), the tidal range even increases for simulations with intertidal flat elevations below mean sea level (Figure 5.6b). This can be attributed to an increase in tidal prism in the most upstream part of the estuary for these scenarios (Figure 5.7), which is not compensated by a significant increase in intertidal storage volume or channel cross-section in the upstream section and hence leads to a stronger amplification of the tide.

### ***5.5.3 The effect of hydro-morphodynamic feedbacks***

With respect to the conclusions on the hydrodynamic impact of intertidal areas, it should be stated that only initial hydrodynamic effects of (changes in) intertidal area location and elevation are obtained by this modelling study. It can be expected that changes in tidal prism, tidal flow velocities and tidal asymmetry initiate morphological changes in the estuarine channels and of the tidal flats itself, towards a new dynamic equilibrium of the estuarine morphology and tidal hydrodynamics (e.g. Dronkers, 1986; Van Dongeren and Vriend, 1994), but these hydro-morphodynamic feedbacks are not taken into account in this study. For instance, an increase in tidal prism and flow velocities in the channels may induce channel deepening and/or widening, while a reduction in tidal prism and tidal flow velocities induces channel infilling according to global relationships between cross-sections of tidal channels and the tidal prism (e.g. Dronkers, 1998; Jarrett, 1976; O'Brien, 1969, 1931). Along with such morphodynamic changes, the impact of intertidal area changes on tidal hydrodynamics may alter as well (e.g. Jeuken et al., 2004; Wang et al., 2002). Decadal scale hydro-morphological modelling by Jeuken et al. (2004) showed that the initial impact of additional storage areas on sediment transport through the channels in the downstream part of the Scheldt Estuary may differ from the decadal scale impact. In particular, they showed that for the specific case of additional intertidal areas along the downstream part of the Western Scheldt, the initial decrease in tidal range is less pronounced on the long-term due to morphological feedback mechanisms (i.e., channel erosion or infilling) and that after some decades an increase in tidal range might even occur. However, these feedback-mechanisms occur on morphological timescales of several decades which is estimated to be around 50-100 years for the Scheldt Estuary, while the hydrodynamic response during the first decades after sudden intertidal area changes such as embankments or de-embankments are expected to be fairly similar to the initial response (Jeuken et al., 2004). Nevertheless, it may be expected that especially very large changes and the relatively sharp transitions in tidal hydrodynamics along the estuary would in reality become smaller and more gradual as a result of hydro-morphodynamic feedbacks.

Besides, the impact of intertidal area changes on tidal hydrodynamics and the morphological development will in reality also interfere with the effects of channel deepening and enlargement through dredging activities. A comparison between the (initial) hydrodynamic impact of intertidal area changes and of channel deepening is made in **Appendix 5C**, in which the results of scenarios with (fictitious) channel enlargement (i.e., deepening and widening) are discussed.

### ***5.5.4 Implications for estuarine management***

Finally, as our results demonstrate the effects of intertidal area characteristics on tidal hydrodynamics along the estuary, this study may help estuarine managers in assessing the impact of human-induced intertidal area changes such as (de-)embankments, as well as with the morphological management of estuaries through dredging and disposal of dredged sediments on intertidal areas. Our model results show the initial hydrodynamic impact of (fictitious) de-embankments or morphological management measures (i.e., altering the elevation of tidal flats). In general, creation of intertidal areas as part of morphological management strategies could be used to enhance channel erosion by increasing tidal prism and ebb-dominance along specific stretches of estuarine channels. Moreover, careful dredging and disposal of sediment could be used to shape intertidal flats at a desired elevation aiming for a specific impact on tidal asymmetry. In addition to human-induced impacts, natural morphological changes in intertidal areas may have considerable impact on along estuary tidal hydrodynamics. In particular, vertical accretion of intertidal areas such as the development from relatively low bare intertidal flats to vegetated marshes which are situated higher in the tidal frame may lead to a temporally varying impact on tidal hydrodynamics along estuarine channels (i.e., the impact on tidal asymmetry strongly depends on tidal flat elevation) according to the present model results. As several marsh restoration projects are being realized or will be realized along the Scheldt estuary in the near future, the present model results are of special interest to this area. For example, the model results suggest that the flood control areas along the Belgian part of the Scheldt estuary that do not contribute to the flow-carrying cross-section of the estuarine channel have a different impact on estuarine tidal hydrodynamics than the intertidal flats located within the estuarine channel system, especially for tidal flats that are situated low in the tidal frame. All these spatial and temporal variations in hydrodynamic effects but also morphodynamic impact should be taken in consideration when it comes to the implementation of marsh restoration, managed realignment and other ecosystem-based adaptation schemes along the Scheldt estuary and other estuaries worldwide.

## **5.6 References**

Anon, 2010. Bodemberoerende activiteiten. Indicatoren voor het Schelde-estuarium., in: VLIZ Information Sheets. Vlaams Instituut voor de Zee (VLIZ), Oostende, p. 11.

Aubrey, D.G., Speer, P.E., 1985. A Study of Non-linear Tidal Propagation in shallow inlet / estuarine systems Part I : Observations. *Estuar. Coast. Shelf Sci.* 21, 185–205.

- Barbier, E.B., Georgiou, I.Y., Enchelmeyer, B., Reed, D.J., 2013. The value of wetlands in protecting Southeast Louisiana from hurricane storm surges. *PLoS One* 8, e58715. doi:10.1371/journal.pone.0058715
- Blott, S.J., Pye, K., van der Wal, D., Neal, A., 2006. Long-term morphological change and its causes in the Mersey Estuary, NW England. *Geomorphology* 81, 185–206. doi:10.1016/j.geomorph.2006.04.008
- Brown, J.M., Davies, A.G., 2010. Flood/ebb tidal asymmetry in a shallow sandy estuary and the impact on net sand transport. *Geomorphology* 114, 431–439. doi:10.1016/j.geomorph.2009.08.006
- Coen, L., Peeters, P., Mostaert, F., 2008. Inventarisatie en historische analyse Zeeschelde habitats: Effect antropogene ingrepen en natuurlijke evoluties op de getij-indringing in de Zeeschelde - Ondersteunende numerieke 1D-modellering. WL Rapporten, 713\_21. Antwerpen.
- Costanza, R., Arge, R., Groot, R. De, Farberk, S., Grasso, M., Hannon, B., Limburg, K., Naeem, S., O'Neill, R. V., Paruelo, J., Raskin, R.G., Suttonk, P., van den Belt, M., 1997. The value of the world 's ecosystem services and natural capital. *Nature* 387, 253–260. doi:10.1038/387253a0
- Cox, T., Maris, T., De Vleeschauwer, P., De Mulder, T., Soetaert, K., Meire, P., 2006. Flood control areas as an opportunity to restore estuarine habitat. *Ecol. Eng.* 28, 55–63. doi:10.1016/j.ecoleng.2006.04.001
- De Mulder, T., Vercruyssen, J., Peeters, P., Maris, T., Meire, P., 2013. Inlet sluices for flood control areas with controlled reduced tide in the Scheldt estuary: an overview, in: Bung, D.B. et al. (Ed.), *Proceedings of the International Workshop on Hydraulic Design of Low-Head Structures*. Aachen, Germany, pp. 43–53.
- Dronkers, J., 1998. Morphodynamics of the Dutch Delta, in: *Physics of Estuaries and Coastal Seas*. The Hague, Netherlands, pp. 297–304.
- Dronkers, J., 1986. Tidal asymmetry and estuarine morphology. *Netherlands J. Sea Res.* 20, 117–131. doi:10.1016/0077-7579(86)90036-0
- Fortunato, A.B., Oliveira, A., 2005. Influence of Intertidal Flats on Tidal Asymmetry. *J. Coast. Res.* 21, 1062–1067. doi:10.2112/03-0089.1
- French, P.W., 2006. Managed realignment - The developing story of a comparatively new approach to soft engineering. *Estuar. Coast. Shelf Sci.* 67, 409–423. doi:10.1016/j.ecss.2005.11.035
- Friedrichs, C.T., Aubrey, D.G., 1994. Tidal propagation in strongly convergent channels. *J. Geophys. Res.* 99, 3321–3336. doi:10.1029/93JC03219
- Friedrichs, C.T., Aubrey, D.G., 1988. Non-linear Tidal Distortion in Shallow Well-Mixed Estuaries: a Synthesis. *Estuar. Coast. Shelf Sci.* 27, 521–545. doi:10.1016/0272-7714(90)90054-U
- Friedrichs, C.T., Madsen, O.S., 1992. Nonlinear diffusion of the tidal signal in frictionally dominated embayments. *J. Geophys. Res.* 97, 5637–5650. doi:10.1029/92JC00354
- Hervouet, J.-M., 2007. Hydrodynamics of Free Surface Flows: Modelling with the finite element method. doi:10.1002/9780470319628
- Jarrett, J.T., 1976. *Tidal Prism - Inlet Area Relationships*. Vicksburg, MS, U.S.
- Jeuken, C., Wang, Z.B., van der Kaaij, T., Van Helvert, M., Van Ormondt, M., Bruinsma, R., Tanczos, I., 2004. Morfologische ontwikkelingen in het Schelde estuarium bij voortzetting van het huidige beleid en effecten van een verdere verdieping van de vaargeul en uitpoldering langs de Westerschelde. Deelovereenkomst 2 en 3. Morfologie.
- Jeuken, M.C.J.L., Wang, Z.B., 2010. Impact of dredging and dumping on the stability of ebb-flood channel systems. *Coast. Eng.* 57, 553–566. doi:10.1016/j.coastaleng.2009.12.004
- Jongepier, I., Wang, C., Missiaen, T., Soens, T., Temmerman, S., 2015. Intertidal landscape response time to dike breaching and stepwise re-embankment: A combined historical and geomorphological study. *Geomorphology* 236, 64–78. doi:10.1016/j.geomorph.2015.02.012
- Kirwan, M.L., Megonigal, J.P., 2013. Tidal wetland stability in the face of human impacts and sea-level rise. *Nature* 504, 53–60. doi:10.1038/nature12856
- Lanzoni, S., Seminara, G., 2002. Long-term evolution and morphodynamic equilibrium of tidal channels. *J. Geophys. Res.* 107, --. doi:10.1029/2000JC000468
- Li, C., Schuttelaars, H.M., Roos, P.C., Damveld, J.H., Gong, W., Hulscher, S.J.M.H., 2016. Influence of retention basins on tidal dynamics in estuaries: Application to the Ems estuary. *Ocean Coast. Manag.* 134, 216–225. doi:10.1016/j.ocecoaman.2016.10.010
- Maris, T., Cox, T., Temmerman, S., De Vleeschauwer, P., Van Damme, S., De Mulder, T., Van Den Bergh, E., Meire, P., 2007. Tuning the tide: Creating ecological conditions for tidal marsh development in a flood control area. *Hydrobiologia* 588, 31–43. doi:10.1007/s10750-007-0650-5
- Maximova, T., Ides, S., Plancke, Y., De Mulder, T., Mostaert, F., 2010. Vervolgstudie inventarisatie en historische analyse van slikken en schorren langs de Zeeschelde - Scenario analyse 2D model. WL Rapporten, 713\_21. Antwerpen.

- Meire, P., Ysebaert, T., Van Damme, S., Van Den Bergh, E., Maris, T., Struyf, E., 2005. The Scheldt estuary: A description of a changing ecosystem. *Hydrobiologia* 540, 1–11. doi:10.1007/s10750-005-0896-8
- Möller, I., Kudella, M., Rupprecht, F., Spencer, T., Paul, M., van Wesenbeeck, B.K., Wolters, G., Jensen, K., Bouma, T.J., Miranda-Lange, M., Schimmels, S., 2014. Wave attenuation over coastal salt marshes under storm surge conditions. *Nat. Geosci.* 7, 727–731. doi:10.1038/ngeo2251
- Möller, I., Spencer, T., French, J.R., Leggett, D.J., Dixon, M., 2001. The Sea-Defence Value of Salt Marshes: Field Evidence from North Norfolk. *J. Chart. Inst. Water Environ. Manag.* 15, 109–116. doi:DOI: 10.1111/j.1747-6593.2001.tb00315.x
- Moore, R.D., Wolf, J., Souza, A.J., Flint, S.S., 2009. Morphological evolution of the Dee Estuary, Eastern Irish Sea, UK: A tidal asymmetry approach. *Geomorphology* 103, 588–596. doi:10.1016/j.geomorph.2008.08.003
- O'Brien, M.P., 1969. Equilibrium flow areas of tidal inlets on sandy coasts, in: *Proceedings of the American Society of Civil Engineers. Journal of the Waterways and Harbors Division.* pp. 43–52-. doi:10.9753/icce.v10.25p
- O'Brien, M.P., 1931. Estuary and tidal prisms related to entrance areas. *Civ. Eng.* 1, 738–739.
- Parker, B.B., 1984. Frictional effects on the tidal dynamics of a shallow estuary, Ph.D. thesis. John Hopkins University, Baltimore, Md., U.S.A.
- Pawlowicz, R., Beardsley, B., Lentz, S., 2002. Classical tidal harmonic analysis including error estimates in MATLAB using T\_TIDE. *Comput. Geosci.* 28, 929–937. doi:10.1016/S0098-3004(02)00013-4
- Pendleton, L., Donato, D.C., Murray, B.C., Crooks, S., Jenkins, W.A., Sifleet, S., Craft, C., Fourqurean, J.W., Kauffman, J.B., Marb??, N., Megonigal, P., Pidgeon, E., Herr, D., Gordon, D., Baldera, A., 2012. Estimating Global “Blue Carbon” Emissions from Conversion and Degradation of Vegetated Coastal Ecosystems. *PLoS One* 7. doi:10.1371/journal.pone.0043542
- Pieters, T., 2002. “Het Scheldegetij” Beschrijving en analyse van het getij in het Schelde-estuarium (Rapport BGW-0102). Middelburg.
- Roos, P.C., Schuttelaars, H.M., 2015. Resonance properties of tidal channels with multiple retention basins: role of adjacent sea. *Ocean Dyn.* 65, 311–324. doi:10.1007/s10236-015-0809-y
- Rupp-Armstrong, S., Nicholls, R.J., 2007. Coastal and estuarine retreat: a comparison of the application of managed realignment in England And Germany. *J. Coast. Res.* 236, 1418–1430. doi:10.2112/04-0426.1
- Shepard, C.C., Crain, C.M., Beck, M.W., 2011. The protective role of coastal marshes: a systematic review and meta-analysis. *PLoS One* 6, e27374. doi:10.1371/journal.pone.0027374
- Sherwood, C.R., Jay, D.A., Harvey, R.B., Hamilton, P., Simenstad, C.A., 1990. Historical changes in the Columbia River Estuary. *Prog. Oceanogr.* 25, 299–352. doi:Doi 10.1016/0079-6611(90)90011-P
- Small, C., Nicholls, R.J., 2003. A Global Analysis of Human Settlement in Coastal Zones. *J. Coast. Res.* 19, 584–599.
- Smolders, S., Ides, S., Plancke, Y., Meire, P., Temmerman, S., 2012. Calibrating Discharges in a 2D Hydrodynamic Model of the Scheldt Estuary : Which Parameters Can Be Used and What Is Their Sensitivity ?, in: *Proceedings of 10th International Conference on Hydroinformatics, HIC 2012, Hamburg, Germany.* p. 8.
- Smolders, S., Plancke, Y., Ides, S., Meire, P., Temmerman, S., 2015. Role of intertidal wetlands for tidal and storm tide attenuation along a confined estuary: A model study. *Nat. Hazards Earth Syst. Sci.* 15, 1659–1675. doi:10.5194/nhess-15-1659-2015
- Speer, P.E., Aubrey, D.G., 1985. A study of non-linear tidal propagation in shallow inlet/estuarine systems Part II: Theory. *Estuar. Coast. Shelf Sci.* 21, 207–224. doi:10.1016/0272-7714(85)90097-6
- Speer, P.E., Aubrey, D.G., Friedrichs, C.T., 1991. Nonlinear hydrodynamics of shallow tidal inlet/bay systems. *Tidal Hydrodyn.* 321–339.
- Swinkels, C.M., Jeuken, C.M.C.J.L., Wang, Z.B., Nicholls, R.J., 2009. Presence of connecting channels in the Western Scheldt Estuary. *J. Coast. Res.* 627–640. doi:10.2112/06-0719.1
- Temmerman, S., De Vries, M.B., Bouma, T.J., 2012. Coastal marsh die-off and reduced attenuation of coastal floods: A model analysis. *Glob. Planet. Change* 92–93, 267–274. doi:10.1016/j.gloplacha.2012.06.001
- Temmerman, S., Kirwan, M.L., 2015. Building land with a rising sea. *Science* (80-. ). 349, 588–589. doi:10.1126/science.aac8312
- Temmerman, S., Meire, P., Bouma, T.J., Herman, P.M.J., Ysebaert, T., De Vriend, H.J., 2013. Ecosystem-based coastal defence in the face of global change. *Nature* 504, 79–83. doi:10.1038/nature12859
- Townend, I., Pethick, J., 2002. Estuarine flooding and managed retreat. *Philos. Trans. R. Soc. Ser. A Math. Phys. Eng. Sci.* 360, 1477–1495. doi:10.1098/rsta.2002.1011
- Van de Kreeke, J., Robaczewska, K., 1993. Tide-induced residual transport of coarse sediment; Application to the EMS estuary. *Netherlands J. Sea Res.* 31, 209–220. doi:10.1016/0077-7579(93)90022-K

- Van der Spek, A.J.F., 1997. Tidal asymmetry and long-term evolution of Holocene tidal basins in the Netherlands: Simulation of palaeo-tides in the Schelde estuary. *Mar. Geol.* 141, 71–90. doi:10.1016/S0025-3227(97)00064-9
- Van Dongeren, A.R., Vriend, H.J. de, 1994. A model of morphological behaviour of tidal basins. *Coast. Eng.* 22, 287–310. doi:10.1016/0378-3839(94)90040-X
- Van Rijn, L.C., 2011. Analytical and numerical analysis of tides and salinities in estuaries; part I: tidal wave propagation in convergent estuaries. *Ocean Dyn.* 61, 1719–1741. doi:10.1007/s10236-011-0453-0
- Vanlierde, E., Ferket, B., Michielsen, S., Vereycken, K., Van Hoestenbergh, T., Levy, Y., Plancke, Y., Deschamps, M., Verwaest, T., Mostaert, F., 2014. MONEOS - jaarboek monitoring WL 2013: Factual data rapportage van monitoring hydrodynamiek en fysische parameters zoals gemeten door WL in het Zeescheldebekken in 2013. Versie 4.0. WL Rapporten, 12\_070. Antwerpen.
- Wamsley, T. V., Cialone, M. a., Smith, J.M., Atkinson, J.H., Rosati, J.D., 2010. The potential of wetlands in reducing storm surge. *Ocean Eng.* 37, 59–68. doi:10.1016/j.oceaneng.2009.07.018
- Wang, C., Temmerman, S., 2013. Does biogeomorphic feedback lead to abrupt shifts between alternative landscape states?: An empirical study on intertidal flats and marshes. *J. Geophys. Res.* 118, 229–240. doi:10.1029/2012JF002474
- Wang, Z., Jeuken, C., De Vriend, H., 1999. Tidal asymmetry and residual sediment transport in estuaries. A literature study and applications to the Western Scheldt, Z2749.
- Wang, Z.B., Jeuken, M.C.J.L., Gerritsen, H., De Vriend, H.J., Kornman, B.A., 2002. Morphology and asymmetry of the vertical tide in the Westerschelde estuary. *Cont. Shelf Res.* 22, 2599–2609. doi:10.1016/S0278-4343(02)00134-6
- Yang, S.L., Li, M., Dai, S.B., Liu, Z., Zhang, J., Ding, P.X., 2006. Drastic decrease in sediment supply from the Yangtze River and its challenge to coastal wetland management. *Geophys. Res. Lett.* 33, 4–7. doi:10.1029/2005GL025507





## Appendix 5A – Tidal constituent analysis

### *Theoretical background*

In addition to the more straightforward indicators for tidal asymmetry such as the difference or ratio between the period of the rising and falling tide or the ratio between peak flood and peak ebb velocities, tidal asymmetry can also be analyzed by the relative contribution of various tidal constituents to the tidal signal (e.g. Friedrichs and Aubrey, 1988; Parker, 1984; Wang et al., 1999, 2002). The amplitude ratios and phase differences between the principal tidal constituents and superharmonic tides (i.e., overtides or compound tides) determine the strength and nature of the tidal asymmetry. Amplitude ratios between the overtides and the principal tidal constituent are indicators for the strength of the tidal asymmetry. Higher amplitude ratios imply stronger tidal asymmetry, while lower ratios indicate more symmetric tides. Phase differences between the overtides and the main tidal constituent determine the nature of the tidal asymmetry.

Here, we assess the impact of the M4 overtide of the lunar M2 tide (see Figure A1 for an overview of asymmetries that may occur as a result of interaction between the M2 and M4 constituents), which is the main tidal constituent in the Scheldt Estuary. The M4 overtide originates from the nonlinear terms in the momentum and continuity equations, including advective inertia and bottom friction (Parker, 1984). The  $2\varphi_{M2}-\varphi_{M4}$  phase difference between the M2 constituent and the M4 overtide is considered representative for phase differences between other semi-diurnal and quarter-diurnal constituents (Speer et al., 1991; Wang et al., 1999) and can be used to indicate the nature of the asymmetry of the tidal signal (i.e., whether the tide is flood-dominant or ebb-dominant).

If the M2 and M4 constituents of the vertical tide are considered, phase differences between  $0^\circ < 2\varphi_{M2-wl}-\varphi_{M4-wl} < 180^\circ$  indicate that the vertical tidal asymmetry tends to be flood dominant with a shorter water level rise than fall, whereas a phase difference between  $-180^\circ < 2\varphi_{M2-wl}-\varphi_{M4-wl} < 0^\circ$  indicates an ebb-dominant asymmetry with a longer water level rise (Figure A1) (e.g. Wang et al., 1999, 2002). For the horizontal tide, phase differences between  $-90^\circ < 2\varphi_{M2-vel}-\varphi_{M4-vel} < 90^\circ$  indicate that the peak flood velocities are higher than the peak ebb velocities implying flood dominance of the horizontal tide, which is the strongest for  $2\varphi_{M2-vel}-\varphi_{M4-vel} = 0^\circ$ . Conversely, phase differences of  $-180^\circ < 2\varphi_{M2-vel}-\varphi_{M4-vel} < -90^\circ$  or  $90^\circ < 2\varphi_{M2-vel}-\varphi_{M4-vel} < 180^\circ$  indicate higher peak ebb velocities and ebb-dominance, which is the strongest for  $2\varphi_{M2-vel}-\varphi_{M4-vel} = 180^\circ$  (Figure A1) (e.g. Friedrichs and Aubrey, 1988).

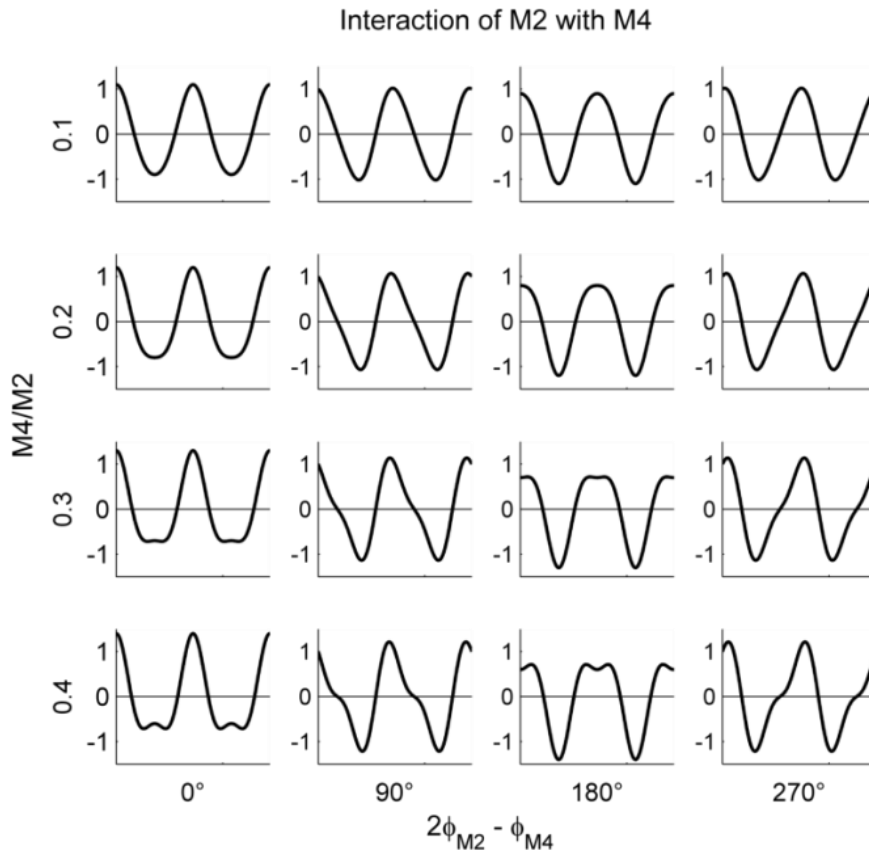


**Figure A1:** Characteristic tidal signals based on the interaction between the M2 and M4 tidal constituents with varying phase differences and amplitude ratios.

### Method

Harmonic analyses are performed on the model results that are presented in **Chapter 5** with the T-TIDE toolbox for Matlab by Pawlowicz et al. (2002). In particular, amplitudes and phases of the M2 and M4 tidal constituents are extracted from the modelled series of water levels and cross-sectional averaged velocities at the cross-sections in Figure 5.1. Harmonic analyses are first used to extend the model validation with a tidal constituent analysis of observed and modelled water level time series at tidal stations along the Scheldt estuary (see Figure 5.1). For the model validation, the North Sea boundary is forced by 28 days of water level observations (i.e. 31/8/2013-28/9/2013); while the upstream discharge boundaries are forced by constant monthly averaged discharges of the same period (calculated based on available discharge data from <http://www.waterinfo.be>). In particular, the monthly averaged discharge input at the different tributaries varies between 3.0 and 12.0 m<sup>3</sup>s<sup>-1</sup>. Secondly, the harmonic analyses are also performed on the results of the model scenarios in which the elevation and location of intertidal areas along the Scheldt Estuary is varied (Table 5.1). The strength and type of the vertical and horizontal tidal asymmetry are then quantified based on the phase differences ( $2\phi_{M2-wl}-\phi_{M4-wl}$  and  $2\phi_{M2-vel}-\phi_{M4-vel}$ ) and amplitude ratios ( $M4/M2_{wl}$  and  $M4/M2_{vel}$ ) between the M2 and M4 constituents.

### Comparing harmonic analysis results for the observed and modelled tidal signal

In Table A1, the results of comparison between the harmonic analyses of the observed and simulated tidal signal are depicted for several water level stations along the Scheldt Estuary. The M2 amplitude increases gradually along the estuary between the estuary

mouth (i.e., Vlissingen) and KM-100 (i.e., Hemiksem). The model represents the observed amplitudes fairly well in the Western Scheldt (i.e., until the Prosperpolder tidal station), but M2 amplitudes are slightly underestimated at some upstream tidal stations (i.e., Liefkenshoek and Antwerpen) and M4 amplitudes are slightly overestimated at all tidal stations along the Sea Scheldt (i.e., Liefkenshoek, Antwerpen and Hemiksem). The M2 phase is modelled with a phase lag of 0-4° (i.e., up until 8 minutes) relative to the observations at up until the Antwerp tidal station, from where the phase lag increases to 22° at KM-100. In general, the representation of the M4 phase also worsens upstream of KM-87 (i.e., upstream of Antwerpen). The modelled M4 phases are within -11° in the Sea Scheldt and +6° near the estuary mouth. Again, the model performance is worsens significantly towards the Hemiksem tidal station at KM-100.

**Table A1:** Comparison between observed (bold) and modelled (italic) amplitudes and phases of the M2 and M4 tidal constituents at tidal stations in Vlissingen (VLIS), Terneuzen (TERN), Hansweert (HANS), Baalhoek (BAAL), Prosperpolder (PROS), Liefkenshoek (LIEF), Antwerpen (ANTW) and Hemiksem (HEMI) (see Figure 5.1 for locations).

Tidal station	VLIS	TERN	HANS	BAAL	PROS	LIEF	ANTW	HEMI
<i>Distance from mouth</i>	<i>3 km</i>	<i>24 km</i>	<i>41 km</i>	<i>51 km</i>	<i>64 km</i>	<i>73 km</i>	<i>87 km</i>	<i>100 km</i>
<b>M2 amplitude</b>	<b>1,73 m</b>	<b>1,86 m</b>	<b>1,98 m</b>	<b>2,07 m</b>	<b>2,13 m</b>	<b>2,20 m</b>	<b>2,27 m</b>	<b>2,28 m</b>
	<i>1,72 m</i>	<i>1,85 m</i>	<i>1,98 m</i>	<i>2,05 m</i>	<i>2,12 m</i>	<i>2,15 m</i>	<i>2,19 m</i>	<i>2.28 m</i>
<b>M2 phase</b>	<b>166°</b>	<b>176°</b>	<b>-174°</b>	<b>-167°</b>	<b>-161°</b>	<b>-159°</b>	<b>-150°</b>	<b>-112°</b>
	<i>166°</i>	<i>175°</i>	<i>-174°</i>	<i>-166°</i>	<i>-159°</i>	<i>-156°</i>	<i>-146°</i>	<i>-138°</i>
<b>M4 amplitude</b>	<b>0,13 m</b>	<b>0,12 m</b>	<b>0,11 m</b>	<b>0,12 m</b>	<b>0,11 m</b>	<b>0,11 m</b>	<b>0,11 m</b>	<b>0,12 m</b>
	<i>0,14 m</i>	<i>0,13 m</i>	<i>0,13 m</i>	<i>0,13 m</i>	<i>0,13 m</i>	<i>0,14 m</i>	<i>0,14 m</i>	<i>0.16 m</i>
<b>M4 phase</b>	<b>-26°</b>	<b>-10°</b>	<b>16°</b>	<b>34°</b>	<b>38°</b>	<b>42°</b>	<b>53°</b>	<b>117°</b>
	<i>-20°</i>	<i>-3°</i>	<i>20°</i>	<i>31°</i>	<i>28°</i>	<i>31°</i>	<i>43°</i>	<i>56°</i>

#### Tidal constituent analysis for scenarios with additional intertidal storage

Based on the M4 and M2 constituents of the vertical tide (Figure A2), the vertical tidal asymmetry is in general slightly ebb-dominant in the downstream part of the estuary (i.e. up until KM-60) and becomes gradually more flood-dominant in the upstream part of the estuary. This result differs from the analysis of tidal asymmetry based on the ratio between the duration of the rising and falling tide and the ratio between peak flood and peak ebb velocities (Figure 5.5), in which the asymmetry was flood-dominant along the entire estuary.

Nevertheless, the impact of additional storage areas to the tidal asymmetry is fairly similar for the tidal constituent analysis. That is, the vertical tidal asymmetry becomes more flood-dominant downstream of an additional intertidal storage area (i.e.,  $2\varphi_{M2-wl} - \varphi_{M4-wl}$  increases), while ebb-dominance is slightly enhanced upstream of the additional storage (i.e.,  $2\varphi_{M2-wl} - \varphi_{M4-wl}$  decreases). The increase in flood-dominance downstream and enhanced ebb-dominance upstream is most pronounced in the scenario with additional storage at KM-97, where the storage volume is approximately 59% of the local tidal prism. Furthermore, adding intertidal storage generally reduces the strength of the vertical tidal asymmetry along the estuary (i.e.,  $M4/M2_{wl}$  decreases). However, for the

scenario in which intertidal storage is added far upstream at KM-97, tidal asymmetry increases further than  $\sim 20$  km downstream of the additional intertidal storage area.

Based on the M4 and M2 constituents of the horizontal tide (Figure A3), the horizontal tidal asymmetry is also almost symmetric or slightly ebb-dominant in the most downstream part of the estuary (i.e.,  $2\varphi_{M2-vel}-\varphi_{M4-vel} \approx -90^\circ$  or slightly below) and becomes also increasingly flood-dominant further upstream (i.e.,  $0^\circ < 2\varphi_{M2-vel}-\varphi_{M4-vel} < -90^\circ$ ). Adding intertidal storage generally enhances ebb-dominance. The peak of enhanced flood-dominance directly downstream of the added storage areas, as observed in Figure 5.5, is not present in  $2\varphi_{M2-vel}-\varphi_{M4-vel}$ . However, there is a peak in the strength of the tidal asymmetry  $M4/M2_{vel}$ . Only in the scenario in which intertidal storage is added at KM-97, flood-dominance is further enhanced in the most downstream part and ebb-dominance increases (i.e.,  $2\varphi_{M2-vel}-\varphi_{M4-vel} < -90^\circ$ ) between KM-65 and the additional storage area itself. Although the relative importance of  $M4_{vel}$  varies a lot along the estuary, it can be noted that the strength of the horizontal asymmetry peaks just downstream of the upstream located intertidal storage areas (i.e., at KM-66 and KM-97).

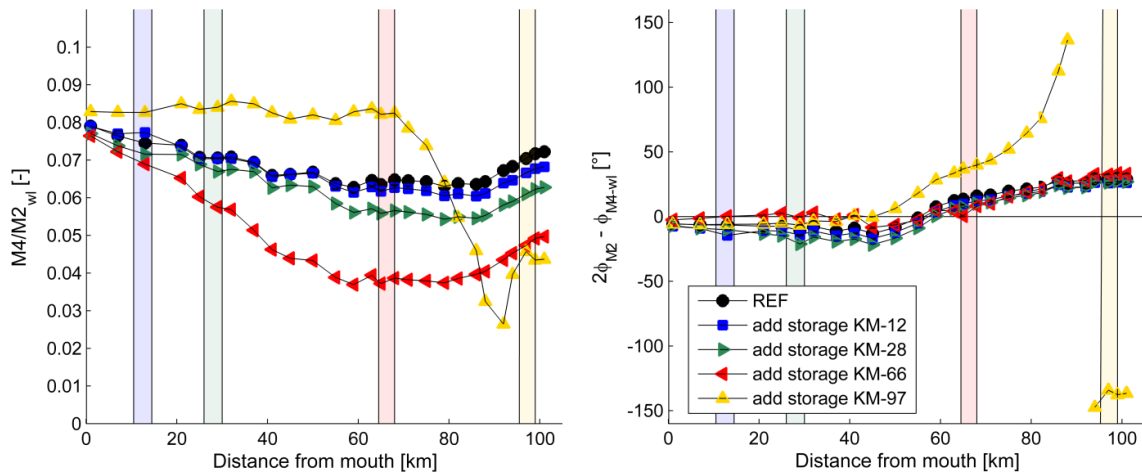


**Figure A2:** Modelled  $M4/M2_{wl}$  amplitude ratios (left) and  $2\varphi_{M2-wl}-\varphi_{M4-wl}$  phase differences (right) of the vertical tide for the reference simulation (black) and for scenarios with additional intertidal storage at KM-12 (blue), KM-28 (green), KM-66 (red) and KM-97 (yellow).

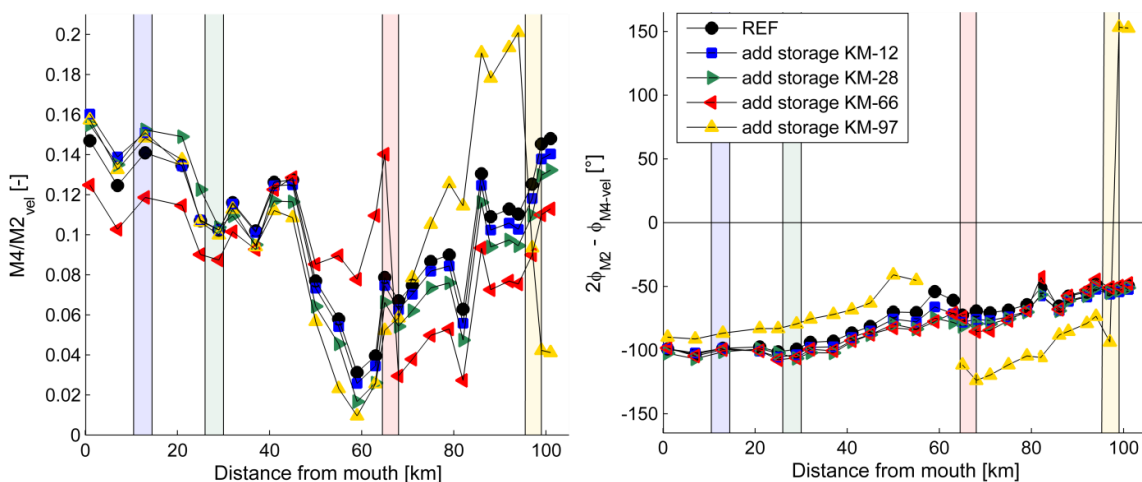


**Figure A3:** Modelled  $M4/M2_{vel}$  amplitude ratios (left) and  $2\varphi_{M2-wl}-\varphi_{M4-vel}$  phase differences (right) of the horizontal tide for the reference simulation (black) and for scenarios with additional intertidal storage at KM-12 (blue), KM-28 (green), KM-66 (red) and KM-97 (yellow).

Tidal constituent analysis for scenarios with varying tidal flat elevation

Based on the amplitude ratios between the M4 and M2 constituents, the strength of both the vertical and horizontal tidal asymmetry varies with the elevation of the intertidal flats (Figures A4 and A5). For the vertical tide, tidal asymmetry is stronger if the tidal flats are situated low in the tidal frame and weaker if the tidal flats are situated higher in the tidal frame. However, the strength of the tidal asymmetry is weakest for tidal flat elevations close to and 1 m above mean sea level and increases again for higher tidal flat elevations and for the scenario without intertidal flats. Upstream of KM-40, the relative importance of M4 is strongest for lower intertidal flats (i.e.  $z_{\text{flat}} = -2.0$  m NAP).

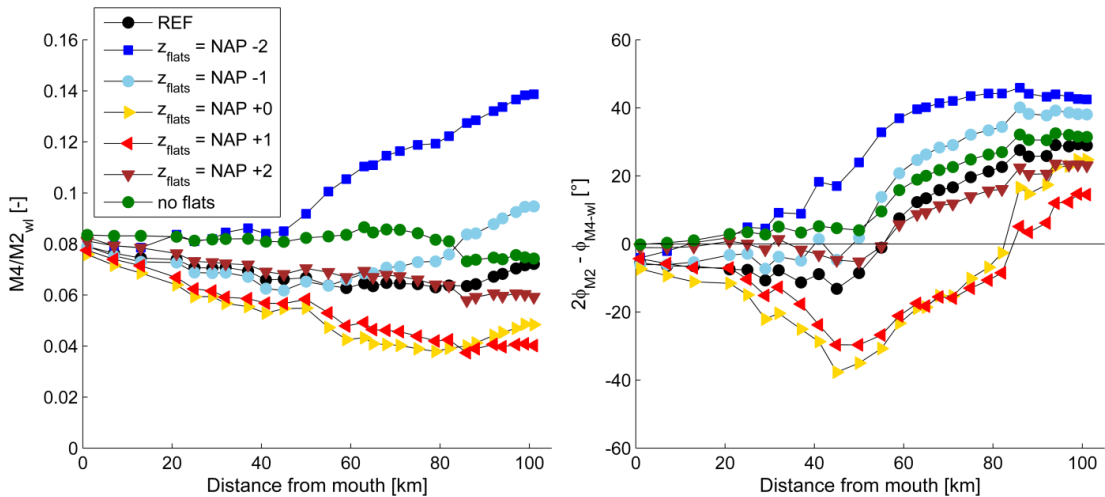


**Figure A4:** Modelled  $M4/M2_{wl}$  amplitude ratios (left) and  $2\phi_{M2-wl} - \phi_{M4-wl}$  phase differences (right) of the vertical tide for the reference scenario and for scenarios in which the elevation of the intertidal flats is varied.

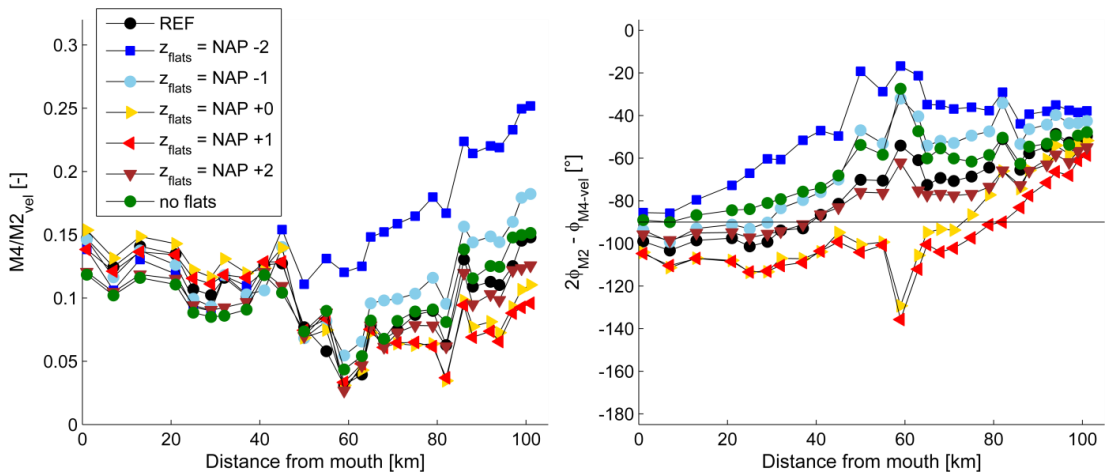


**Figure A5:** Modelled  $M4/M2_{vel}$  amplitude ratios (left) and  $2\phi_{M2-wl} - \phi_{M4-vel}$  phase differences (right) of the horizontal tide for the reference scenario and for scenarios in which the elevation of the intertidal flats is varied.

The type of the horizontal and of the vertical tidal asymmetry also varies between scenarios with a different tidal flat elevation (Figures A4 and A5). In particular, ebb-dominance is enhanced up until  $\sim$ KM-80 along the estuary for the scenarios with  $z_{\text{flat}} = +0.0$  m NAP and  $z_{\text{flat}} = +1.0$  m NAP based on the phase differences between M4 and M2 (i.e.,  $2\phi_{M2-wl} - \phi_{M4-wl} < 0^\circ$  and  $2\phi_{M2-vel} - \phi_{M4-vel} < -90^\circ$ ), while flood-dominance is also reduced further upstream for these scenarios. In contrast, flood-dominance is enhanced for the

scenarios in which the elevation of the tidal flats is lower (i.e.,  $z_{\text{flat}} = -2.0$  m NAP and  $z_{\text{flat}} = -1.0$  m) or higher (i.e., scenarios with  $z_{\text{flat}} = +2.0$  m NAP and without tidal flats) as the  $2\varphi_{M2-wl} - \varphi_{M4-wl}$  phase difference of the vertical tide increases and the  $2\varphi_{M2-vel} - \varphi_{M4-vel}$  phase difference of the horizontal tide is between  $0^\circ < 2\varphi_{M2-vel} - \varphi_{M4-vel} < -90^\circ$ . The above described effects of tidal flat elevation on tidal asymmetry based on the tidal constituent analysis are again similar to the results based on the ratio between peak flood and peak ebb velocities and the ratio between the duration of the rising and falling tide. However, an ebb-dominant asymmetry of the vertical tide and the horizontal tide arises up until KM-80 for the model scenarios with  $z_{\text{flat}} = 0.0$  m NAP and  $z_{\text{flat}} = +1.0$  m NAP based on the phase difference between the M4 and M2 tidal constituents, whereas the ratio between peak flood and peak ebb velocities and the ratio between the duration of the rising and falling tide only become less flood-dominant in these scenarios.

## Appendix 5B – Effects of the Saeftinghe marsh and its elevation on tidal hydrodynamics in the Scheldt estuary

### *Introduction*

Here we assess how tidal hydrodynamics are influenced by elevation changes of the largest intertidal area along the Scheldt estuary: the '*Verdronken Land van Saeftinghe*' (which translates as 'Drowned Land of Saeftinghe or simply Saeftinghe marsh). The 3000 ha Saeftinghe accounts for approximately  $43 \cdot 10^6$  m<sup>3</sup> (i.e., ~17% of the total  $248 \cdot 10^6$  m<sup>3</sup> intertidal storage, calculated as the storage volume below highest high water). The marsh is situated between KM-50 and KM-60 from the estuary mouth (Figure B1). Nowadays, the Saeftinghe marsh is surrounded by levees in the south and the west and bordered by the estuary channel in the north and east. The marsh used to be bigger but stepwise embankments between the 17<sup>th</sup> century and the early 20<sup>th</sup> century confined the marsh to its current size (Jongepier et al., 2015). The elevation, vegetation cover and geomorphology of the marsh changed significantly since the last embankments. Over the last decades, large parts of the marsh developed from a bare intertidal flat to a higher elevated vegetated marsh platform dissected by intertidal channels (Wang and Temmerman, 2013). Accordingly, the mean elevation of the marsh (i.e., including the marsh platform and the channels) increased from 1.1 m in the 1930s to 2.4 m in the 2010s (Wang and Temmerman, 2013; **Chapter 4**).

It can be expected that elevation changes of the largest tidal marsh along the Scheldt estuary have a significant impact on tidal hydrodynamics, especially because of its location upstream of most other intertidal flats. In particular, model results in **Chapter 5** indicate that (local) changes in intertidal storage volume may have an along-estuary varying effect on tidal prism, tidal range and tidal asymmetry along a large stretch of the estuarine channels. Moreover, the impact on tidal hydrodynamics increases if the intertidal storage volume is situated further upstream and affects a larger part of the local tidal prism, as is the case for the Saeftinghe marsh. Furthermore, model scenarios in **Chapter 5** in which the tidal flat elevation is altered throughout the estuary show that the elevation of intertidal flats may determine the strength and type of tidal asymmetry (i.e., whether the asymmetry is flood- or ebb-dominant) in estuarine channels. Generally, ebb-dominance is most strongly enhanced by a larger intertidal storage volume through the storage term in the momentum and continuity equations (e.g. Friedrichs and Aubrey, 1988; Friedrichs and Madsen, 1992; Wang et al., 1999). If the intertidal areas are situated relatively low in the tidal frame and their location within the estuarine channel system is such that they contribute to the along-estuary propagation of the tidal wave, frictional effects may slow the propagation of the low tide as well, enhancing flood-dominance (Fortunato and Oliveira, 2005). However, if the elevation of intertidal flats is such that they only affect the along-estuary propagation of the high tide, friction and advective inertia still enhance ebb-dominance by slowing the high tide more than the low tide (e.g. Fortunato and Oliveira, 2005; Friedrichs and Aubrey, 1988; Friedrichs and Madsen, 1992).

In case of the Saeftinghe marsh, the position within the estuarine channel- and flat system is such that part of the marsh contributes to the along-estuary propagation of the tidal wave (i.e., based on visual examination of simulated flow fields in the model scenarios and also depending on the marsh elevation), whereas other parts mainly have a storage function. An example is given in Figure B2, which shows that tidal propagation occurs over the northeastern part of the intertidal area during both flood and ebb, while the southwestern part of the marsh merely has a storage function. The effect of the Saeftinghe marsh on the along-estuary propagation of storm tides and high water levels in general was assessed in a previous study by Smolders et al. (2015), who showed with a hydrodynamic model that the presence of the Saeftinghe marsh reduces high water levels along the estuary by up to 0.2 m. Here, we extend this study by performing an additional scenario analysis in which we assess the effect of the presence and elevation of the Saeftinghe marsh on tidal hydrodynamics, including tidal asymmetry, along the Scheldt estuary.

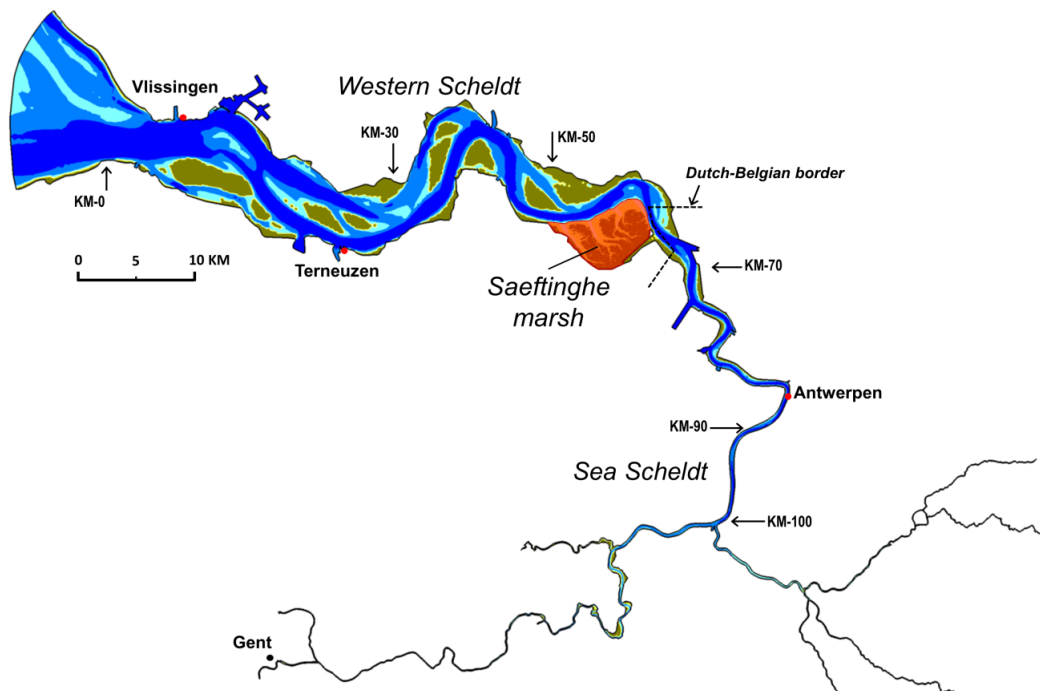


**Figure B1:** Bathymetrical map of the Scheldt Estuary model with the surface area of the Saeftinghe marsh (marked in transparent red) of which the elevation is varied in the model scenarios.

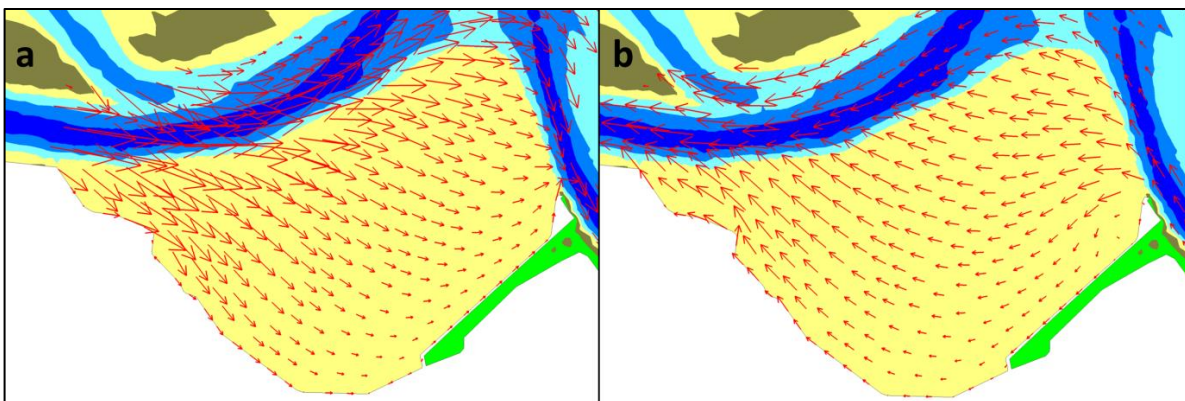


**Figure B2:** Simulated flow fields over the Saeftinghe marsh (a) during flood ( $T_{HW} - 90$  min) and (b) during ebb ( $T_{HW} + 90$  min) for the simulation in which the elevation of the marsh is set at  $z_{saef} = -2.0$  m NAP.



### Methods

Five additional model scenarios are set up with the Scheldt Estuary model in which the elevation of the Saeftinghe marsh (i.e., defined in Figure B1) is varied within the tidal frame (Table B1). The reference simulation is similar to the reference simulation in **Chapter 5** and is set up by implementing the 2011 bathymetry in the model. In the other simulations, the elevation of the Saeftinghe marsh is varied between NAP -2.0 m and NAP +1.0 m with a one meter interval, along with a scenario in which the tidal flat elevation is increased above the highest high water level (HHW) and hence excluding the Saeftinghe marsh from the model. Besides, the mean elevation of the marsh corresponds to  $z_{saeft} = +2.4$  m NAP in the reference simulation. Furthermore, the model scenarios are simulated with the same settings as the model scenarios in **Chapter 5**. In particular, bottom friction is implemented by spatially varying Manning's coefficients as calibrated by Smolders et al. (2015) and in this thesis (**Chapter 3**). The Manning's bottom friction coefficient for the Saeftinghe marsh is in all cases set to  $n = 0.02 \text{ s}\cdot\text{m}^{-1/3}$  (representative for bare sand). The model boundaries are forced by 28 days of water level observations (i.e. 31/8/2013-28/9/2013), while the upstream river discharge is forced by constant monthly averaged discharges ranging between  $3.0 \text{ m}^3\text{s}^{-1}$  and  $12.0 \text{ m}^3\text{s}^{-1}$  at the upstream boundary of the Sea Scheldt near Ghent and at six other tributaries.

**Table B1:** Overview of model scenarios with varying elevation of the Saeftinghe marsh, including the additional intertidal storage volume relative to the reference scenario ( $z_{saeft} = +2.4$  m NAP) and the percentage of the storage volume change relative to the local spring tidal prism.

Scenario description	abbreviation	$\Delta V_{\text{storage}}$
<i>Reference scenario based on the 2011 bathymetry (mean elevation of the Saeftinghe marsh is <math>z = +2.4</math> m NAP)</i>	REF	-
<i>Scenario in which the elevation of the Saeftinghe marsh is set to <math>z = -2.0</math> m NAP</i>	$z_{saeft} = -2.0 \text{ m}$	$+132 \cdot 10^6 \text{ m}^3$ (+44%)
<i>Scenario in which the elevation of the Saeftinghe marsh is set to <math>z = -1.0</math> m NAP</i>	$z_{saeft} = -1.0 \text{ m}$	$+100 \cdot 10^6 \text{ m}^3$ (+33%)
<i>Scenario in which the elevation of the Saeftinghe marsh is set to <math>z = 0.0</math> m NAP</i>	$z_{saeft} = +0.0 \text{ m}$	$+68 \cdot 10^6 \text{ m}^3$ (+23%)
<i>Scenario in which the elevation of the Saeftinghe marsh is set to <math>z = +1.0</math> m NAP</i>	$z_{saeft} = +1.0 \text{ m}$	$+36 \cdot 10^6 \text{ m}^3$ (+12%)
<i>Scenario in which the Saeftinghe marsh is removed from the model</i>	no saeftinghe	$-43 \cdot 10^6 \text{ m}^3$ (-14%)

As in **Chapter 5**, tidal hydrodynamics of the vertical tide are quantified by the mean tidal range ( $TR$ ), mean high water level ( $MHWL$ ), mean low water level ( $MLWL$ ) and the phase of the high water ( $T_{HW}$ ) and low water ( $T_{LW}$ ). The horizontal tide is described by the cross-sectional averaged peak velocities during flood ( $V_{CS-flood}$ ) and during ebb ( $V_{CS-ebb}$ ). Vertical tidal asymmetry is described by the ratio ( $R_T$ ) between the period of water level rise ( $T_{rising}$ ) and the period of water level fall ( $T_{falling}$ ) and the horizontal tidal

asymmetry is quantified by the ratio between cross-sectional averaged peak velocities during flood and ebb:  $R_{V-CS} = \max(V_{CS-flood}) / \max(V_{CS-ebb})$ , both calculated per tide and averaged over the 28-days model simulation period. Furthermore, the flood tidal prism ( $P$ ) is calculated through all these cross-sections. The results of the additional model scenarios are compared with the reference scenario and with the results of simulations in which the tidal flat elevation is varied throughout the estuary (in **Chapter 5**). The additional intertidal storage volumes as compared to the reference scenario are given in Table B1 and compared to the local tidal prism of approximately  $300 \cdot 10^6 \text{ m}^3$  as computed directly downstream of Saeftinghe. In particular, removing Saeftinghe from the model corresponds to removing an intertidal storage volume of 14% of the local tidal prism, while stepwise lowering the elevation of the marsh increases the intertidal storage volume by up to 44% of the local tidal prism.

#### Effects for the vertical tide

The model results indicate that the present-day Saeftinghe marsh reduces the mean tidal range and MHWLs by up to 0.08 m along the estuary channels upstream of the marsh, while its impact on MLWLs is negligible (i.e., comparing the scenario without Saeftinghe with the reference scenario; Figure B3a/b/c). The reduction in MHWL is almost half of the impact of all the other tidal flats from the estuary mouth up until KM-80 (**Chapter 5**). The effect of the marsh on the tidal range and MHWLs quickly diminishes downstream. Scenarios in which the elevation of the Saeftinghe marsh is stepwise lowered within the tidal frame indicate that the additional storage volume can further reduce the tidal range by up to 0.4 m depending on the elevation of the marsh surface area. Tidal range reduction is again mainly the result of lower MHWLs, except for the scenarios with  $z_{saef} = -1.0 \text{ m NAP}$  and  $z_{saef} = -2.0 \text{ m NAP}$  in which the low water levels are also affected. Remarkably, the decrease in tidal range and MHWL in these scenarios is strongest downstream of the marsh around KM-40, from which MHWLs increase up until  $\sim$ KM-55 near the marsh location, and upstream of which the reduction in MHWLs increases again to a more or less constant level far upstream (Figure B3a/b). Apparently, the presence of a large intertidal storage volume along the estuary may locally lead to a higher tidal range and higher mean high water levels relative to the (strong) reduction upstream and downstream of the intertidal storage area. This can possibly be explained by the local reduction in flow velocities in the channels adjacent to the marsh surface (Figure B4), as lower flow velocities imply a reduction in bottom friction and hence a relative reduction in tidal damping (or a relative increase in amplification of the tide).

The Saeftinghe marsh at its present day elevation (i.e.,  $z_{saef} = +2.4 \text{ m NAP}$ ) barely affects the high and low water phase along the estuary (Figure B3d/e). In particular, both the high water phase and low water phase are slowed down by less than 5 minutes. However, if the elevation of Saeftinghe is lowered, the intertidal storage area does have a significant effect on the propagation of the high water as well as the low water. The high water phase is slowed down by 10 to 20 minutes upstream of the Saeftinghe marsh for scenarios with a lowered marsh surface, while the propagation of the low water is slowed by up to 18 minutes. The effects on high water phase and low water phase are

different downstream of the marsh, where the high water phase is slightly accelerated whereas the phase lag of the low water due to the Saeftinghe marsh gradually decreases towards the estuary mouth.

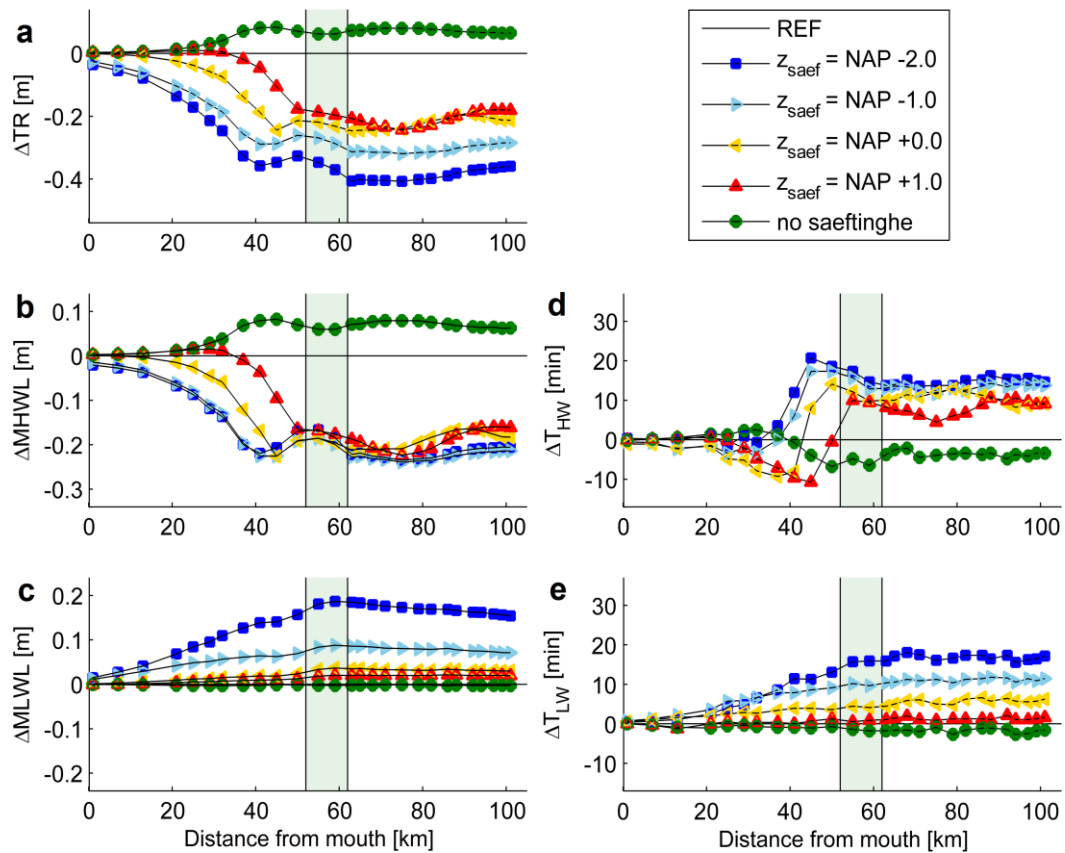


**Figure B3:** Modelled difference in (a) tidal range, (b) mean high water level (MHWL), (c) mean low water level (MLWL) and the phase differences of (d) high water ( $T_{HW}$ ) and (e) low water ( $T_{LW}$ ) for scenarios in which the elevation of the Saeftinghe marsh is varied, compared to the reference scenario.

#### *Effects for the horizontal tide*

The cross-sectional averaged peak velocities during flood and ebb (Figure B4) are only slightly affected by the presence of the Saeftinghe marsh (i.e., removing the marsh from the model only alters the peak velocities by less than 0.05 m/s). Lowering the marsh elevation and thereby increasing the storage volume leads to a strong reduction in both flood and ebb velocities in the channel section along the marsh and a strong increase in peak velocities directly downstream of the marsh. Generally, the peak flood velocities are more affected than the peak ebb velocities. These effects on peak flood and peak ebb velocities are similar to the effect of additional intertidal storage areas described in **Chapter 5**. The Saeftinghe marsh at its present-day elevation has only little effect on the mean tidal prism in the estuary (Figure B5) as removing the marsh only reduces the mean tidal prism by up to 5%, even though the storage volume of the marsh corresponds to approximately 14% of the local tidal prism (Table B1). It should however be stated that the (relative) storage volumes in Table B1 are based on the spring tidal prism and highest high water, whereas Figure B5 depicts the effect on the mean tidal prism, and hence includes lower tides during which large parts of the marsh platform are not inundated at all.

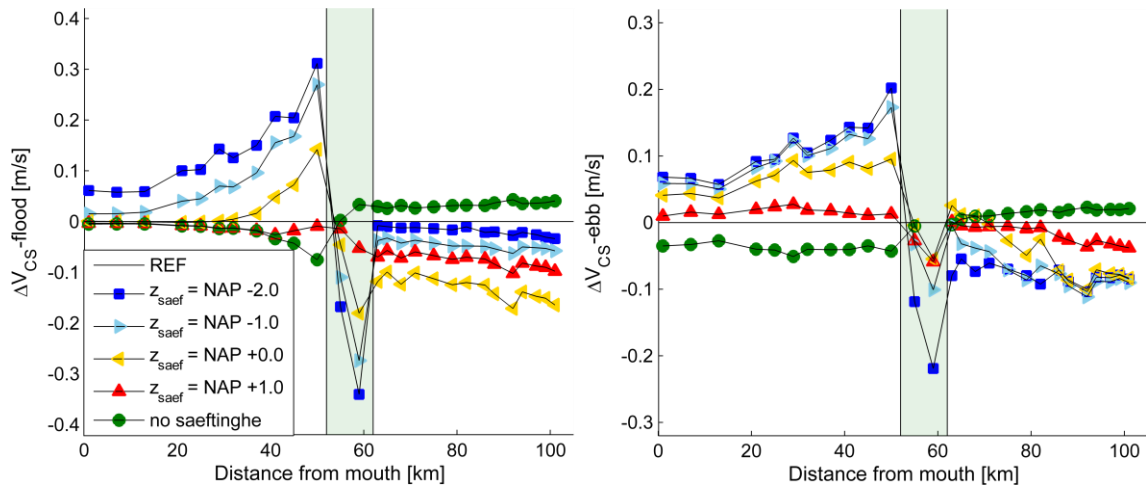


**Figure B4:** Modelled difference in cross-sectional averaged peak flood velocities (left) and cross-sectional averaged peak ebb velocities (right) between scenarios in which the elevation of the Saeftinghe marsh is varied and the reference scenario.

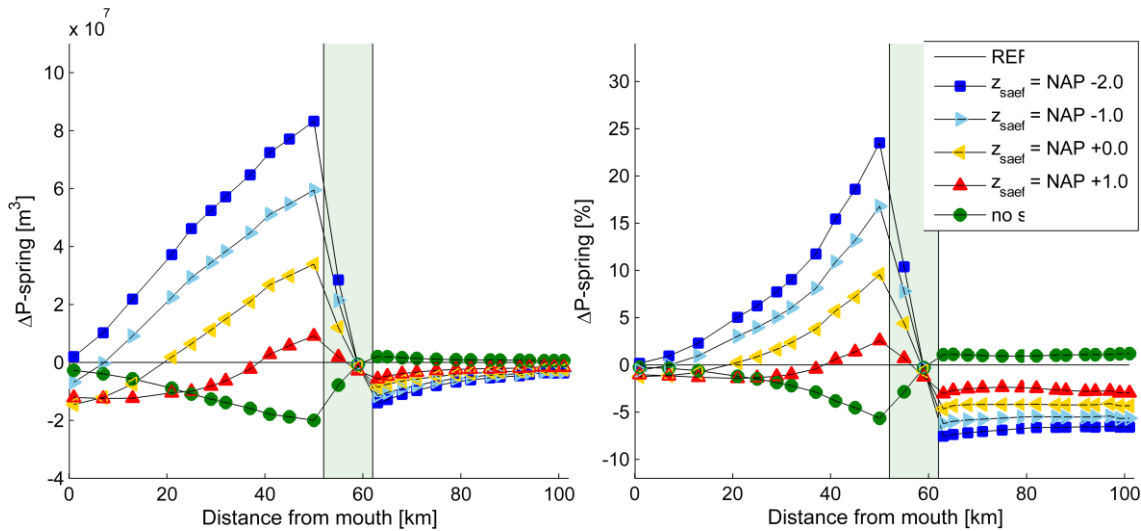


**Figure B5:** Modelled absolute (left) and relative (right) difference in tidal prism for scenarios in which the elevation of the Saeftinghe marsh is varied, compared to the reference scenario.

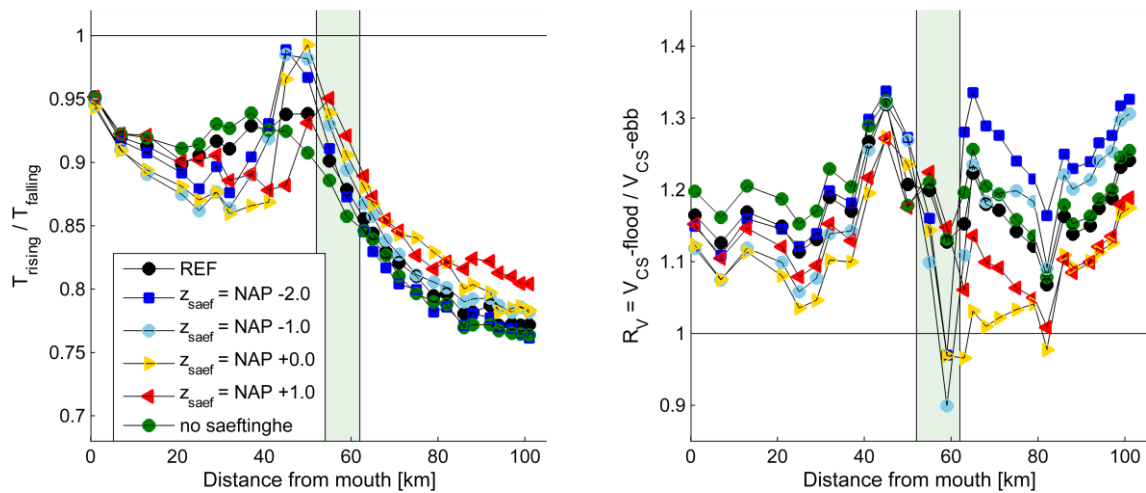


**Figure B6:** Modelled vertical tidal asymmetry based on the ratio between the duration of the rising tide and of the falling tide (left) and horizontal tidal asymmetry based on the ratio between cross-sectional averaged peak flood and peak ebb velocities (right) for scenarios in which the elevation of the Saeftinghe marsh is varied.

For the other scenarios, the effect of lowering the platform elevation of the marsh and thereby enlarging the intertidal storage volume is again largely similar to the effect of adding additional storage areas as described in **Chapter 5**. That is, a decrease in tidal prism upstream of the marsh (up to 8% of the total tidal prism for  $z_{saef} = -2.0$  m NAP), a strong increase in tidal prism directly downstream of the marsh (up to 25% for  $z_{saef} = -2.0$  m NAP) and a gradual reduction in tidal prism increase further downstream towards the estuary mouth. The latter can be explained by the decrease in tidal range as a result of the additional intertidal storage (Figure B3a). In particular, as the tidal prism strongly increases due to the added storage volume without any increase in the channel cross-section downstream, flow velocities in the tidal channels increase as well (Figure B5), leading to higher bottom friction and hence a reduced tidal range (e.g. Jeuken et al., 2004; Maximova et al., 2010). This reduction in tidal range also implies a reduction in tidal prism, which becomes larger downstream as a greater surface area is affected. In case that the elevation of the Saeftinghe marsh is lowered to  $z_{saef} = +1.0$  m and  $z_{saef} = +0.0$  m NAP, this second-order effect of tidal range reduction becomes even stronger than the first-order effect of storage volume increase at the estuary mouth where a net decrease in tidal prism is simulated. In the simulations in which the elevation of the marsh is lowered even further, the tidal prism at the estuary mouth is fairly similar to the reference scenario. In conclusion, elevation changes of the Saeftinghe marsh have along estuary-varying effects on the tidal prism, which on its turn may induce morphological changes in the channel morphology through relationships between tidal prism and channel geometry (e.g. Dronkers, 1998; Jarrett, 1976; O'Brien, 1969, 1931). In particular, the decrease in tidal prism upstream and far downstream of the marsh likely enhances channel infilling, whereas the increase in tidal prism directly downstream of the marsh enhances channel scouring.

#### Effects for tidal asymmetry

Based on  $R_T$  (i.e., the ratio between the duration of the rising and the falling tide) and  $R_V$  (i.e., the ratio between peak flood and peak ebb velocities), different marsh elevations of Saeftinghe cause varying effects on tidal asymmetry along the estuarine channels (Figure B6). The present-day Saeftinghe marsh enhances ebb dominance throughout the estuary (i.e., comparing the reference scenario with the scenario without Saeftinghe), although the vertical tidal asymmetry (i.e.,  $R_T$ ) becomes slightly more flood-dominant downstream of Saeftinghe. The impact of elevation changes of the Saeftinghe marsh on vertical tidal asymmetry is opposite upstream and downstream of the marsh, whereas the impact on horizontal tidal asymmetry is largely similar along the estuarine channels. Based on both  $R_T$  and  $R_V$ , flood-dominance is most strongly reduced upstream of the Saeftinghe marsh for  $z_{saef} = 0.0$  m NAP and  $z_{saef} = +1.0$  m NAP. On the other hand, if the elevation of Saeftinghe would be lower in the tidal frame (i.e.,  $z_{saef} = -1.0$  m NAP and  $z_{saef} = -2.0$  m NAP), the vertical and horizontal tidal asymmetry even become more flood-dominant upstream of the marsh. Downstream of Saeftinghe, the effects on horizontal asymmetry are different from the effects on vertical tidal asymmetry. While  $R_V$  is least flood-dominant for the scenarios with  $z_{saef} = 0.0$  m NAP and  $z_{saef} = -1.0$  m NAP,  $R_T$  is most

flood-dominant for these scenarios in the downstream part of the estuary (i.e., up until ~KM-40).

Overall, the effect on vertical asymmetry is largely similar to the effect of additional intertidal storage areas as described in **Chapter 5**, which also differs upstream and downstream of the intertidal storage area. However, the effect of the Saeftinghe marsh on tidal asymmetry is not strongest for the largest storage volume (i.e., for the lowest elevation) but for elevations around MSL, which corresponds more to the effect of tidal flat elevation in **Chapter 5** and hence is linked to variations in depth-dependent friction and depth-dependent storage that affect the propagation of the tidal wave differently at varying water levels. Similarly, the impact on horizontal asymmetry also corresponds to the effect of elevation changes of tidal flats, for which ebb-dominance is enhanced the most if tidal flats are around or slightly above mean sea level.

## Appendix 5C – Effects of channel enlargement on tidal hydrodynamics in the Scheldt estuary

### *Introduction*

The channels of the Scheldt estuary form the main shipping lane to the port of Antwerp. Dredging and dumping activities to deepen and maintain this navigation route have been the main human interference to the geomorphology of the Scheldt Estuary during the last decades (i.e., after numerous large scale embankments in previous centuries until the 1960s; Van der Spek, 1997). A first channel enlargement (i.e., deepening and widening) took place in the 1970s during which the depth of the sills in the navigation channel along the Western Scheldt was increased by 3 to 4 m. Sills in the navigation channel refer to the shallow parts of the estuary channel, which are typically present where the braiding ebb and flood channels merge (Swinkels et al., 2009). A second enlargement was carried out in 1997/1998 during which the channel depth was increased by about 1.8 m, assuring a tide-independent navigable depth of 11.8 m. This stepwise channel deepening or enlargement led to an increase in annual dredging works from  $\sim 0.5 \text{ Mm}^3$  per year before the 1950s to  $\sim 7\text{-}10 \text{ Mm}^3$  per year in the early 2000s (Jeuken and Wang, 2010). Recently, a third enlargement was carried out in which the water depth was increased by another 1.3 m to assure a tide-independent navigable channel depth of 13.10 m (or a minimum guaranteed water depth of 14.1 m). Besides maintenance and capital dredging, sand mining caused removal of large amounts of sand from the estuarine system. In particular, a total of about  $116 \text{ Mm}^3$  of sediment was removed from the estuary between 1931 and 2008 (Anon, 2010). Nowadays, all dredged sediment is redistributed in the estuary.

While stepwise enlargement of the navigation channel have increased the depth of the channels along the Scheldt estuary over time, embankments and de-embankments and the morphological development of tidal flats and marshes have historically altered the intertidal storage area characteristics. Both processes affect tidal hydrodynamics and tidal asymmetry in the estuarine channels (e.g. Dronkers, 1986; Friedrichs and Aubrey, 1988; Friedrichs and Madsen, 1992; Speer and Aubrey, 1985). Variations in channel depth are expected to affect tidal asymmetry as the relative tidal amplitude (i.e., ratio between the tidal amplitude and the channel depth) is a determining factor for tidal asymmetry in estuarine channels (e.g. Friedrichs and Madsen, 1992; Speer and Aubrey, 1985). In particular, deep tidal channels (along with large intertidal storage volumes) are known to enhance ebb-dominance as the frictional distortion decreases, whereas shallow channels (along with little intertidal storage) generally enhance flood-dominance (e.g. Dronkers, 1986; Friedrichs and Aubrey, 1988; Friedrichs and Madsen, 1992; Speer and Aubrey, 1985). Wang et al. (2002) showed that historical changes in tidal asymmetry along the Scheldt estuary channels are indeed largely explained by the amplitude to water depth ratio. The effect of specific intertidal storage area properties is assessed in **Chapter 5**. Here, we perform an additional scenario analysis (as to the scenarios with varying intertidal storage area characteristics in **Chapter 5**) in which the minimum water depth of the estuary channels is increased. The intention is to compare

the impact of channel enlargement (i.e., deepening of the sills along the estuary channels) with the effect of intertidal area changes, which are the two major human impacts on the Scheldt Estuary during the last centuries. In particular, fictitious model scenarios are set up in which the estuarine channels are enlarged by similar volumes as the variations in intertidal storage volume in the model scenarios in **Chapter 5** (Table C1; Table 5.1), allowing for a quantitative comparison between channel deepening or enlargement and intertidal area changes.

### Method

Two additional scenarios are set up in which the minimum depth of the channel bed is set to 16.0m below NAP (i.e., comparable with the current navigation depth) and 20.0 m below NAP (implying a further deepening of approximately 4.0 m). The channel bed is altered along the estuary channels as defined in Figure C1. In particular, the navigation channel is manually defined up until Antwerpen. Upstream of Antwerpen the channel bed is kept constant. It should be stated that these model scenarios are fictitious, implying that they do not represent the actual navigation channel, nor the actual dredging and deepening activities along the shipping lanes. Moreover, in reality the dredged sediment is redistributed in the estuary (Jeuken and Wang, 2010), which is not the case in the additional model scenarios in which all sediment is removed. The model scenarios are simulated with the same settings as the model scenarios in **Chapter 5**. That is, bottom friction is implemented by spatially varying Manning's coefficients as calibrated by Smolders et al. (2015) and in this thesis (**Chapter 3**). Furthermore, in the scenario analysis, the model boundaries are forced by 28 days of water level observations (i.e. 31/8/2013-28/9/2013), while the upstream river discharge is forced by constant monthly averaged discharges ranging between 3.0 and 12.0 m<sup>3</sup>s<sup>-1</sup> at the upstream boundary of the Sea Scheldt near Ghent and at six other tributaries.

As in **Chapter 5**, tidal hydrodynamics of the vertical tide are again assessed by the mean tidal range ( $TR$ ), mean high water level ( $MHWL$ ), mean low water level ( $MLWL$ ) and the phase of the high water ( $T_{HW}$ ) and low water ( $T_{LW}$ ), while the horizontal tide is assessed by the cross-sectional averaged peak velocities during flood ( $V_{CS-flood}$ ) and during ebb ( $V_{CS-ebb}$ ). Vertical tidal asymmetry is described by the ratio ( $R_T$ ) between the period of water level rise ( $T_{rising}$ ) and the period of water level fall ( $T_{falling}$ ) and the horizontal tidal asymmetry is quantified by the ratio between cross-sectional averaged peak velocities during flood and ebb:  $R_{V-CS} = \max(V_{CS-flood}) / \max(V_{CS-ebb})$ , both calculated per tide and averaged over the 28-days model simulation period. Furthermore, the flood tidal prism ( $P$ ) is calculated through all these cross-sections. The results of the additional model scenarios are compared with the reference scenario based on the 2011 bathymetry of the Western Scheldt. The additional basin volumes as compared to the reference scenario are given in Table C1. The volume increase of the tidal basin as a result of channel enlargement is in the same range as the additional volumes created by varying the elevation of the intertidal flats (Table 5.1), allowing for a comparison between the effect of volumetric changes as a result of channel deepening and volumetric changes in intertidal storage.



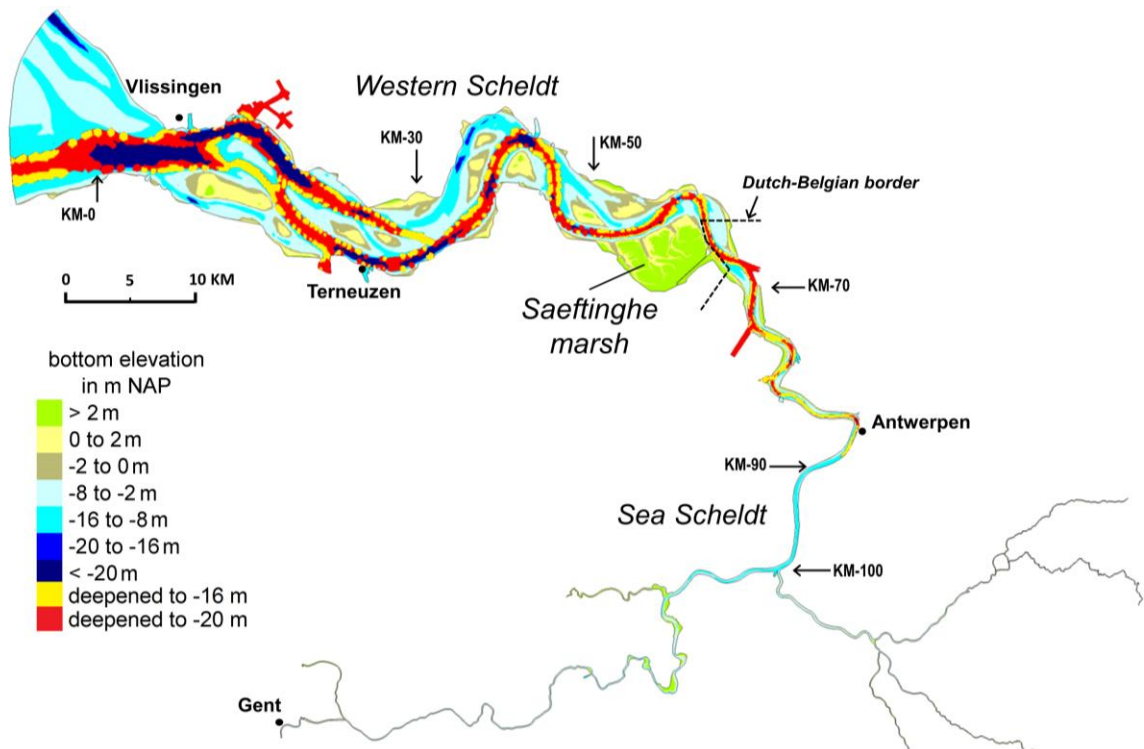


**Figure C1:** Bathymetrical map of the Scheldt Estuary model in which the parts of the channel that are lowered in the simulation with  $z_{\text{channel}} \leq 16$  m NAP is indicated in yellow and the part of the channel that is further lowered in the simulation with  $z_{\text{channel}} \leq 20$  m NAP is indicated in red.

**Table C1:** Overview of model scenarios with varying channel depth and the additional volume (below mean sea level) relative to the reference scenario.

Scenario description	abbreviation	additional tidal basin volume
Reference scenario based on the 2011 bathymetry	REF	-
Scenario with channel elevation $z_{\text{channel}} \leq 16.0$ m	$z_{\text{channel}} \leq 16.0$ m NAP	43 Mm <sup>3</sup>
Scenario with channel elevation $z_{\text{channel}} \leq 20.0$ m	$z_{\text{channel}} \leq 20.0$ m NAP	311 Mm <sup>3</sup>

#### Effects of channel enlargement on the vertical tide

Channel enlargement leads to an increase in tidal range to which higher MHWLs and lower MLWLs evenly contribute (Figure C2a-c). If the minimum channel depth is increased to 20 m below NAP, tidal range increases by up to 0.12 m, which is the same order of magnitude as the tidal range decrease due to the presence of intertidal flats (i.e., tidal flats reduce the tidal range by up to 0.20 m along the Western Scheldt, depending on their elevation) or due to the inclusion of additional intertidal storage volume of ~20% of the tidal prism (i.e., simulation with additional intertidal storage at KM-66 in **Chapter 5**). The propagation of the high water as well as the low water is accelerated as a result of channel deepening (Figure C2d/e). However, the low water phase lead in scenarios with deeper channels is larger than the high water phase lead, implying that the low water propagation is accelerated more.

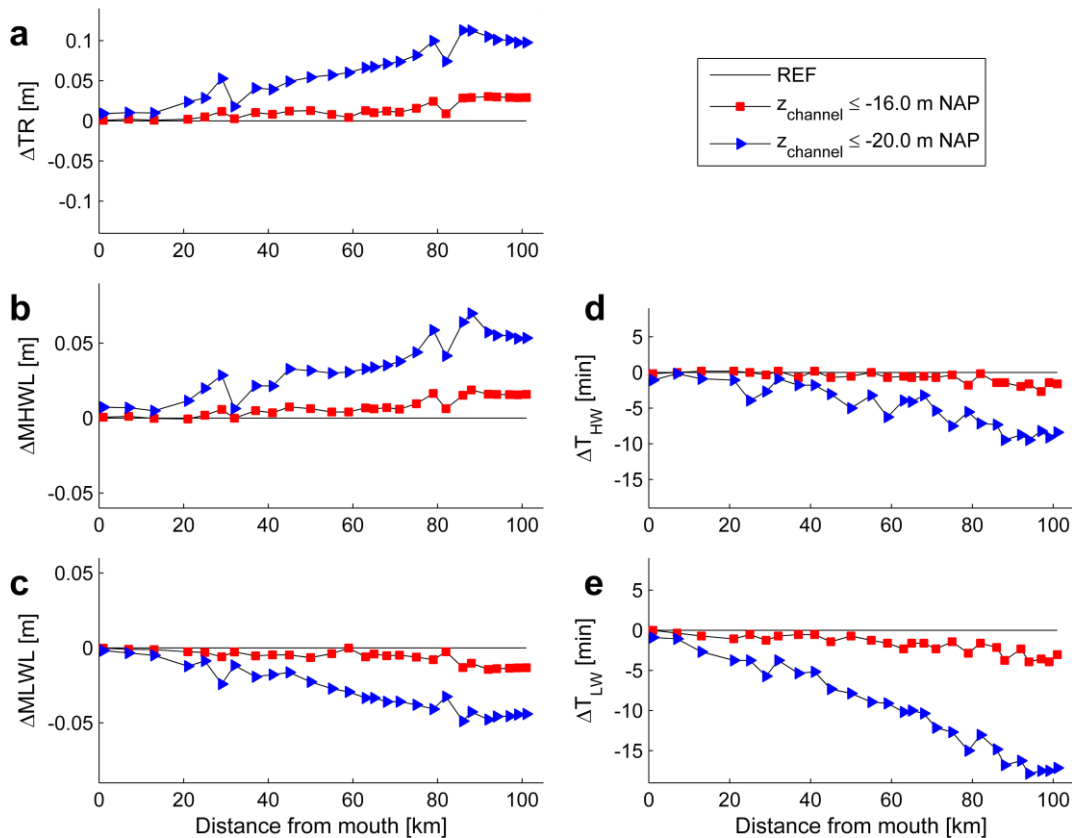


**Figure C2:** Modelled difference in (a) tidal range, (b) mean high water level (MHWL), (c) mean low water level (MLWL) and the phase differences of (d) high water ( $T_{HW}$ ) and (e) low water ( $T_{LW}$ ) for scenarios with a varying minimum channel depth, compared to the reference scenario.

#### *Effects of channel enlargement on the horizontal tide*

For the peak flood and peak ebb velocities (Figure C3), the effect of channel enlargement is the reverse of the effect of adding intertidal storage. While the latter leads to stronger peak ebb and flood velocities along most parts of the estuary, channel enlargement generally reduces the peak velocities. The peak flood and peak ebb velocities are barely affected in the scenario with a minimum channel depth of NAP -16.0 m, whereas the scenario with a minimum channel depth of NAP -20.0 m generally reduces the peak flood and peak ebb velocities along the estuarine channels. However, the effect on the peak velocities is variable along the estuary. In particular, changes in peak velocities range from a small increase at some locations to a decrease of  $\sim 0.15$  m/s at other locations. In the upstream part of the estuary, where the channel depth is not increased in the additional model scenarios (Figure C1), there is a small but continuous increase in peak flood and peak ebb velocities as a result of the downstream channel depth increase. The increase in peak ebb velocities is herein larger than in peak flood-velocities.

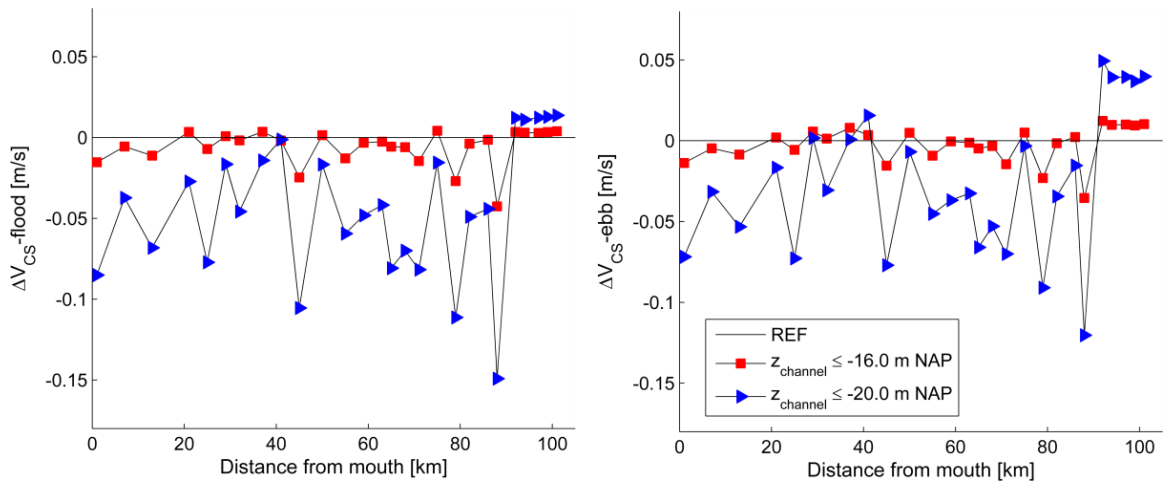


**Figure C3:** Modelled difference in cross-sectional averaged peak flood velocities (left) and cross-sectional averaged peak ebb velocities (right) between scenarios with a varying minimum channel depth and the reference scenario.

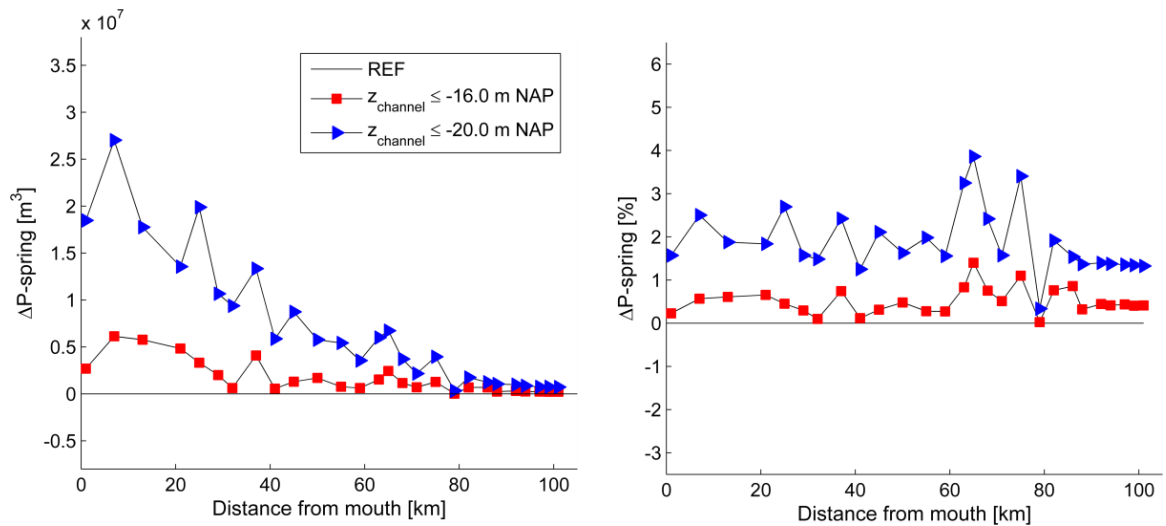


**Figure C4:** Modelled absolute (left) and relative (right) difference in tidal prism for scenarios with a varying minimum channel depth, compared to the reference scenario.

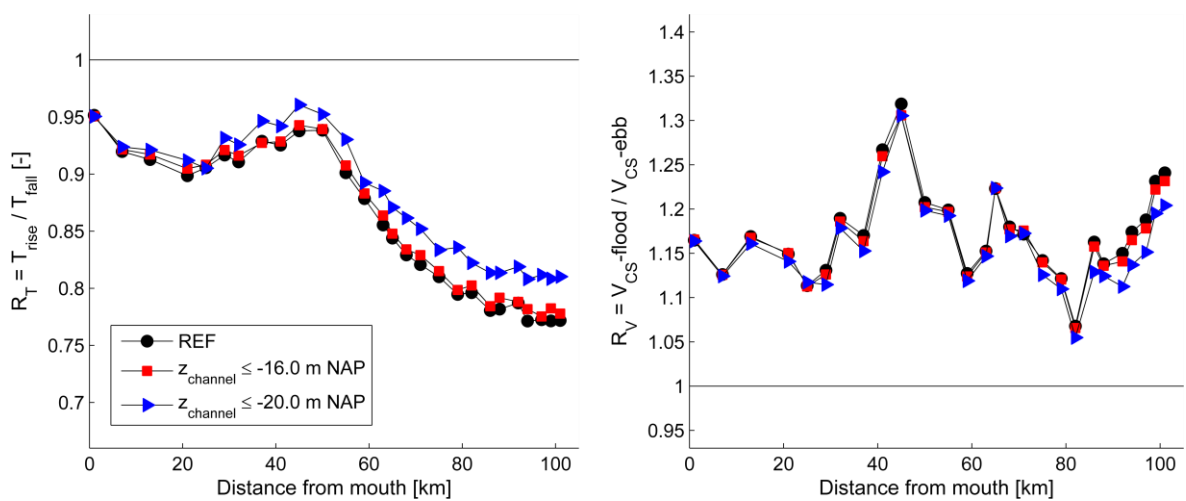


**Figure C5:** Modelled vertical tidal asymmetry based on the ratio between the duration of the rising tide and of the falling tide (left) and horizontal tidal asymmetry based on the ratio between cross-sectional averaged peak velocities during flood and during ebb for scenarios with a varying minimum channel depth and the reference scenario.

As channel enlargement leads to an increase in tidal range, the tidal prism also increases in the simulations with deeper channels (Figure C4). If the minimum channel depth is increased to NAP -20.0 and the subtidal volume of the estuary is enlarged by 311 Mm<sup>3</sup> (Table C1), the tidal prism at the mouth increases by about 2 Mm<sup>3</sup>. The tidal prism increase along the estuary, from the mouth up to KM-100 ranges from approximately 1.5% to 4% for this scenario. This is fairly similar to the effect of intertidal flats with an elevation of NAP +2.0 m (as compared to a situation without tidal flats; Figure 5.8). However, the latter scenario only enlarges the storage volume of the estuary by 137 Mm<sup>3</sup>. Furthermore, the scenario in which the channel depth is set to NAP -16.0 m only leads to a tidal prism increase along the estuary of 0% to 1.5%.

### *Effects of channel enlargement on tidal asymmetry*

Vertical and horizontal tidal asymmetry generally become less flood-dominant or more ebb-dominant as a result of channel enlargement (i.e.,  $R_T$  increases and  $R_V$  decreases; Figure C5). Nevertheless, tidal asymmetry remains flood-dominant along the entire channel in both scenarios. The impact of channel elevation on tidal asymmetry along the Scheldt Estuary channels is small relative to the impact of changes in tidal flat elevation. In particular, the value of  $R_T$  only increases by up to 0.04 in the upstream part of the estuary, while in the scenarios with varying tidal flat elevations the maximum impact on  $R_T$  ranges between -0.10 for tidal flats that are situated low in the tidal frame and +0.06 for scenarios with higher tidal flats. Similarly,  $R_V$  decreases by up to 0.04 upstream, whereas the impact of tidal flat elevation ranges from -0.15 to +0.20, depending on the elevation relative to mean sea level. However, when compared to the impact of adding (or removing) intertidal storage at specific locations along the estuary, the effect of channel deepening and changes in intertidal storage volume are of the same order. More specifically, the impact of deepening the channel to  $z_{\text{channel}} \leq 20.0$  m NAP on tidal asymmetry is similar to the impact that downstream located intertidal storage areas have to the upstream part of the estuary (Figure 5.5). Hence, the effect of channel enlargement or deepening on tidal asymmetry is the inverse of the effect that embankments have on tidal asymmetry in the estuarine channels upstream.

## References used in Appendix 5A-C

- Anon, 2010. Bodemberoerende activiteiten. Indicatoren voor het Schelde-estuarium., in: VLIZ Information Sheets. Vlaams Instituut voor de Zee (VLIZ), Oostende, p. 11.
- Dronkers, J., 1998. Morphodynamics of the Dutch Delta, in: *Physics of Estuaries and Coastal Seas*. The Hague, Netherlands, pp. 297–304.
- Dronkers, J., 1986. Tidal asymmetry and estuarine morphology. *Netherlands J. Sea Res.* 20, 117–131. doi:10.1016/0077-7579(86)90036-0
- Fortunato, A.B., Oliveira, A., 2005. Influence of Intertidal Flats on Tidal Asymmetry. *J. Coast. Res.* 21, 1062–1067. doi:10.2112/03-0089.1
- Friedrichs, C.T., Aubrey, D.G., 1988. Non-linear Tidal Distortion in Shallow Well-Mixed Estuaries: a Synthesis. *Estuar. Coast. Shelf Sci.* 27, 521–545. doi:10.1016/0272-7714(90)90054-U
- Friedrichs, C.T., Madsen, O.S., 1992. Nonlinear diffusion of the tidal signal in frictionally dominated embayments. *J. Geophys. Res.* 97, 5637–5650. doi:10.1029/92JC00354
- Jarrett, J.T., 1976. Tidal Prism - Inlet Area Relationships. Vicksburg, MS, U.S.
- Jeuken, C., Wang, Z.B., van der Kaaij, T., Van Helvert, M., Van Ormondt, M., Bruinsma, R., Tanczos, I., 2004. Morfologische ontwikkelingen in het Schelde estuarium bij voortzetting van het huidige beleid en effecten van een verdere verdieping van de vaargeul en uitpoldering langs de Westerschelde. Deelovereenkomst 2 en 3. Morfologie.
- Jeuken, M.C.J.L., Wang, Z.B., 2010. Impact of dredging and dumping on the stability of ebb-flood channel systems. *Coast. Eng.* 57, 553–566. doi:10.1016/j.coastaleng.2009.12.004
- Jongepier, I., Wang, C., Missiaen, T., Soens, T., Temmerman, S., 2015. Intertidal landscape response time to dike breaching and stepwise re-embankment: A combined historical and geomorphological study. *Geomorphology* 236, 64–78. doi:10.1016/j.geomorph.2015.02.012
- Maximova, T., Ides, S., Plancke, Y., De Mulder, T., Mostaert, F., 2010. Vervolgstudie inventarisatie en historische analyse van slikken en schorren langs de Zeeschelde - Scenario analyse 2D model. WL Rapporten, 713\_21. Antwerpen.
- O'Brien, M.P., 1969. Equilibrium flow areas of tidal inlets on sandy coasts, in: *Proceedings of the American Society of Civil Engineers. Journal of the Waterways and Harbors Division.* pp. 43–52. doi:10.9753/icce.v10.25p
- O'Brien, M.P., 1931. Estuary and tidal prisms related to entrance areas. *Civ. Eng.* 1, 738–739.
- Parker, B.B., 1984. Frictional effects on the tidal dynamics of a shallow estuary, Ph.D. thesis. John Hopkins University, Baltimore, Md., U.S.A.
- Pawlowicz, R., Beardsley, B., Lentz, S., 2002. Classical tidal harmonic analysis including error estimates in MATLAB using T\_TIDE. *Comput. Geosci.* 28, 929–937. doi:10.1016/S0098-3004(02)00013-4
- Smolders, S., Plancke, Y., Ides, S., Meire, P., Temmerman, S., 2015. Role of intertidal wetlands for tidal and storm tide attenuation along a confined estuary: A model study. *Nat. Hazards Earth Syst. Sci.* 15, 1659–1675. doi:10.5194/nhess-15-1659-2015
- Speer, P.E., Aubrey, D.G., 1985. A study of non-linear tidal propagation in shallow inlet/estuarine systems Part II: Theory. *Estuar. Coast. Shelf Sci.* 21, 207–224. doi:10.1016/0272-7714(85)90097-6
- Speer, P.E., Aubrey, D.G., Friedrichs, C.T., 1991. Nonlinear hydrodynamics of shallow tidal inlet/bay systems. *Tidal Hydrodyn.* 321–339.
- Swinkels, C.M., Jeuken, M.C.J.L., Wang, Z.B., Nicholls, R.J., 2009. Presence of connecting channels in the Western Scheldt Estuary. *J. Coast. Res.* 627–640. doi:10.2112/06-0719.1
- Van der Spek, A.J.F., 1997. Tidal asymmetry and long-term evolution of Holocene tidal basins in the Netherlands: Simulation of palaeo-tides in the Schelde estuary. *Mar. Geol.* 141, 71–90. doi:10.1016/S0025-3227(97)00064-9
- Wang, C., Temmerman, S., 2013. Does biogeomorphic feedback lead to abrupt shifts between alternative landscape states?: An empirical study on intertidal flats and marshes. *J. Geophys. Res.* 118, 229–240. doi:10.1029/2012JF002474
- Wang, Z., Jeuken, C., De Vriend, H., 1999. Tidal asymmetry and residual sediment transport in estuaries. A literature study and applications to the Western Scheldt, Z2749.
- Wang, Z.B., Jeuken, M.C.J.L., Gerritsen, H., De Vriend, H.J., Kornman, B.A., 2002. Morphology and asymmetry of the vertical tide in the Westerschelde estuary. *Cont. Shelf Res.* 22, 2599–2609. doi:10.1016/S0278-4343(02)00134-6



# Chapter 6

## General discussion & conclusions



*Intertidal channel in the Saeftinghe marsh at dawn*

This thesis addresses the impact of intertidal ecosystems on estuarine tidal hydrodynamics, including storm tide propagation. The size and morphology of intertidal areas along estuaries and coasts change over time as a result of the natural eco-geomorphological development of marshes (e.g. Allen, 2000; D'Alpaos et al., 2005; Kirwan and Murray, 2007; Stefanon et al., 2010) and as a result of human impacts, such as embankments, de-embankments and estuarine management practices (e.g. dredging activities, sand mining, dam construction, etc.) (e.g. Blott et al., 2006; Meire et al., 2005; Naik and Jay, 2011; Sherwood et al., 1990; Yang et al., 2006). In addition, relative sea level rise may also affect intertidal area characteristics as marshes could die off and drown if the sediment supply is insufficient (e.g. Kirwan and Megonigal, 2013; Kirwan et al., 2010), transforming former marsh habitat to non-vegetated intertidal flats or shallow water bodies. Restoration and conservation of intertidal areas is nowadays starting to be implemented in estuarine management schemes (e.g. French, 2006; Rupp-Armstrong and Nicholls, 2007; Temmerman et al., 2013). Driving forces behind this development are the potential to reduce flood risks from storm surges (e.g. **Chapters 2 & 3**; McIvor et al., 2012; Wamsley et al., 2010) and wind waves (e.g. Möller et al., 2014), and the ecological value provided by these areas (e.g. Barbier et al., 2013). Moreover, the implementation of intertidal areas is considered to be sustainable as biophysical feedback processes are known to enhance the vertical growth of marshes in case of sea level rise (e.g. de Vriend et al., 2014; Kirwan et al., 2016; Temmerman et al., 2013).

As the coastal defense value of tidal wetlands is often an important reason for the restoration of intertidal habitat (Borsje et al., 2011), such as for the Belgian Sigmaphan (Maris et al., 2007; Meire et al., 2014) or several managed realignment projects in Germany and the U.K. (French, 2006; Rupp-Armstrong and Nicholls, 2007), a main objective for this thesis is to improve scientific insights on the importance of intertidal area changes (i.e., changes in marsh size, geomorphology and vegetation cover) on its potential to reduce flood risks. In particular, new insights are developed in this thesis on the impact of marsh size and geometry on along-wetland attenuation rates. This is assessed with new field observations (**Chapter 2**) and with numerical modelling (**Chapter 3**), while the impact of intertidal area characteristics on along-estuary attenuation of storm surges was already assessed in a previous study by Smolders et al. (2015), who modelled along estuary attenuation of storm tides in the Scheldt Estuary. In addition, this thesis provides new insights about the impact of intertidal area changes on tidal hydrodynamics and in particular on tidal asymmetry, both on marsh scale (**Chapters 2 & 4**) as well as on estuary scale (**Chapter 5**).

The results and findings in this thesis may assist coastal and estuarine managers worldwide in optimizing the design, implementation and morphological management of intertidal ecosystems, including tidal flats and tidal marshes, with special attention for the potential positive effects that intertidal ecosystems can have on regular estuarine hydrodynamics and storm tide hydrodynamics. For example, the results can be used in favor of ecosystem-based flood risk mitigation or studies on the effects of intertidal areas for tidal asymmetry, which is relevant for the net transport of sediments and other



materials or for risks of high turbidity and even sediment infilling of estuaries or marshes.

## 6.1 Potential for storm surge reduction

Both in-situ water level observations and numerical modelling results in this thesis indicate that marshes, and in a broader sense intertidal ecosystems, have the potential to attenuate peak water levels and reduce storm surges locally across marsh transects (**Chapters 2 & 3**) and reduce peak water levels on a larger scale along estuary channels (**Chapter 5**). The present results increase generic insights on the coastal defense potential of these wetlands and may support coastal and estuarine managers in areas at risk around the world (e.g. Table 2.1 in **Chapter 2**), for example with the design or management of nature-based coastal defense structures. More specifically, the findings in this thesis show the effect of variations in the eco-geomorphology of coastal wetlands on storm surge attenuation rates. The effects of variations in wetland geomorphology on storm surge reduction inside wetlands and along estuaries are summarized in a general scheme in Figure 6.1 (i.e., based on developmental stages of intertidal wetlands). Below, we discuss these effects and relations between inside-wetland attenuation and along-estuary attenuation in more detail.

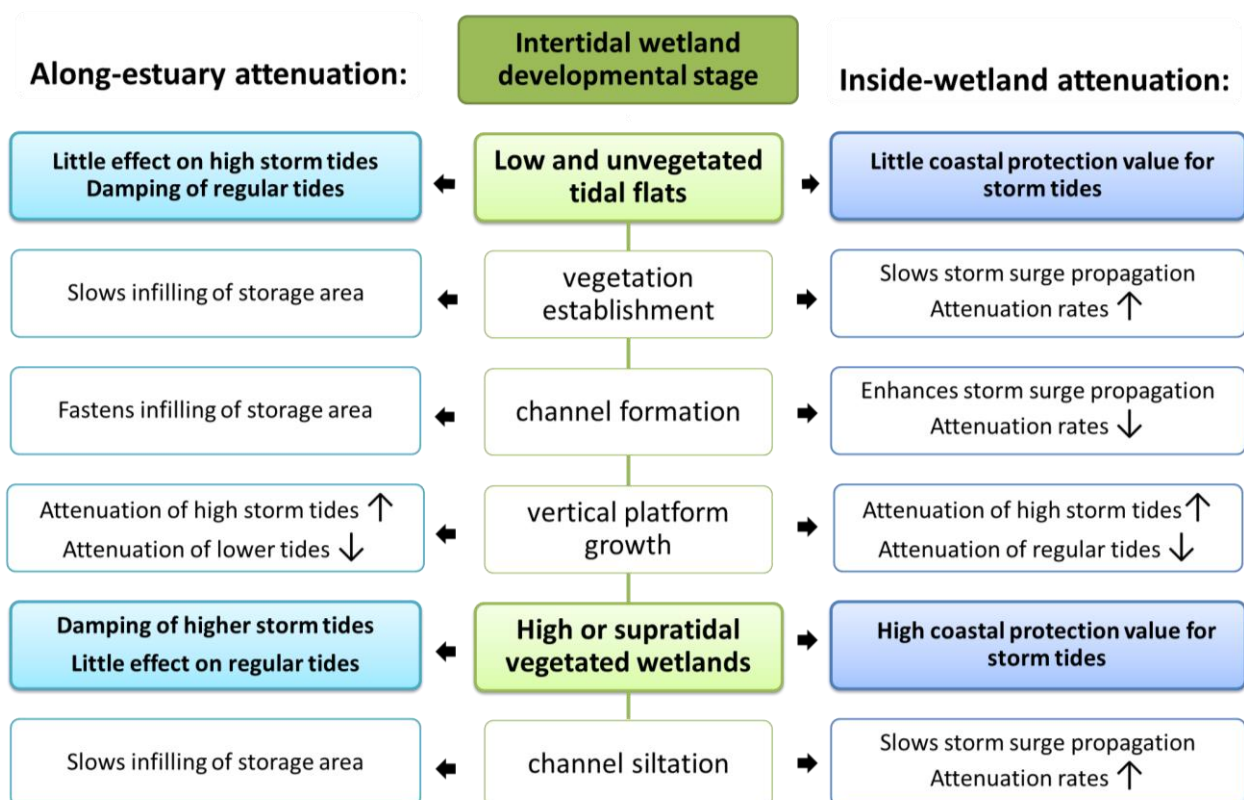


**Figure 6.1:** Scheme showing the effect of wetland eco-geomorphology, based on different stages of marsh development, on along-estuary storm surge attenuation (based on findings of Smolders et al, 2015) and on inside-wetland attenuation (based on findings in **Chapters 2 & 3**).

Generally, tidal marsh vegetation damps the tidal propagation across wetlands for overmarsh tides and thereby attenuates the peak water levels. The amount of peak water level reduction is a function of the hydrodynamic boundary conditions (i.e., the

storm surge height and duration) and marsh geomorphology (i.e., elevation, size, channel geometry and vegetation cover), implying that the coastal defense value of tidal wetlands is related to the combined effect of hydrodynamic and geomorphological parameters. Model results in this thesis (**Chapter 3**) indicate that attenuation rates can be predicted by the ratio between the water volume flowing over the marsh platform and the total water volume in the marsh channels and on the marsh platform ( $\alpha_v = V_{platform} / (V_{channel} + V_{platform})$ ). The parameter  $\alpha_v$  is indeed dependent on both marsh characteristics (i.e., channel depth, channel width and platform width) as well as hydrodynamic characteristics (i.e., flood wave height).

### **6.1.1 Effect of wetland channel geometry**

The dependency on  $\alpha_v$  implies that attenuation rates are partly determined by marsh channel geometry and more specifically by the channel depth and by the channel width relative to the platform width. Narrow and shallow channels induce higher attenuation rates, whereas wide and deep channels induce lower attenuation rates or may even lead to amplification. Similar conclusions can be drawn based on field observations and an analytical approximation for tidal flow through estuaries and tidal channels (Van Rijn, 2011), which is adopted for tidal flow through intertidal channels surrounded by vegetated marsh platforms (**Chapter 2**). Moreover, these conclusions are also consistent with general knowledge on tidal propagation in convergent estuary channels for which frictional distortion decreases if the channel depth increases, leading to less damping or more amplification (e.g. Friedrichs and Madsen, 1992). Although the effect of wetland channel geometry on along estuary storm surge attenuation was found to be small in modelling efforts by Smolders et al. (2015), the effect could be more profound in situations where the flow resistance on the marsh platform is higher as channels enhance the tidal propagation across the wetland (e.g. **Chapters 2 & 3**; Temmerman et al., 2012). Besides, the presence of (larger) channels also increases the total storage volume provided by the wetland.

### **6.1.2 Effect of the elevation of tidal wetlands**

The elevation of the marsh platform determines which tides or flood waves are most effectively attenuated, both locally across wetlands, as well as along estuary channels. Generally, higher tidal marshes (or supratidal wetlands) are more efficient in attenuating higher flood waves, while lower tidal marshes are more efficient in attenuating lower flood waves (Figure 6.1).

For peak water level reduction across tidal wetlands, a distinct shift in attenuation rates is present between undermarsh tides that only inundate the marsh channels on one hand and overmarsh tides that also inundate the marsh platform on the other hand (**Chapters 2 & 3**). Undermarsh tides are generally not attenuated or even slightly amplified, whereas overmarsh tides are increasingly attenuated for higher peak water levels up until a maximum attenuation rate depending on  $\alpha_v$  (**Chapter 3**). In addition, the analytical approximation of tidal flow through marsh channels indicates that attenuation rates may be limited for very high flood waves as the effect of (vegetation-induced) bottom friction reduces for higher inundation depths (**Chapter 2**).

On the estuary scale, similar conclusions can be drawn for peak water level attenuation rates along the estuary channels. Based on hydrodynamic model simulations of storm tides in the Scheldt estuary, Smolders et al. (2015) show that higher storm tides are more effectively attenuated by higher marshes, even though the total storage area is less. They argue that the inflow during higher water levels is relatively faster for low wetland elevations as the wetland is already flooded by a (significant) water depth and hence flow resistance is smaller. Besides, results in this thesis (**Chapter 5**) suggest that while the intertidal storage volume increases for lower tidal wetlands, the friction exerted on the propagating high water level will decrease as the water depth on the tidal wetland becomes larger. This interaction between depth-varying intertidal storage on one hand and depth-dependent friction on the other hand causes the damping of regular spring-to neap tides along the estuary to be optimized for intermediate intertidal area elevations between MSL and MHWL (**Chapter 5**), whereas the damping of higher storm tides is optimized for high intertidal area elevations.

### ***6.1.3 Effect of the size of tidal wetlands***

Another important issue for peak water level reduction is wetland size (or marsh width). Field observations suggest (**Chapter 2**) and numerical model results show (**Chapter 3**; Liu et al., 2013; Resio and Westerink, 2008) that storage area limitations may lead to blockage and reflection against levees or other structures confining the marsh or coastal wetland area. If the flood wave duration is long enough, the propagating flood wave is blocked or reflected before the peak water levels reach the landward edge of the tidal wetland, leading to higher HWLs at the levee and hence lower attenuation rates or even amplification towards the landward edge of the marsh. This suggests that a minimum wetland size or marsh width exists, for which the inside-wetland attenuation capacity is optimized and attenuation rates are not anymore affected by levees or other confining structures behind the marshes. The minimum wetland size or minimum marsh width depends on the flood wave duration and marsh characteristics affecting flood wave propagation (i.e., such as vegetation cover and marsh elevation). However, while peak water level attenuation rates are optimized at a certain minimum wetland size, the total inside wetland peak water level reduction may still increase for larger wetland sizes and marsh widths as the distance over which these attenuation rates are present increases with the size of the marsh.

Marsh size is also important for the coastal defense value of tidal wetlands on estuary scale. Along-estuary peak water level reduction also increases with the size of intertidal areas (**Chapter 5**; Smolders et al., 2015). More specifically, Smolders et al. (2015) showed that once a certain wetland size is exceeded, along-estuary peak water level reduction does not increase further as the duration of the flood wave is then too short to fill the entire storage volume. Hence, blockage against levees or other structures confining the marsh size can again be considered as limiting factor. This implies that a similar minimum wetland size for which the attenuation capacity is optimized may also exist for the along-estuary attenuation of storm tides. In contrast to the total inside wetland attenuation which may increase further for even larger wetlands, the total

along-estuary peak water level reduction does not increase further if the wetland size is increased beyond its 'optimal' size.

### **6.1.4 Implications towards coastal and estuarine management**

Findings in this thesis could be applied in coastal and estuarine areas at risk around the world (e.g. Table 2.1 in **Chapter 2**). The present model results on the impact of tidal wetland geomorphology on peak water level attenuation rates may open the way to create design guidelines for the implementation of tidal marshes or coastal wetlands in general as part of the coastal defense structures. In particular, the relationship that is developed in this thesis between the ratio  $\alpha_v$  (i.e.,  $V_{platform} / (V_{channel} + V_{platform})$ ) and peak water level reduction rates (**Chapter 3**) is potentially applicable to tidally induced sheet flow over marshes dominated by flexible wetland grasses. Moreover, similar relationships can potentially be found for other types of tidal wetlands, with different vegetation types such as mangroves or different forcing conditions such as hurricanes or diurnal storm tides.

Furthermore, this thesis shows the importance of wetland size for the attenuation of storm tides, which may have implications for the applicability of nature-based coastal defense structures in vulnerable areas around the world. In particular, a certain minimum marsh width or wetland size is required to efficiently reduce storm surges across coastal wetlands. In this perspective, it is also important to realize that the type of hydrodynamic forcing for which the protection is intended largely determines this minimum wetland size. An 'optimal' geometry of tidal wetlands is always linked to specific hydrodynamic forcing conditions. Larger storms with longer durations ask for larger wetlands, both on a local scale (**Chapter 3**) as well as for the along estuary attenuation (Smolders et al., 2015). When the duration of a the hydrodynamic forcing or flood wave is known (e.g. storm tides have a specific duration linked to the tidal period), design guidelines can be developed for the marsh width at which blockage effects do not play a role anymore (e.g. **Chapter 3**; Resio and Westerink, 2008) and the inside-wetland attenuation rate or along-estuary attenuation is maximized. However, for inside wetland attenuation, the total peak water level reduction will still increase for larger wetland sizes as it is the attenuation rate and not the total attenuation that is optimized at a certain minimum wetland size.

Similarly, design guidelines for marsh or wetland elevation are also linked to specific forcing conditions. An example is that higher marsh platforms or intertidal areas that are situated higher in the tidal frame are more effective for the attenuation of higher storm tides, both locally across the area itself (**Chapter 3**) as well as on estuary scale (Smolders et al., 2015), but they are less effective for attenuating lower flood waves. Hence, optimizing the design and geometry of tidal wetlands based on a very high (design) storm surge may lead to less efficient peak water level reduction during lower but more frequent storm surges or flood waves.

## 6.2 Intertidal area changes and tidal hydrodynamics

Model results in this thesis indicate that changes in the size and geometry of intertidal ecosystems, including (de-)embankments and the eco-geomorphological development of tidal marshes, affect tidal hydrodynamics locally along marsh channels (**Chapters 2 & 4**) and on estuary scale (**Chapter 5**). In particular, the present results clearly show the impact of depth-dependent friction and storage volume (i.e., varying intertidal area or marsh platform elevation) on tidal asymmetry (Figure 6.2), expanding existing general insights about the effect of estuarine geometry on tidal asymmetry (e.g. Dronkers, 1986; Friedrichs and Aubrey, 1988; Friedrichs and Madsen, 1992; Speer and Aubrey, 1985). Below, we again discuss the effect of some characteristics and eco-geomorphological development steps of intertidal areas on tidal hydrodynamics on marsh scale and on estuary scale. It should be stated that the conclusions on the hydrodynamic impact of intertidal area characteristics concern initial hydrodynamic effects and that hydro-morphodynamic feedbacks and the morphological development that is initiated by the hydrodynamic changes are not taken into account.

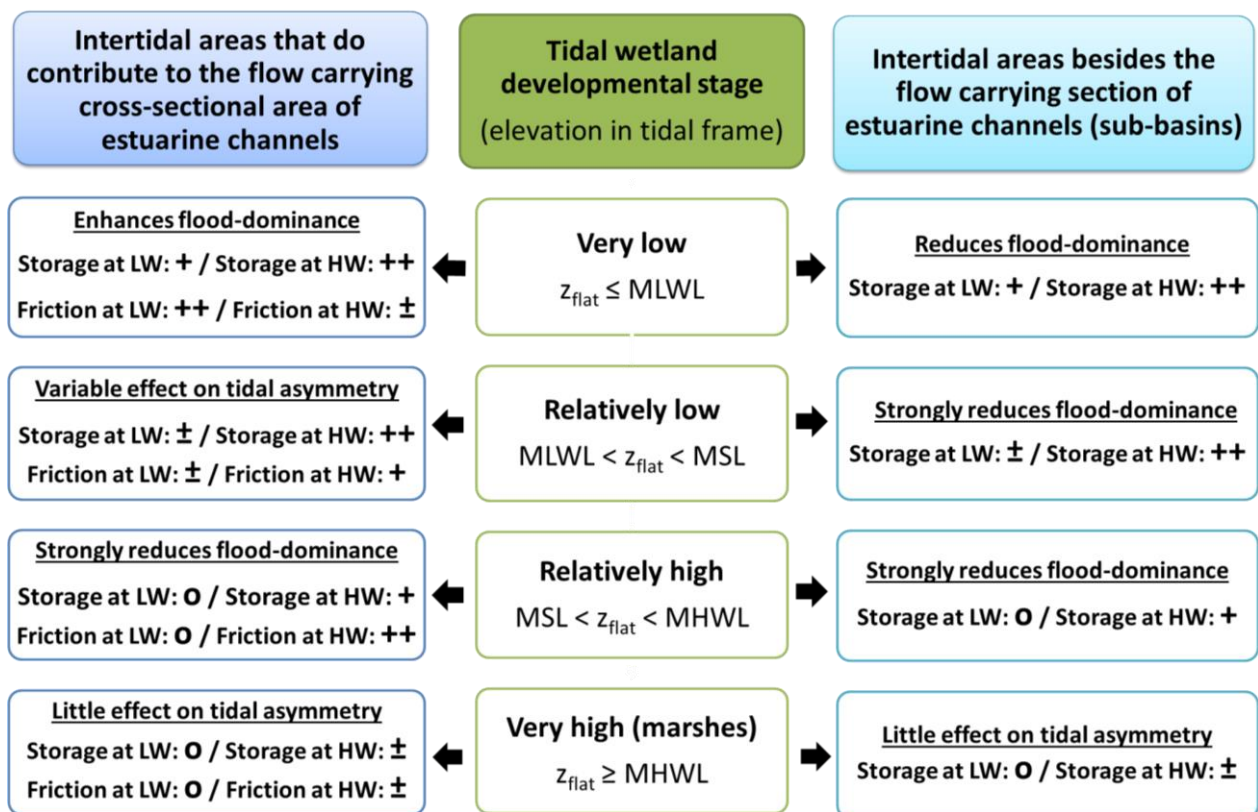


**Figure 6.2:** Conceptual scheme of the effect of intertidal area elevation within the tidal frame on tidal asymmetry in estuarine channels for intertidal areas that are part of the momentum-carrying cross-section of the estuary (left) and for intertidal areas that do not contribute to the flow-carrying cross-section (right), based on the friction exerted and storage provided at high and low water levels. The contribution of storage and friction effects at different water levels is ranked between non-existing/negligible (0), weak ( $\pm$ ), strong (+) and very strong (++). The elevation of the tidal wetlands within the tidal frame ( $z_{\text{flat}}$ ) is given relative to mean low water level (MLWL), mean sea level (MSL) and mean high water level (MHWL).

**6.2.1 Effect of (intertidal) storage volume**

Depending on their size and storage volume relative to the local tidal prism, the presence of intertidal ecosystems (i.e., tidal flats and tidal marshes) along estuarine channels has an increasingly large effect on estuarine tidal hydrodynamics. Intertidal storage areas reduce the tidal range and the high water levels (i.e., including peak water level reduction of storm tides) along the estuary and have an along-estuary varying effect on the tidal prism. More specifically, in addition to the known effect of tidal prism decrease upstream and tidal prism increase downstream of intertidal storage areas (e.g. Coen et al., 2008; Jeuken et al., 2004), model results in this thesis show that far downstream the second-order effect of tidal range reduction on the tidal prism can become larger than the intertidal storage volume itself (**Chapter 5**). Hence, adding intertidal storage can (initially) reduce the tidal prism far downstream.

For tidal asymmetry, model results in this thesis indicate that adding intertidal storage volume reduces flood-dominance in estuarine channels upstream of the intertidal area (**Chapter 5**). This finding is consistent with analytical results by Speer and Aubrey (1985) and Tambroni and Seminara (2008) who show that sufficiently large tidal flats may turn an initially flood-dominant channel into ebb-dominant. The strength of the ebb-dominance due to intertidal storage depends on the amount of storage provided at different water levels (Figure 6.2). Conversely, intertidal storage areas may enhance flood-dominance along a stretch of several kilometers downstream due to a velocity surge effect, which is stronger during flood than during ebb in the model results presented in this thesis (**Chapter 5**). On marsh scale, the effect of additional storage volume can best be illustrated by the distinct shift from strong flood-dominance for undermarsh tides towards a less flood-dominant or even ebb-dominant asymmetry for overmarsh tides (**Chapter 2**). Hence, adding storage volume reduces flood-dominance (or enhances ebb-dominance) on estuary scale as well as on marsh scale. However, the impact on tidal asymmetry (i.e., reduction of flood-dominance) might be less pronounced if storage effects already influence the tidal propagation at relatively low water levels (Figure 6.2).

**6.2.2 Effect of the elevation of intertidal areas and marsh platforms**

While previous studies often only considered the storage function of tidal flats, which enhances ebb-dominance in estuarine channels (e.g. Friedrichs and Aubrey, 1994, 1988; Friedrichs and Madsen, 1992), an important finding in this thesis is that bottom friction exerted by the tidal flats on along-estuary tidal propagation is also important for tidal asymmetry. In particular, intertidal areas that are situated in the momentum-carrying cross-section of the estuary and hence exert friction on the propagating tidal wave (Speer and Aubrey, 1985) may have a different impact on tidal hydrodynamics than intertidal areas that only provide for storage volume (i.e., such as tidal sub-basins that are located besides the estuarine channel), depending on their elevation (Figure 6.2). For example, if the intertidal storage volume is increased by creating intertidal side-basins that do barely contribute to the along-estuary tidal propagation, flood-dominance is generally reduced. In contrast, if the intertidal storage volume is increased by lowering tidal flats that are part of the flow-carrying cross-section and exert friction on

the propagating tidal wave, flood-dominance might be enhanced upstream as bottom friction decreases for higher water levels while storage and friction effects increase for lower water levels (Figure 6.2), especially if the tidal flats are situated very low in the tidal frame and remain inundated during tides with relatively high low water levels (i.e., neap tides). On the other hand, tidal wetlands that are situated very high in the tidal frame (e.g. marshes) barely have any effect on tidal asymmetry as a majority of the tides during a spring-neap cycle is confined in the estuarine channels. Moreover, flood-dominance will prevail in this situation as a frictionally dominated tidal channel with insignificant intertidal storage is known to be flood-dominated (Lanzoni and Seminara, 2002). It can be concluded that if intertidal areas are situated in the momentum-conveying cross-section of an estuary and hence exert friction on the propagating tidal wave, their elevation determines the influence of tidal flats on the type of tidal asymmetry (i.e., whether tidal flats enhance ebb-dominance or flood-dominance). The influence of intertidal area elevation also implies that the eco-geomorphological development of intertidal areas, from relatively low and unvegetated tidal flats to high elevated and vegetated marshes, alters the impact of intertidal areas on tidal asymmetry in estuaries over time.

The effect of elevation changes of the marsh platform on tidal hydrodynamics in marsh channels (**Chapter 4**) is largely similar to the effect of elevation changes of the intertidal areas as a whole on tidal hydrodynamics in estuarine channels (**Chapter 5**) based on Figure 6.2. On marsh scale, an increase in platform elevation implies a decrease in storage volume and hence a decrease in tidal prism in the intertidal marsh channels. In addition to differences in storage volume, variations in the elevation of the marsh platform also imply differences in depth-dependent friction exerted on the tidal flow. Generally, frictional effects on the marsh platform cause the tidal asymmetry in marsh channels to become more ebb-dominant (or less flood-dominant) for higher marsh platforms, even though the decrease in storage volume would enhance flood-dominance (**Chapter 4**). However, if the marsh platform elevation becomes too high in the tidal frame, and hence a majority of the tides during a spring-neap cycle is confined in the marsh channels, the effect of the platform is minimized (similar to the effect of very high tidal flats in Figure 6.2) and flood-dominance increases again.

### **6.2.3 Effect of channel geometry**

The geometry of the marsh channels itself has an impact on tidal hydrodynamics on marsh scale, while the impact on estuary scale is more indirect as marsh channels reduce the average elevation of the intertidal area as a whole and hence increase the intertidal storage volume, especially during neap tides when the marsh platform is not inundated. The effect of changes in channel size (i.e., cross-sectional area) on tidal hydrodynamics can largely be explained by relationships between tidal prism and the cross-sectional area of marsh channels (e.g. **Chapter 4**; Rinaldo et al., 1999; Steel and Pye, 1997; Vandenbruwaene et al., 2015), similar to the typical prism to cross-sectional area relationships for tidal inlets (e.g. Jarrett, 1976; O'Brien, 1969, 1931; Stive et al., 2010). For example, a decrease in tidal prism leads to lower flow velocities and bottom shear stresses, which on its turn induces channel infilling and hence a smaller cross-

sectional area, or vice versa. Nevertheless, the effect of marsh channel infilling on tidal asymmetry can be twofold as channel infilling reduces both the cross-sectional area (enhancing ebb-dominance associated with channel scouring), as well as the tidal prism because the storage volume in the channel network itself decreases (enhancing flood-dominance associated with further channel infilling). The resulting impact of variations in marsh channel geometry on marsh tidal hydrodynamics is thus dependent on the relative importance of changes in water storage in the channel network for the total tidal prism.

The impact of changes in the size and depth of the subtidal estuarine channels on tidal asymmetry in the Scheldt Estuary, briefly assessed in **Appendix C**, could not be explained by tidal prism to cross-sectional area relationships. In particular, enlargement of the estuarine channels appears to lead to a less flood-dominant asymmetry instead of enhanced flood-dominance associated with channel infilling. This is considered to be the result of a decrease in frictional distortion (e.g. Friedrichs and Aubrey, 1988; Speer and Aubrey, 1985).

### **6.2.4 Effect of marsh vegetation**

The presence and establishment of marsh vegetation mainly influences tidal hydrodynamics on the intertidal area itself (**Chapter 4**). Vegetation-induced flow resistance induces flow concentration towards the marsh channels and leads to a shift towards a more ebb-dominant (or less flood-dominant) asymmetry of the horizontal tide associated with net export (or a reduced import) of sediments and materials. In contrast, the vertical tide appears to become more flood-dominant (i.e., shorter rising) in marsh channels if vegetation is present. This means that the lag effect vegetation has on tidal flow damps the peak flood velocities more than the peak ebb velocities, but it also elongates the ebb outflow. Another possibility is that the total ebb volume exceeds the total flood volume in the marsh channels because part of the inflow during flood occurs as so-called sheet flow over the marsh platform (e.g. Temmerman et al., 2005a, 2005b), whereas the outflow during ebb is more concentrated towards the channels.

The direct effect of the presence of vegetation on tidal flats for tidal hydrodynamics along the estuarine channels is not assessed in this thesis, but is expected to be minor relative to significant changes in the size and elevation of intertidal areas, the effects of which are discussed below. In particular, sensitivity analysis reveals that if the bottom friction coefficients of the vegetated part of the Saeftinghe marsh are varied in model scenarios representing the present-day situation (not presented in this thesis), the effect of this large intertidal ecosystem on estuarine tidal hydrodynamics barely changes. Nevertheless, the effect of vegetation establishment on estuarine tidal hydrodynamics can be indirect as vegetation traps sediments, enhances vertical accretion (e.g. Mudd et al., 2010) and hence induces changes in the elevation of intertidal areas, which may have pronounced effects on estuary-scale tidal hydrodynamics (paragraph 6.2.2).



### **6.2.5 Implications towards estuarine and wetland management**

Creation and restoration of tidal wetlands is nowadays taking place in numerous estuaries around the world (e.g. French, 2006; Maris et al., 2007; Rupp-Armstrong and Nicholls, 2007). A better understanding of the effects of specific intertidal area properties on tidal hydrodynamics is therefore of interest for estuarine scientists and managers. In general, when assessing the impact of additional intertidal storage on tidal hydrodynamics for estuarine management, the location of intertidal areas (i.e., position along the estuary and relative to the flow-carrying cross-section) should be taken into account. Firstly, the position along the estuary determines the relative impact of intertidal storage areas, as well as the part of the estuary along which a certain hydrodynamic impact takes place. Secondly, the physio-topographical position of an intertidal storage area relative to the estuarine channels determines whether the intertidal area contributes to the momentum-conveying or flow-carrying cross-section (i.e., allowing along-estuary propagation across the intertidal area), which particularly affects the impact that intertidal areas have on tidal asymmetry for lower tidal flat elevations (Figure 6.2).

The spatially varying effects of intertidal areas or de-embankments in particular could potentially be used in favor of estuarine management. For example, findings on intertidal area characteristics that enhance ebb-dominance the most (i.e., intermediate to high tidal flat elevations or tidal flats that do not exert friction on the propagating tidal wave) could be of particular interest in estuaries or tidal channels in which tidal pumping as a result of a strong flood-dominant tidal asymmetry is considered to be a problem (e.g. Mitchell, 2013). By choosing an optimal location for de-embankments or the creation of intertidal storage, ebb-dominance can be enhanced along specific channel sections upstream of the additional intertidal area. Similarly, the tidal prism can be reduced or increased along specific sections of the estuarine channel by carefully choosing the location of de-embankments.

Another important issue for estuarine management is how the hydrodynamic impact of de-embankments, marsh restoration or former embankments compares to other human-induced impacts such as dredging and disposal of dredged material. For the Scheldt Estuary or other estuaries where both large-scale embankments and intensive dredging activities have taken place, questions could be raised whether the impact of historical embankments on tidal hydrodynamics can be counteracted by dredging activities in the estuarine channels. The results in this thesis indicate that this may indeed be possible for the impact on tidal asymmetry as removing a large intertidal storage volume enhances flood-dominance (**Chapter 5**), while enlarging the channel size appears to reduce flood-dominance in the Scheldt Estuary channels (**Appendix C**). However, in this perspective it should be stated that, although they have an opposite impact on tidal asymmetry, embankments and channel deepening both lead to a larger tidal prism and tidal range in estuarine channels, which is often considered as a negative impact for coastal safety reasons.

### **6.3 Recommendations**

Some of the findings in this thesis open the way for additional research to further improve insights about the impact of specific intertidal area characteristics on the potential for storm surge reduction and estuarine tidal hydrodynamics.

Firstly, research efforts could be done to find additional relationships between storm surge attenuation rates, marsh geometry and hydrodynamic boundary conditions, similar to the relationship found in **Chapter 3** (i.e., Eq. 3.9). This relationship is developed for a storm tide propagating over a relatively high tidal marsh occupied by (short) wetland grasses. Similar relationships probably exist for other wetland types such as mangroves, where the flow resistance is different from the marsh we studied (e.g. Hu et al., 2015; Sheng et al., 2012). In particular, mangrove trees are generally tall, emergent and have a higher stiffness compared to the flexible short wetland grasses in marshlands. In terms of bottom friction, typical Manning's friction coefficients for mangrove forests are  $n = 0.08 \text{ s}\cdot\text{m}^{-1/3}$  to  $n = 0.15 \text{ s}\cdot\text{m}^{-1/3}$  (e.g. Wamsley et al., 2010; Zhang et al., 2012), whereas typical values for marshlands with shorter flexible vegetation range between  $n = 0.04 \text{ s}\cdot\text{m}^{-1/3}$  and  $n = 0.08 \text{ s}\cdot\text{m}^{-1/3}$  for marshlands (e.g. **Chapter 3**; Temmerman et al., 2012; Zhang et al., 2012). Sensitivity analysis in **Chapter 3** already gives an indication of this relationship for higher bottom friction coefficients, showing how much attenuation rates would increase for higher friction coefficients. While this thesis only addresses storm tides in a semi-diurnal tidal environment, the relationship may also vary for different types of flood waves, such as hurricane- or cyclone-induced storm surges, depending on their flood wave period and forward propagation speed (Resio and Westerink, 2008). These research questions could potentially be addressed numerically, but the demand for additional field observations remains large.

Although this thesis has provided quite unique field measurements of storm surge propagation through tidal wetlands (**Chapter 2**), in-situ observations in other marsh systems are still scarce and mainly exist of measurements during specific hurricane events (Table 2.1). Systematic field measurements of flood wave or tidal propagation in different wetland types, with varying vegetation cover, varying channel geometry and most importantly for a wide range of tidal and storm surge-induced inundation events (i.e., ranging from regular tides to elongated storm surges) are therefore still needed. The demand for this kind of field observations is nowadays especially urgent as wetlands are increasingly considered as part of the coastal defense system (e.g. Borsje et al., 2011; Temmerman et al., 2013). Moreover, insights on the relation between vegetation characteristics and storm surge attenuation capacity could also be improved this way. Examples are the effects of vegetation height, stem diameter and stem density, which are included in the Baptist et al. (2007) formula for vegetation-induced flow resistance, or the effects of vegetation stiffness, linked to the flow-resistance of flexible submerged vegetation (Verschoren et al., 2016). Ultimately, all these additional insights on the impact of the eco-geomorphology of tidal wetlands on storm surge attenuation rates could contribute to a global model of storm surge impact and a more accurate estimation of the coastal defense value of wetlands and mangroves worldwide.

Furthermore, future studies on the coastal defense potential of tidal wetlands could focus on the feasibility of the implementation of tidal wetlands to simultaneously reduce flood risks locally on marsh scale as well as on estuary scale. Field observations and model results in this thesis indicate that the effectiveness of wetlands in attenuating flood waves locally across the wetland itself is related to the flood wave height relative to the platform height (**Chapters 2 & 3**). In particular, it was found that higher wetlands are more efficient in attenuating higher flood waves. Smolders et al. (2015) found that higher wetlands are also more efficient in reducing the peak water levels of higher storm tides along estuary channels. It has however not yet been assessed whether the elevation for which a specific storm tide is most effectively attenuated locally coincides with the elevation that provides the largest peak water level reduction on estuary scale. In addition, results in this thesis suggest that there might be a minimum wetland size, related to the duration of the flood wave, for which the attenuation capacity of the tidal wetland is fully used on a local scale (**Chapter 3**). Similar results were found for the effect of wetland size on estuary-scale peak water level reduction, which also increased up until a certain wetland size for which the storm surge reduction was maximized (Smolders et al., 2015). It may be expected that these ‘optimal’ wetland sizes for marsh scale and estuary scale attenuation are similar, as blockage against confining levees or other structures is in both cases considered to be the limiting factor, but this has not yet been assessed either. Additional modelling efforts could be used to test this hypothesis.

For the impact of intertidal areas on tidal hydrodynamics, the main aspects that still ask for a better understanding are variations in the impact of intertidal areas on tidal hydrodynamics on longer time scales (i.e., decadal time scale) due to interactions between the morphological development and changing tidal hydrodynamics (Jeuken et al., 2004). In this thesis, only the initial impact of (sudden) changes in intertidal area properties, covering the first years to decades, is assessed (**Chapter 5**). It is likely that the relatively strong initial impact of sudden changes in intertidal area properties gradually decreases over time as a consequence of morphodynamic response to the changed hydrodynamics. Moreover, Jeuken et al. (2004) showed that after several decades the impact on tidal hydrodynamics may even be reverse. The effects on longer time scales may also interfere with other processes such as channel deepening and maintenance dredging and disposal activities that affect estuarine morphodynamics and alter the estuarine morphology on the long term (Van der Wegen and Roelvink, 2012). Decadal scale morphological modelling is deemed necessary to better assess long-term effects of intertidal area changes. This is however a challenging task as decadal scale morphological modelling tends to be difficult as the model performance on decadal time scale is often poor due to the initial morphological adaptation time (Van der Wegen and Roelvink, 2012). Nevertheless, the model performance of decadal scale morphological modelling is improving and, for example, Dam et al. (2015) obtained good results with a decadal to centennial scale morphological model of the Scheldt Estuary, starting from a realistic bathymetry. In their case, it appeared that the long-term development of the estuarine geomorphology is largely determined by the interactions between (tidal)

boundary conditions and the planform shape of the estuarine geometry (i.e., confinement by fixed banks).

Finally, another opportunity for further research is to implement specific types of connections that allow for the water exchange between the estuarine channels and restored marshes or flood control areas (i.e., overflow dykes, weir- and sluice systems) into hydrodynamic or morphological models. In this perspective, a numerical code was recently developed to implement such controlled reduced tide systems in TELEMAC-3D (Smolders et al., 2014; Teles et al., 2015), which opens a way to assess the impact of this type of intertidal areas and flood control areas on estuarine tidal hydrodynamics. By doing so, the impact of these areas on tidal hydrodynamics can be assessed and their impact on estuarine tidal hydrodynamics can potentially be optimized as the tidal exchange can be altered by the design or configuration of weirs and in- or outlet sluices. For example, the water level at which inflow starts and the total amount of tidal exchange in the flood control areas with so-called controlled reduced tide along the Scheldt Estuary (e.g. Cox et al., 2006; Maris et al., 2007) are determined by the configuration of the sluices (De Mulder et al., 2013). This allows not only for a regulation of the hydraulic regime on the restored marsh itself, it also implies that the site's impact on estuarine hydrodynamics can be altered by the configuration of the inlet sluices. Moreover, these intertidal areas with a 'controlled' tidal forcing can have a very low elevation in the tidal frame (or even be subtidal) and provide for a significant intertidal storage volume at high water levels without exerting friction on the tidal propagation. Potentially undesirable frictional effects of very low intertidal or subtidal flats (i.e., enhancing flood-dominance or high sedimentation rates) may therefore be avoided by implementing them according to this scheme.

## 6.4 References

- Allen, J.R.L., 2000. Morphodynamics of Holocene salt marshes: A review sketch from the Atlantic and Southern North Sea coasts of Europe. *Quat. Sci. Rev.* 19, 1155–1231. doi:10.1016/S0277-3791(99)00034-7
- Baptist, M.J., Babovic, V., Rodríguez Uthurburu, J., Keijzer, M., Uittenbogaard, R.E., Mynett, A., Verwey, A., 2007. On inducing equations for vegetation resistance. *J. Hydraul. Res.* 45, 435–450.
- Barbier, E.B., Georgiou, I.Y., Enchelmeyer, B., Reed, D.J., 2013. The value of wetlands in protecting Southeast Louisiana from hurricane storm surges. *PLoS One* 8, e58715. doi:10.1371/journal.pone.0058715
- Blott, S.J., Pye, K., van der Wal, D., Neal, A., 2006. Long-term morphological change and its causes in the Mersey Estuary, NW England. *Geomorphology* 81, 185–206. doi:10.1016/j.geomorph.2006.04.008
- Borsje, B.W., van Wesenbeeck, B.K., Dekker, F., Paalvast, P., Bouma, T.J., van Katwijk, M.M., de Vries, M.B., 2011. How ecological engineering can serve in coastal protection. *Ecol. Eng.* 37, 113–122. doi:10.1016/j.ecoleng.2010.11.027
- Coen, L., Peeters, P., Mostaert, F., 2008. Inventarisatie en historische analyse Zeeschelde habitats: Effect antropogene ingrepen en natuurlijke evoluties op de getij-indringing in de Zeeschelde - Ondersteunende numerieke 1D-modellering. WL Rapporten, 713\_21. Antwerpen.
- Cox, T., Maris, T., De Vleeschauwer, P., De Mulder, T., Soetaert, K., Meire, P., 2006. Flood control areas as an opportunity to restore estuarine habitat. *Ecol. Eng.* 28, 55–63. doi:10.1016/j.ecoleng.2006.04.001
- D'Alpaos, A., Lanzoni, S., Marani, M., Fagherazzi, S., Rinaldo, A., 2005. Tidal network ontogeny: Channel initiation and early development. *J. Geophys. Res. Earth Surf.* 110, 1–14. doi:10.1029/2004JF000182

- Dam, G., Van der Wegen, M., Roelvink, D., Labeur, R., Bliet, B., 2015. Simulation of long-term morphodynamics of the Western Scheldt, in: E-Proceedings of the 36th IAHR World Congress. The Hague, p. 9.
- De Mulder, T., Vercruyse, J., Peeters, P., Maris, T., Meire, P., 2013. Inlet sluices for flood control areas with controlled reduced tide in the Scheldt estuary: an overview, in: Bung, D.B. et al. (Ed.), Proceedings of the International Workshop on Hydraulic Design of Low-Head Structures. Aachen, Germany, pp. 43–53.
- De Vriend, H., Aarninkhof, S., van Koningsveld, M., 2014. "Building with nature": the new Dutch approach to coastal and river works. *Proc. ICE - Civ. Eng.* 167, 18–24. doi:10.1680/cien.13.00003
- Dronkers, J., 1986. Tidal asymmetry and estuarine morphology. *Netherlands J. Sea Res.* 20, 117–131. doi:10.1016/0077-7579(86)90036-0
- French, P.W., 2006. Managed realignment - The developing story of a comparatively new approach to soft engineering. *Estuar. Coast. Shelf Sci.* 67, 409–423. doi:10.1016/j.ecss.2005.11.035
- Friedrichs, C.T., Aubrey, D.G., 1994. Tidal propagation in strongly convergent channels. *J. Geophys. Res.* 99, 3321–3336. doi:10.1029/93JC03219
- Friedrichs, C.T., Aubrey, D.G., 1988. Non-linear Tidal Distortion in Shallow Well-Mixed Estuaries: a Synthesis. *Estuar. Coast. Shelf Sci.* 27, 521–545. doi:10.1016/0272-7714(90)90054-U
- Friedrichs, C.T., Madsen, O.S., 1992. Nonlinear diffusion of the tidal signal in frictionally dominated embayments. *J. Geophys. Res.* 97, 5637–5650. doi:10.1029/92JC00354
- Hu, K., Chen, Q., Wang, H., 2015. A numerical study of vegetation impact on reducing storm surge by wetlands in a semi-enclosed estuary. *Coast. Eng.* 95, 66–76. doi:10.1016/j.coastaleng.2014.09.008
- Jarrett, J.T., 1976. *Tidal Prism - Inlet Area Relationships*. Vicksburg, MS, U.S.
- Jeuken, C., Wang, Z.B., van der Kaaij, T., Van Helvert, M., Van Ormondt, M., Bruinsma, R., Tanczos, I., 2004. *Morfologische ontwikkelingen in het Schelde estuarium bij voortzetting van het huidige beleid en effecten van een verdere verdieping van de vaargeul en uitpoldering langs de Westerschelde. Deelovereenkomst 2 en 3. Morfologie.*
- Kirwan, M.L., Guntenspergen, G.R., D'Alpaos, A., Morris, J.T., Mudd, S.M., Temmerman, S., 2010. Limits on the adaptability of coastal marshes to rising sea level. *Geophys. Res. Lett.* 37, n/a–n/a. doi:10.1029/2010GL045489
- Kirwan, M.L., Megonigal, J.P., 2013. Tidal wetland stability in the face of human impacts and sea-level rise. *Nature* 504, 53–60. doi:10.1038/nature12856
- Kirwan, M.L., Murray, a B., 2007. A coupled geomorphic and ecological model of tidal marsh evolution. *Proc. Natl. Acad. Sci. U. S. A.* 104, 6118–6122. doi:10.1073/pnas.0700958104
- Kirwan, M.L., Temmerman, S., Skeehean, E.E., Guntenspergen, G.R., Fagherazzi, S., 2016. Overestimation of marsh vulnerability to sea level rise. *Nat. Clim. Chang.* 6, 253–260. doi:10.1038/nclimate2909
- Lanzoni, S., Seminara, G., 2002. Long-term evolution and morphodynamic equilibrium of tidal channels. *J. Geophys. Res.* 107, ---. doi:10.1029/2000JC000468
- Liu, H., Zhang, K., Li, Y., Xie, L., 2013. Numerical study of the sensitivity of mangroves in reducing storm surge and flooding to hurricane characteristics in southern Florida. *Cont. Shelf Res.* 64, 51–65. doi:10.1016/j.csr.2013.05.015
- Maris, T., Cox, T., Temmerman, S., De Vleeschauwer, P., Van Damme, S., De Mulder, T., Van Den Bergh, E., Meire, P., 2007. Tuning the tide: Creating ecological conditions for tidal marsh development in a flood control area. *Hydrobiologia* 588, 31–43. doi:10.1007/s10750-007-0650-5
- McIvor, A., Spencer, T., Möller, I., Spalding, M., 2012. *Storm surge reduction by mangroves. Natural Coastal Protection Series: Report 2, Cambridge Coastal Research Unit Working Paper 41.*
- Meire, P., Dauwe, W., Maris, T., Peeters, P., Deschamps, M., Rutten, J., Temmerman, S., Ministry, F., Albert, K., 2014. The recent "Saint Nicholas" storm surge in the Scheldt estuary: the Sigma plan proves its efficiency. *ECSA Bull.* 62, 19–23.
- Meire, P., Ysebaert, T., Van Damme, S., Van Den Bergh, E., Maris, T., Struyf, E., 2005. The Scheldt estuary: A description of a changing ecosystem. *Hydrobiologia* 540, 1–11. doi:10.1007/s10750-005-0896-8
- Mitchell, S.B., 2013. Turbidity maxima in four macrotidal estuaries. *Ocean Coast. Manag.* 79, 62–69. doi:10.1016/j.ocecoaman.2012.05.030
- Möller, I., Kudella, M., Rupprecht, F., Spencer, T., Paul, M., van Wesenbeeck, B.K., Wolters, G., Jensen, K., Bouma, T.J., Miranda-Lange, M., Schimmels, S., 2014. Wave attenuation over coastal salt marshes under storm surge conditions. *Nat. Geosci.* 7, 727–731. doi:10.1038/ngeo2251
- Mudd, S.M., D'Alpaos, A., Morris, J.T., 2010. How does vegetation affect sedimentation on tidal marshes? Investigating particle capture and hydrodynamic controls on biologically mediated sedimentation. *J. Geophys. Res.* 115, F03029. doi:10.1029/2009JF001566

- Naik, P.K., Jay, D.A., 2011. Distinguishing human and climate influences on the Columbia River: Changes in mean flow and sediment transport. *J. Hydrol.* 404, 259–277. doi:10.1016/j.jhydrol.2011.04.035
- O'Brien, M.P., 1969. Equilibrium flow areas of tidal inlets on sandy coasts, in: *Proceedings of the American Society of Civil Engineers. Journal of the Waterways and Harbors Division.* pp. 43–52-. doi:10.9753/icce.v10.25p
- O'Brien, M.P., 1931. Estuary and tidal prisms related to entrance areas. *Civ. Eng.* 1, 738–739.
- Resio, D.T., Westerink, J.J., 2008. Modelling the physics of storm surges. *Phys. Today* 61, 33–38. doi:10.1063/1.2982120
- Rinaldo, A., Fagherazzi, S., Lanzoni, S., Marani, M., Dietrich, W.E., 1999. Tidal networks: 3. Landscape-forming discharges and studies in empirical geomorphic relationships. *Water Resour. Res.* 35, 3919–3929.
- Rupp-Armstrong, S., Nicholls, R.J., 2007. Coastal and estuarine retreat: a comparison of the application of managed realignment in England And Germany. *J. Coast. Res.* 236, 1418–1430. doi:10.2112/04-0426.1
- Sheng, Y.P., Lapetina, A., Ma, G., 2012. The reduction of storm surge by vegetation canopies: Three-dimensional simulations. *Geophys. Res. Lett.* 39, 1–5. doi:10.1029/2012GL053577
- Sherwood, C.R., Jay, D.A., Harvey, R.B., Hamilton, P., Simenstad, C.A., 1990. Historical changes in the Columbia River Estuary. *Prog. Oceanogr.* 25, 299–352. doi:10.1016/0079-6611(90)90011-P
- Smolders, S., Maximova, T., Vanlede, J., Teles, M.J., 2014. Implementation of controlled reduced tide and flooding areas in the TELEMAC 3D model of the Scheldt Estuary, in: *Proceedings of the 21st TELEMAC-MASCARET User Conference.* Grenoble, France, p. 8.
- Smolders, S., Plancke, Y., Ides, S., Meire, P., Temmerman, S., 2015. Role of intertidal wetlands for tidal and storm tide attenuation along a confined estuary: A model study. *Nat. Hazards Earth Syst. Sci.* 15, 1659–1675. doi:10.5194/nhess-15-1659-2015
- Speer, P.E., Aubrey, D.G., 1985. A study of non-linear tidal propagation in shallow inlet/estuarine systems Part II: Theory. *Estuar. Coast. Shelf Sci.* 21, 207–224. doi:10.1016/0272-7714(85)90097-6
- Steel, T.J., Pye, K., 1997. The development of saltmarsh tidal creek networks: evidence from the UK, in: *Proceedings of the Canadian Coastal Conference,* 22-25 May 1997. pp. 267–280.
- Stefanon, L., Carniello, L., D'Alpaos, A., Lanzoni, S., 2010. Experimental analysis of tidal network growth and development. *Cont. Shelf Res.* 30, 950–962. doi:10.1016/j.csr.2009.08.018
- Stive, M.J.F., Ji, L., Brouwer, R.L., van de Kreeke, J., Ranasinghe, R., 2010. Empirical relationship between inlet cross-sectional area and tidal prism: a re-evaluation, in: *Coastal Engineering Proceedings.* pp. 1–10.
- Tambroni, N., Seminara, G., 2008. Effects of tidal flats on tide propagation and sediment transport in tidal channels, in: P. Campostrini (Ed.), *Scientific Research and Safeguarding of Venice: Research Programme Corila 2004-2006 Vol VI.* Corila, Venice, pp. 597–611.
- Teles, M.J., Smolders, S., Maximova, T., Rocabado, I., Vanlede, J., 2015. Numerical modelling of flood control areas with controlled reduced tide, in: *E-Proceedings of the 36th IAHR World Congress.* The Hague, Netherlands, p. 10.
- Temmerman, S., Bouma, T.J., Govers, G., Lauwaet, D., 2005a. Flow paths of water and sediment in a tidal marsh: Relations with marsh developmental stage and tidal inundation height. *Estuaries* 28, 338–352. doi:10.1007/BF02693917
- Temmerman, S., Bouma, T.J., Govers, G., Wang, Z.B., De Vries, M.B., Herman, P.M.J., 2005b. Impact of vegetation on flow routing and sedimentation patterns: Three-dimensional modelling for a tidal marsh. *J. Geophys. Res.* 110, F04019. doi:10.1029/2005JF000301
- Temmerman, S., De Vries, M.B., Bouma, T.J., 2012. Coastal marsh die-off and reduced attenuation of coastal floods: A model analysis. *Glob. Planet. Change* 92–93, 267–274. doi:10.1016/j.gloplacha.2012.06.001
- Temmerman, S., Meire, P., Bouma, T.J., Herman, P.M.J., Ysebaert, T., De Vriend, H.J., 2013. Ecosystem-based coastal defence in the face of global change. *Nature* 504, 79–83. doi:10.1038/nature12859
- Van der Wegen, M., Roelvink, J.A., 2012. Reproduction of estuarine bathymetry by means of a process-based model: Western Scheldt case study, the Netherlands. *Geomorphology* 179, 152–167. doi:10.1016/j.geomorph.2012.08.007
- Van Rijn, L.C., 2011. Analytical and numerical analysis of tides and salinities in estuaries; part I: tidal wave propagation in convergent estuaries. *Ocean Dyn.* 61, 1719–1741. doi:10.1007/s10236-011-0453-0
- Vandenbruwaene, W., Schwarz, C., Bouma, T.J., Meire, P., Temmerman, S., 2015. Landscape-scale flow patterns over a vegetated tidal marsh and an unvegetated tidal flat: implications for the landform properties of the intertidal floodplain. *Geomorphology* 231, 40–52. doi:10.1016/j.geomorph.2014.11.020

- Verschoren, V., Meire, D., Schoelynck, J., Buis, K., Bal, K.D., Troch, P., Meire, P., Temmerman, S., 2016. Resistance and reconfiguration of natural flexible submerged vegetation in hydrodynamic river modelling. *Environ. Fluid Mech.* 16, 245–265. doi:10.1007/s10652-015-9432-1
- Wamsley, T. V., Cialone, M. a., Smith, J.M., Atkinson, J.H., Rosati, J.D., 2010. The potential of wetlands in reducing storm surge. *Ocean Eng.* 37, 59–68. doi:10.1016/j.oceaneng.2009.07.018
- Yang, S.L., Li, M., Dai, S.B., Liu, Z., Zhang, J., Ding, P.X., 2006. Drastic decrease in sediment supply from the Yangtze River and its challenge to coastal wetland management. *Geophys. Res. Lett.* 33, 4–7. doi:10.1029/2005GL025507
- Zhang, K., Liu, H., Li, Y., Xu, H., Shen, J., Rhome, J., Smith, T.J., 2012. The role of mangroves in attenuating storm surges. *Estuar. Coast. Shelf Sci.* 102-103, 11–23. doi:10.1016/j.ecss.2012.02.021





## Curriculum Vitae



Jeroen Stark was born in Schiedam, the Netherlands, on March 1<sup>st</sup> 1989 and lived most of his life in Rotterdam. He graduated from secondary school (VWO) at the Emmauscollege in Rotterdam in 2006. His academic education started afterwards at Delft University of Technology where he studied Civil Engineering. Jeroen obtained his BSc degree in 2009 and his MSc degree at the Section of Hydraulic Engineering in 2012. As part of his study, he gained work experience during an internship at Witteveen+Bos in Rotterdam. His graduation research, entitled ‘The influence of dredging activities on the long-term morphological development of the Columbia River Mouth: a Delft3D modelling study’, was supervised by prof. dr. ir. Marcel Stive, dr. ir. Edwin Elias, ir. Arjen Luijendijk, dr. ir. Dirk-Jan Walstra, dr. Guy Gelfenbaum and dr. ir. Joep Storms. This graduation research was conducted at Deltares in Delft (NL) and at the USGS Pacific Coastal & Marine Science Center in Santa Cruz (CA, U.S.A.).

After graduation, Jeroen worked for a short period as coastal engineer at the Hydraulic Engineering department of Deltares before starting his PhD research at the University of Antwerp in December 2012. This PhD research, in which he studied the impact of intertidal ecosystems on tidal hydrodynamics and flood wave propagation in estuaries and tidal wetlands, resulted in the present thesis.

## List of publications

### *Journal articles as first author:*

**Stark, J.**, Plancke, Y., Ides, S., Meire, P., Temmerman, S. (2016). Coastal flood protection by a combined nature-based and engineering approach: Modeling the effects of marsh geometry and surrounding dikes. *Estuarine, Coastal and Shelf Science*, 175: 34-45. doi: 10.1016/j.ecss.2016.03.027

**Stark, J.**, Van Oyen, T., Meire, P., Temmerman, S. (2015). Observations of tidal and storm surge attenuation in a large tidal marsh. *Limnology and Oceanography*, 60: 1371–1381. doi: 10.1002/lno.10104

**Stark, J.**, Meire, P., Temmerman, S. (n/a). Changing tidal hydrodynamics during different stages of eco-geomorphological development of a tidal marsh: a numerical modeling study. *Submitted*

**Stark, J.**, Smolders, S., Meire, P., Temmerman, S. (n/a). Impact of intertidal area characteristics on estuarine tidal hydrodynamics: a modeling study for the Scheldt estuary. *Submitted*

Conference proceedings, abstracts and other publications:

- Stark, J.**, Ides, S., Plancke, Y., Meire, P., Temmerman, S. (2016). Modelling the effect of intertidal area changes on tidal hydrodynamics in estuary channels. in: Meire, P. (Ed.) (2016). Book of abstracts – ECSA Local Meeting 2016. Estuarine Restoration: from theory to practice and back, University of Antwerp, Antwerp, Belgium, 5-9 July 2016: pp. 98
- Stark, J.**, Meire, P., Temmerman, S. (2016). Do marshes attenuate storm surges? Modelling the effects of marsh geometry and marsh size on storm surge reduction rates. in: Meire, P. (Ed.) (2016). Book of abstracts – ECSA Local Meeting 2016. Estuarine Restoration: from theory to practice and back, University of Antwerp, Antwerp, Belgium, 5-9 July 2016: pp. 98
- Stark, J.**, Ides, S., Plancke, Y., Meire, P., Temmerman, S. (2016). Do marshes attenuate storm surges? A numerical study on the effects of marsh geometry and marsh size on storm surge reduction rates. in: Jan Mees and Jan Seys (Eds.) (2016). Book of abstracts – VLIZ Marine Scientist Day. Brugge, Belgium, 12 February 2016: pp. 103
- Stark, J.**, Plancke, Y., Ides, S., Meire, P., Temmerman, S. (2015). Storm surge attenuation in a large intertidal marsh: Impact of marsh geomorphology. in: E-proceedings of the 36th IAHR World Congress, Den Haag, The Netherlands, 28/6-3/7 2015.
- Stark, J.**, Ides, S., Plancke, Y., Meire, P., Temmerman, S. (2015). In-situ observations and numerical modelling of tidal propagation and storm surge attenuation in a large tidal marsh. in: Proceedings of the 55th Estuaries & Coastal Sciences Association (ECSA) Conference, London, UK, 6-9 September 2015.
- Stark, J.**, Meire, P., Temmerman, S. (2015). Do marshes attenuate storm surges? Observations of peak water levels along channelized marsh transects. in: Mees, J. et al. (Eds.) (2015). Book of abstracts – VLIZ Young Scientists' Day. Brugge, Belgium, 20 February 2015: pp. 120
- Stark, J.**, Meire, P., Temmerman, S. (2014). 2D modeling of tidal wave propagation through a large vegetated marsh. in: Proceedings of the 21st TELEMAC-MASCARET User Conference, Grenoble, France, 15–17 October 2014: pp. 101
- Stark, J.**, Smolders, S., Plancke, Y., Ides, S., Meire, P., Temmerman, S. (2013). Tidal wave propagation in a marsh along the Western Scheldt. in: Book of Abstracts – Coastal Ecology Workshop, Spiekeroog, Germany, 28-31 October 2013: pp. 20
- Raaijmakers, T., van Velzen, G., Hoffmans, G., Bijlsma, A., Verbruggen, W., **Stark J.** (2012). Stormvloedkering Oosterschelde: ontwikkeling ontgrondingskuilen en stabiliteit bodembescherming, deelrapportage "Ontgrondingen". 1206907-003-GEO-0003, november 2012, Deltares. *In Dutch*.
- Stark, J.** (2012). The influence of dredging activities on the morphological development of the Columbia River mouth. MSc Thesis, July 2012, Delft University of Technology. [uid:e5d65bb4-5aef-432e-b6a2-871fb22f0de4](https://doi.org/10.1001/10.1001/e5d65bb4-5aef-432e-b6a2-871fb22f0de4)